



**Process Development for the Continuous  
Epoxidation of Renewable Terpenes using  
“Mesoscale” 3D-printed Oscillatory Baffled Reactor**

A thesis submitted to the Newcastle University for the  
Degree of Doctor of Philosophy

by

**Mohamad Faiz Mukhtar Gunam Resul**

School of Engineering  
Newcastle University, United Kingdom

**August 2020**



## Abstract

A continuous process was developed for the epoxidation of (R)-(+)-limonene and  $\alpha$ -pinene with an oxidant ( $\text{H}_2\text{O}_2$ ) using a polytungstophosphate catalyst in a mesoscale Oscillatory Baffled Reactor (mesoOBR). Waste biomass derived (R)-(+)-limonene and  $\alpha$ -pinene were used as an alternative to petrochemical-based epoxides. A selective process towards the epoxides was investigated by the screening of process parameters including temperature, oxidant molar ratio, sodium sulphate ( $\text{Na}_2\text{SO}_4$ ) amount, acid ( $\text{H}_2\text{SO}_4$ ) concentration and solvent type. The mass and heat transfer limitation associated with the exothermic and biphasic epoxidation reaction was overcome using new 3D-printed baffles in the mesoOBR platform.

Screening the process parameters for the epoxidation of (R)-(+)-limonene revealed that a high  $\text{H}_2\text{O}_2$  conversion (~95 %) and selectivity to the limonene-1,2-epoxide (100 %), was able to achieve in 15 minutes with a single-step addition of  $\text{H}_2\text{O}_2$ . The operating conditions included a 50 °C temperature in an organic solvent-free environment, with a (R)-(+)-limonene/ $\text{H}_2\text{O}_2$ /catalyst molar ratio of 4:1:0.005. To prevent the hydrolysis of the epoxide, the reaction mixture was saturated with  $\text{Na}_2\text{SO}_4$  (5.7 g). An acid concentration of lower than 0.04 M was used and found to have a significant effect on the selectivity. Kinetic studies were performed to allow modelling of the reaction scheme. A kinetic investigation showed that the reaction was first-order in terms of (R)-(+)-limonene and catalyst concentration, and fractional order (~0.5) with respect to the  $\text{H}_2\text{O}_2$  concentration. The activation energy for the formation of limonene-1,2-epoxide and limonene-1,2-diol was determined to be ~36 and 79  $\text{kJ mol}^{-1}$ , respectively.

The epoxidation of  $\alpha$ -pinene with  $\text{H}_2\text{O}_2$  was also performed using polytungstophosphate catalyst. The variables in the screening parameters were temperatures (30–70 °C), oxidant amount (100-200 mol%), acid concentrations (0.02-0.09 M) and solvent types (1,2-dichloroethane, toluene, *p*-cymene, and acetonitrile). Screening the process parameters revealed that a 100% selective epoxidation of  $\alpha$ -pinene to  $\alpha$ -pinene oxide was possible with negligible side-product formation within a short reaction time (~20 minutes), using process conditions of a 50 °C temperature in an organic solvent-free environment and a  $\alpha$ -pinene/ $\text{H}_2\text{O}_2$ /catalyst molar ratio of 5:1:0.01. A kinetic investigation also showed that the reaction was first-order in terms of  $\alpha$ -pinene and catalyst concentration, and fractional order (~0.5) with respect to the  $\text{H}_2\text{O}_2$  concentration. The activation energy of ~35  $\text{kJ mol}^{-1}$  was obtained for the epoxidation of  $\alpha$ -pinene, which was similar to ~36  $\text{kJ mol}^{-1}$  for (R)-(+)-limonene.

Novel 3D-printed orifice baffles were integrated with a mesoscale oscillatory baffled reactor for the continuous epoxidation of terpenes ((R)-(+)-limonene and  $\alpha$ -pinene) with  $H_2O_2$  in an organic solvent-free environment. The biphasic reaction is highly exothermic, usually requiring solvent, tight temperature control and effective multiphase mixing. The performance of the new 3D-printed single, tri- and multi-orifice baffles was compared to conventional helical and integral baffles. The performance investigated were the mixing intensity, induction period, multi steady state and heat removal capability. Passive isothermalisation was also investigated using mesoOBR in a heat pipe assembly. The tri- and multi-orifice baffles were able to overcome mixing limitation in continuous epoxidation and achieved a comparable rate of reaction to batch epoxidation at mixing condition of oscillatory Reynolds number ( $Re_o$ )  $>850$  and  $Re_o >500$ , respectively. Both baffles exhibited rapid steady state attainment, shorter induction period at  $t = 1.5$  residence time ( $\tau$ ) and better reproducibility with product variation of  $\sim 1.3\%$ . Other mesoOBRs designs had induction times of  $2.0 \tau - 3.0 \tau$  and product variations in the range of  $1.6 - 2.1 \%$ . The helically baffled mesoOBR designs demonstrated effective heat transfer capability, allowing the reaction to being operated isothermally with  $\pm 1$  °C temperature variation in an organic solvent-free condition. This removes the need of a solvent, thus reducing reaction volume by a 5-fold. The timescale for the reaction was reduced from  $\sim 8$  hours in a conventional process to 30 minutes in the multi-orifice mesoOBR, a 16-fold reduction. Therefore, a better process has been developed for a continuous epoxidation of (R)-(+)-limonene and  $\alpha$ -pinene with  $H_2O_2$  using multi-orifice mesoOBRs, with a potential intensification factor of  $\sim 80$ .



## **Dedication**

Dedicated to

Zeenat, Zara, Zaira, Uzair and Umar

## **Acknowledgements**

First and foremost, I would like to express my profound gratitude to God Almighty for giving me the strength and courage to complete my PhD. Special thanks to my supervisor, Prof. Adam P. Harvey for his mentorship, encouragement, keen supervision, and insightful contributions to this research. I am indebted to my second supervisor, Dr. Ana Maria Lopez Fernandez, for her tireless efforts over the last 3 years on many aspects of this research. Many thanks to Dr. Valentine Eze for your guidance and sharp criticism during the write-up of this thesis.

I also express my deepest appreciations to my beloved wife, Zeenat and daughters, Zara Fizrina and Zaira Firzana for their patience and understanding throughout the years. I am forever indebted to my parents, Gunam Resul and Shamshad Begum who had inspired me to continuously seek knowledge. Special thanks to them, my siblings and in-laws for their sacrifices and prayers.

To my friend, Abdul Rehman, thank you for the many help and favours you had given. I also thank the members of Process Intensification Group who also helped contribute to this work.

Special appreciation to the technical staff in School of Engineering, Rob Dixon, Ian Ditchburn, Ian Strong, Paul Sterling and Stewart Latimer who had assisted in the technical aspect of this project.

Finally, I express my gratitude for the financial support provided by Universiti Putra Malaysia, The Ministry of Education, Malaysia and an Engineering and Physical Sciences Research Council (EPSRC) grant (Sustainable Polymers, grant number EP/L017393/1).

## Table of Contents

Abstract .....	i
Dedication .....	iii
Acknowledgements.....	iv
List of Publications .....	ix
List of Figures.....	x
List of Schemes.....	xxi
List of Tables.....	xxiii
List of Abbreviations .....	xxv
List of Nomenclature .....	xxvii
Chapter 1 Introduction .....	1
1.1 Background.....	1
1.2 Importance of this research project .....	6
1.3 Research aims and objective.....	7
Chapter 2 Literature Review .....	8
2.1 Waste biomass as a feedstock for bio-based polymers .....	8
2.2 Terpenes.....	10
2.3 Epoxidation.....	12
2.3.1 Routes for epoxidation process .....	14
2.3.2 Prilezhaev epoxidation .....	14
2.3.3 Hydroperoxide routes .....	16
2.3.4 Catalytic route using molecular oxygen and $H_2O_2$ .....	17
2.4 The effect of sodium sulphate ( $Na_2SO_4$ ) in the epoxidation reaction .....	26
2.5 Biphasic reactions .....	27
2.5.1 Surfactants .....	28
2.5.2 Phase transfer catalyst (PTC).....	31
2.5.3 Polyoxometalates.....	34
2.6 Process intensification .....	42

2.6.1 The Oscillatory baffled reactor (OBR) .....	43
2.6.2 The Mesoscale oscillatory baffled reactor .....	46
2.6.3 Heat pipe OBR.....	49
2.6.4 Additive manufacturing (AM).....	51
Chapter 3 Materials and Methods.....	53
3.1 Materials .....	53
3.2 Experimental set-up and equipment .....	56
3.2.1 Batch reactor.....	56
3.2.2 Helically and integrally baffled mesoOBR .....	57
3.2.3 Additive manufacturing for fabrication of orifice baffles using a 3D- printer .....	58
3.2.4 Laboratory equipment and accessories .....	63
3.3 Experimental procedure.....	63
3.3.1 Preparation of the oxidant .....	63
3.3.2 Batch epoxidation.....	64
3.3.3 Screening of process parameters.....	65
3.3.4 Continuous epoxidation .....	67
3.3.5 Heat pipe mesoOBR and temperature monitoring .....	70
3.3.6 Sampling and product purification.....	73
3.4 Product analysis techniques .....	73
3.4.1 H <sub>2</sub> O <sub>2</sub> titration method.....	73
3.4.2 In situ Fourier transform infrared (FTIR) spectroscopy analysis .....	74
3.4.3 FTIR spectroscopy Calibration .....	76
3.4.4 Gas chromatography .....	78
3.4.5 GC quantification via a calibration curve .....	78
3.4.6 GC sample analysis and quantification .....	80
3.4.7 Nuclear magnetic resonance spectroscopy (NMR) .....	82
3.5 Kinetic modelling of the epoxidation of (R)-(+)-limonene and $\alpha$ -pinene with H <sub>2</sub> O <sub>2</sub> ....	83
3.5.1 Kinetic study and models .....	83

3.5.2 Modelling procedure .....	85
Chapter 4 Epoxidation of (R)-(+)-limonene.....	86
4.1 Introduction.....	86
4.2 Epoxidation of (R)-(+)-limonene with tungstic acid.....	86
4.3 Effects of mixing on (R)-(+)-limonene epoxidation .....	89
4.4 Effect of addition of a phase transfer catalyst on (R)-(+)-limonene epoxidation.....	90
4.5 Effects of metal catalyst and temperatures on decomposition of H <sub>2</sub> O <sub>2</sub> .....	92
4.6 Study of kinetics of (R)-(+)-limonene epoxidation.....	94
4.7 Effect of temperature on the (R)-(+)-limonene epoxidation.....	99
4.8 Effect of H <sub>2</sub> O <sub>2</sub> oxidant amount on (R)-(+)-limonene epoxidation .....	104
4.9 Effect of Na <sub>2</sub> SO <sub>4</sub> on the yield of limonene-1,2-epoxide .....	107
4.10 Effect of acid concentration on (R)-(+)-limonene epoxidation .....	111
4.11 Effects of various solvents on the epoxidation of (R)-(+)-limonene .....	115
4.12 Summary.....	117
Chapter 5 Epoxidation of $\alpha$ -pinene.....	119
5.1 Introduction.....	119
5.2 Kinetics of $\alpha$ -pinene epoxidation.....	119
5.3 Effect of temperature on $\alpha$ -pinene epoxidation .....	124
5.4 Effect of H <sub>2</sub> O <sub>2</sub> oxidant amount on the $\alpha$ -pinene epoxidation.....	127
5.5 Effect of acid concentrations on the $\alpha$ -pinene epoxidation .....	129
5.6 Effects of solvents on $\alpha$ -pinene epoxidation.....	131
5.7 Summary.....	134
Chapter 6 Continuous Epoxidation of (R)-(+)-limonene and $\alpha$ -pinene .....	136
6.1 Introduction.....	136
6.2 Process limitation of an organic solvent-free epoxidation at equimolar conditions ....	136
6.3 Mixing study for epoxidation of (R)-(+)-limonene in the continuous mesoOBR reactor .....	137
6.4 Steady states performance of the mesoOBRs .....	140

6.5 Effect of temperature on the continuous epoxidation in mesoOBR.....	143
6.6 Effect of residence time on the continuous epoxidation in mesoOBR.....	145
6.7 Effect of molar ratio of (R)-(+)-limonene and $\alpha$ -pinene to H <sub>2</sub> O <sub>2</sub> on the continuous epoxidation in mesoOBR .....	146
6.8 Passive isothermalisation of continuous epoxidation using heat-pipe OBR (HPOBR).....	148
6.9 Summary.....	153
Chapter 7 Conclusions and Future Work.....	154
7.1 Conclusions.....	154
7.1.1 Batch (R)-(+)-limonene epoxidation .....	155
7.1.2 Batch $\alpha$ -pinene epoxidation .....	156
7.1.3 Continuous (R)-(+)-limonene epoxidation using mesoOBR.....	156
7.2 Future Work.....	158
7.2.1 Heterogeneous catalyst.....	158
7.2.2 Residence Time Distributions (RTD).....	158
7.2.3 Scalability of the mesoOBR.....	158
7.2.4 Heat transfer study .....	159
7.2.5 Droplet diameter .....	159
7.2.6 Kinetic model.....	159
References .....	160
Appendix A. Calculation for Na <sub>2</sub> SO <sub>4</sub> solubility.....	175
Appendix B. Syringe pump commands.....	176
Appendix C. Flow condition used in the continuous experiments using mesoOBR.....	178
Appendix D. Full FTIR spectra.....	179
Appendix E. GC response factor and calibration curves.....	181
Appendix F. NMR Spectra.....	184
Appendix G. MATLAB code (epoxidation of limonene).....	186
Appendix H. Initial rates values (limonene epoxidation).....	189
Appendix I. Initial rates values ( $\alpha$ -pinene epoxidation).....	191

## List of Publications

1. **Resul, M.F.M.G.**, Fernández, A.M.L., Rehman, A., and Harvey, A.P. (2018) 'Development of a selective, solvent-free epoxidation of limonene using hydrogen peroxide and a tungsten-based catalyst', *Reaction Chemistry & Engineering*, 3(5), pp. 747-756.
2. Rehman, A., Fernández, A.M.L., **Resul, M.G.** and Harvey, A., (2018) 'Kinetic investigations of styrene carbonate synthesis from styrene oxide and CO<sub>2</sub> using a continuous flow tube-in-tube gas-liquid reactor', *Journal of CO<sub>2</sub> Utilization*, 24, pp. 341-349
3. Rehman, A., Fernández, A.M.L., **Resul, M.G.** and Harvey, A. (2019) 'Highly selective, sustainable synthesis of limonene cyclic carbonate from bio-based limonene oxide and CO<sub>2</sub>: A kinetic study', *Journal of CO<sub>2</sub> Utilization*, 29, pp. 126-133.
4. Rehman, A., Eze, V.C., **Resul, M.F.M.G.** and Harvey, A. (2018) 'Kinetics and mechanistic investigation of epoxide/CO<sub>2</sub> cycloaddition by a synergistic catalytic effect of pyrrolidinopyridinium iodide and zinc halides', *Journal of Energy Chemistry*, 37, pp. 35-42.
5. Durkin, A., Tapygin, I., Kong, Q., **Resul, M.F.G.**, Rehman, A., Fernández, A.M., Harvey, A.P., Shah, N. and Guo, M., (2019) 'Scale-up and Sustainability Evaluation of Biopolymer Production from Citrus Waste Offering Carbon Capture and Utilisation Pathway', *ChemistryOpen*, 8(6), pp.668.
6. **Resul, M.F.M.G.**, Fernández, A.M.L., Rehman, A., Eze, V. and Harvey, A.P. (under review). 'Continuous epoxidation of renewable terpenes using novel, "mesoscale" 3D-printed oscillatory baffled reactors'

## List of Figures

Figure 1.1. A typical epoxidation process using solvent and a fed-batch reactor. ....	3
Figure 1.2. Commonly used baffled type in MesoOBR; (a) integral baffles and (b) helical baffles. ....	4
Figure 1.3. An envisaged epoxidation process using Oscillatory Baffled Reactor in an organic solvent-free environment. ....	6
Figure 2.1. Bio-based alternatives to petrochemical for the manufacturing of polymers (Zhu et al., 2016). ....	9
Figure 2.2. Commonly used peracids for epoxidation; (1) peroxyformic acid,(2) peroxyacetic acid, (3) m-chloroperoxybenzoic and (4) p-nitroperoxybenzoic. ....	15
Figure 2.3. From biomass to polymer, the versatility of epoxides. ....	22
Figure 2.4. A simplified version of a biphasic reaction system showing product separation and recycling. ....	27
Figure 2.5. Schematic of a ‘water-in-oil’ emulsion where the hydrophobic tail of the surfactant stretches towards the organic phase (gold background), while the hydrophilic head remains in the aqueous phase (blue background). ....	29
Figure 2.6. Mechanism of PTC in a biphasic mixture. ....	32
Figure 2.7. Influence of acidity on the structure of the polyoxometalates complex, (a) Keggin, (b) lacunary Keggin, (c) Wells-Dawson and (d) Anderson structure (Zhu et al., 2003). ....	35
Figure 2.8. The visualisation of the structure of Venturello anion (PW4) (Mizuno et al., 2005). ....	37
Figure 2.9. Overall reaction scheme for the epoxidation of (R)-(+)-limonene, the formation of oxidative species, the decomposition of H <sub>2</sub> O <sub>2</sub> and the hydrolytic decomposition of the epoxides. The schematic diagram visualises the phase where each reaction occurs (blue background: aqueous phase, gold background: organic phase). ....	40



Figure 2.10. Conventional OBR fitted with single orifice baffles (Zheng et al., 2007). .....	43
Figure 2.11. Formation of vortices in oscillatory baffled reactor; (a) vortex forms downstream of the baffle, (b) vortex grow in baffle cavity, (c) vortex swept into bulk fluid and (d) interact with vortices from previous cycle (McDonough et al., 2015). .....	44
Figure 2.12. Type of baffles in mesoOBR: (a) integral, (b) central axial, (c) round edge helical, (d) sharp edge helical, (e) sharp edge helical with central rod, and (f) wire wool (McDonough et al., 2015). .....	47
Figure 2.13. The mechanism of a heat pipe OBR (Reay et al., 2006). .....	49
Figure 2.14. Various design of 3D-printed reactors (McDonough et al., 2019). .....	52
Figure 3.1. Jacketed four-neck batch reactor.....	57
Figure 3.2. Configuration and schematics of the conventional mesoOBRs design: (A) helical baffles and (B) integral baffles. ....	58
Figure 3.3. Application of the AM technique for the fabrication of orifice baffles at the millimetre scale: (A) Form2 SLA 3D-printer, (B) a SketchUp drawing model showing a tri-orifice baffle, and (C) a printed, cured and cleaned multi-orifice baffled mesoOBR reactor. ....	59
Figure 3.4. Configuration and schematics of the 3D-printed orifice mesoOBRs designs: (A) single orifice, (B) tri-orifice, and (C) multi-orifice.....	60
Figure 3.5. FTIR spectra of pure component and samples taken after submersion of 3D-printed materials for 72 hours; (A) (R)-(+)-limonene, (B) limonene-1,2-epoxide, (C) $\alpha$ -pinene and (D) $\alpha$ -pinene oxide. $8\text{cm}^{-1}$ resolution, 40 averaged scans, 15 seconds per scan set. ....	62
Figure 3.6. NMR spectra of (A) the prepared polytungstophosphate catalyst $\{\text{PO}_4[\text{WO}(\text{O}_2)_2]_4\}^{3-}$ and (B) polytungstophosphate characterized in (Duncan et al., 1995). ....	64
Figure 3.7. Experimental set-up for batch epoxidation using in situ FTIR spectroscopy.....	65

Figure 3.8. (A) Experimental set-up and (B) schematics for the continuous epoxidation of terpenes with H <sub>2</sub> O <sub>2</sub> using helically baffled mesoOBR.....	68
Figure 3.9. (A) Schematic diagram and (B) photograph of the heat pipe oscillatory baffled reactor (HPOBR) for continuous solvent-free epoxidation of terpenes with H <sub>2</sub> O <sub>2</sub> . .....	72
Figure 3.10. FTIR spectra of pure; (A) $\alpha$ -pinene and $\alpha$ -pinene oxide and (B) (R)-(+)-limonene and limonene-1,2-epoxide; collected between 1200 cm <sup>-1</sup> and 650 cm <sup>-1</sup> at 8 cm <sup>-1</sup> resolution, 40 co-added and averaged scans and 15 seconds per scan set. ....	75
Figure 3.11. FTIR spectroscopy calibration curves showing the relationship between FTIR spectra peak area and pure component concentrations for (A) $\alpha$ -pinene and $\alpha$ -pinene oxide and (B) (R)-(+)-limonene and limonene-1,2-epoxide.....	77
Figure 3.12. GC calibration curve for (A) (R)-(+)-limonene, (B) limonene-1,2-epoxide, (C) $\alpha$ -pinene, and (D) $\alpha$ -pinene oxide. The value of y-axis represents the ratio between the peak area of the analyte (A <sub>s</sub> ) and the peak area of the internal standard (A <sub>i</sub> ). The value of x-axis represents the ratio between the concentration of the analyte (C <sub>s</sub> ) and the concentration of the internal standard (C <sub>i</sub> ). The gradient of the curve represents the response factor (R <sub>f</sub> ). The trendlines in Figure 3.12 each pass-through origin. ....	80
Figure 3.13. GC chromatogram of (A) $\alpha$ -pinene, its oxidative products and the internal standard and (B) (R)-(+)-limonene, its oxidative products, and the internal standard. ....	81
Figure 4.1. FTIR spectra of reaction sample from the batch epoxidation of (R)-(+)-limonene using tungstic acid catalyst at reaction condition of (R)-(+)-limonene (1.0 M), H <sub>2</sub> O <sub>2</sub> (1.6 M), H <sub>2</sub> WO <sub>4</sub> (0.009 M), phase transfer catalyst (PTC) amount 1 g, mixing speed of 1250 rpm, reaction time 2 hour, and temperature 50 °C. FTIR spectra collected between 1500 cm <sup>-1</sup> and 650 cm <sup>-1</sup> at 8 cm <sup>-1</sup> resolution, 40 averaged scans and 15 seconds per scan set.....	87

- Figure 4.2. FTIR spectra of reaction sample from the batch epoxidation of (R)-(+)-limonene using polytungstophosphate catalyst at reaction condition of (R)-(+)-limonene (1.0 M), H<sub>2</sub>O<sub>2</sub> (1.6 M), Na<sub>2</sub>WO<sub>4</sub>·2H<sub>2</sub>O (0.009 M), phase transfer catalyst (PTC) amount 1 g, mixing speed of 1250 rpm, reaction time 2 hour, and temperature 50 °C. FTIR spectra collected between 1500 cm<sup>-1</sup> and 650 cm<sup>-1</sup> at 8 cm<sup>-1</sup> resolution, 40 averaged scans and 15 seconds per scan set. .... 88
- Figure 4.3. Batch epoxidation of (R)-(+)-limonene at reaction conditions of (R)-(+)-limonene (1.25 M), H<sub>2</sub>O<sub>2</sub> (1.25 M), Na<sub>2</sub>WO<sub>4</sub>·2H<sub>2</sub>O (0.006 M), Na<sub>2</sub>SO<sub>4</sub> (5.7 g), H<sub>2</sub>SO<sub>4</sub> (0.04 M), 1.0 g PTC, temperature (50 °C), toluene (500 mol%) and mixing speeds of 250 – 1500 rpm, (A) The concentration of limonene-1,2-epoxide versus time at various mixing speed. (B) The relationship between the initial reaction rate and the mixing speed. .... 89
- Figure 4.4. Batch epoxidation of (R)-(+)-limonene at reaction conditions of (R)-(+)-limonene (1.25 M), H<sub>2</sub>O<sub>2</sub> (1.25 M), Na<sub>2</sub>WO<sub>4</sub>·2H<sub>2</sub>O (0.006 M), Na<sub>2</sub>SO<sub>4</sub> (5.7 g), H<sub>2</sub>SO<sub>4</sub> (0.04 M), PTC ( 0 – 2.0 g), temperature (50 °C), toluene (500 mol%) and mixing speed of 1250 rpm, (A) The concentration of limonene-1,2-epoxide versus time at various amount of PTC. (B) The relationship between the initial reaction rate and the amount of PTC. .... 91
- Figure 4.5. Effects of catalyst concentration and temperature on the decomposition of H<sub>2</sub>O<sub>2</sub>, (A) concentration of H<sub>2</sub>O<sub>2</sub> with increasing Na<sub>2</sub>WO<sub>4</sub>·2H<sub>2</sub>O catalyst concentration from 0.002 - 0.02 M at 70 °C temperature and 60 min, (B) concentration of H<sub>2</sub>O<sub>2</sub> with increasing temperature from 30 – 80 °C, 0.02 M Na<sub>2</sub>WO<sub>4</sub>·2H<sub>2</sub>O catalyst and 60 min. .... 93
- Figure 4.6. Batch epoxidation at reaction conditions of (R)-(+)-limonene (1.25 M), H<sub>2</sub>O<sub>2</sub> (1.25 M), Na<sub>2</sub>WO<sub>4</sub>·2H<sub>2</sub>O (0.003 M – 0.009 M), Na<sub>2</sub>SO<sub>4</sub> (5.7 g), H<sub>2</sub>SO<sub>4</sub> (0.04 M), 1.0 g PTC, temperature (50 °C), toluene (500 mol%), and 1250 rpm mixing speed, (A)

The concentration of limonene-1,2-epoxide versus time at various concentration of  $\text{Na}_2\text{WO}_4 \cdot 2\text{H}_2\text{O}$ , (B) The plot of the natural log of the initial reaction rates and  $\text{Na}_2\text{WO}_4 \cdot 2\text{H}_2\text{O}$  concentrations. The lines in (A) are fitted to the kinetic model by using Equations (3.6) – (3.11) and the rate constant in Table 4.1..... 95

Figure 4.7. Batch epoxidation at reaction conditions of (R)-(+)-limonene (0.25 M - 1.25 M),  $\text{H}_2\text{O}_2$  (1.25 M),  $\text{Na}_2\text{WO}_4 \cdot 2\text{H}_2\text{O}$  (0.006 M),  $\text{Na}_2\text{SO}_4$  (5.7 g),  $\text{H}_2\text{SO}_4$  (0.04 M), 1.0 g PTC, temperature (50 °C), toluene (500 mol%), and 1250 rpm mixing speed, (A) The concentration of limonene-1,2-epoxide versus time at various initial (R)-(+)-limonene concentrations, (B) The plot of the natural log of the initial reaction rates and initial (R)-(+)-limonene concentrations. The lines in (A) are fitted to the kinetic model by using Equations (3.6) – (3.11) and the rate constant in Table 4.1..... 96

Figure 4.8. Batch epoxidation at reaction conditions of (R)-(+)-limonene (1.25 M),  $\text{H}_2\text{O}_2$  (0.25 M - 1.25 M),  $\text{Na}_2\text{WO}_4 \cdot 2\text{H}_2\text{O}$  (0.006 M),  $\text{Na}_2\text{SO}_4$  (5.7 g),  $\text{H}_2\text{SO}_4$  (0.04 M), 1.0 g PTC, temperature (50 °C), toluene (500 mol%), and 1250 rpm mixing speed, (A) The concentration of limonene-1,2-epoxide versus time at various initial  $\text{H}_2\text{O}_2$  concentrations, (B) The plot of the natural log of the initial reaction rates and initial  $\text{H}_2\text{O}_2$  concentrations. The lines in (A) are fitted to the kinetic model by using Equations (3.6) – (3.11) and the rate constant in Table 4.1..... 98

Figure 4.9. The effects of temperature on (R)-(+)-limonene epoxidation at reaction conditions of (R)-(+)-limonene (1.25 M),  $\text{H}_2\text{O}_2$  (1.25 M),  $\text{Na}_2\text{WO}_4 \cdot 2\text{H}_2\text{O}$  (0.006 M),  $\text{Na}_2\text{SO}_4$  (5.7 g),  $\text{H}_2\text{SO}_4$  (0.06M), 1.0 g PTC, temperature (30 – 60 °C), toluene (500 mol%) and 1250 rpm mixing. (A) conversion of (R)-(+)-limonene, (B) yield of limonene-1,2-epoxide, (C) yield of limonene bis-epoxide and (D) yield of limonene-1,2-diol. The lines are fitted to the kinetic model by using Equations (3.6) – (3.11) and the rate constant in Table 4.1..... 100

Figure 4.10. (A) The plot of the natural log of (R)-(+)-limonene concentration versus time at various temperatures for the formation of limonene-1,2-epoxide for batch epoxidation at reaction conditions of (R)-(+)-limonene (1.25 M), H<sub>2</sub>O<sub>2</sub> (1.25 M), Na<sub>2</sub>WO<sub>4</sub>·2H<sub>2</sub>O (0.006 M), H<sub>2</sub>SO<sub>4</sub> (0.04 M), 1.0 g PTC, toluene (500 mol%) and 1250 rpm mixing, and (B) limonene-1,2-diol formation for reactions at limonene-1,2-epoxide (1.27 M), H<sub>2</sub>O<sub>2</sub> (1.27 M), Na<sub>2</sub>WO<sub>4</sub>·2H<sub>2</sub>O (0.006 M), Na<sub>2</sub>SO<sub>4</sub> (5.7 g), H<sub>2</sub>SO<sub>4</sub> (0.04 M), 1.0 g PTC, toluene (500 mol%) and 1250 rpm mixing, (C) Arrhenius activation energies (E<sub>a</sub>) and temperature dependence of the rate constant for the formation of limonene-1,2-epoxide and limonene-1,2-diol..... 103

Figure 4.11. The effect of the H<sub>2</sub>O<sub>2</sub> amount on (R)-(+)-limonene epoxidation for reactions at (R)-(+)-limonene (1.25 M), H<sub>2</sub>O<sub>2</sub> (1.25 M – 2.50 M), Na<sub>2</sub>WO<sub>4</sub>·2H<sub>2</sub>O (0.006 M), H<sub>2</sub>SO<sub>4</sub> (0.06 M), Na<sub>2</sub>SO<sub>4</sub> (5.7 g), 1.0 g PTC, temperature (50 °C), toluene (500 mol%) and 1250 rpm mixing, (A) conversion of (R)-(+)-limonene, (B) yield of limonene-1,2-epoxide, (C) yield of limonene bis-epoxide, and (D) yield of limonene-1,2-diol. .... 106

Figure 4.12. The effect of the Na<sub>2</sub>SO<sub>4</sub> amount on (R)-(+)-limonene epoxidation at reaction conditions of (R)-(+)-limonene (1.25 M), H<sub>2</sub>O<sub>2</sub> (1.25 M), Na<sub>2</sub>WO<sub>4</sub>·2H<sub>2</sub>O (0.006 M), H<sub>2</sub>SO<sub>4</sub> (0.06 M), 1.0 g PTC, temperature (50 °C), toluene (500 mol%) and 1250 rpm mixing, (A) conversion of (R)-(+)-limonene, (B) yield of limonene-1,2-epoxide, (C) yield of limonene bis-epoxide and (D) yield of limonene-1,2-diol. .... 109

Figure 4.13. Gas chromatograph of samples at reaction time 120 min for the epoxidation of (R)-(+)-limonene using 5.7 g Na<sub>2</sub>SO<sub>4</sub>. .... 111

Figure 4.14. The effect of acid concentration on (R)-(+)-limonene epoxidation for reactions at (R)-(+)-limonene (1.25 M), H<sub>2</sub>O<sub>2</sub> (1.25 M), Na<sub>2</sub>WO<sub>4</sub>·2H<sub>2</sub>O (0.006 M), Na<sub>2</sub>SO<sub>4</sub> (5.7 g), H<sub>2</sub>SO<sub>4</sub> (0.02 M - 0.06 M), 1.0 g PTC, temperature (50 °C), toluene (500

mol%) and 1250 rpm mixing (A) conversion of (R)-(+)-limonene, (B) yield of limonene-1,2-epoxide, (C) yield of limonene bis-epoxide and (D) yield of limonene-1,2-diol..... 113

Figure 4.15. The effects of different solvents on (R)-(+)-limonene epoxidation for reactions at (R)-(+)-limonene (1.25 M), H<sub>2</sub>O<sub>2</sub> (1.25 M), Na<sub>2</sub>WO<sub>4</sub>·2H<sub>2</sub>O (0.006 M), Na<sub>2</sub>SO<sub>4</sub> (5.7 g), H<sub>2</sub>SO<sub>4</sub> (0.06 M), PTC, temperature (50 °C), reaction time (120 min) and solvent amount (500 mol%) for 1.0 g each solvent. (R)-(+)-limonene is represented by the calculated conversion on the y-axis, while limonene-1,2-epoxide, limonene bis-epoxide and limonene-1,2-diol are represented by the calculated yield. .... 115

Figure 4.16. The yield of limonene-1,2-epoxide versus time as a function of the amount of (R)-(+)-limonene at reaction conditions of H<sub>2</sub>O<sub>2</sub> (1.25 M), Na<sub>2</sub>WO<sub>4</sub>·2H<sub>2</sub>O (0.006 M), Na<sub>2</sub>SO<sub>4</sub> (5.7 g), and H<sub>2</sub>SO<sub>4</sub> (0.04 M), 1.0 g PTC, temperature (50 °C) and 1250 rpm mixing. The lines are fitted to the kinetic model by using Equations (3.6) – (3.11) and the rate constant in Table 4.1. .... 117

Figure 5.1. Batch epoxidation of  $\alpha$ -pinene at reaction conditions of  $\alpha$ -pinene (1.25 M), H<sub>2</sub>O<sub>2</sub> (1.25 M), Na<sub>2</sub>WO<sub>4</sub>·2H<sub>2</sub>O (0.008 M – 0.016 M), Na<sub>2</sub>SO<sub>4</sub> (5.7 g), H<sub>2</sub>SO<sub>4</sub> (0.05 M), 1.0 g PTC, temperature (50 °C), toluene (500 mol%) and 1250 rpm mixing, (A) The concentration of  $\alpha$ -pinene oxide versus time at various concentrations of Na<sub>2</sub>WO<sub>4</sub>·2H<sub>2</sub>O, (B) The plot of the natural log between the initial reaction rate and Na<sub>2</sub>WO<sub>4</sub>·2H<sub>2</sub>O concentration. The lines in (A) are fitted to the kinetic model using Equations (3.12) – (3.14) and the rate constant in Table 5.1..... 120

Figure 5.2. Batch epoxidations of  $\alpha$ -pinene at reaction conditions of  $\alpha$ -pinene (0.25 M - 1.25 M), H<sub>2</sub>O<sub>2</sub> (1.25 M), Na<sub>2</sub>WO<sub>4</sub>·2H<sub>2</sub>O (0.012 M), Na<sub>2</sub>SO<sub>4</sub> (5.7 g), H<sub>2</sub>SO<sub>4</sub> (0.05 M), 1.0 g PTC, temperature (50 °C), toluene (500 mol%) and 1250 rpm mixing, (A) The concentration of  $\alpha$ -pinene oxide versus time at various initial  $\alpha$ -pinene concentration, (B) The plot of the natural log between the initial reaction rate and

initial  $\alpha$ -pinene concentration. The lines in (A) are fitted to the kinetic model using Equations (3.12) – (3.14) and the rate constant in Table 5.1..... 122

Figure 5.3. Batch epoxidations of  $\alpha$ -pinene at reaction conditions of  $\alpha$ -pinene (0.25 M),  $H_2O_2$  (0.25 M - 1.25 M),  $Na_2WO_4 \cdot 2H_2O$  (0.012 M),  $Na_2SO_4$  (5.7 g),  $H_2SO_4$  (0.05 M), 1.0 g PTC, temperature (50 °C), toluene (500 mol%) and 1250 rpm mixing, (A) The concentration of  $\alpha$ -pinene oxide versus time at various  $H_2O_2$  initial concentration. (B) The plot of the natural log between the initial reaction rate and initial  $H_2O_2$  concentration. The lines in (A) are fitted to the kinetic model using Equations (3.12)–(3.14) and the rate constant in Table 5.1. .... 123

Figure 5.4. The effects of temperature on the epoxidation of  $\alpha$ -pinene at reaction conditions of  $\alpha$ -pinene (1.25 M),  $H_2O_2$  (1.25 M),  $Na_2WO_4 \cdot 2H_2O$  (0.012 M),  $Na_2SO_4$  (5.7 g),  $H_2SO_4$  (0.05 M), 1.0 g PTC, temperature (30 – 70 °C), toluene (500 mol%) and 1250 rpm mixing, (A) conversion of  $\alpha$ -pinene, (B) yield of  $\alpha$ -pinene oxide. The lines represent the trends between data points. .... 125

Figure 5.5. Arrhenius activation energy for the formation of  $\alpha$ -pinene oxide at reaction conditions of  $\alpha$ -pinene (1.25 M),  $H_2O_2$  (1.25 M),  $Na_2WO_4 \cdot 2H_2O$  (0.006 M),  $Na_2SO_4$  (5.7 g),  $H_2SO_4$  (0.04 M), 1.0 g PTC, temperature (30 – 70 °C), toluene (500 mol%) and 1250 rpm mixing, (A) The plot of the natural log of  $\alpha$ -pinene concentrations versus time at various temperatures for the epoxidation of  $\alpha$ -pinene. (B) Temperature dependence of the rate constant for the formation of  $\alpha$ -pinene oxide. .... 126

Figure 5.6. The effect of the oxidant amount on the epoxidation of  $\alpha$ -pinene and distribution of the products at reaction conditions of  $\alpha$ -pinene (1.25 M),  $H_2O_2$  (0.25 M - 1.25 M),  $Na_2WO_4 \cdot 2H_2O$  (0.012 M),  $Na_2SO_4$  (5.7 g),  $H_2SO_4$  (0.05 M), 1.0 g PTC, temperature (50 °C), reaction time (120 min), toluene (500 mol%) and 1250 rpm mixing. ... 128

Figure 5.7. The effect of acid concentration on the epoxidation of $\alpha$ -pinene and distribution of the products at reaction conditions of $\alpha$ -pinene (1.25 M), $\text{H}_2\text{O}_2$ (1.25 M), $\text{Na}_2\text{WO}_4 \cdot 2\text{H}_2\text{O}$ (0.012 M), $\text{Na}_2\text{SO}_4$ (5.7 g), $\text{H}_2\text{SO}_4$ (0.04 M – 0.09 M), 1.0 g PTC, temperature (50 °C), reaction time (120 min), toluene (500 mol%) and 1250 rpm mixing. ....	129
Figure 5.8. The effects of solvents on $\alpha$ -pinene epoxidation at reaction conditions of $\alpha$ -pinene (1.25 M), $\text{H}_2\text{O}_2$ (1.25 M), $\text{Na}_2\text{WO}_4 \cdot 2\text{H}_2\text{O}$ (0.012 M), $\text{Na}_2\text{SO}_4$ (5.7 g), $\text{H}_2\text{SO}_4$ (0.05 M), 1.0 g PTC, temperature (50 °C), reaction time (120 min), solvent amount (500 mol%) for each solvent and 1250 rpm mixing. ....	132
Figure 5.9. The yield of $\alpha$ -pinene oxide versus time as a function of the amount of $\alpha$ -pinene at reaction conditions of $\text{H}_2\text{O}_2$ (1.25 M), $\text{Na}_2\text{WO}_4 \cdot 2\text{H}_2\text{O}$ (0.012 M), $\text{Na}_2\text{SO}_4$ (5.7 g), $\text{H}_2\text{SO}_4$ (0.05 M), 1.0 g PTC, temperature (50 °C), reaction time (120 min), and 1250 rpm mixing. The lines represent the trends between data points. ....	133
Figure 6.1. Simulated yield of limonene-1,2-epoxide. Reaction conditions: (R)-(+)-limonene (1.25 M), $\text{H}_2\text{O}_2$ (1.25 M), $\text{Na}_2\text{WO}_4 \cdot 2\text{H}_2\text{O}$ (0.006 M), $\text{H}_2\text{SO}_4$ (0.04 M) and temperature (50 °C). The model is fitted using Equation (3.6) – (3.11) and the rate constant in Table 4.1. ....	137
Figure 6.2. Effect of mixing on the initial rate of reaction for the epoxidation of (R)-(+)-limonene using various type of baffles. Reaction condition: (R)-(+)-limonene (1.25 M), $\text{H}_2\text{O}_2$ (1.25 M), $\text{Na}_2\text{WO}_4 \cdot 2\text{H}_2\text{O}$ (0.006 M), $\text{H}_2\text{SO}_4$ (0.04 M), temperature (50 °C), $\text{Re}_0 \sim 1300$ , residence times ( $\tau$ ) 5 min to 15 min ( $\text{Re}_n$ 2.0 – 5.7). Dashed line represents data from simulated model. ....	138
Figure 6.3. Comparison of the yield of limonene-1,2-epoxide of the simulated model and continuous mesoOBR using various baffles. Reaction condition: (R)-(+)-limonene (1.25 M), $\text{H}_2\text{O}_2$ (1.25 M), $\text{Na}_2\text{WO}_4 \cdot 2\text{H}_2\text{O}$ (0.006 M), $\text{H}_2\text{SO}_4$ (0.04 M), temperature (50 °C), $\text{Re}_0 \sim 1300$ , residence times ( $\tau$ ) 30 min ( $\text{Re}_n$ 2.0 – 5.7). ....	139



- Figure 6.4. The effect of various baffle types on the achievement of steady states for the continuous epoxidation of (R)-(+)-limonene. Reaction condition: (R)-(+)-limonene (1.25 M), H<sub>2</sub>O<sub>2</sub> (1.25 M), Na<sub>2</sub>WO<sub>4</sub>·2H<sub>2</sub>O (0.006 M), H<sub>2</sub>SO<sub>4</sub> (0.04 M), temperature 50 °C, residence time ( $\tau$ ) 15 min ( $Re_n \sim 2.0$ ),  $Re_o \sim 1300$ ..... 140
- Figure 6.5. Comparison between the multi-orifice baffle and helically baffled mesoOBR for the screening of residence time for the continuous epoxidation of (R)-(+)-limonene in multi steady state mode. The dashed line represents ramped residence times. Reaction condition: (R)-(+)-limonene (1.25 M), H<sub>2</sub>O<sub>2</sub> (1.25 M), Na<sub>2</sub>WO<sub>4</sub>·2H<sub>2</sub>O (0.006 M), H<sub>2</sub>SO<sub>4</sub> (0.04 M) temperature 50 °C,  $Re_n$  1.0 – 5.7,  $Re_o \sim 1300$ . ..... 142
- Figure 6.6. Comparison of yield for the continuous epoxidation using helical and multi-orifice mesoOBR at various temperature. (A) yield of limonene-1,2-epoxide (B) yield of  $\alpha$ -pinene oxide. Reaction conditions: (R)-(+)-limonene (1.25 M), H<sub>2</sub>O<sub>2</sub> (1.25 M), Na<sub>2</sub>WO<sub>4</sub>·2H<sub>2</sub>O (0.006 M), H<sub>2</sub>SO<sub>4</sub> (0.04 M), residence time ( $\tau$ ) 30 minutes ( $Re_n$  1.0), multi-orifice  $Re_o \sim 500$ , helical  $Re_o \sim 1300$ ..... 144
- Figure 6.7. Comparison of yield for the continuous epoxidation using helical and multi-orifice mesoOBR at various residence time. (A) yield of limonene-1,2-epoxide (B) yield of  $\alpha$ -pinene oxide. Reaction conditions: (R)-(+)-limonene (1.25 M), H<sub>2</sub>O<sub>2</sub> (1.25 M), Na<sub>2</sub>WO<sub>4</sub>·2H<sub>2</sub>O (0.006 M), H<sub>2</sub>SO<sub>4</sub> (0.04 M), temperature 50 °C, ( $Re_n$  1.0 – 5.7), multi-orifice  $Re_o \sim 500$ , helical  $Re_o \sim 1300$ ..... 145
- Figure 6.8. Comparison of yield for the continuous epoxidation using helical and multi-orifice mesoOBR at various molar ratio. (A) yield of limonene-1,2-epoxide (B) yield of  $\alpha$ -pinene oxide. Reaction conditions: Na<sub>2</sub>WO<sub>4</sub>·2H<sub>2</sub>O (0.006 M), H<sub>2</sub>SO<sub>4</sub> (0.04 M), residence time 30 minutes ( $Re_n$  1.0), multi-orifice  $Re_o \sim 500$ , helical  $Re_o \sim 1300$ , 400 mol% = 4:1 substrate:H<sub>2</sub>O<sub>2</sub>. ..... 147

Figure 6.9. Temperature profile comparison between jacketed flask and mesoOBR. Condition for mesoOBR; 5 min residence time ( $Re_n = 5.7$ ) and 30 min residence time ( $Re_n = 1.0$ ).	149
Figure 6.10. Comparison of yield of limonene-1,2-epoxide for the continuous epoxidation using helical mesoOBR, multi-orifice mesoOBR and helically baffled HPOBR at various residence time. Reaction conditions: (R)-(+)-limonene (1.25 M), $H_2O_2$ (1.25 M), $Na_2WO_4 \cdot 2H_2O$ (0.006 M), $H_2SO_4$ (0.04 M), $Re_n$ 1.0 – 5.7, multi-orifice $Re_o \sim 500$ , helical $Re_o \sim 1300$ , HPOBR $Re_o \sim 1300$ .	151
Figure 6.11. Temperature profile for HPOBR showing hot spot at certain reactor length. Reaction conditions: (R)-(+)-limonene (1.25 M), $H_2O_2$ (1.25 M), $Na_2WO_4 \cdot 2H_2O$ (0.006 M), $H_2SO_4$ (0.04 M), initial temperature 50 °C, ( $Re_n$ 1.0 – 11.2), HPOBR $Re_o \sim 1300$ .	152
Figure D.1. Full (4000 – 650 $cm^{-1}$ ) FTIR spectra for A) $\alpha$ -pinene and $\alpha$ -pinene oxide B) limonene and limonene oxide C) toluene (solvent).	180
Figure E.1. GC Calibration curve for (A) Limonene bis-epoxide (B) Limonene-1,2-diol (C) Campholenic aldehyde (D) Sobrerol (E) Pinanediol (F) Verbenol (G) Verbenone.	183
Figure F.1. NMR spectra for A) limonene, limonene-1,2-epoxide and limonene bis-epoxide B) limonene-1,2-diol C) $\alpha$ -pinene and $\alpha$ -pinene oxide.	185

## List of Schemes

Scheme 1.1. The epoxidation of terpenes with H <sub>2</sub> O <sub>2</sub> . (1) (R)-(+)-limonene, (2) trans-limonene-1,2-epoxide, (3) $\alpha$ -pinene and (4) trans- $\alpha$ -pinene oxide. ....	2
Scheme 1.2. Cycloaddition of CO <sub>2</sub> to limonene epoxides for the synthesis of limonene cyclic carbonates (Rehman et al., 2019). ....	6
Scheme 2.1. Biosynthetic route and common skeleton for monoterpenes in plants (Erman, 1985). ....	11
Scheme 2.2. Ethylene oxide (EO), propylene oxide (PO) and their respective polyether's, polyethylene glycol (PEG) and polypropylene glycol (PPG).....	13
Scheme 2.3. Epoxidation of ethylene to ethylene oxide with molecular oxygen using silver catalyst. ....	13
Scheme 2.4. Peroxide-based epoxidation of propylene to propylene oxide using titanium catalyst. ....	14
Scheme 2.5. The reaction scheme and mechanism of the epoxidation of alkene using peracid. ....	15
Scheme 2.6. Epoxidation of (1) $\alpha$ -pinene with (2) TBHP producing (3) $\alpha$ -pinene oxide,(4) verbenol, (5) verbenone and (6) tert-butanol. ....	17
Scheme 2.7. Epoxidation of (1) (R)-(+)-limonene with molecular oxygen producing (2) limonene-1,2-epoxide, (3) limonene-8,9-epoxide, (4) carveol and (5) carvone. ....	18
Scheme 2.8. Epoxidation of (1) (R)-(+)-limonene with Ti-MCM-41 producing (2) limonene-1,2-epoxide, (3) limonene bis-epoxide, (4) limonene-1,2-diol, (5) carveol and (6) carvone. ....	19
Scheme 2.9. Epoxidation of (1) $\alpha$ -pinene with Ti-MCM-41 catalyst producing (2) $\alpha$ -pinene oxide, (3) verbenol, (4) verbenone and (5) campholenic aldehyde. ....	20
Scheme 2.10. Epoxidation of 1-dodecene to 1,2-epoxydodecane using quaternary ammonium salt (Q <sup>+</sup> X <sup>-</sup> ) as phase transfer catalyst. ....	20

Scheme 2.11. The epoxidation of cyclooctene with H <sub>2</sub> O <sub>2</sub> in a halide- and solvent-free system. .....	21
Scheme 2.12. Products of (R)-(+)-limonene epoxidation with hydrogen peroxide (H <sub>2</sub> O <sub>2</sub> ) as oxidant in the presence of tungsten-based catalyst;(1) (R)-(+)-limonene, (2) cis-limonene-8,9-epoxide, (3) trans-limonene-8,9-epoxide, (4) cis-limonene-1,2-epoxide, (5) trans-limonene-1,2-epoxide, (6) RSS limonene bis-epoxide, (7) SRS limonene bis-epoxide, (8) RSR limonene bis-epoxide, (9) SRR limonene bis-epoxide, (10) trans-limonene-1,2-diol,(11) carveol and (12) carvone. ....	23
Scheme 2.13. Product of $\alpha$ -pinene epoxidation with hydrogen peroxide (H <sub>2</sub> O <sub>2</sub> ) as oxidant in the presence of tungsten-based catalyst;(1) $\alpha$ -pinene,(2) $\alpha$ -pinene oxide, (3) pinanediol, (4) campholenic aldehyde,(5) sobrerol, (6) verbenol and (7) verbenone.....	24
Scheme 2.14. Products of isomerisation of $\alpha$ -pinene oxide; (1) $\alpha$ -pinene oxide, (2) isopinocampone, (3) pinocarveol, (4) trans-carveol, (5) 2-methyl-5-(propan-2-ylidene) cyclohex-2-enol, (6) p-cymene, (7) campholenic aldehyde and (8) fencholenic aldehydes (Stekrova et al., 2014). ....	25
Scheme 2.15. Reaction mechanism of alkene epoxidation using Venturello anion as the catalyst (Mouret et al., 2014). ....	36
Scheme 2.16. Mechanism of active species formation (Yadav and Satoskar, 1997). ....	38
Scheme 3. 1. Decomposition of H <sub>2</sub> O <sub>2</sub> to H <sub>2</sub> O and O <sub>2</sub> .....	83

## List of Tables

Table 2.1. Classification of terpenes and examples (Breitmaier, 2006). .....	10
Table 2.2. Classifications of surfactants and examples of common surfactants. ....	30
Table 2.3. Common quaternary ammonium salts used in biphasic reactions. ....	31
Table 2.4. List of research on alkene epoxidation using POM as a catalyst. ....	41
Table 2.5. Examples of working fluids and their temperature range (Reay et al., 2006). ....	50
Table 3.1 List of chemicals used. ....	55
Table 3.2 Properties of the reactant, solvents, and products. ....	56
Table 3.3. Experimental conditions for the epoxidation of terpenes. ....	66
Table 3.4 Flow rate at each residence time for the continuous epoxidation in mesoOBR .....	69
Table 3.5. Various concentrations of $\alpha$ -pinene, $\alpha$ -pinene oxide, (R)-(+)-limonene and limonene-1,2-epoxide pure samples for FTIR spectroscopy calibration. ....	76
Table 3.6. Various concentrations of $\alpha$ -pinene, $\alpha$ -pinene oxide, (R)-(+)-limonene and limonene-1,2-epoxide pure samples for GC calibration. ....	79
Table 4.1 The pre-exponential factor and the activation energy for the formation of limonene-1,2-epoxide, limonene bis-epoxide and limonene-1,2-diol. ....	104
Table 5.1. The pre-exponential factor and the activation energy for the formation of $\alpha$ -pinene-oxide. ....	127
Table A.1. Solubility of Na <sub>2</sub> SO <sub>4</sub> in H <sub>2</sub> O at various temperature. ....	175
Table B.1. Commonly used pump commands. ....	176
Table B.2. Description of abbreviations in Table B.1. ....	176
Table B.3. q and r parameters and its corresponding frequency and amplitude when using two 12.5 mL syringe for oscillation. ....	177
Table C.1. Mixing condition (Re <sub>0</sub> ), strouhal number (St) and its corresponding centre-to-peak amplitude (X <sub>0</sub> ) and frequency (f). ....	178
Table E.1. GC response factor for limonene, $\alpha$ -pinene and all oxidative products. ....	181

Table H.1. Initial rates obtained from the mixing study of limonene epoxidation.....	189
Table H.2. Initial rates obtained from the PTC amount study for limonene epoxidation.....	189
Table H.3. Initial rates obtained from the kinetic study of limonene epoxidation (catalyst concentration). .....	189
Table H.4. Initial rates obtained from the kinetic study of limonene epoxidation (limonene concentration). .....	190
Table H.5. Initial rates obtained from the kinetic study of limonene epoxidation (H <sub>2</sub> O <sub>2</sub> concentration). .....	190
Table I.1. Initial rates obtained from the kinetic study of $\alpha$ -pinene epoxidation (catalyst concentration).....	191
Table I.2. Initial rates obtained from the kinetic study of $\alpha$ -pinene epoxidation ( $\alpha$ -pinene concentration).....	191
Table I.3. Initial rates obtained from the kinetic study of $\alpha$ -pinene epoxidation (H <sub>2</sub> O <sub>2</sub> concentration).....	191

## List of Abbreviations

3D	three-dimensional
AM	additive manufacturing
CFD	computational fluid dynamics
CHP	cumene hydroperoxides
COBR	continuous oscillatory baffled reactor
CPU	central processing unit
CSTR	continuous stirred tank reactor
DCM	dichloromethane
DMF	N,N-dimethylformamide
EBHP	ethylbenzene hydroperoxides
FDCA	furan dicarboxylic acid
FDM	fused deposit modelling
FID	flame ionisation detector
FTIR	fourier transform infrared
GC	gas chromatograph
HPA	heteropolyacid
HPLC	High-Performance Liquid Chromatography
HPOBR	heat-pipe oscillatory baffled reactor
IER	ion exchange resin
m-CPBA	<i>meta</i> -chloroperbenzoic acid
MesoOBR	mesoscale oscillatory baffled reactor
MTO	methyltrioxorhenium
OBR	oscillatory baffled reactor
PE	polyethylene
PEF	poly(ethylene furanoate)
PET	poly(ethylene terephthalate)
PI	process intensification
PIV	particle image velocimetry

PLA	polylactide
POM	polyoxometalates
PTC	phase transfer catalyst
Rpm	revolutions per minute
RTD	residence time distribution
SLA	stereolithography
SPC	smooth periodic constrictions
SPS	subsequent peroxy species
TBHP	tert-butyl hydroperoxide
TOF	turn over frequency
UHP	urea hydrogen peroxide



## List of Nomenclature

$\rho$	density ( $\text{kg m}^{-3}$ )
$\mu$	dynamic viscosity (Pas)
$\psi$	velocity ratio
$\nu$	kinematic viscosity ( $\text{m}^2 \text{s}^{-1}$ )
$u$	fluid superficial velocity ( $\text{m s}^{-1}$ )
$\tau$	residence time (s)
$A_i$	GC peak area of internal standard (mVs)
$A_s$	GC peak area of sample (mVs)
$C_i$	concentration of internal standard ( $\text{mg L}^{-1}$ )
$C_s$	concentration of sample ( $\text{mg L}^{-1}$ )
$d_0$	orifice diameter
$D$	diameter of baffled reactor (m)
$E_a$	Arrhenius activation energy ( $\text{kJ mol}^{-1}$ )
$f$	oscillation frequency (Hz)
$k$	reaction rate constant ( $\text{L mol}^{-1}\text{s}^{-1}$ )
$K_{\text{eq}}$	equilibrium constant
$L$	baffle spacing
$R$	universal gas constant ( $\text{J mol}^{-1}\text{K}^{-1}$ )
$R_f$	relative response factor for GC calibration
$Re_n$	net flow Reynolds number
$Re_0$	oscillatory Reynolds number
$S$	baffle open space area
$St$	Strouhal number
$t$	time (s)
$T$	temperature ( $^{\circ}\text{C}$ )
$u$	superficial velocity
wt.	weight
$x_0$	centre-to-peak amplitude (m)

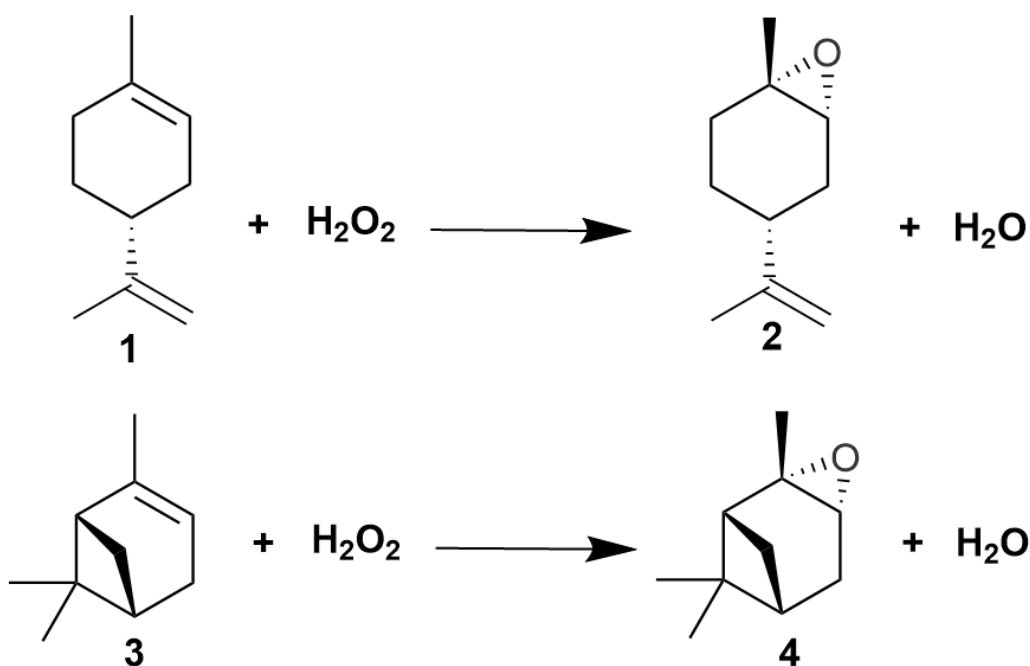
# Chapter 1 Introduction

## 1.1 Background

Epoxides (oxiranes) derived from petrochemicals, such as ethylene oxide and propylene oxide, are among the primary sources for many processes, especially in the polymer industries. Industries such as packaging, textiles and electronics have become dependent on these polymers derived from epoxides. In 2011, synthetic polymer production, which include non-epoxide driven polymers such as polyethylene (PE), polypropylene (PP) and polyethylene terephthalate (PET) accounted for about 280 Mt worldwide (Thompson *et al.*, 2009).

However, in recent years, concerns about the environment and sustainability have led researchers to develop processes that could utilise waste biomass as an alternative feedstock to the petrochemical-based epoxides (Zhu *et al.*, 2016). Utilisation of waste biomass such as terpenes for sustainable production of valuable chemicals would reduce waste and be closer to carbon dioxide (CO<sub>2</sub>) neutrality (Belgacem and Gandini, 2008). Biomass-derived terpenes, such as (R)-(+)-limonene and  $\alpha$ -pinene, have many applications, including use as flavours, fragrances and pharmaceutical precursors (Erman, 1985; Chapuis and Jacoby, 2001; Bauer *et al.*, 2008; Silvestre and Gandini, 2008). Epoxidation of these terpenes could be used to produce epoxides, such as limonene-1,2-epoxide and  $\alpha$ -pinene oxide, which are useful intermediates for many industrial processes. For instance, limonene-1,2-epoxide has been investigated as a potential monomer to produce limonene polycarbonate (Hauenstein *et al.*, 2016; Martín and Kleij, 2016; Reiter *et al.*, 2017; Pagliaro *et al.*, 2018), whereas isomerisation of  $\alpha$ -pinene oxide could be used to produce valuable chemicals, such as campholenic aldehyde, a precursor for the production of fragrances (Fráter *et al.*, 1998; Stekrova *et al.*, 2014).

Epoxidation of (R)-(+)-limonene and  $\alpha$ -pinene with a green oxidant such as hydrogen peroxide (H<sub>2</sub>O<sub>2</sub>), has received a great deal of research interest (Chiker *et al.*, 2003; Casuscelli *et al.*, 2004; Casuscelli *et al.*, 2005; Silva *et al.*, 2006; Zapata *et al.*, 2009a; Cánepa *et al.*, 2011; Kon *et al.*, 2011; Egusquiza *et al.*, 2012; Michel *et al.*, 2012; Zheng *et al.*, 2012; Bonon *et al.*, 2014). Hydrogen peroxide is preferred over other oxidants as it has water (H<sub>2</sub>O) as its only by-product as shown in Scheme 1.1, making it “environmentally friendly”.



Scheme 1.1. The epoxidation of terpenes with H<sub>2</sub>O<sub>2</sub>. (1) (R)-(+)-limonene, (2) trans-limonene-1,2-epoxide, (3) α-pinene and (4) trans-α-pinene oxide.

Nonetheless, the epoxidation of terpenes with H<sub>2</sub>O<sub>2</sub> is challenging, for three reasons:

- i) selectivity can be low, as multiple oxidative products can be formed.
- ii) mass transfer limitations can limit the rate, due to the biphasic nature of the reaction, as the hydrophobic terpenes are not miscible with the aqueous H<sub>2</sub>O<sub>2</sub>.
- iii) heat removal can be difficult, as the highly exothermic epoxidation reaction could readily undergo a runaway reaction without a proper temperature control or mitigation.

In a conventional process, the exothermicity is mitigated either by the addition of organic solvent or by drop-wise addition of the oxidant (Santacesaria *et al.*, 2011; Santacesaria *et al.*, 2012; Wu *et al.*, 2017). For instance, a fed-batch reactor is commonly used for this type of epoxidation, and oxidants are added at specific time intervals to achieve an overall isothermal condition. Furthermore, the use of organic solvent necessitates multiple distillation process for product purifications, see Figure 1.1. This method, however, necessarily reduces the reaction rate leading to long reaction times and reduced throughput for a given reactor volume. It is therefore timely to propose a more efficient, greener and "intensified" process with effective multiphase and high heat transfer capabilities to overcome those challenges.

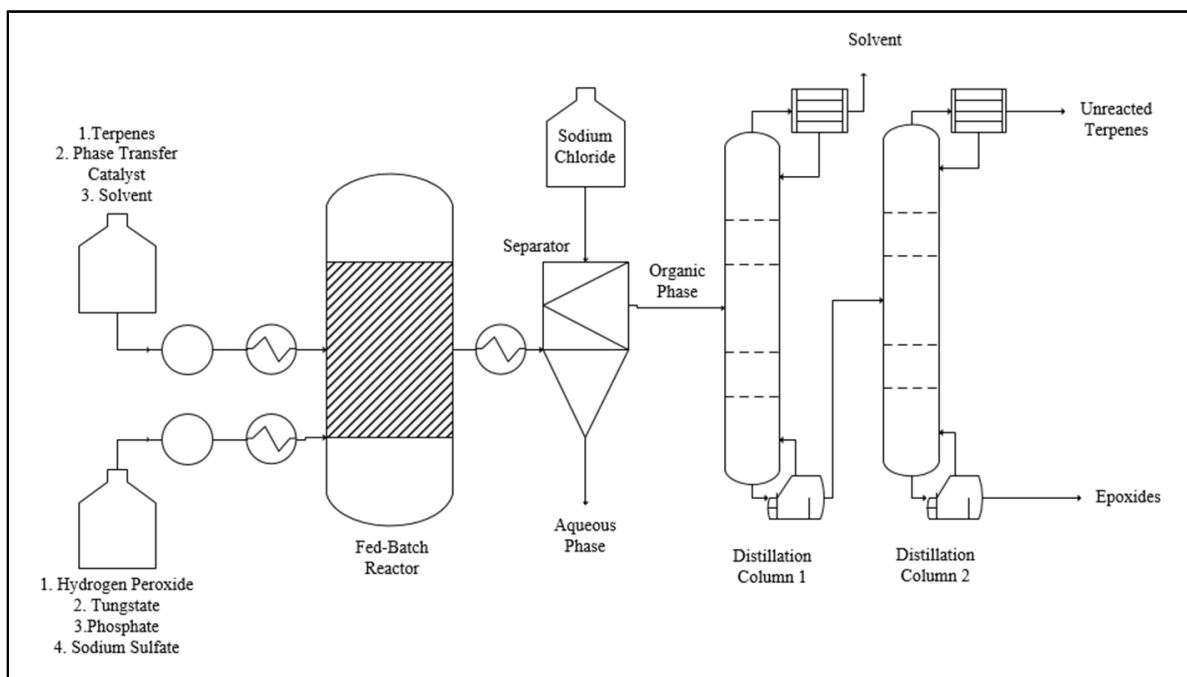


Figure 1.1. A typical epoxidation process using solvent and a fed-batch reactor.

Development of a continuous process for the epoxidation reaction process capable of addressing the mass and heat transfer bottlenecks is required for an intensified bio-based terpene epoxidation. It is envisaged that such a continuous process would require intensified reactors such as the oscillatory baffled reactor (OBR) to provide effective multi-phase fluid mixing and heat removal from the reaction mixture (Mackley *et al.*, 1993; Ni and Pereira, 2000; Stonestreet and Harvey, 2002b; Harvey *et al.*, 2003b; Reis *et al.*, 2004; Reis *et al.*, 2005).

Generally, the OBR is a tubular reactor fitted with baffles, which could provide a plug flow behaviour, at a net flow rate in the laminar region (Stonestreet and Van Der Veeke, 1999; Stonestreet and Harvey, 2002a; Harvey *et al.*, 2003b; Al-Abduly *et al.*, 2014; Ahmed *et al.*, 2017; Law *et al.*, 2018). The multiphase mixing and heat transfer in the OBR is independent of net flow and controlled by an oscillatory flow, allowing reactions that require long residence times (up to hours) to be operated in a continuous mode using OBRs of greatly reduced length to diameter ratio. The extent of mixing and radial transport in OBRs are controlled by dimensionless numbers including net flow Reynolds number ( $Re_n$ ) and the oscillatory Reynolds number ( $Re_o$ ) (Harvey *et al.*, 2003a). The effective radial fluid mixing and heat transfer in the OBR results from oscillatory mixing where vortices are formed from the interaction between the oscillating fluid and the baffles (Brunold *et al.*, 1989; Ni *et al.*, 2002). These interactions

lead to the formation and dissipation of the vortices which enhance the mass and heat transfer between the reactants.

The mesoOBR is a millimetre scale diameter ( $\sim 5$  mm) version of the “conventional” OBR (typically  $> 24$  mm diameter), fitted with various types of baffles for rapid process screening (Harvey *et al.*, 2001; Harvey *et al.*, 2003a; Phan and Harvey, 2010; Phan *et al.*, 2011a; Phan and Harvey, 2011; Phan *et al.*, 2011b; Phan and Harvey, 2012; Phan *et al.*, 2012; Eze *et al.*, 2013; Rasdi *et al.*, 2013; McDonough *et al.*, 2015; Eze *et al.*, 2017). The small volumes of the mesoOBRs allow them to operate at lower flow rates, which in turn uses fewer reagents and produces less waste. The mesoOBRs have been studied for the biphasic reaction of biodiesel productions (Phan *et al.*, 2012; Eze *et al.*, 2013; Eze *et al.*, 2017; Eze and Harvey, 2018). It has been found that a sufficient interfacial area is required to obtain proper mixing for the biphasic mixture (Phan *et al.*, 2012). For a biphasic reaction, the rate of reaction is mostly influenced by the contact area between the immiscible reactants. This requirement necessitates an appropriate design of a continuous reactor that facilitates intense mixing. However, baffle designs commonly used in mesoOBR, such as the integral and the helical, lack sharp edges necessary to induce droplets breakage in a biphasic mixture, see Figure 1.2.

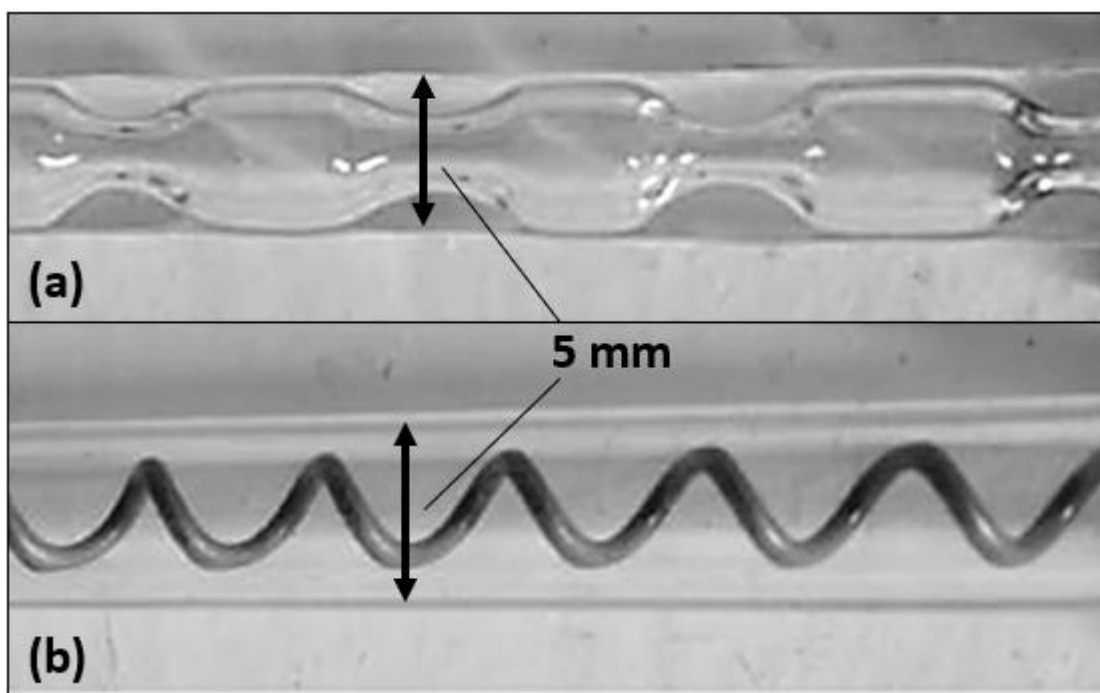


Figure 1.2. Commonly used baffled type in MesoOBR; (a) integral baffles and (b) helical baffles.

The design limitation can be remedied by designing baffles with sharp edges, such as orifice baffles, which generate high interfacial areas, by droplet break-up. Fabrication of orifice baffles at these scales using conventional methods is difficult and labour-intensive. Nowadays, however, Additive Manufacturing (AM) can provide a solution. Complex designs, such as multi-orifice baffles, can now be fabricated rapidly via 3D-printing (Kitson *et al.*, 2012; Symes *et al.*, 2012; Dragone *et al.*, 2013; Mathieson *et al.*, 2013; Kitson *et al.*, 2016; Okafor *et al.*, 2017). This new baffle design could be easily fitted to obtain a new design of mesoOBR in a ‘plug-and-play’ concept, such that capability of various designs mesoOBRs multiphase mixing and heat transfer could potentially be rapidly screened in a system of mesoOBRs platform. Design optimisation for reactors at this scale, to address a wide variety of duties, will be greatly accelerated by 3D-printing.

This work investigates process development for the epoxidation of (R)-(+)-limonene and  $\alpha$ -pinene with  $H_2O_2$  using polyoxometalates catalyst. Batch screening of a few parameters on the epoxidation of (R)-(+)-limonene and  $\alpha$ -pinene were performed with the focus on obtaining a highly selective process towards the epoxides. A kinetic study was also performed to develop a predictive model for the reaction. The optimised reaction was transferred to a continuous process using mesoOBR. Various designs of mesoOBR baffles were evaluated. New designs of mesoscale orifice baffles were fabricated through 3D-printing, and some mesoOBRs of various baffles designs were evaluated for multiphase and heat transfer effectiveness in the terpene’s epoxidation process. The mesoOBRs’ performances in terms of the induction period, quality of steady states, and heat transfer capability in terms of rapid isothermalisation of the epoxidation reaction in an organic solvent-free condition, were evaluated. The reaction product contains mainly terpenes and its epoxide without solvent, which reduces the number of distillation stages required as shown in Figure 1.3. The possibility of using mesoOBR in a heat pipe assembly as a means of low energy and passive isothermalisation was also investigated.

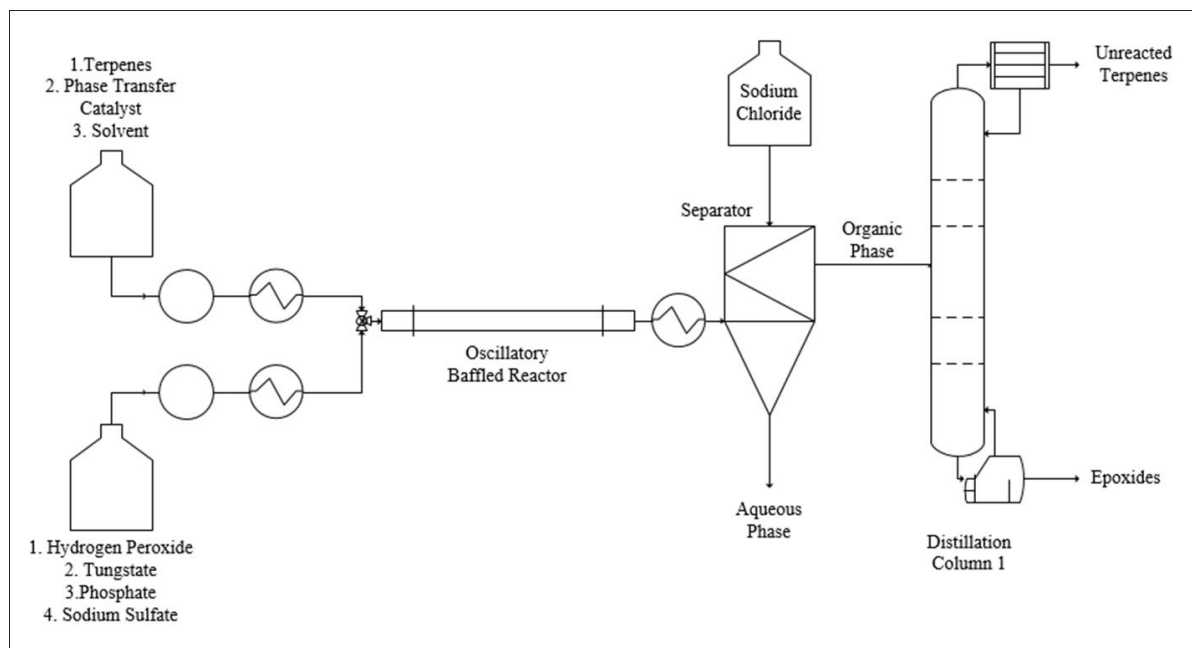
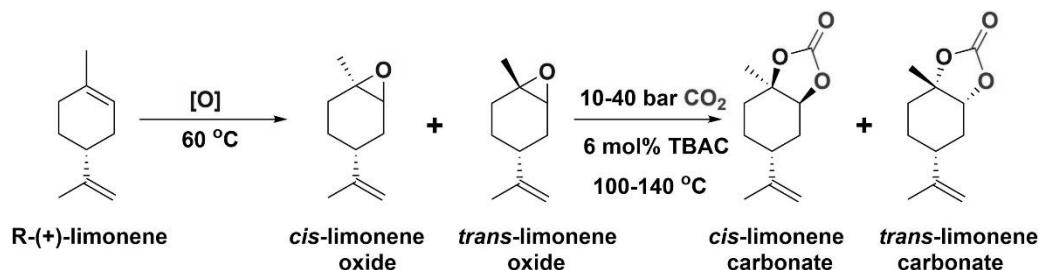


Figure 1.3. An envisaged epoxidation process using Oscillatory Baffled Reactor in an organic solvent-free environment.

## 1.2 Importance of this research project

This research is a part of an ongoing EPSRC research project (Sustainable Polymers, grant number: EP/L017393/1) that aims to replace petrochemical-based polymers with polymers made from sustainable and renewable resources. Waste biomass such as terpenes was identified as a potential resource as the starting material for these polymers. Epoxides derived from the waste biomass were identified as one of the feasible routes to produce bio-based polymers. Biomass derived polymers are a way of capturing and potentially storing CO<sub>2</sub>, for instance the formation of limonene cyclic carbonates from (R)-(+)-limonene and CO<sub>2</sub>, see Scheme 1.2. Such processes should, in principle, reduce waste, whilst generating wealth.



Scheme 1.2. Cycloaddition of CO<sub>2</sub> to limonene epoxides for the synthesis of limonene cyclic carbonates (Rehman et al., 2019).

MesoOBRs will be used to intensify the process by allowing conversion to continuous processing, and mixing the reactants well, thereby allowing them to react at their “inherent” rate. This will result in lower reaction times, thereby increasing the overall output for a given reactor volume. It will also eliminate or reduce the solvent requirements, mainly due to the enhanced heat transfer capabilities. Overall, the research is intended to underpin the development of a feasible commercial process to produce bio-based epoxides from waste biomass.

### **1.3 Research aims and objective**

The aim of this project was to develop a ‘green’ and intensified continuous solvent-free process for the biphasic epoxidation of terpenes ((R)-(+)-limonene and  $\alpha$ -pinene) with H<sub>2</sub>O<sub>2</sub> in a mesoOBR. To achieve the aim, a series of objectives were defined:

- i) To identify the conditions necessary for mixing-independence in the batch reactor.
- ii) To identify the process optima where high conversion of (R)-(+)-limonene or  $\alpha$ -pinene can be achieved with the highest selectivity to their epoxides. The effects of temperature, oxidant amount, addition of inorganic salt (Na<sub>2</sub>SO<sub>4</sub>), acid concentration and type of solvent were evaluated.
- iii) To perform a kinetic study for the epoxidation of (R)-(+)-limonene and  $\alpha$ -pinene and develop a predictive model for the reaction.
- iv) To design and fabricate new baffle designs using 3D-printing technology to enhance mass transfer in the mesoOBR.
- v) To identify the mixing-independent area in the mesoOBR for various baffle designs
- vi) To evaluate the steady state performance of the OBRs by investigating the induction period, for all baffle design.
- vii) To evaluate reaction parameters, such as residence time in a multi-steady state mode to reduce process development time.
- viii) To evaluate the temperature profile of the mesoOBR and to compare this with a novel Heat-Pipe Oscillatory baffled reactor (HPOBR).



## Chapter 2 Literature Review

### 2.1 Waste biomass as a feedstock for bio-based polymers

Fossil fuel-derived synthetic polymers are widely used in many industries including packaging, textile, toys, electronics, among others. In 2014, approximately 300 Mt of polymers produced globally were fossil fuel-derived (Shen *et al.*, 2010). Although the demand for fossil fuel-based polymers is increasing, stocks of the feedstock itself are diminishing (Anastas and Kirchhoff, 2002). Environmental concerns associated with petrochemical polymers have raised awareness of the raw materials used and the end-of-life options of these polymers (Zhu *et al.*, 2016). The risk of diminishing fossil fuels and environmental concerns drives the need for alternative measures that focus on the development of polymers derived from renewable resources. Recent advances in sustainable development have increased interest in bio-based polymers (Belgacem and Gandini (2008). The growth is also supported by policy and legislation such as the international agreement on reducing carbon dioxide (CO<sub>2</sub>) emissions at the 2015 United Nations Climate Change Conference (COP21) in Paris (Philp *et al.*, 2013).

Waste biomass has recently gained interest as a resource for sustainable bio-based polymers (Zhu *et al.*, 2016). The conversion of waste biomass to a valuable product has many benefits, including reducing waste and maintaining CO<sub>2</sub> neutrality. Waste biomass can be derived from various resources such as agricultural waste, forestry, waste CO<sub>2</sub>, paper and food waste, with waste biomass extraction and conversion producing platform chemicals that can be used as feedstocks for bio-based polymers, see Figure 2.1. Many of these bio-based polymers can be manufactured using existing facilities used for petrochemical derivatives, thus reducing capital required for investment (Zhu *et al.*, 2016). It should be noted that some of the bio-based polymers are not biodegradable while a number of petrochemical based polymers could biodegrade (Belgacem and Gandini, 2008).

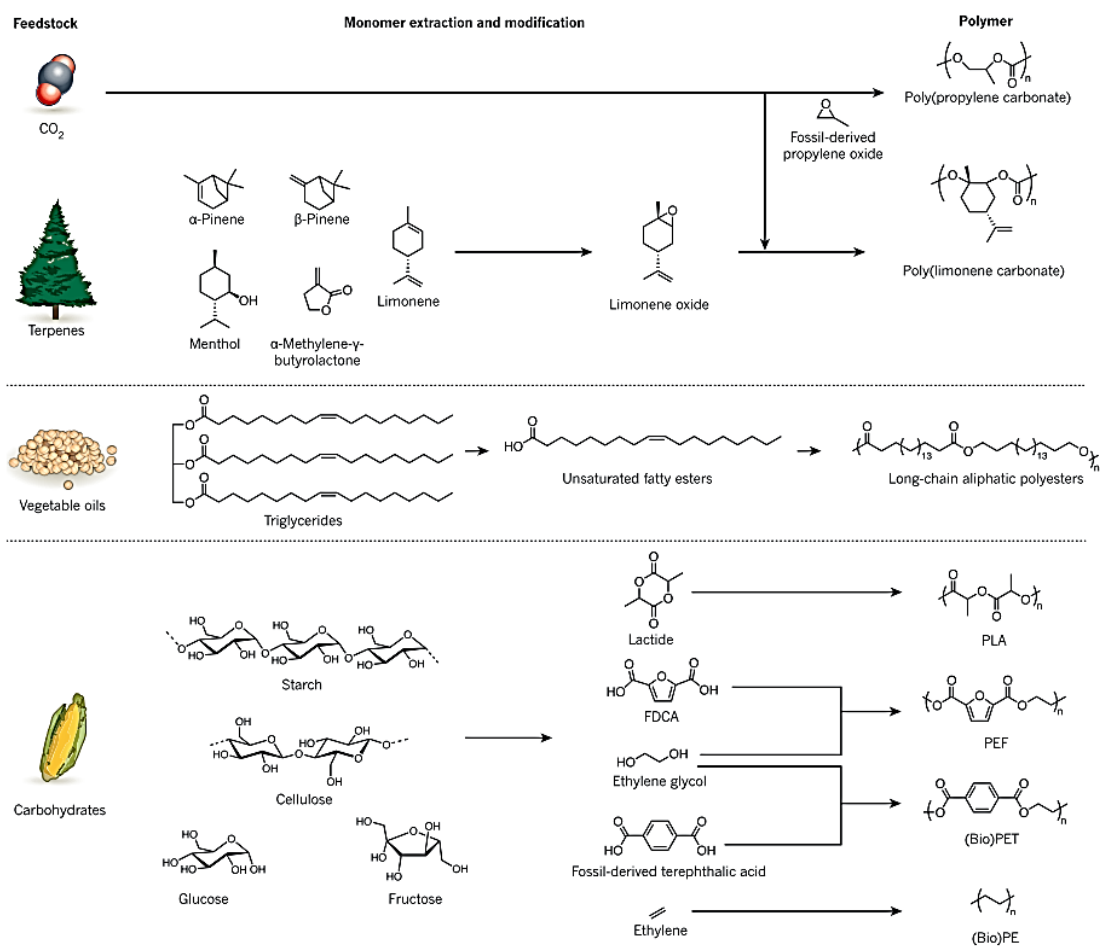


Figure 2.1. Bio-based alternatives to petrochemical for the manufacturing of polymers (Zhu *et al.*, 2016).

As can be seen in Figure 2.1, poly(limonene carbonate), which are synthesised from terpenes oxide and CO<sub>2</sub> can potentially be an alternative to petrochemical based poly(propylene carbonate). Vegetable oil derived triglycerides can be a source for the long-chain aliphatic polyester for use in industries such as PVC manufacturing (Yadav and Satoskar, 1997). More research has focused on the use of carbohydrates in its various forms such a starch, cellulose, glucose and fructose to synthesise molecules such as lactide, furandicarboxylic acid (FDCA), ethylene glycol and ethylene (Zhu *et al.*, 2016). These molecules can be converted to bio-based polymers such as polylactide (PLA), poly(ethylene furanoate) (PEF), bio-derived poly(ethylene terephthalate) (bio-PET) and bio-derived polyethylene (bio-PE) (Zhu *et al.*, 2016).

Some common platform chemicals include terpenes (e.g., (R)-(+)-limonene and  $\alpha$ -pinene), various diacids (e.g., itaconic, muconic and succinic acid) and levoglucosenone (Gallezot, 2007). In this work, terpenes were used as a feedstock as they are more abundant than other waste biomass-derived platform chemicals, with the exception of natural rubbers (Zhu *et al.*, 2016).

## 2.2 Terpenes

Terpenes are naturally occurring hydrocarbons found in plants, animals and some insects (Breitmaier, 2006). Modified terpenes containing functional groups are classified as terpenoids. These alkenes can be classified by the number of isoprene units in the molecule, with the general formula  $(C_5H_8)_n$ . Table 2.1 lists the classification of terpenes and examples for each class.

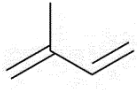
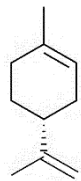
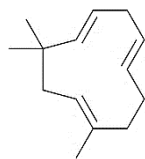
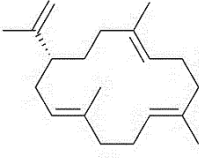
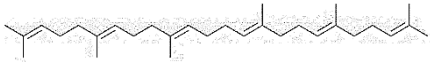
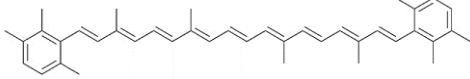
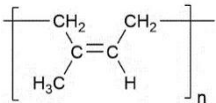
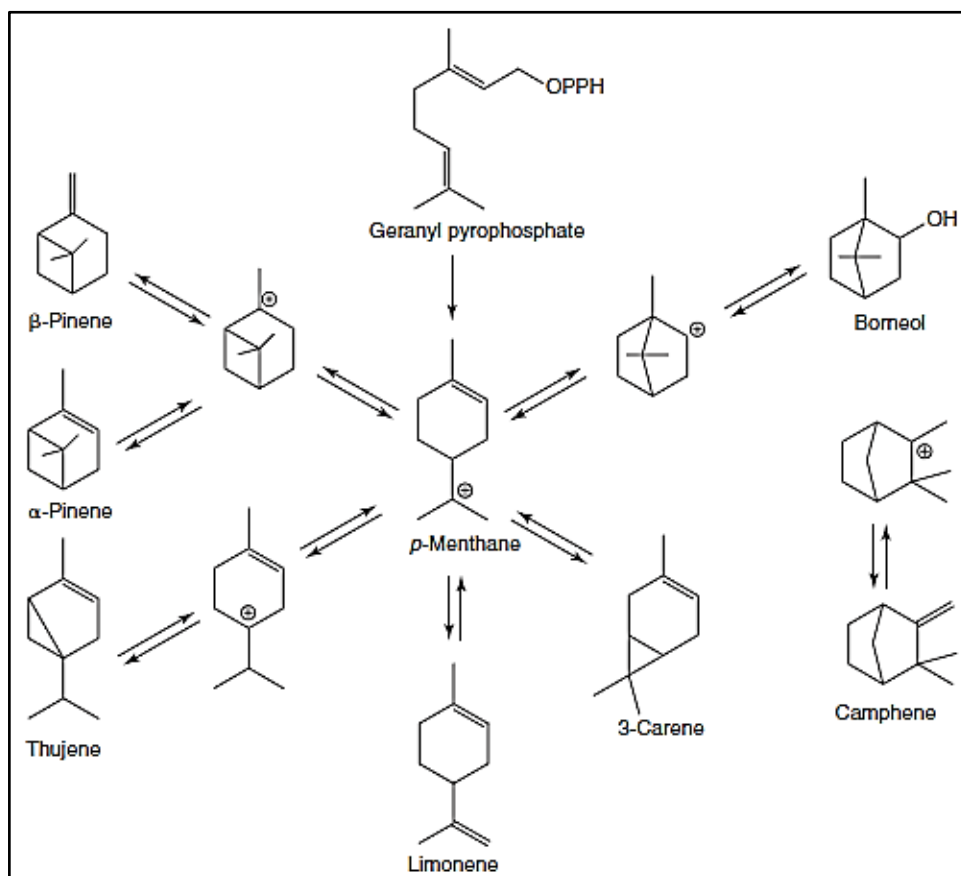
Classification	General formula	Examples	Molecular Structure
hemiterpenes	$C_5H_8$	isoprene	
monoterpenes	$C_{10}H_{16}$	(R)-(+)-limonene	
sesquiterpenes	$C_{15}H_{24}$	humulene	
diterpenes	$C_{20}H_{32}$	cembrene,	
triterpenes	$C_{30}H_{48}$	squalene	
tetraterpenes	$C_{40}H_{64}$	carotenoids	
polyterpenes	> 8 isoprene units	rubber	

Table 2.1. Classification of terpenes and examples (Breitmaier, 2006).

Low molecular weight terpenes, such as monoterpenes, are highly volatile and commonly used as fragrances, while the heavier terpenes, such as rubbers are used in latex industries. Natural rubbers (polyisoprene) are the most abundant bio-based terpenes (Breitmaier, 2006). Monoterpenes produced by plants are highly flexible compounds, exhibiting structural diversity via biosynthetic routes from a common structural skeleton (Erman, 1985). Scheme 2.1 shows the common skeleton and biosynthetic routes for monoterpenes.



Scheme 2.1. Biosynthetic route and common skeleton for monoterpenes in plants (Erman, 1985).

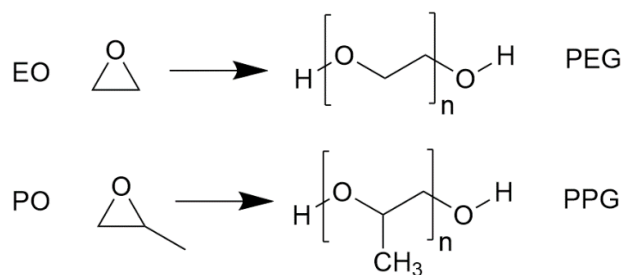
Monoterpenes, such as  $\alpha$ -pinene and (R)-(+)-limonene, are commonly used as ingredients in flavours and fragrances, as well as in the pharmaceutical industry (Albert and Webb, 1989; Breitmaier, 2006). The use of these terpenes as polymers (polyterpenes) has also been demonstrated (Ruckel and Arlt, 1989). These monoterpenes are mostly derived from turpentine oil, consisting mainly of  $\alpha$ -pinene (45-97 %),  $\beta$ -pinene (0.5-28 %) and other monoterpenes, including (R)-(+)-limonene (Derfer and Traynor, 1989). Two abundant terpenes,  $\alpha$ -pinene and (R)-(+)-limonene, have recently gained attention as they can be extracted from waste biomass, specifically from wood pulp processing ( $\alpha$ -pinene) and from citrus peel waste ((R)-(+)-limonene) (Becerra *et al.*, 2018).

It is estimated that 71.6 million tonnes of orange were produced in 2013 (Becerra *et al.*, 2018). In the orange juice industry, up to 60 % of the orange mass becomes peel waste (Garcia-Castello *et al.*, 2011). Furthermore, orange oil extracted from orange peel is up to 96 wt.% (R)-(+)-limonene (Xiong *et al.*, 2013), consequently there is a significant potential to convert this waste into many valuable products such as bio-based polymers (Wikandari *et al.*, 2015).

Waste biomass-derived terpenes, such as  $\alpha$ -pinene (C<sub>10</sub>H<sub>16</sub>), are important sources of flavours, fragrances and pharmaceuticals precursors (Erman, 1985; Fdil *et al.*, 1996; Mimoun, 1996; Calogirou *et al.*, 1999; Chapuis and Jacoby, 2001; Bauer *et al.*, 2008; Silvestre and Gandini, 2008). The central component of turpentine oil,  $\alpha$ -pinene, is a useful co-product of the wood and paper industries. Indeed, the epoxidation of  $\alpha$ -pinene generates many valuable products, such as verbenol, verbenone and  $\alpha$ -pinene oxide (Wender and Mucciari, 1992; Paquette, 1999),  $\alpha$ -pinene oxide being an important intermediate in many processes, with many applications (Fráter *et al.*, 1998). The isomerisation of  $\alpha$ -pinene oxide into products such as campholenic aldehyde is also useful for the production of sandalwood fragrances (Stekrova *et al.*, 2014). In this work, (R)-(+)-limonene and  $\alpha$ -pinene were selected as the raw materials for the development of a continuous epoxidation process based on their abundance and potential use of the resulting epoxides.

### 2.3 Epoxidation

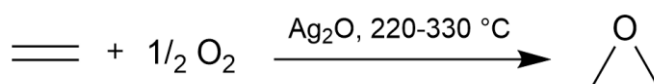
Epoxide or 'oxirane' is a cyclic ether consisting of a three-membered ring. The strained ring causes the epoxides to be highly reactive and versatile, hence suitable for use as intermediates in many reactions (Sienel *et al.*, 2003). Epoxides derived from petrochemicals, such as ethylene oxide and propylene oxide, are among the primary sources for many processes, especially in the polymer industries, see Scheme 2.2 (Zhu *et al.*, 2016). As of 2014, the estimated world production of ethylene oxide and propylene oxide was 25 and 8 million tonnes/year, respectively (Herzberger *et al.*, 2015). However, in recent years, environmental and sustainability concerns have led researchers to develop processes that could utilise waste biomass as a potential alternative for petrochemical-based epoxides (Zhu *et al.*, 2016).



*Scheme 2.2. Ethylene oxide (EO), propylene oxide (PO) and their respective polyether's, polyethylene glycol (PEG) and polypropylene glycol (PPG).*

Epoxidation of alkenes is an important industrial process and has various commercial applications. Epoxides have been used as starting materials for many chemical processes such as in the production of glycols, alcohols, carbonyl compounds and polymers such as polyesters, polyurethanes, and epoxy resins. Long-chain alkenes, such as soybean oil, have been commercially epoxidised to produce plasticisers and stabilisers for PVC manufacturing (Yadav and Satoskar, 1997).

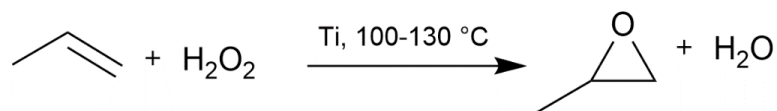
There are several processes for the production of epoxides including the Prilezhaev route, also known as the Prileschajew (using peracids as oxidants), Sharpless epoxidation (using organic hydroperoxides), Jacobsen-Katsuki epoxidation (using hypochlorites), Shi epoxidation (using dioxiranes) and the use of aqueous hydrogen peroxides ( $\text{H}_2\text{O}_2$ ) (Kurti and Czako, 2005). Commonly used starting materials include alkenes,  $\alpha$ -halocarbonyl compounds, carbonyl compounds, epichlorohydrin, and substituted hydroxyl compounds (Swern, 1971; Wilkinson, 1975; Duncan *et al.*, 1995). One of the conventional epoxidation processes involves the oxidation of ethylene to ethylene oxide. The process occurs in the gas phase employing a silver-based catalyst at temperatures between 220 and 330 °C, see Scheme 2.3.



*Scheme 2.3. Epoxidation of ethylene to ethylene oxide with molecular oxygen using silver catalyst.*

Propylene can be epoxidised to propylene oxide via several routes. Traditionally, a non-catalytic chlorohydrin-based process was used. Alternatively, a peroxide-based process is used

commercially at a temperature between 100 and 130 °C using either molybdenum (Mo) or titanium (Ti) based catalyst, see Scheme 2.4 (Kobe *et al.*, 2002; Sienel *et al.*, 2003).



*Scheme 2.4. Peroxide-based epoxidation of propylene to propylene oxide using titanium catalyst.*

However, these hydroperoxide processes have limitations in terms of the formation of side-products. This method was replaced by more favourable stoichiometric processes using peracids and catalytic processes using oxidants such as O<sub>2</sub>, organic peroxides and H<sub>2</sub>O<sub>2</sub> (Kamata *et al.*, 2003).

### **2.3.1 Routes for epoxidation process**

Epoxidation of alkenes can be achieved by three main routes, prilezhaev, hydroperoxides and catalytic routes. The prilezhaev route is typically performed using peracids as oxidants, hydroperoxides routes used organic peroxide such tert-butyl hydrogen peroxide (TBHP), while the catalytic route usually uses molecular oxygen or H<sub>2</sub>O<sub>2</sub> as oxidants. Active oxygen from these oxidants are transferred to the double bonds, forming an epoxide.

### **2.3.2 Prilezhaev epoxidation**

As mentioned, the prilezhaev epoxidation of alkene is commonly performed using peracids as oxidant. Peracids are strong electrophiles, epoxidising alkenes without the presence of any metal catalyst. Prileschajew (1909) first demonstrated the epoxidation of alkene using peracids, subsequently his methods become widely accepted as the most common technique to synthesise epoxides. Commonly used peracids are peroxyacetic acid, peroxybenzoic acid, peroxyformic acid, *m*-chloroperoxybenzoic and *p*-nitroperoxybenzoic, see Figure 2.2. These peracids have been used due to their relative availability, lower cost, stoichiometric yield of epoxides and stability at mild temperatures. The peracids also offer flexibility of reaction medium, as they can be used in aqueous, organic, homogeneous and heterogeneous media (Yadav and Satoskar, 1997).

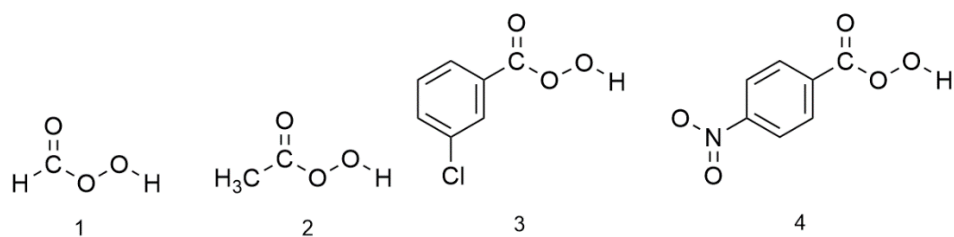
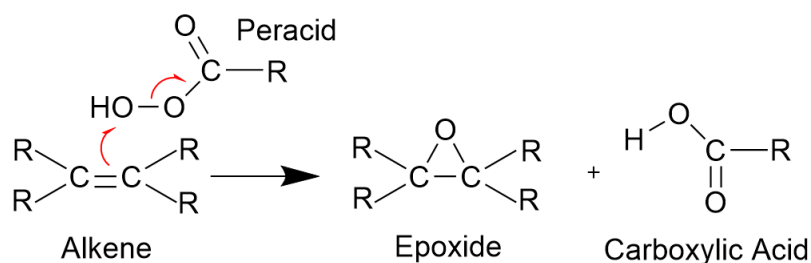


Figure 2.2. Commonly used peracids for epoxidation; (1) peroxyformic acid, (2) peroxyacetic acid, (3) *m*-chloroperoxybenzoic and (4) *p*-nitroperoxybenzoic.

Despite several advantages, peracids are hazardous, as it generates acid waste (Grigoropoulou *et al.*, 2003). The reaction scheme and mechanism of the epoxidation of alkene using peracid is shown in Scheme 2.5.



Scheme 2.5. The reaction scheme and mechanism of the epoxidation of alkene using peracid.

There are two methods to perform epoxidation using peracids: (i) preformed peracid epoxidation and (ii) *in situ* peracid epoxidation. In both methods, aqueous H<sub>2</sub>O<sub>2</sub> is reacted with carboxylic acid over an acidic catalyst (e.g. H<sub>2</sub>SO<sub>4</sub>) to form a peracid (Yao *et al.*, 2016). The methods differ only in the way the peracids were formed. Preformed peracids usually necessitate rigorous storage procedures to minimise the risk of explosions due to exothermic decomposition (Yadav and Satoskar, 1997). Consequently, the alternative *in situ* peracids method of epoxidation is favoured, the benefit of which is that it requires minimal amounts of reactants to generate the oxidative species in the reaction, making the process much safer (Yadav and Satoskar, 1997). It usually requires the addition of a mineral acid such as H<sub>2</sub>SO<sub>4</sub> as a catalyst to generate the oxidative species. Alternatively, a heterogeneous catalyst such as an ion exchange resin (IER) could be used to overcome separation and purification issues usually associated with homogeneous catalysts. Yadav and Satoskar (1997) demonstrated that the recyclability and selectivity of heterogeneous IERs for *in situ* peracids are better than for preformed peracids for the epoxidation of undecylinic acid. According to their findings, the



heterogeneous IER catalyst has an additional advantage over the preformed peracids, as fewer side reactions occurred during the epoxidation (Yadav and Satoskar, 1997).

Goud *et al.* (2007) compared the performance of two types of peracids formed *in situ*, peroxyacetic acid and peroxyformic acid, for the epoxidation of jatropha oil using IER (Amberlite IR-120) as catalyst at a temperature of up to 70 °C. They investigated the performance of the peracids with and without the presence of solvent (toluene), showing that peroxyformic acid is more efficient for *in situ* peracid epoxidation than the peroxyacetic acid at temperatures below 80 °C. However, at temperatures above 80 °C, they found that peroxyacetic acid was as effective as peroxyformic acid (Goud *et al.*, 2007).

One of the preferred industrial methods for epoxidation is the stoichiometric peracid route, which employs peracetic acids, such as m-chloroperoxybenzoic acid, as an oxidant (Swern, 1971). However, safety and environmental issues arise as these chemicals are toxic, producing a significant amount of acid waste (Grigoropoulou and Clark, 2006; Yao *et al.*, 2016). Peracids have also been shown to be unsuitable for acid-sensitive epoxides, such as terpene oxide, as they cause severe hydrolysis of the epoxides (Grigoropoulou *et al.*, 2003). These concerns have led to the search for a selective, safe, and “clean” alternative to the peracid epoxidation method.

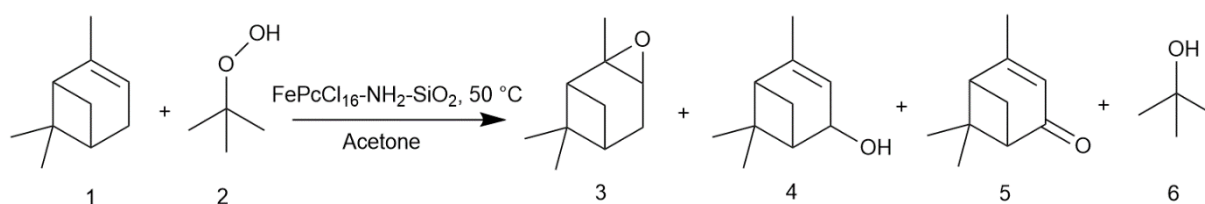
### 2.3.3 Hydroperoxide routes

The catalytic epoxidation of alkene using hydroperoxides, such as cumene hydroperoxides (CHP), ethylbenzene hydroperoxides (EBHP) and tert-butyl hydroperoxides (TBHP), has been shown to be a better alternative to peracids (Yadav and Pujari, 2000). The organic peroxides are easier to handle than peracids, thus less hazardous for industrial epoxidation. The organic peroxides have also been successfully used for the epoxidation of acid-labile epoxides, such as the epoxides of terpenes and styrene, which typically resulted in a poor yield if peracids were used (Swern, 1971; Yadav and Satoskar, 1997). Balula *et al.* (2012) studied the epoxidation of (R)-(+)-limonene with TBHP using dichlorodioxomolybdenum(VI)-pyridylimine as catalyst at 55 °C under solvent-free conditions. They reported a 99 % conversion of (R)-(+)-limonene at 100 % selectivity to limonene-1,2-epoxide, highlighting the advantage of using organic hydroperoxides for the epoxidation of alkenes such as (R)-(+)-limonene.

Studies have also focussed on developing a heterogeneous catalyst for the epoxidation using organic peroxides as oxidants. Charbonneau and Kaliaguine (2017) reported epoxidation of (R)-(+)-limonene with TBHP using a titanium-based heterogeneous catalyst (Ti-SBA-16) at a

temperature of 75 °C in acetonitrile. They reported a (R)-(+)-limonene conversion of 80 % at 79 % selectivity to limonene-1,2-epoxide, observing that at more than double the amount of TBHP to (R)-(+)-limonene, the TBHP decomposes to form radicals that reacted with (R)-(+)-limonene to produce many oxidative products. They also found that solvents with higher polarity, such as acetonitrile, facilitate higher activity for the epoxidation reaction with TBHP compared to solvents with lower polarity, such as ethyl acetate and cyclohexane.

The formation of radicals associated with the use of TBHP as oxidant in epoxidation can also be observed for the epoxidation of  $\alpha$ -pinene using similar oxidants. Becerra *et al.* (2016) demonstrated the epoxidation of  $\alpha$ -pinene with TBHP using an iron-based heterogeneous catalyst ( $\text{FePcCl}_{16}\text{-NH}_2\text{-SiO}_2$ ) at a temperature of 50 °C in acetone, see Scheme 2.6. They obtained  $\alpha$ -pinene conversion of 83 % after 23 hours to many oxidative products, mainly verbenone (23 %). Their study concluded that under both catalytic and non-catalytic conditions, TBHP decomposes to form radicals which promotes allylic oxidation of  $\alpha$ -pinene.



*Scheme 2.6. Epoxidation of (1)  $\alpha$ -pinene with (2) TBHP producing (3)  $\alpha$ -pinene oxide, (4) verbenol, (5) verbenone and (6) tert-butanol.*

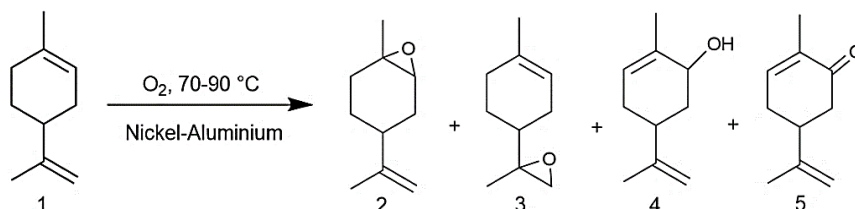
The use of organic peroxides, such as TBHP, also generates organic by-products that require additional separation processes. For instance, tert-butanol is produced from the epoxidation of both (R)-(+)-limonene and  $\alpha$ -pinene with TBHP that necessitates further separation of the alcohol from the epoxide products (Guidotti *et al.*, 2011). In this regard, a greener and more selective oxidant is required to develop a selective epoxidation process for (R)-(+)-limonene and  $\alpha$ -pinene.

#### **2.3.4 Catalytic route using molecular oxygen and $\text{H}_2\text{O}_2$**

Catalytic epoxidation has gained interest over the past few decades as it offers many advantages over peracids. Some researchers focussed on developing a green epoxidation process using molecular oxygen as the oxidant of choice since it is cheaper, easily available and does not

produce as many by-products as other oxidants. Examples of commercial epoxidation processes using molecular oxygen include the epoxidation of ethylene and propylene to form their respective epoxides. The epoxidation of ethylene represents the only example of an epoxidation process using a heterogeneous silver catalyst. However, this catalyst is not suitable for the epoxidation of propylene or any other alkene due to the oxidation at the allylic C-H bond.

Although molecular oxygen offers the advantage of being a green oxidant, there are some limitations that have not been addressed. Molecular oxygen has been found to be less reactive towards organic molecules at low temperature and has less selectivity towards the main products due to the formation of radicals (Pena *et al.*, 2012). Furthermore, the unstable radicals tend to oxidise the substrate into many side-products (Ishii *et al.*, 2001; Vanoye *et al.*, 2016). Pena *et al.* (2012) demonstrated the liquid-phase oxidation of (R)-(+)-limonene with molecular oxygen using nickel-aluminium hydrotalcites as catalysts under atmospheric pressure at temperatures between 70 and 90 °C in solvent-free conditions, see Scheme 2.7. They achieved a (R)-(+)-limonene conversion of up to 50 %, to many oxidative products including limonene-1,2-epoxide, limonene-8,9-epoxide, carveol and carveone. They confirmed that the selectivity to epoxides was lower when using molecular oxygen due to the thermal decomposition of limonene hydroperoxides that initiate autooxidation (Pena *et al.*, 2012).



Scheme 2.7. Epoxidation of (1) (R)-(+)-limonene with molecular oxygen producing (2) limonene-1,2-epoxide, (3) limonene-8,9-epoxide, (4) carveol and (5) carveone.

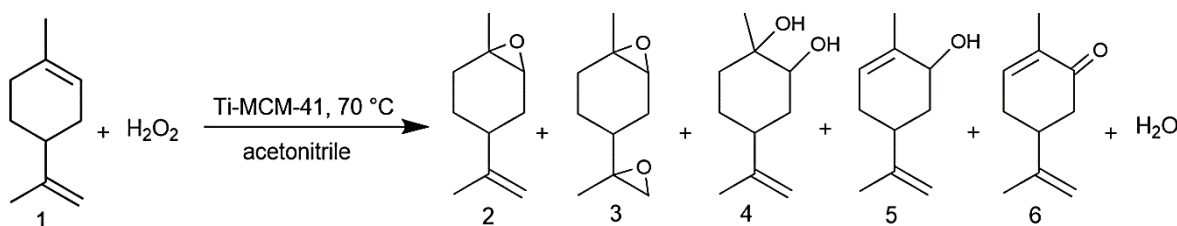
Similar observations were reported for the epoxidation of  $\alpha$ -pinene with molecular oxygen. Patil *et al.* (2007) investigated the epoxidation of  $\alpha$ -pinene with molecular oxygen using a cobalt (II)-based heterogeneous catalyst at temperature of 100 °C and pressure of up to 6 bar using dimethylformamide (DMF) as a solvent. They reported a 47 % conversion of  $\alpha$ -pinene, with 61 % selectivity to  $\alpha$ -pinene oxide, concluding that the oxidation occurs through a free radical mechanism, which also caused a reduced selectivity to the epoxides (Patil *et al.*, 2007).

Epoxidation of alkene with a sustainable oxidant, such as aqueous hydrogen peroxide (H<sub>2</sub>O<sub>2</sub>), has received a great deal of research interest (Chiker *et al.*, 2003; Casuscelli *et al.*, 2004;

Casuscelli *et al.*, 2005; Silva *et al.*, 2006; Zapata *et al.*, 2009a; Cánepa *et al.*, 2011; Kon *et al.*, 2011; Egusquiza *et al.*, 2012; Michel *et al.*, 2012; Zheng *et al.*, 2012; Bonon *et al.*, 2014). Hydrogen peroxide is preferred over other oxidants as it has H<sub>2</sub>O as the only by-product, making it environmentally friendly (Schirmann and Delavarenne, 1979; Strukul, 1992; Jones, 1999). Studies on the epoxidation using H<sub>2</sub>O<sub>2</sub> as oxidant involve many types of catalysts using metals such as molybdenum (Mo), rhenium (Re), titanium (Ti) and tungsten (W).

Michel *et al.* (2012) reported the epoxidation of (R)-(+)-limonene with H<sub>2</sub>O<sub>2</sub> using methyltrioxorhenium (MTO) as catalyst at a temperature of 25 °C in dichloromethane (DCM), showing 96 % selectivity to epoxide with a yield of 77 % after 1 hour. According to their findings, the catalyst requires a pyridine-based compound to lower the acid centre of the catalyst to prevent the formation of diol. The catalyst is more selective towards limonene-1,2-epoxide at a lower temperature, with more limonene bis-epoxides formed at a higher temperature (> 25 °C).

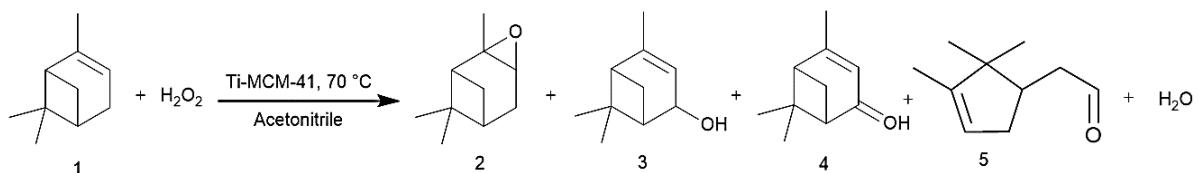
Cagnoli *et al.* (2005) demonstrated epoxidation of (R)-(+)-limonene with H<sub>2</sub>O<sub>2</sub> using a titanium-based heterogeneous catalyst (Ti-MCM-41) at temperature of 70 °C in acetonitrile, reporting up to 60 % conversion of (R)-(+)-limonene to many oxidative products including limonene-1,2-epoxide, limonene bis-epoxide, limonene-1,2-diol, carveol and carvone, see Scheme 2.8. They observed only 60 % selectivity to the epoxide using the catalyst and argued that the heterogeneous catalyst had better activity than other titanium-based catalysts with minimal leaching.



Scheme 2.8. Epoxidation of (1) (R)-(+)-limonene with Ti-MCM-41 producing (2) limonene-1,2-epoxide, (3) limonene bis-epoxide, (4) limonene-1,2-diol, (5) carveol and (6) carvone.

There is a lack of literature regarding the selective epoxidation of  $\alpha$ -pinene to  $\alpha$ -pinene oxide with H<sub>2</sub>O<sub>2</sub> using metal catalyst. Cánepa *et al.* (2011) studied the epoxidation of  $\alpha$ -pinene with H<sub>2</sub>O<sub>2</sub> using a titanium-based catalyst (Ti-MCM-41) at temperature of 70 °C in acetonitrile, showing that the reaction was less selective to  $\alpha$ -pinene oxide and more selective to verbenone (41 %), verbenol (16 %) and campholenic aldehyde (27 %), see Scheme 2.9. In a more recent

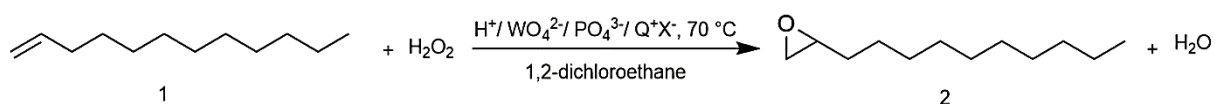
report, Cánepa *et al.* (2015) investigated the epoxidation of  $\alpha$ -pinene with  $\text{H}_2\text{O}_2$  using heterogeneous vanadium-based catalyst at a temperature of  $70\text{ }^\circ\text{C}$  in acetonitrile. They observed a 91 % conversion of  $\text{H}_2\text{O}_2$  ( $\alpha$ -pinene in higher molar ratio, 4:1) after 7 hours to many oxidative products, mainly verbenone (46 %), achieving only less than 3 % selectivity to  $\alpha$ -pinene oxide.



Scheme 2.9. Epoxidation of (1)  $\alpha$ -pinene with Ti-MCM-41 catalyst producing (2)  $\alpha$ -pinene oxide, (3) verbenol, (4) verbenone and (5) campholenic aldehyde.

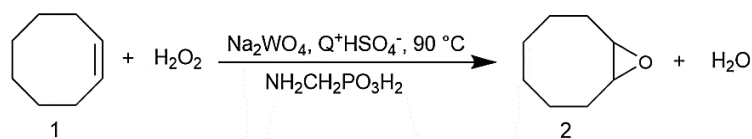
Among the many types of catalyst employed in the epoxidation reaction, tungsten-based polyoxometalates catalysts have been found to be very effective when used with  $\text{H}_2\text{O}_2$  as the oxidant (Venturello *et al.*, 1983). Jimtaisong and Luck (2006) demonstrated and compared the performance of a molybdenum-based catalyst and a tungsten-based catalyst for the epoxidation of cyclooctene using both TBHP and  $\text{H}_2\text{O}_2$ . They concluded that tungsten-based catalyst showed superior activity to the molybdenum-based catalyst if  $\text{H}_2\text{O}_2$  was used as an oxidant. However, the tungsten-based catalyst had lower activity when TBHP was used.

Ishii *et al.* (1988) and Venturello and D'Aloisio (1988) demonstrated the efficient epoxidation of an alkene with  $\text{H}_2\text{O}_2$  by using tungsten-based polyoxometalates under biphasic conditions in the presence of a quaternary ammonium salts as phase transfer catalyst. Venturello and D'Aloisio (1988) reported a 1-dodecene conversion of up to 98 % at 96 % selectivity to the epoxides at  $70\text{ }^\circ\text{C}$  in 1,2-dichloroethane (see Scheme 2.10), whereas Ishii *et al.*, (1988) reported 96 % conversion of cyclooctene at 98 % selectivity to epoxides in chloroform. However, both methods are limited due to the requirement of chlorinated solvents, so an alternative approach was developed.



Scheme 2.10. Epoxidation of 1-dodecene to 1,2-epoxydodecane using quaternary ammonium salt ( $\text{Q}^+\text{X}^-$ ) as phase transfer catalyst.

The improved method for the epoxidation of alkene using tungsten-based polyoxometalates in an organic solvent-free system used aminomethylphosphonic acid ( $\text{NH}_2\text{CH}_2\text{PO}_3\text{H}_2$ ) and a halide-free, quaternary ammonium hydrogensulfate ( $\text{Q}^+\text{HSO}_4^-$ ) as phase transfer catalyst, see Scheme 2.11 (Noyori *et al.*, 2003). This method had a large impact on further research on epoxidation reactions using tungsten-based catalysts and  $\text{H}_2\text{O}_2$  as oxidant, as the process was able to be conducted in an environmentally friendly way. However, their method was prone to hydrolytic decomposition of acid-labile epoxides in acidic conditions, and the acid used was expensive.



*Scheme 2.11. The epoxidation of cyclooctene with  $\text{H}_2\text{O}_2$  in a halide- and solvent-free system.*

Grigoropoulou and Clark (2003) reported the epoxidation of (R)-(+)-limonene under an improved ‘Noyori’ method without using expensive aminomethylphosphonic acid. They studied the epoxidation of (R)-(+)-limonene with  $\text{H}_2\text{O}_2$  using a sodium tungstate ( $\text{Na}_2\text{WO}_4$ ) catalyst at a temperature of  $70\text{ }^\circ\text{C}$  in an organic solvent-free conditions, showing 94 % conversion of (R)-(+)-limonene at 81 % selectivity to limonene-1,2-epoxide. They used an inorganic salt ( $\text{Na}_2\text{SO}_4$ ) to increase the selectivity to epoxide and to prevent the ring-opening reaction in acidic conditions. Their findings had substantial impact on further development of selective epoxidation of terpenes using  $\text{H}_2\text{O}_2$  as an oxidant. Hachiya *et al.* (2012) and Takumi *et al.* (2014) reported a similar addition of inorganic salt for the solvent-free epoxidation of (R)-(+)-limonene with  $\text{H}_2\text{O}_2$  using a tungsten-based catalyst and were able to produce a stable epoxide in acidic environments. The effect of  $\text{Na}_2\text{SO}_4$  on the stability of epoxides requires further understanding and as such, will be discussed in the relevant section (section 2.4).

Maheswari *et al.* (2005) performed another improve on the ‘Noyori’ method. They demonstrated the epoxidation of cyclooctene with  $\text{H}_2\text{O}_2$  using a tungsten-based ( $\text{Na}_2\text{WO}_4/\text{H}_2\text{WO}_4$ ) catalyst at  $60\text{ }^\circ\text{C}$  under solvent-free conditions in a biphasic system. They proposed a new approach for the catalytic system where chloroacetic acids were added to imitate the effect of peracids, reporting a 90 % conversion of cyclooctene at 99 % selectivity to cyclooctene oxide. They highlighted the importance of residual acidity of the aqueous medium to increase the catalytic activity of the tungsten-based catalyst. Their results show the positive effect of acid ( $\text{H}^+$ ) on the epoxidation rate. However, this approach may not be suitable for an

acid-labile epoxide, such as terpenes oxide, as with increasing acidity, the epoxides are susceptible to hydrolytic decomposition (Maheswari *et al.*, 2005).

Kaur *et al.* (2010) reported the possibility of handling H<sub>2</sub>O<sub>2</sub> in a much safer way, employing solid urea hydrogen peroxide (UHP) as an oxidant for the epoxidation of terpenes. The reaction was catalysed by a tungsten-based catalyst, and they reported a comparable yield to a similarly conditioned aqueous H<sub>2</sub>O<sub>2</sub> based epoxidations.

Although the methods of producing limonene-1,2-epoxide at high selectivity and without significant hydrolytic decomposition were reported by the above-cited authors over recent years, the process has not been optimised, and the reaction kinetics are unclear. Furthermore, little attention was paid to the conditions that would actively promote the ring opening of the epoxides. In this work, aqueous H<sub>2</sub>O<sub>2</sub> was chosen as oxidant for the epoxidation of (R)-(+)-limonene and  $\alpha$ -pinene due to higher selectivity to the epoxides and its 'green' properties. A tungsten-based polyoxometalates catalyst was employed since it shows better activity with H<sub>2</sub>O<sub>2</sub> compared to other catalysts. Further discussion of the chemistry, structure, and mechanism of the polyoxometalates catalyst is provided in Section 2.5.3

#### ***Epoxidation of (R)-(+)-limonene and $\alpha$ -pinene: reaction scheme***

Epoxidation is one of the most versatile routes for polymerisation of terpenes derived from waste biomass. An epoxide can be derived from more than one source, also being further polymerised to more than one type of polymer. Figure 2.3 shows various routes to polymerisation highlighting the versatility of epoxides as intermediates.

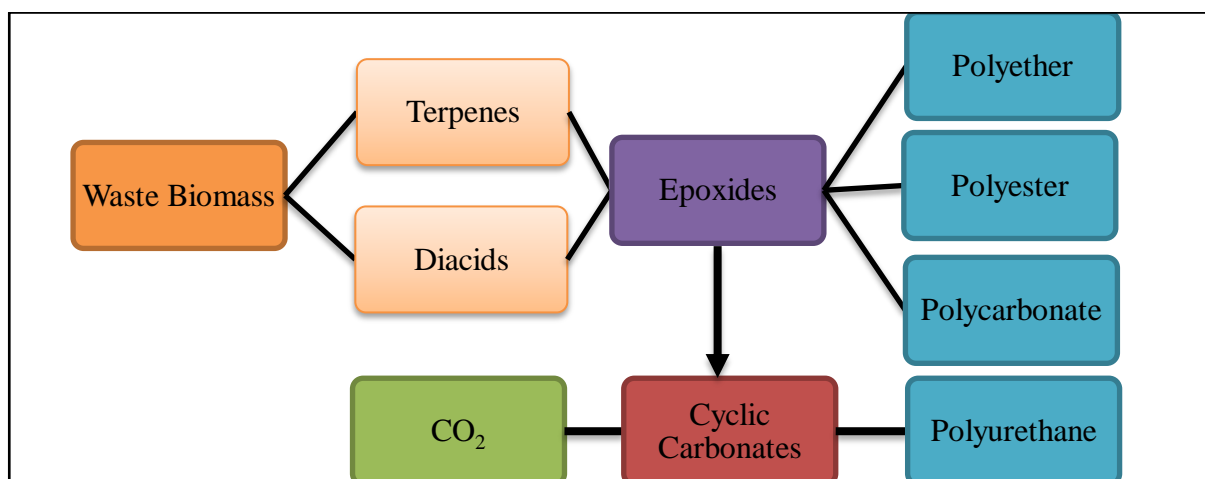
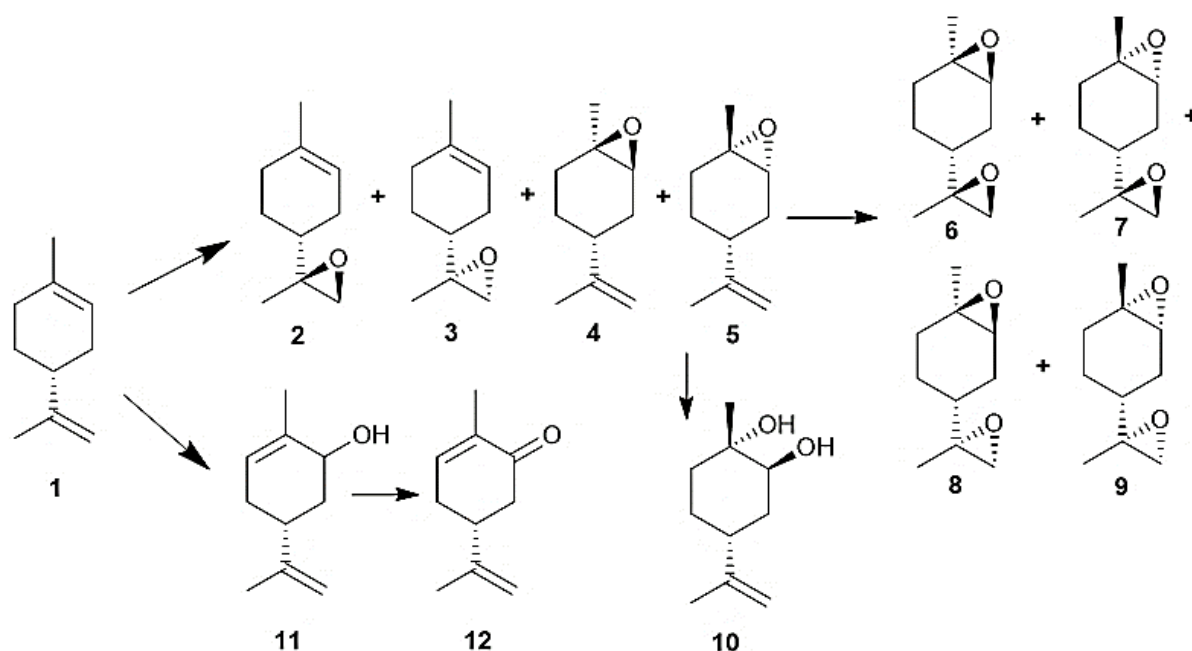


Figure 2.3. From biomass to polymer, the versatility of epoxides.

Traditionally, terpenes, such as (R)-(+)-limonene and  $\alpha$ -pinene, have many applications, including use as flavours, fragrances and as pharmaceutical precursors (Erman, 1985; Chapuis and Jacoby, 2001; Bauer *et al.*, 2008; Silvestre and Gandini, 2008). Epoxidation of these terpenes ((R)-(+)-limonene and  $\alpha$ -pinene) could be used to produce epoxides such as limonene-1,2-epoxide and  $\alpha$ -pinene oxide, which are useful intermediates for many industrial processes. For instance, limonene-1,2-epoxide has been investigated as a potential monomer to produce limonene polycarbonate by incorporating carbon dioxide (CO<sub>2</sub>) (Hauenstein *et al.*, 2016; Martín and Kleij, 2016; Reiter *et al.*, 2017; Pagliaro *et al.*, 2018), whereas isomerisation of  $\alpha$ -pinene oxide could be used to produce valuable chemicals such as campholenic aldehyde, a precursor for the production of sandalwood fragrances (Fráter *et al.*, 1998; Stekrova *et al.*, 2014).

The catalytic epoxidation of (R)-(+)-limonene with H<sub>2</sub>O<sub>2</sub> could generate many oxidative products. Scheme 2.12 shows products of (R)-(+)-limonene epoxidation, including their respective stereoisomers.

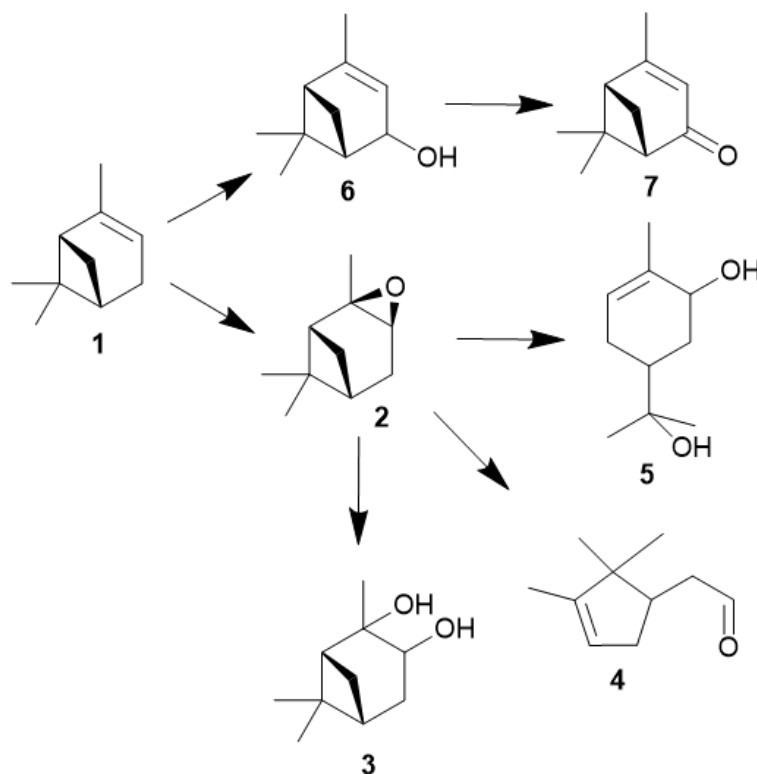


Scheme 2.12. Products of (R)-(+)-limonene epoxidation with hydrogen peroxide (H<sub>2</sub>O<sub>2</sub>) as oxidant in the presence of tungsten-based catalyst; (1) (R)-(+)-limonene, (2) cis-limonene-8,9-epoxide, (3) trans-limonene-8,9-epoxide, (4) cis-limonene-1,2-epoxide, (5) trans-limonene-1,2-epoxide, (6) RSS limonene bis-epoxide, (7) SRS limonene bis-epoxide, (8) RSR limonene bis-epoxide, (9) SRR limonene bis-epoxide, (10) trans-limonene-1,2-diol, (11) carveol and (12) carvone.



Epoxidation of (R)-(+)-limonene (**1**) with H<sub>2</sub>O<sub>2</sub> using a tungsten-based polyoxometalates would produce both limonene-8,9-epoxide (**2** and **3**) and limonene-1,2-epoxide (**4** and **5**) (a mixture of *cis*- and *trans* isomers). Due to the electrophilic nature of the oxidative species, epoxidation would more likely occur at more substituted double bonds, causing limonene-1,2-epoxide to be the primary product (Charbonneau and Kaliaguine, 2017). Limonene-bis-epoxide (**6,7,8** and **9**; a mixture of four stereoisomers) would be produced by the epoxidation of external double bonds of limonene-1,2-epoxide. Moreover, limonene-1,2-epoxide could undergo hydrolytic decomposition to form limonene-1,2-diol (**10**) in the presence of acid (H<sup>+</sup>) and H<sub>2</sub>O. (R)-(+)-limonene could also, in principle, undergo allylic oxidation to form (i) carveol (**11**), which could be further converted to carvone (**12**) by oxidative dehydrogenation (Wroblewska, 2014).

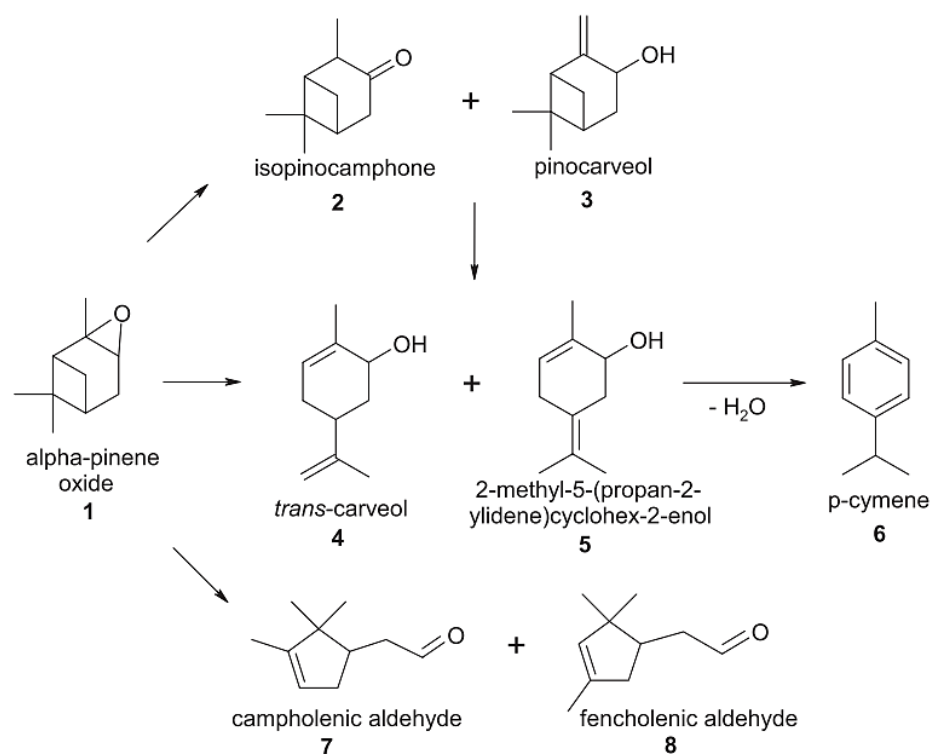
In the presence of a metal catalyst, the epoxidation of  $\alpha$ -pinene with H<sub>2</sub>O<sub>2</sub> can generate many oxidative products. Scheme 2.13 presents a simplified version of the reaction scheme.



Scheme 2.13. Product of  $\alpha$ -pinene epoxidation with hydrogen peroxide (H<sub>2</sub>O<sub>2</sub>) as oxidant in the presence of tungsten-based catalyst; (1)  $\alpha$ -pinene, (2)  $\alpha$ -pinene oxide, (3) pinanediol, (4) campholenic aldehyde, (5) sobrerol, (6) verbenol and (7) verbenone.

The epoxidation of  $\alpha$ -pinene (**1**) with H<sub>2</sub>O<sub>2</sub> using tungsten-based catalyst produced  $\alpha$ -pinene oxide (mixture of *cis*- and *trans* isomers) (**2**) as the main product due to the electrophilic nature

of the peroxy species, which are attracted to more substituted  $\pi$  bonds (Noyori *et al.*, 2003). In the presence of  $H^+$  and  $H_2O$ ,  $\alpha$ -pinene oxide can undergo hydrolytic decomposition to form pinanediol (**3**) and sobrerol (**5**). Moreover,  $\alpha$ -pinene oxide can rearrange to form campholenic aldehyde (**4**) and undergo allylic oxidation to form verbenol (**6**), which can be further converted to verbenone (**7**) by oxidative dehydrogenation. The predominance of either epoxidation or allylic oxidation is due to the nature of the catalyst and the formation of radicals during the reaction (Becerra *et al.*, 2016). In addition, an active catalyst could abstract H atoms from more than one position, and various hydroperoxides could be formed as intermediates, such as verbenyl hydroperoxides (Neuenschwander *et al.*, 2010; Neuenschwander *et al.*, 2011). Research had shown that  $\alpha$ -pinene could isomerise during oxidation process to form many products, including  $\beta$ -pinene, (R)-(+)-limonene, terpineol, camphene and 3-carene (Sienel *et al.*, 2003; Swift, 2004; Corma *et al.*, 2007). Moreover, many products, such as pinocarveol, isopinocampone and trans-carveol, have been formed from the rearrangement process of  $\alpha$ -pinene oxide (Carr *et al.*, 1994; Stekrova *et al.*, 2014), with polymeric compounds also be formed during the oxidation process, see Scheme 2.14.



Scheme 2.14. Products of isomerisation of  $\alpha$ -pinene oxide; (1)  $\alpha$ -pinene oxide, (2) isopinocampone, (3) pinocarveol, (4) trans-carveol, (5) 2-methyl-5-(propan-2-ylidene)cyclohex-2-enol, (6) p-cymene, (7) campholenic aldehyde and (8) fencholenic aldehydes (Stekrova *et al.*, 2014).

## 2.4 The effect of sodium sulphate (Na<sub>2</sub>SO<sub>4</sub>) in the epoxidation reaction

Sodium sulphate (Na<sub>2</sub>SO<sub>4</sub>) is an inorganic salt commonly used as a drying agent. The salt exhibits a neutral pH (7) in aqueous solutions as it ionises into Na<sup>+</sup> and SO<sub>4</sub><sup>2-</sup> ions. In aqueous solution, the salt can form a decahydrate, mopping up to 10 molecules of H<sub>2</sub>O per molecule of the salt (Hyde *et al.*, 2017). In the biphasic epoxidation reaction using aqueous H<sub>2</sub>O<sub>2</sub>, the use of acidic catalyst and the presence of H<sub>2</sub>O was found to be detrimental to the stability of the epoxides (Campanella and Baltanás, 2006). The addition of sodium sulphate to prevent the hydrolysis of the epoxides was reported by Grigoropoulou *et al.* (2006) for the epoxidation of alkenes with H<sub>2</sub>O<sub>2</sub> using a tungsten-based catalyst. They found that the addition of Na<sub>2</sub>SO<sub>4</sub> increases the ionic strength of the aqueous phase, thus improving the selectivity towards acid-labile epoxides (Grigoropoulou and Clark, 2006). In a more recent report, Hachiya *et al.* (2012) studied the addition of various inorganic salts including Na<sub>2</sub>SO<sub>4</sub> for the epoxidation of terpenes, such as  $\alpha$ -pinene, with H<sub>2</sub>O<sub>2</sub>. They found that only Na<sub>2</sub>SO<sub>4</sub> was able to successfully suppress the hydrolysis and ring-opening of the epoxide, hypothesising that the unique combination of sulphate anion and sodium cation plays a crucial role in preventing the hydrolysis. They also found that saturation with the salt was required to achieve the highest selectivity to the epoxides. Their report highlights the peculiarities of using Na<sub>2</sub>SO<sub>4</sub> since other salts, commonly used as a drying agent such as MgSO<sub>4</sub>, failed to achieve a similar effect as Na<sub>2</sub>SO<sub>4</sub> in terms of suppressing the hydrolysis of epoxides.

To better understand this effect, the role of Na<sub>2</sub>SO<sub>4</sub> could be regarded as a salting-out agent rather than a drying agent. Salting-out extractions facilitate the recovery of organic compounds in an aqueous medium (Kojima and Davis, 1984; Korenman *et al.*, 2010) and are commonly used in biochemistry, for instance, the isolation of proteins using ammonium sulphate (Englard and Seifter, 1990), protein crystallisation (Mcperson, 2001) and purification of bio-molecules (DNA, RNA) (Mazzola *et al.*, 2008).

The salting-out process affects the solubility of non-electrolytes in water, where the solubility decreases with increasing salt concentration (Randall and Failey, 1927). Long and McDevit (1952) proposed that the salting-out process was caused by an electronic repulsion of high density-charged dissolved anions which enhances the hydrophobic effect of the solution. The hydrophobic effect, in turn, causes solutes to aggregate and be repulsed. A report by Hyde *et al.* (2017) on the general principle of the salting-out phenomenon suggests that the SO<sub>4</sub><sup>2-</sup> ions show remarkable repulsion on non-electrolytes compared to other anions (Hyde *et al.*, 2017). According to their findings, the effect was further enhanced in the presence of Na<sup>+</sup> cations,

which show synergism with the  $\text{SO}_4^{2-}$  anions. This salting-out effect could explain the peculiarities of using  $\text{Na}_2\text{SO}_4$  in preventing the hydrolysis of acid-labile epoxides.

## 2.5 Biphasic reactions

A biphasic reaction system occurs when reactants form two separate phases. The advantages of this system are potential rapid phase separation and reactant recovery. This approach could reduce energy costs, where a simple separator might be used rather than a distillation column. In many cases, the catalyst used is usually dissolved in one of the phases, typically the aqueous phase if a metal catalyst was used. Figure 2.4 illustrates a simplified biphasic reaction system in which product separation and recycle could be realised.

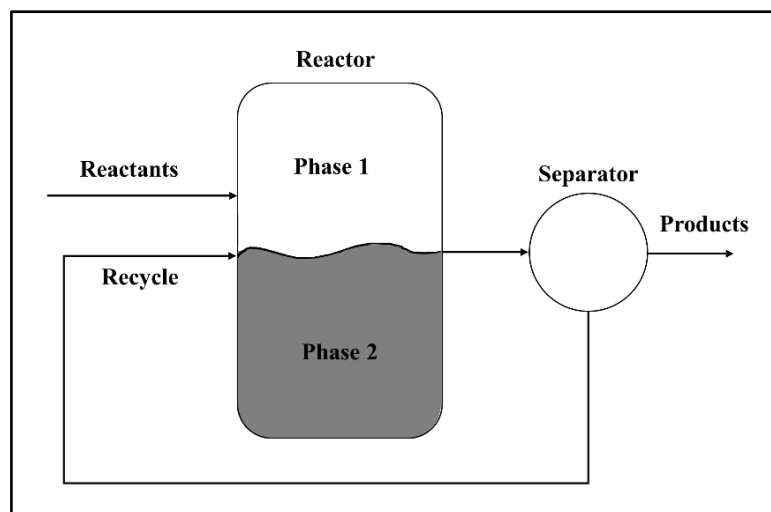


Figure 2.4. A simplified version of a biphasic reaction system showing product separation and recycling.

Typically, a water-based aqueous phase is used as one of the phases in a biphasic mixture due to the high immiscibility with the organic phase. However, a biphasic system consists of two fluoruous organic phases or involving ionic liquids also have been used (Wiebus and Cornils, 2006). Examples of biphasic reactions involving the aqueous-organic system includes alkylation (Sinou *et al.*, 2003), carbonylation (da Rosa *et al.*, 2000), Diels-Alder reaction (Loncaric *et al.*, 2003), epoxidation (Venturello *et al.*, 1983), and hydrogenation (Yang *et al.*, 2000).

In general, most organic reactions involving a biphasic system were either performed by using a phase transfer catalyst or in emulsifications. Both approaches have been shown to have many benefits, especially their effect on the reaction rates (Duynstee and Grunwald, 1959; Letts and

Mackay, 1975; Weber and Gokel, 1977; Chen *et al.*, 2004; Yang *et al.*, 2005; Holmberg, 2007). Although the dominance of one method over another is usually negligible, there are instances where for a process, the use of one method significantly alters the reaction rates. For instance, Menger and Elrington (1991) found that the oxidation of mustard (bis(2-chloroethyl) sulfide) was 80 times faster in an emulsification than in a non-emulsified system using a phase transfer catalyst. There are also studies which investigated the prospect of having both methods in one system, for example, Häger and Holmberg (2000) investigated the ring opening of an aliphatic epoxide using quaternary ammonium salts as a phase transfer catalyst in an emulsified system.

Emulsification in a biphasic reaction could also be achieved in a microfluidic and membrane reactor. De Bellefon *et al.* (2000) demonstrated the use of a microfluidic reactor to emulsify the isomerisation of allylic alcohol. They concluded that the use of a microfluidic reactor enhances the emulsification, allowing for a rapid screening of process variables.

An example of a biphasic epoxidation reaction involving (R)-(+)-limonene was demonstrated by Villa *et al.* (2002). They reported the biphasic epoxidation of (R)-(+)-limonene using H<sub>2</sub>O<sub>2</sub> with heterogeneous peroxotungstophosphate (Venturello anion) on Amberlite IRA-900 in acetonitrile. According to their results, acetonitrile increased the (R)-(+)-limonene concentration in the aqueous phase, highlighting the relationship between the concentration of (R)-(+)-limonene and the mass transfer rate in the biphasic system (Villa *et al.*, 2002).

### **2.5.1 Surfactants**

Surfactants are generally used to lower the surface tension between two liquids (Kosswig, 2000) and are primarily amphiphilic organic compounds consisting of two components, hydrophobic ‘tails’ and hydrophilic ‘heads’. This unique feature allows each component of the surfactant to be soluble either in aqueous or organic medium. An ‘oil-in-water’ emulsion is formed when the surfactant’s hydrophobic tail aggregates in an organic droplet, while the hydrophilic head is in contact with the bulk aqueous phase. In a bulk organic phase, particularly in a non-polar solvent environment, the surfactant molecules tend to form a ‘water-in-oil’ emulsion, where the hydrophilic heads encapsulate the aqueous droplets, while the hydrophobic tails stretch towards the organic phase. Figure 2.5 illustrates the formation of a ‘water-in-oil’ emulsion by the action of surfactant molecules in a biphasic mixture.

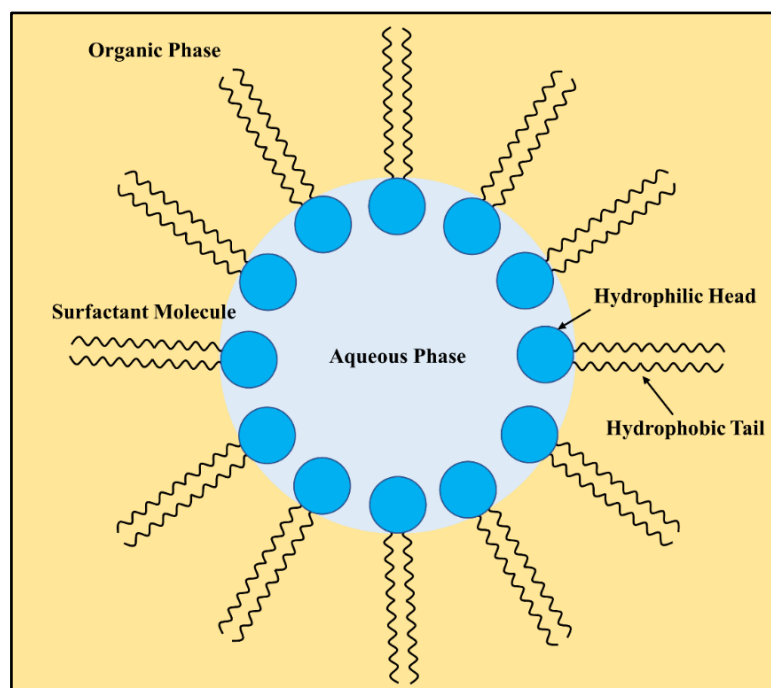


*Figure 2.5. Schematic of a 'water-in-oil' emulsion where the hydrophobic tail of the surfactant stretches towards the organic phase (gold background), while the hydrophilic head remains in the aqueous phase (blue background).*

In a chemical reaction involving two immiscible liquids (biphasic reaction), surfactants are typically utilised to form an emulsion. The stability of the emulsions formed depends on the type of the surfactant. Surfactants are commonly classified according to the polarity of the hydrophilic head. Table 2.2 shows the classification of surfactants and examples of surfactant for each class.

Class	Surfactant head net charge	Examples
nonionic	no charge	alkylphenol ethoxylates (Triton™ X-100) (Doong <i>et al.</i> , 1998), sorbitan monolaurate (SPAN® 20), polyethylene glycol sorbitan monolaurate (TWEEN® 20) (Bishopp <i>et al.</i> , 2014)
anionic	negative	sulfonate: perfluorooctanesulfonate (PFOS) (Vecitis <i>et al.</i> , 2008), carboxylate: sodium stearate (Wang <i>et al.</i> , 2010)
cationic	positive	quaternary ammonium salts: cetyl methyl ammonium bromide (CTAB) (Doong <i>et al.</i> , 1998), methyltrialkyl (C <sub>8</sub> -C <sub>10</sub> ) ammonium chloride (Adogen® 464) (Lee and Chang, 1978)
zwitterionic	negative and positive (two heads)	cocamidopropyl betaine (CAPB) (Hunter and Fowler Jr, 1998), phosphatidylethanolamine (Attwood <i>et al.</i> , 1992)

Table 2.2. Classifications of surfactants and examples of common surfactants.

The surfactant acts as a phase transfer catalyst in a biphasic reaction, which allows the formation of emulsions, providing a higher contact area between the immiscible reactants. In such biphasic reactions, the absence of surfactants could result in mass transfer limited conditions. In biphasic epoxidation, quaternary ammonium salts such as methyltrialkyl-(C<sub>8</sub>-C<sub>10</sub>)-ammonium chloride (Adogen® 464) and trioctylmethylammonium chloride (Aliquat® 336) are commonly used as phase transfer catalysts (Maheswari *et al.*, 2005; Mahha *et al.*, 2007; Wang and Rajendran, 2007; Seki and Baiker, 2009; Egusquiza *et al.*, 2012; Albanese *et al.*, 2016).

### 2.5.2 Phase transfer catalyst (PTC)

Phase transfer catalyst (PTC) is a term used to describe a chemical agent that facilitates the transfer of a reactant from one phase to another where the reaction occurs (Starks, 1971; Weber and Gokel, 1977). It is typically classified as a type of heterogeneous catalyst since the product is not in the same phase as the catalyst. PTC offers a better rate of reaction for a biphasic reaction, potentially reducing the use of solvents to achieve uniform mixture (Makosza, 2000). PTC is widely used in industry, for instance, the process of producing bisphenol-A involves the use of a PTC (Halpern, 2000). Quaternary ammonium salts are commonly used as PTC for biphasic reaction involving anionic reactants or oxidants. Table 2.3 lists common quaternary ammonium salts used as PTC.

Type	Example reaction	References
benzyltriethylammonium chloride	alkylation	(Kimura <i>et al.</i> , 1983)
methyltricaprylammonium chloride / methyltrioctylammonium chloride	oxidation	(Venturello and D'Aloisio, 1988; Neumann and Gara, 1994)
methyltributylammonium chloride	esterification	(Desikan and Doraiswamy, 2000)

Table 2.3. Common quaternary ammonium salts used in biphasic reactions.

The PTC agent typically consists of a cation part (e.g., quaternary ammonium,  $Q^+$ ) and an anion part (e.g., chloride,  $X^-$ ). Figure 2.6 shows the general mechanism of a PTC in a biphasic mixture.



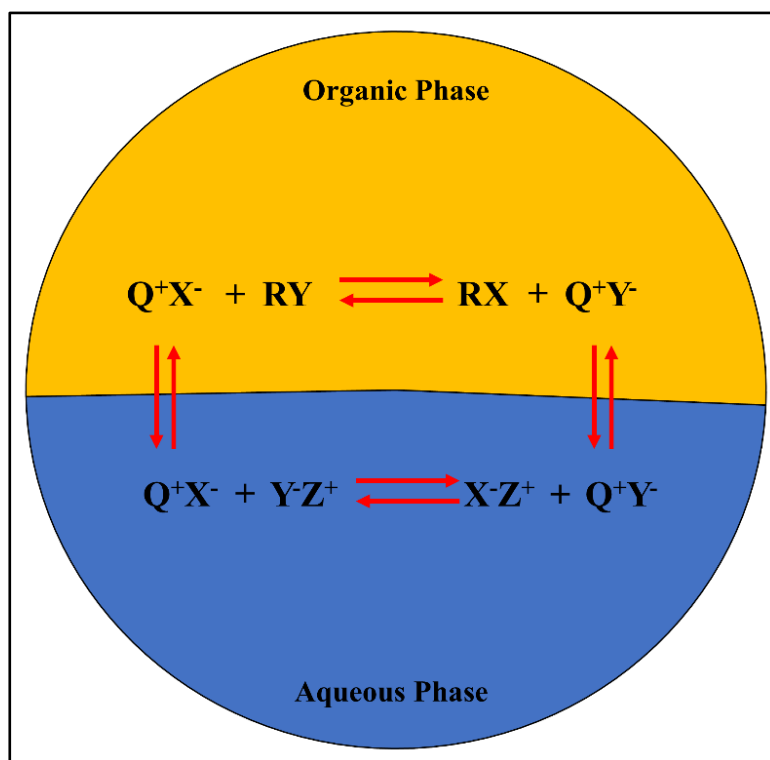


Figure 2.6. Mechanism of PTC in a biphasic mixture.

The  $Q^+$  ion pairs with the anionic reactants or oxidants ( $Y^-$ ) in the aqueous phase before shuttling to the organic phase. In the organic phase, the active oxygen is transferred to the alkene ( $R$ ) allowing the  $Q^+$  to return to the aqueous phase to complete the cycle.

PTC epoxidations gained interest due to high conversions and yields associated with the reactions typically performed in a two-phase system. PTCs can be immobilised as solid support, making them reusable, hence avoiding waste problems completely. Higher temperatures can be employed since the PTCs is stable at higher temperatures, resulting in higher conversions in less time, making the process commercially attractive. This method has been reported to be suitable for unreactive  $\alpha$ -olefins (Venturello *et al.*, 1983; Matoba *et al.*, 1984; Venturello and D'Aloisio, 1988; Duncan *et al.*, 1995).

PTCs are known to enhance the rate of reaction in biphasic systems such as those in typical terpene epoxidation processes using  $H_2O_2$  as oxidant (Weber and Gokel, 1977). Duncan *et al.* (1995) demonstrated the epoxidation of alkenes, such as 1-octene, using heteropolyacids in the presence of a PTC.

A study was conducted to observe the performance of tungsten (VI) and molybdenum (IV) based catalyst for the epoxidation of alkenes under a PTC system. The oxidation of alkenes

depends mainly on the amount and nature of the PTC in addition to the assembling anion of the catalyst (Piquemal *et al.*, 1997). They also found that the presence of the sulphate anion in acidic media was found to increase the selective epoxidation yield when using both tungsten and Mo (IV) catalysts.

Likewise, Sato *et al.* (1996) described the catalytic epoxidation of alkenes using  $H_2O_2$  in a system comprised of sodium tungstate catalyst, aminomethyl-phosphonic acid and methyltri-n-octylammonium hydrogensulphate as the PTC. The epoxidation resulted in a high yield of the product, corresponding to the amount of the PTC with or without solvent. Another study which employed quaternary ammonium heteropolyoxo-tungstate found that the phase transfer agent degraded to a few oxo-peroxophosphate ions, which enhanced the epoxidation yields (Gao *et al.*, 2004).

Chen *et al.* (2004) investigated the epoxidation of alkenes in a phase transfer catalysed system using acidic media and an organic solvent. They concluded that the system works best using  $H_2O_2$  as an oxidant while employing sodium tungstate and phosphoric acid as a catalyst. A more recent study was conducted to evaluate the effect of phosphate and sulphate anions on the epoxidation of alkene in various PTC system which included Arquad 2HT® (Mahha *et al.* (2007). The anion was found to work best when both anions were present in the reaction. Furthermore, it was also reported that tungsten (IV) shows stronger activity compared to sodium tungstate in the phase transfer catalysed system.

Bishopp *et al.* (2014) reported epoxidation of sunflower seed oil with  $H_2O_2$  using a tungsten-based catalyst in absence of common PTC. In the biphasic system, they used nonionic surfactant to create emulsions, showing that the mass transfer limitation associated with the biphasic system can be overcome through emulsification, that is, reducing the diameter of the droplets. They found that above a certain catalyst concentration,  $H_2O_2$  decomposition increases exponentially, reducing the epoxidation rate as the system was starved of oxidant. However, at lower catalyst concentration, the  $H_2O_2$  decomposition was exceptionally low. Addition of acetic acid to the tungsten catalyst sufficiently decrease  $H_2O_2$  decomposition to be almost negligible. They also found that  $H_2O_2$  was first order at lower catalyst concentration.

Growing concerns regarding the separation of PTC from the reaction mixture has led to research on polymer-supported PTC. Desikan and Doraiswamy (2000) compared the performance of a polymer-supported methyltributylammonium chloride as a phase transfer agent and its analogous soluble form for the esterification of benzyl chloride with aqueous sodium acetate.

They observed about 50 % higher activity of the supported PTC compared to the soluble form in addition to the easy post-reaction separation.

### ***2.5.3 Polyoxometalates***

Polyoxometalates (POM) were first reported by Berzelius in 1826, without specifying the arrangement and structure of the compound (Hill, 1998). The structure of POM was discovered later in 1933 by Keggin, where to this day, the most common POM structure is named after him (Keggin, 1934). A wide variety of POM exist due to the fact that many elements from the periodic table can be fused into its structural framework (Hill, 1998). This feature allows POM to be versatile and continuously used in applications such as catalysis (Katsoulis, 1998; Hill, 2007).

POM composed of transition metals in the highest oxidation state form oxo-anionic clusters through the dissolution of metal ions in an aqueous solution (Cavani, 1998). Water molecules coordinate to the cations, forming metal-oxygen bonds, followed by the ionisation of the OH bond. The acidity of the proton centre is related to the metal ion charge, with an unstable complex tending to dimerise by forming oxo or hydroxy groups. The dimer further polymerises until it forms a polyhedral structure, with strong repulsions from its edges. The metals in the structure can be interconnected at the edges via metal-oxygen-metal bridges.

The structure of the complex and its stability depends largely on the pH of the solution. Figure 2.7 illustrates the influence of pH on the stability and structure of the POM complex based on tungsten (W) and phosphorus (P) atoms.

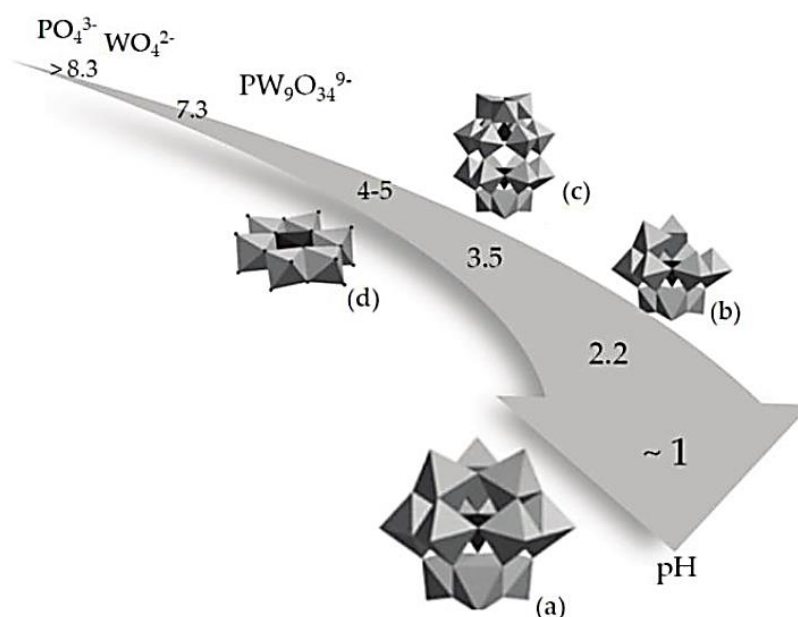


Figure 2.7. Influence of acidity on the structure of the polyoxometalates complex, (a) Keggin, (b) lacunary Keggin, (c) Wells-Dawson and (d) Anderson structure (Zhu *et al.*, 2003).

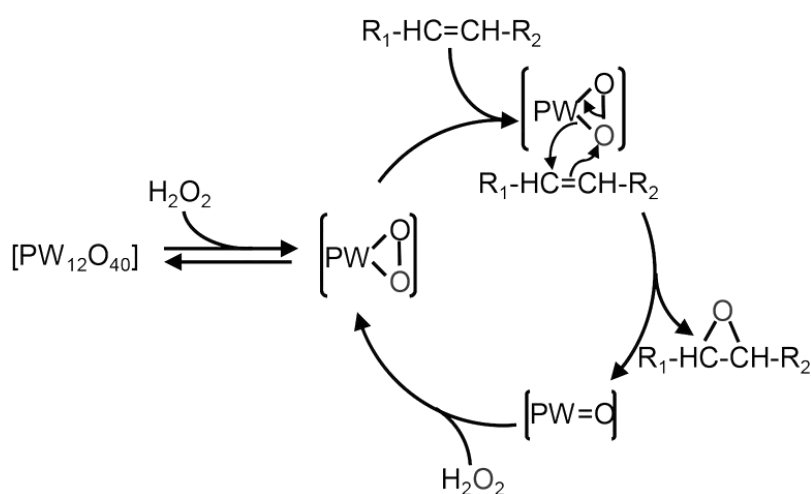
As can be seen from Figure 2.7, a Keggin structure can be formed when the pH is about 1. The Keggin structure of the POM is easily synthesised and highly stable with the general formula  $[X^{n+}M_{12}O_{40}]^{(8-n)-}$ . The structure is commonly formed using P or silica (Si) as central atom (X) with molybdenum (Mo) and W as the addenda atom (M). A lacunary Keggin can be formed by the hydrolysis of the Keggin structure by simply increasing the pH to about 2.2. The general formula for the lacunary Keggin is  $[XM_{11}O_{39}]^{n-}$ , with other metal ions, such as iron ( $Fe^{2+}$ ), nickel ( $Ni^{2+}$ ) or cobalt ( $Co^{2+}$ ), can be fused into the lacunary Keggin structure. Balula *et al.* (2013) demonstrated the use of lacunary Keggin phosphotungstates catalyst for the epoxidation of (R)-(+)-limonene with hydrogen peroxide at 80 °C using acetonitrile as a solvent. They reported high activity of the catalyst, and complete conversion of (R)-(+)-limonene to limonene-1,2-epoxide, bis-epoxide and limonene-1,2-diol was achieved. A Wells-Dawson structure with a general formula  $[X_2^{n+}M_{18}O_{62}]^{(2n-16)-}$  and planar Anderson structure with general formula  $[X^{n+}M_6O_{24}]^{(12-n)-}$  are typically obtained in the pH range between 3.5 – 5.

Heteropolyoxometalates (heteropolyanions) are formed by the fusion of an anion at the centre of the complex in acidic conditions. Numerous anions can be fused including beryllium (Be), boron (B), aluminium (Al), silicon (Si), germanium (Ge), tin (Sn) and P. This structure could form a secondary structure (salts) when associated with counter-ions such as protons ( $H^+$ ),  $Na^+$ ,  $NH_4^+$ ,  $K^+$  and  $Cs^+$ .

Heteropolyacids (HPA) are formed when solid POM composed of heteropolyoxometalates, hydration water and protons as counter-ions. The HPA have strong acidity, reportedly stronger than mineral acids. A commonly used POM/HPA species,  $\text{H}_3\text{PW}_{12}\text{O}_{40}$ , is considered to be a superacid used in many catalysis process such as alkylation, acylation and oxidation (Mizuno and Misono, 1998). POM catalyst gained popularity in oxidation due to high Brønsted acidity, which shows efficient redox capability that enables rapid reactions and regeneration (Hill, 1998). The redox mechanism of POM in oxidation reactions can be used with either di-oxygen ( $\text{O}_2$ ) or hydrogen peroxide ( $\text{H}_2\text{O}_2$ ) as oxidants, where following the oxidation of the substrate, the POM is re-oxidised by the oxidant.

Many studies have been performed to investigate the suitability of Fe (Dutta *et al.*, 2010), Mn (Gupta *et al.*, 2009), Ru (De Vos *et al.*, 2003), Re (Di Giuseppe *et al.*, 2010), W (Amini *et al.*, 2014), alumina (Lane and Burgess, 2003), as well as compounds such as hydrotalcite (Uguina *et al.*, 2006) with hydrogen peroxide for the epoxidation of alkene. Among these, it was demonstrated that W-based POM was most effective with  $\text{H}_2\text{O}_2$  (Oyama, 2008). The commonly used Mo and Ti-based catalysts were found to be less effective with  $\text{H}_2\text{O}_2$  (Arends and Sheldon, 2002).

The use of POM in epoxidation was first reported by Venturello *et al.* (1983), who studied the epoxidation of 1-dodecene using  $\text{H}_2\text{O}_2$  oxidant with  $\text{Na}_2\text{WO}_4$  and  $\text{H}_3\text{PO}_4$  in biphasic conditions. They managed to identify the active oxidative species  $[\text{PO}_4\{\text{W}(\text{O})(\text{O}_2)_2\}_4]^{3-}$ , which is commonly referred to as the Venturello anion ( $\text{PW}_4$ ) (Venturello and D'Aloisio, 1988). The mechanism of alkene epoxidation with the Venturello anion is shown in Scheme 2.15.



Scheme 2.15. Reaction mechanism of alkene epoxidation using Venturello anion as the catalyst (Mouret *et al.*, 2014).

A similar investigation using POM was performed by Ishii *et al.* (1988) for the epoxidation of alkene. They investigated the activity of phosphotungstate ( $\text{H}_3\text{PW}_{12}\text{O}_{40}$ ),  $\text{H}_4\text{SiW}_{12}\text{O}_{40}$  and  $\text{H}_3\text{PMO}_{12}\text{O}_{12}$  species in biphasic conditions using  $\text{H}_2\text{O}_2$  as oxidant in chloroform solvent, where the phosphotungstate was found to be the most active among all POM tested. In both Ishii and Venturello's works, the use of a PTC (quaternary ammonium salts) as counter-ion was required. Figure 2.8 visualises the structure of the Venturello anion.

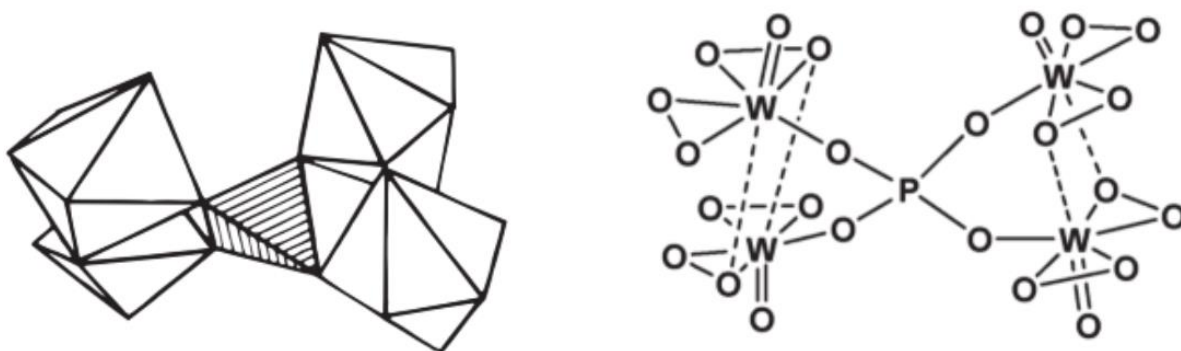
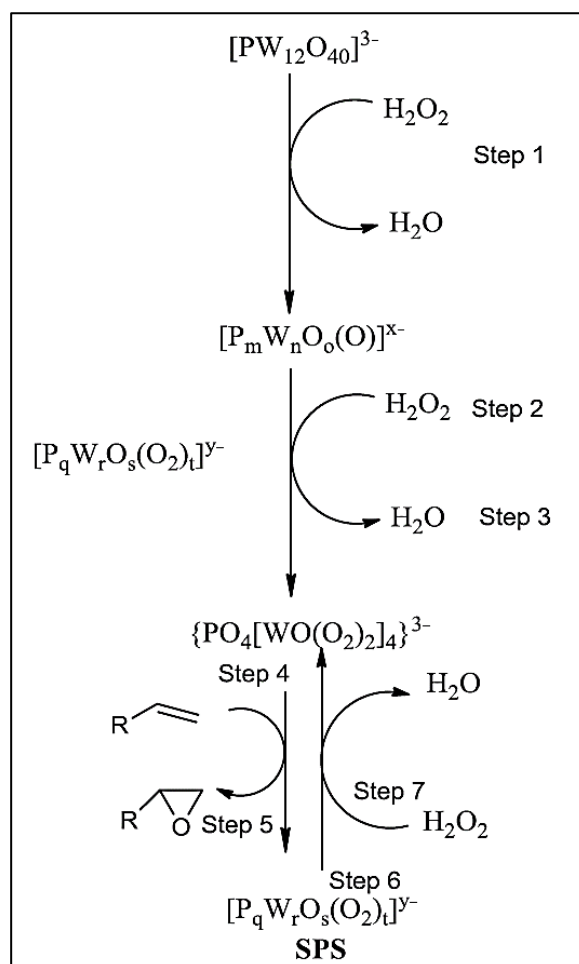


Figure 2.8. The visualisation of the structure of Venturello anion ( $\text{PW}_4$ ) (Mizuno *et al.*, 2005).

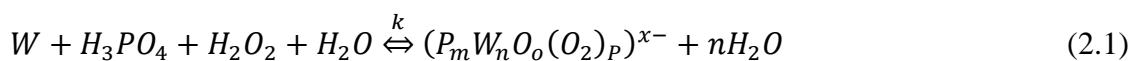
Ishii-Venturello chemistry has gained interest for the epoxidation of alkene. A detailed kinetic investigation on the active species (Venturello anion) was performed by Duncan *et al.* (1995) for the epoxidation of 1-octene with  $\text{H}_2\text{O}_2$ . They investigated the catalytic system, confirming the presence of the  $\text{PW}_4$  as the active species. They compared the activity of 11 POMs and found that the Venturello anion required at least a 50-fold excess of  $\text{H}_2\text{O}_2$  to be formed from the P-W precursors. Interestingly, they observed the formation of subsequent peroxo species (SPS) following the interaction of the  $\text{PW}_4$  species and the substrate. The SPS were found to be rapidly regenerated to form the  $\text{PW}_4$  species by  $\text{H}_2\text{O}_2$ , see Scheme 2.16. They also found that the  $\text{PW}_4$  species was the most active POM for epoxidation, showing more than double the activity of the peroxotungstate species ( $[\text{WO}(\text{O}_2)_2(\text{H}_2\text{O})_2\text{O}]^{2-}$ ). The only disadvantage of this catalytic system is the requirement of chlorinated solvent to facilitate the acid character of the catalyst and the irreversible adsorption of epoxide and diol which deactivates the catalyst (Mouret *et al.*, 2014; Palumbo *et al.*, 2016).



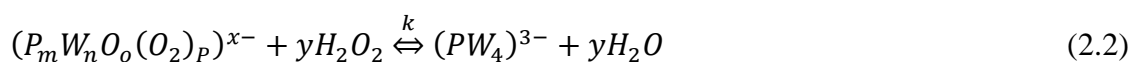
Scheme 2.16. Mechanism of active species formation (Yadav and Satoskar, 1997).

Yadav and Satoskar (1997) investigated the reaction mechanism for the epoxidation of alkene using Venturello anion in the presence of PTC. Their work is largely based on the findings of Duncan *et al.* (1995) and they proposed a mechanism for the epoxidation reaction based on Scheme 2.16 as follows:

Formation of the catalyst complex from tungstate, phosphate and  $H_2O_2$



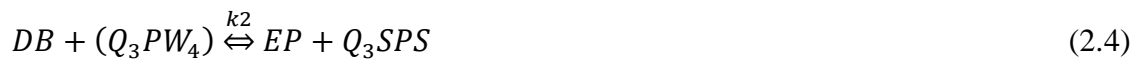
Formation of the Venturello anion ( $PW_4$ )



Venturello anion reacted with quaternary ammonium salt



The epoxidation of double bond (DB) to form epoxide (EP) and SPS



Reactivation of the SPS by H<sub>2</sub>O<sub>2</sub>



The rate law for the formation of the catalyst complex and the epoxidation reaction was written as follows:

$$r_{oxidative} = k_1[aH_2O_2][bW][cH_3PO_4][3Q] - K_{eq}^{-1}[dQ_3PW_4][eH_2O] \quad (2.6)$$

$$r_{epox} = k_2[DB][Q_3PW_4] \quad (2.7)$$

In this work, this mechanism was adopted (simplified in Figure 2.9) for the epoxidation of (R)-(+)-limonene and  $\alpha$ -pinene with H<sub>2</sub>O<sub>2</sub> using polytungstophosphate and PTC. The epoxidation of (R)-(+)-limonene and  $\alpha$ -pinene with H<sub>2</sub>O<sub>2</sub> is biphasic in nature since the hydrophobic substrate and its oxidative products is not miscible with aqueous H<sub>2</sub>O<sub>2</sub>. In order to visualise the process, Figure 2.9 presents the summary of all the involved reactions for the epoxidation of (R)-(+)-limonene.



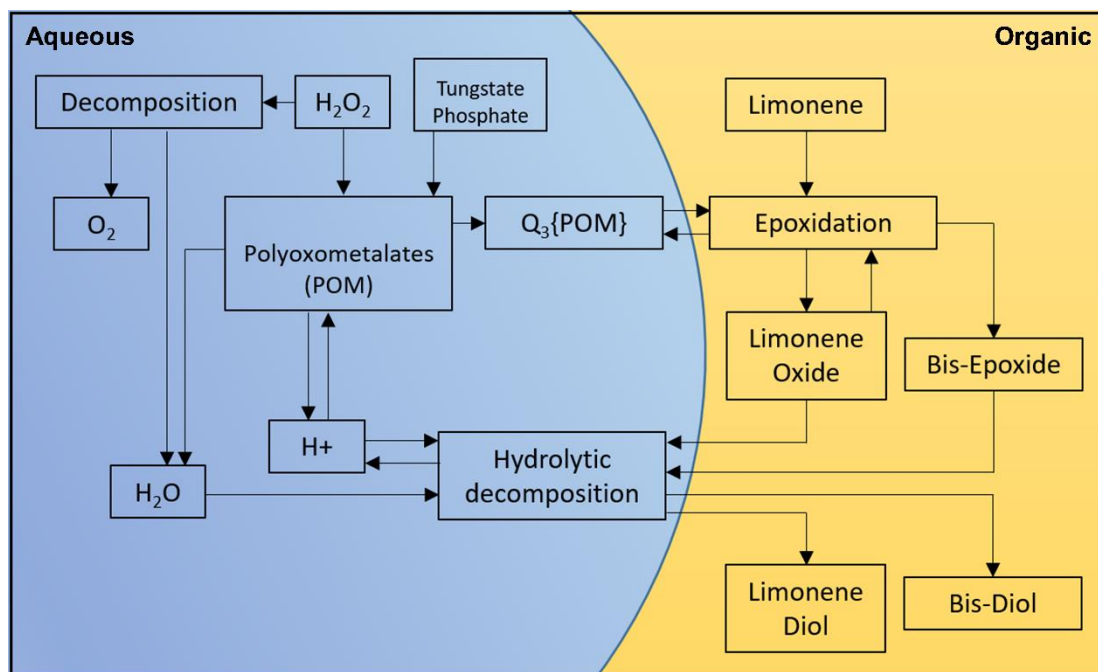


Figure 2.9. Overall reaction scheme for the epoxidation of (R)-(+)-limonene, the formation of oxidative species, the decomposition of  $\text{H}_2\text{O}_2$  and the hydrolytic decomposition of the epoxides. The schematic diagram visualises the phase where each reaction occurs (blue background: aqueous phase, gold background: organic phase).

Figure 2.9 shows that the polytungstophosphate  $\{\text{PO}_4[\text{WO}(\text{O}_2)_2]_4\}^{3-}$  formed from  $\text{H}_2\text{O}_2$ , tungstate and phosphate shuttles to and from the organic phase via a PTC ( $\text{Q}^+$ ). The formation of the oxidative species follows the Ishii-Venturello chemistry, and details of the mechanism are elaborated in the literature (Duncan *et al.*, 1995; Yadav and Satoskar, 1997; Yadav and Pujari, 2000) The active oxygen is transferred to both (R)-(+)-limonene and limonene-1,2-epoxide via the epoxidation reaction. The  $\text{H}^+$  ions participate in the formation of the oxidative species and the protonic attack on the epoxides at the interphase. The epoxides form a diol in the presence of  $\text{H}_2\text{O}$  (nucleophile), following the protonic attack. Table 2.4 below lists notable research on alkene epoxidation employing POM as the catalyst.

POM Catalyst	Substrate	Oxidant	Temperature	Solvent	Conversion (%)	Selectivity (%)	Reference
$[\text{M}_4(\text{H}_2\text{O})_2(\text{PW}_9\text{O}_{34})_2]^{n-}$ , M = Co(II), Mn(II) and Fe(III)	(R)-(+)-limonene	30 wt.% $\text{H}_2\text{O}_2$	80 °C	acetonitrile	Co(II), Mn(II), Fe(III) = 86 %, 68 %, 89 %	Co(II), Mn(II), Fe(III) = 51 %, 82 %, 77 %	Santos <i>et al.</i> , 2017
$\text{K}_{10}[\text{M}_4(\text{H}_2\text{O})_2(\text{PW}_9\text{O}_{34})_2] \cdot 20\text{H}_2\text{O}$ M = Cu(II)	(R)-(+)-limonene	30 wt.% $\text{H}_2\text{O}_2$	2 °C	1,2-dichloroethane	96 %	95 % to limonene-1,2-epoxide	Egusquiza <i>et al.</i> , 2012
$[\text{SeO}_4\{\text{WO}(\text{O}_2)_2\}_2]$	cyclohexene	30 wt.% $\text{H}_2\text{O}_2$	ambient	acetonitrile	99 %	97 % to cyclohexene oxide	Kamata <i>et al.</i> , 2010
$[\text{Ti}_2(\text{OH})_2\text{As}^{2-}\text{W}_{19}\text{O}_{67}(\text{H}_2\text{O})]^{8-}$	(R)-(+)-limonene	30 wt.% $\text{H}_2\text{O}_2$	50 °C	acetonitrile	76 %	75 % to limonene-1,2-epoxide	Donoeva <i>et al.</i> , 2010
$[\text{PW}_4\text{O}_{32}]$	cyclooctene	30 wt.% $\text{H}_2\text{O}_2$	65 °C	ethyl acetate	99 %	99 % to cyclooctene oxide	Ding <i>et al.</i> , 2008
$\text{Na}_2\text{WO}_4/\text{H}_2\text{WO}_4$	cyclooctene	30 wt.% $\text{H}_2\text{O}_2$	60 °C	solvent-free	99 %	99 % to cyclooctene oxide	Maheswari <i>et al.</i> , 2006
$\text{Na}_8\text{H}[\Delta\text{PW}_9\text{O}_{34}] \cdot 19\text{H}_2\text{O}$	(R)-(+)-limonene	35 wt.% $\text{H}_2\text{O}_2$	2 °C	1,2-dichloroethane	100 %	96 % to limonene-1,2-epoxide	Casuscelli <i>et al.</i> , 2005

Table 2.4. List of research on alkene epoxidation using POM as a catalyst.

## 2.6 Process intensification

Process Intensification (PI) is an established concept within the chemical engineering domain, the definition of which has evolved over time. One of the first definitions for PI was presented by Ramshaw in 1995 as: “the strategy of reducing the size of chemical plant needed to achieve a given production objective”. He argued that the size of a chemical plant should be reduced by more than 100 times to achieve a level of intensification. In their review in 2000, Stankiewicz and Moulijn proposed the following definition: “any chemical engineering development that leads to a substantially smaller, cleaner, and more energy efficient technology is process intensification”. They suggest that the PI concept should include the development of new equipment and techniques that could lead to significant improvement in manufacturing and processing, reducing equipment size to production capacity ratio, and reduce waste, which could result in cheaper technologies. Realising the need for appreciation for a safety consideration in the PI concept, Reay *et al.* (2013), refreshed the definition of PI as follows: “any chemical engineering development that leads to a substantially smaller, cleaner, safer and more energy efficient technology is process intensification”.

There have been many types of reactors developed under the domain of PI within the green chemistry principles; integrating efficient energy utilisation, safer system, less footprint and better use of raw materials (Ramshaw, 1999). One of the many reactors that was proven as capable PI reactors are oscillatory baffled reactors (OBRs), which can provide effective multiphase fluid mixing and heat removal from the reaction mixture (Mackley *et al.*, 1993; Ni and Pereira, 2000; Stonestreet and Harvey, 2002b; Harvey *et al.*, 2003b; Reis *et al.*, 2004; Reis *et al.*, 2005). The OBRs have advantages of ease of scale-up, reproducibility of experiments, compatibility with homogeneous and heterogeneous catalysts, and potentials for operations in batch and continuously as a plug flow reactor (Harvey *et al.*, 2003b; Phan *et al.*, 2011b; Phan *et al.*, 2012; Eze *et al.*, 2013; Eze *et al.*, 2017; Eze and Harvey, 2018). This is not necessarily the case for other “intensified” reactors that have been reported for biofuel multiphase reactions, such as microwave reactors (Lin *et al.*, 2014, Liao and Chung, 2013), ultrasonic reactors (Kumar *et al.*, 2010, Okitsu *et al.*, 2010, Colucci *et al.*, 2005) spinning disc reactors (Qiu *et al.*, 2012) and micro-reactors (Kalu *et al.*, 2011, Wen *et al.*, 2009, Sun *et al.*, 2008), where scale-up is unproven or challenging.

### 2.6.1 The Oscillatory baffled reactor (OBR)

The oscillatory baffled reactor (OBR) consists of a tube fitted with periodically spaced baffles along its length (Figure 2.10). The fluid inside the reactor is subjected to oscillating motion via an oscillator. The effective radial fluid mixing and heat transfer in the OBRs result from oscillatory mixing, where vortices are formed from the interaction between the oscillating fluid and the baffles (Brunold *et al.*, 1989; Ni *et al.*, 2002). These interactions lead to the formation and dissipation of the vortices which enhance the mass and heat transfer between the reactants.

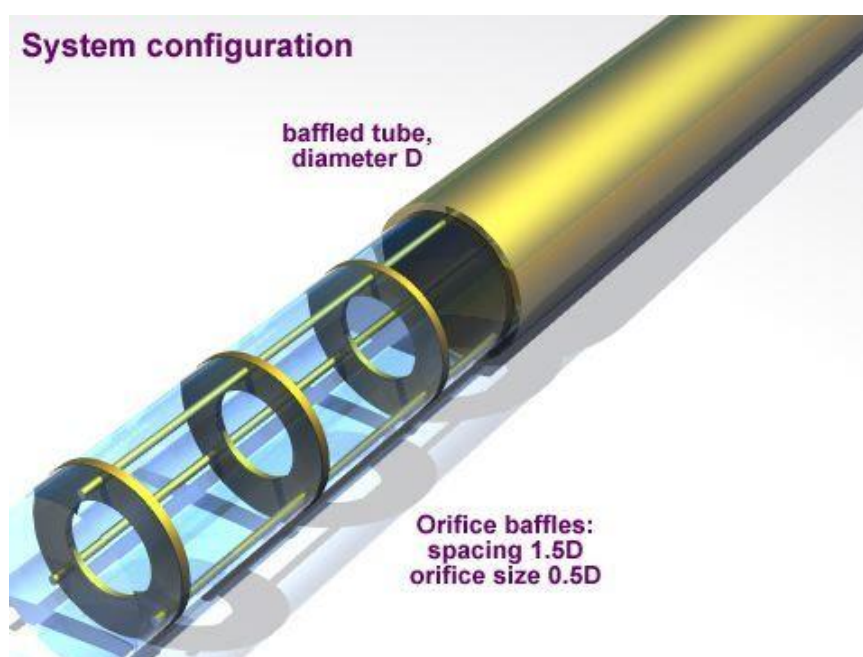


Figure 2.10. Conventional OBR fitted with single orifice baffles (Zheng *et al.*, 2007).

The effect of oscillatory mixing was first reported by Binnie (1945) from the observation of fluid turbulence in a glass pipe. However, the concept evolved decades later during the 80s, when Knott and Mackley (1980) described the formation of eddies and vortices in their study of oscillatory flow movement on sharp edge tubes. Subsequently, Brunold *et al.* (1989) conducted a study to observe the phenomenon of this fluid movement in a tube with fitted baffles, describing how the formation of stable vortices in the baffle cavities could enhance fluid mixing. Dickens *et al.* (1989) observed plug flow behaviour in a laminar net flow condition when the fluid was subjected to both oscillatory and net flow in a baffled tube. Mackley and Ni (1991) compared the mixing profile between an unbaffled and baffled tube to investigate the advantages of fluid oscillation, finding that combining oscillation with periodic baffles results in uniform mixing in each baffle cavity. They observed that the effect originates

from the periodic formation of vortices in the baffled tube. The formation of vortices in OBR can be visualised from Figure 2.11.

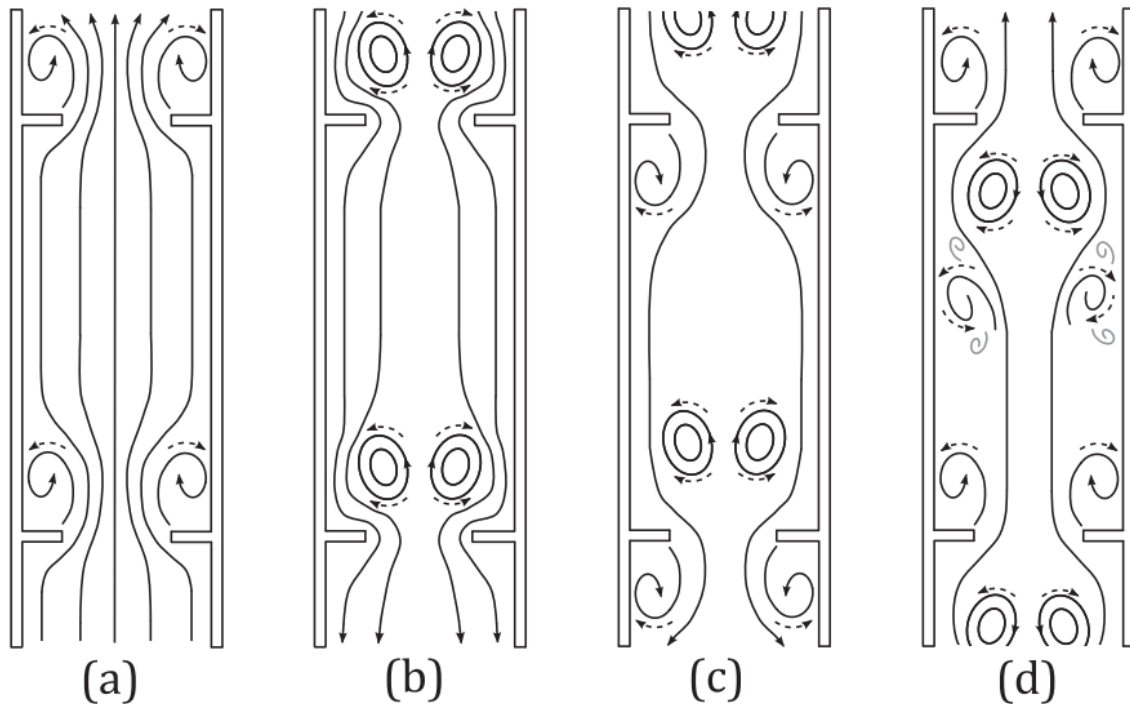


Figure 2.11. Formation of vortices in oscillatory baffled reactor; (a) vortex forms downstream of the baffle, (b) vortex grow in baffle cavity, (c) cortex swept into bulk fluid and (d) interact with vortices from previous cycle (McDonough *et al.*, 2015).

The mixing characteristic inside the OBR was found to be controlled by the oscillation and is independent of the net flow (Harvey *et al.*, 2001). This feature caused the OBR to provide plug flow at low net flow rates in the laminar regime, allowing long reactions to be performed in continuous mode in a reactor of greatly reduced length to diameter ratio. This advantage of the OBR was demonstrated by Harvey *et al.* (2001) in a saponification study where the reactor volume was reduced 100-fold from a stirred tank reactor to a continuous OBR.

In a conventional tubular reactor, plug flow can be achieved when the fluid velocity is sufficiently high net Reynolds number ( $Re_n \geq 2100$ ) to obtain good mixing. In OBR, plug flow can be achieved at a net flow rate in the laminar region (Stonestreet and Van Der Veecken, 1999; Stonestreet and Harvey, 2002a; Harvey *et al.*, 2003b; Al-Abduly *et al.*, 2014; Ahmed *et al.*, 2017; Law *et al.*, 2018). Howes *et al.* (1991) found that at oscillatory Reynolds number,  $Re_0 = 100$ , the vortices formed in a baffled tube are symmetrical, indicating a laminar flow, while at  $Re_0$  above 300, the symmetry was broken showing similar characteristics to turbulent flow.

This was confirmed by Stonestreet and Van Der Veecken (1999), who observed a laminar flow for  $Re_0 < 250$  and a turbulent flow for  $250 < Re_0 < 2000$ .

The fluid mechanics of the OBR are governed by geometrical and dynamic parameters (Ni and Gough, 1997). The geometrical parameter is described by the baffles spacing ( $L$ ) and the baffle open space area ( $S$ ) as defined by equations (2.8) and (2.9), while the dynamic parameter is described by dimensionless numbers, which are the oscillatory Reynolds number ( $Re_0$ ), net flow Reynolds number ( $Re_n$ ) and Strouhal number ( $St$ ) as defined by equations (2.10) – (2.13):

$$L = 1.5D \quad (2.8)$$

$$S = \frac{d_0^2}{D^2} \quad (2.9)$$

$$Re_0 = \frac{2\pi f x_0 \rho D}{\mu} \quad (2.10)$$

$$Re_n = \frac{\rho D u}{\mu} \quad (2.11)$$

$$St = \frac{D}{4\pi x_0} \quad (2.12)$$

$$\psi = \frac{Re_0}{Re_n} \quad (2.13)$$

Where,  $D$  is the tube internal diameter (m),  $d_0$  is the orifice diameter (m),  $f$  is the oscillation frequency (Hz),  $x_0$  is the centre-to-peak amplitude of oscillation (m),  $\rho$  is the fluid density ( $\text{kg m}^{-3}$ ),  $\mu$  is the viscosity ( $\text{m}^2 \text{s}^{-1}$ ), and  $u$  is the fluid superficial velocity ( $\text{m s}^{-1}$ ).

Brunold *et al.* (1989) found that the optimum baffle spacing was 1.5 times the tube diameter for the pulsing oscillation mechanism. The effect and importance of the baffles spacing ( $L$ ) and the baffle open space area ( $S$ ) on the formation of vortices in baffled tube was demonstrated by Ni and Gough (1997). They studied the effect of decreasing the baffle open space area ( $S$ ) from 0.5 to 0.1 at an oscillation frequency ranging from 1 to 5 Hz and oscillation amplitude from 2.5 to 10 mm. According to their findings, the ratio of  $S$  around 0.2 gave the shortest mixing time. In a related work, Ni and Stevenson (1999) observed that increasing the gap size between the baffle and the tube increases the mixing time, regardless of the frequency and amplitude. They found that the intensity of eddy formation reduces with increasing gap size.

The intensity of mixing in the OBR is described by the dimensionless number,  $Re_0$ . The expression is similar to  $Re_n$  except the fluid superficial velocity ( $u$ ) was replaced by maximum

oscillatory velocity ( $2\pi f x_0$ ). Strouhal number (St) measures the effectiveness of eddy propagation within the tube geometry and is inversely proportional to the oscillation amplitude. The velocity ratio ( $\psi$ ) describes the relationship between  $Re_0$  and  $Re_n$  (Equation 2.13). To maintain a fully reversing flow in the OBR, the value of  $\psi$  should be above 1 (Stonestreet and Harvey, 2002a).

Numerous studies have investigated the scalability of OBR through maintaining the geometric and dynamic parameters. For instance, Smith and Mackley (2006) investigated the scalability of OBR from 24, 54 and 150 mm diameter tubes, showing that the axial dispersion value measured in each tube was constant over a wide range of oscillation conditions ( $80 \leq Re_0 \leq 800$ ). Ni *et al.* (2001) observed a linear relationship between the axial dispersion and the tube size for OBR diameter ranging from 40 to 150 mm in both batch and continuous mode. A recent study on the scalability of OBR by Ahmed *et al.* (2017) on the helically baffled OBR between diameter 10 mm to 50 mm showed a similar mixing pattern allowing the reaction conditions to be extrapolated.

The enhancement of mass and heat transfer offered by the OBR renders its application for numerous processes including bioprocessing (Abbott *et al.*, 2014), crystallisation (Lawton *et al.*, 2009), photocatalytic (Fabiyyi and Skelton, 1999), polymerisation (Ni and Stevenson, 1999) and saponifications (Harvey *et al.*, 2001). The advantage of OBR in multiphase mixing has also been demonstrated, especially in biodiesel production (Ghazi *et al.*, 2008).

### **2.6.2 The Mesoscale oscillatory baffled reactor**

Harvey *et al.* (2003a) presented a novel type of reactor, the mesoscale OBR, for process and screening application. The reactor described is much smaller in diameter (5 mm) compared to the previous OBR. The advantage of a smaller dimension reactor is it allows a process to be screened using fewer reagents. Working with fewer reagents effectively reduces the amount of waste compared to a typical screening process in a large OBR. Another advantage of this type of reactor is that it can be operated at much lower net flow rates (Phan *et al.*, 2011a). The reactor can also be fitted with different types of baffles to suit various reaction types, such as biodiesel production (Harvey *et al.*, 2003a). Figure 2.12 shows some baffles commonly used in mesoOBR.

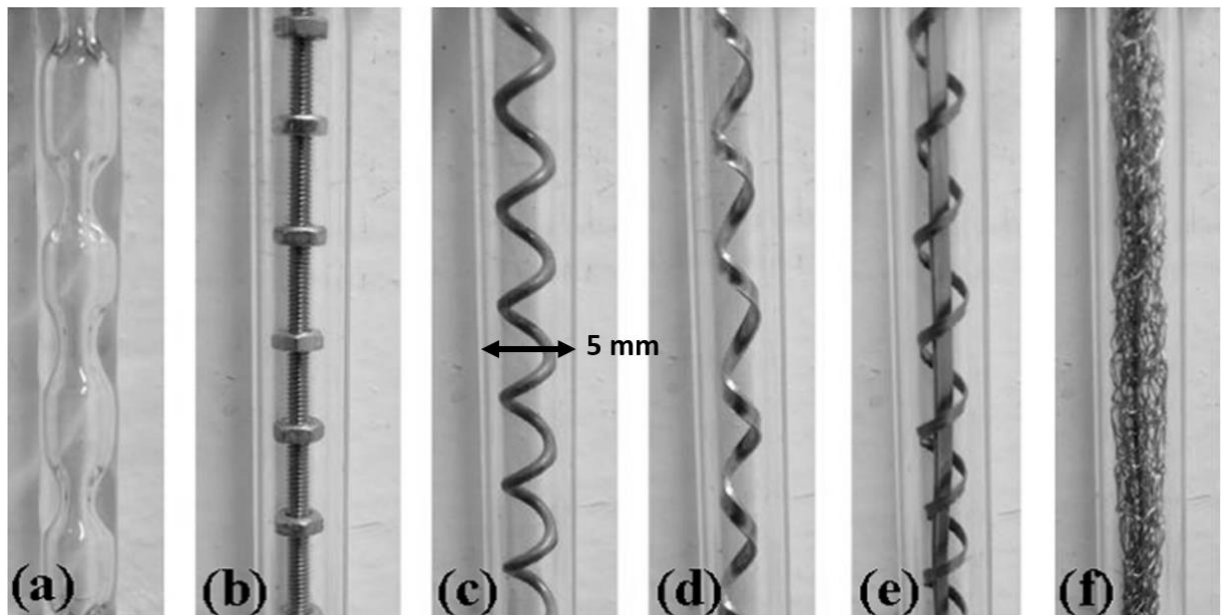


Figure 2.12. Type of baffles in mesoOBR: (a) integral, (b) central axial, (c) round edge helical, (d) sharp edge helical, (e) sharp edge helical with central rod, and (f) wire wool (McDonough *et al.*, 2015).

The integral baffle or smooth periodic column (SPC) design of the mesoOBR platform consists of smooth baffles to reduce shear rate typically associated with sharp edged orifice baffles in OBR. A study by Reis *et al.* (2005) regarding the flow pattern in a SPC mesoOBR using particle image velocimetry (PIV) and computational fluid dynamics (CFD) showed a similar mixing profile to a conventional OBR. They also reported that the critical  $Re_0$  required to form the vortex symmetrically in the SPC mesoOBR was lower ( $Re_0 > 10$ ) than the OBR ( $Re_0 > 50$ ). In another study, Reis *et al.* (2010) characterised the SPC baffle design through a residence time distribution (RTD) study using a tracer, concluding that for the SPC design, the oscillation amplitude ( $x_0$ ) has a more pronounced effect on the mixing than the frequency ( $f$ ). Zheng and Mackley (2008) reported an increase in axial dispersion with the increase in the  $Re_0$  for the SPC design. However, at low amplitude (high  $St$ ), lower axial dispersion was observed for the same  $Re_0$ .

The SPC design has been used in numerous applications. Reis *et al.* (2006) demonstrated the advantages of the SPC in sensitive applications, such as bio-processes. The smooth constriction of the integral baffle also allowed an excellent solid suspension throughout the reactor (Harvey *et al.*, 2003a). The SPC was also used for multiphase mixing such as biodiesel production. Zheng *et al.* (2007) determined the optimal operating conditions for a biodiesel reaction in batch



and continuous mode, showing that the SPC design was able to enhance the mass transfer by inducing droplets breakage and emulsion formation.

Phan and Harvey (2010) developed new baffle designs for the mesoOBR, the central baffle and helical design (Figure 2.12 (B) and (C)). The new design incorporated sharp edges within the geometry to imitate similar mixing conditions to the conventional OBR. The central baffle design was fabricated with a 2 mm threaded rod and fitted with periodically spaced 4 mm diameter hexagonal solid discs. The helical baffle design consisted of 1.2 mm coiled wire with a 7.5 mm pitch, similar to those found in the conventional OBR. Regarding the mixing performance of a helically baffled mesoOBR, they found that the mixing inside the helical baffle was enhanced through the formation of a swirling flow originating from the interaction between the centre flow and the helical geometries. This finding was confirmed by Solano *et al.* (2012) who assessed the flow pattern using a numerical solution. They observed the formation of swirled flow at the centre of the helical design with rotation that depends on the reversing motion of the oscillation.

Phan *et al.* (2010, 2011, 2012) described the benefit of the helical baffle and wire wool for mixing immiscible liquids. They found enhanced mixing of fluids at a higher degree of plug flow over a wider oscillatory range than any other baffle design (Phan and Harvey, 2010; Phan *et al.*, 2011a; Phan and Harvey, 2012). However, they concluded that the helically baffled design exhibits limited performance when used for a biphasic reaction, observing indistinct step changes when different operating parameters were subsequently employed.

Eze *et al.* (2013) demonstrated the advantage of an integral baffle mesoOBR for the continuous esterification of hexanoic acid with methanol using a heterogeneous catalyst (PrSO<sub>3</sub>H-SBA-15). They observed a clear step change in conversion when changing the operating parameters. They also reported an increase in turnover frequency (TOF) from 31 h<sup>-1</sup> in a stirred tank reactor to 57 h<sup>-1</sup> in the integral baffle design mesoOBR due to the reduced level of water poisoning in the continuous tubular reactor compared to the stirred tank.

### 2.6.3 Heat pipe OBR

The heat pipe is a heat transfer device based on two principles, thermal conductivity, and phase transition. In a heat pipe, the thermal energy is transferred from one point to another via the evaporation and condensation of a working fluid (Reay *et al.*, 2006). In this regard, the heat pipe does not function to reduce temperature at any point, but it tends to equalise the temperature between both ends. At a much hotter interface, the working fluid rapidly evaporates, absorbing the latent heat of evaporation, thus increasing the vapour pressure near the interface (McDonough *et al.*, 2016). The vapor pressure difference between the hot interface and cooler interface on the other end acts as a driving force between both ends. The latent heat is released at the cooler end causing condensation of the working fluid, the cooled working fluid then returns to the hot interface to complete the cycle via gravity, capillary or centrifugal force (McDonough *et al.*, 2016). Normally, a wick structure is required to allow the return of the fluid by capillary action, with the wick embedded alongside the heat pipe assembly either by parallel grooves or sintered metal powder. A thermosiphon is a vertically oriented heat pipe, with the condenser part was located above the evaporator (see Figure 2.13). This arrangement allows the condensed working fluid to flow towards the evaporator using gravity.

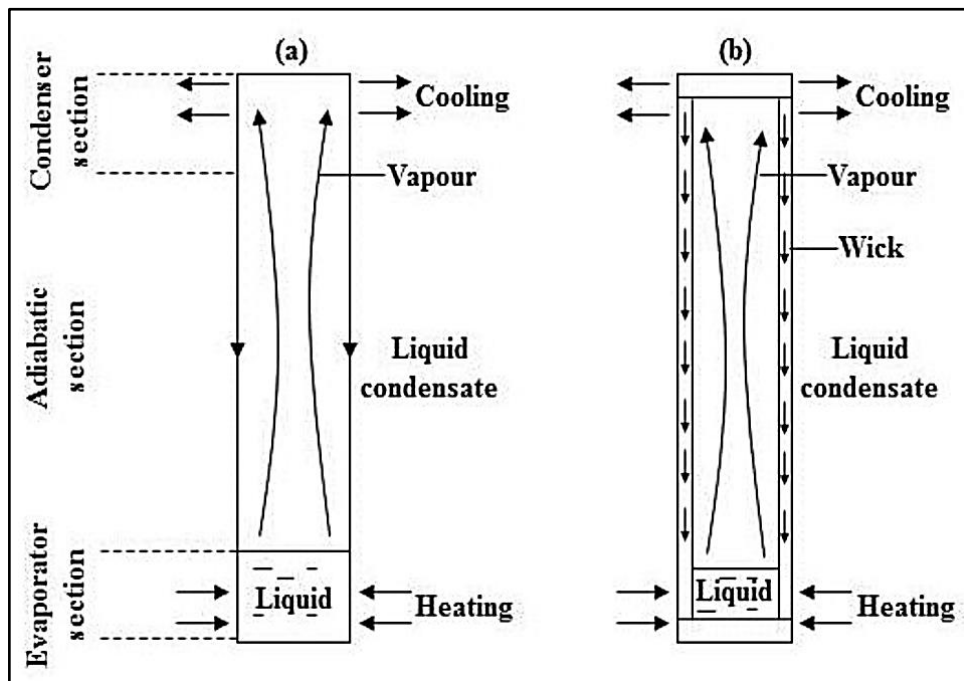


Figure 2.13. The mechanism of a heat pipe OBR (Reay *et al.*, 2006).

The heat pipe is usually built as a sealed pipe where the heat pipe is partially filled with working fluid prior to removing the air to create a vacuum (Reay *et al.*, 2006). The working fluid is selected based on the operating temperature range of the process. A temperature higher than the working fluid boiling point would prohibit condensation, while a lower temperature would not be able to evaporate the working fluid. This system of evaporating and cooling working fluid allows a higher heat transfer coefficient compared to conventional thermal conductor such as copper. Table 2.5 shows examples of working fluids and their temperature range.

<b>Working fluid</b>	<b>Temperature range</b>
liquid helium	2–4 K
ammonia	213–373 K
ethanol	273–403 K
methanol	283–403 K
water	298–573 K
mercury	523–923 K
sodium	873–1473 K
indium	2000–3000 K

Table 2.5. Examples of working fluids and their temperature range (Reay *et al.*, 2006).

The term heat pipe was first used by George Grover in his patent in 1963 (Löwe *et al.*, 2009). Extensive development of heat pipe was later conducted by NASA for space flight applications. Subsequently, there has been worldwide application of heat pipes as part of computer’s central processing unit (CPU) cooling systems. In addition, heat pipes are also applied in solar thermal systems (Wong *et al.*, 2014).

The integration of heat pipes into chemical reactors was reported by Lowe *et al.* (2009) for the synthesis of an ionic liquid. They employed a CPU cooling unit integrated to a chemical reactor, allowing the flow rate of the exothermic reaction to be increased further as the point of thermal runaway shifted higher. Wong *et al.* (2014) demonstrated the use of heat pipe in the CO removal

from a CO/H<sub>2</sub> mixture as an approach to control the temperature. According to their findings, the utilisation of heat pipe facilitates a lower temperature increase at the inlet. In a recent study, McDonough *et al.* (2016) integrated a thermosiphon with a helically baffled mesoOBR (Heat Pipe OBR or HPOBR) for an exothermic imination reaction. They studied the effect of mixing, net flow and working fluid filling ratios on the isothermalisation of the reaction, concluding that the HPOBRs were able to reduce the maximum reaction temperature below the boiling point of the reactant, allowing an isothermal condition. In this work, the utilisation of HPOBR as an approach to reduce energy cost by passive isothermalisation was investigated and compared with the jacketed helically baffled mesoOBR.

#### **2.6.4 Additive manufacturing (AM)**

The advent of additive manufacturing (AM) demonstrated the emerging new concept of manufacturing where items typically made using large machinery and complicated machining process could be made rapidly using a 3D-printer. Three-dimensional objects can be created layer upon layer based on designs made on computers using various design software. Among many technologies that have been developed, stereolithography (SLA) and fused deposit modelling (FDM) are among the most common (Bártolo and Gibson, 2011). SLA was first coined by Charles W. Hull in his patent in 1984, where he described a 3D-printing technique involving photopolymerisation, where light causes resin molecules to link forming polymers (Hull, 1984). This technique has increasingly gained interest in research labs, where many types of apparatus and reactors have been designed and created. Symes *et al.* (2012) and Kitson *et al.* (2016) successfully demonstrated the application of 3D-printed chemical reactors for chemical synthesis. Further development in the AM field for chemical reactions has resulted in the fabrication of fluidic devices for continuous flow applications (Kitson *et al.*, 2012; Dragone *et al.*, 2013; Mathieson *et al.*, 2013). Recently, Okafor *et al.* (2017) studied the possibility of manufacturing a continuous flow oscillatory baffled reactor (COBR) using SLA techniques for the synthesis of silver nanoparticles. They observed an improved mixing pattern over conventional tubular reactor besides able to work under back pressure. Their report showed the flexibility of designing a complex reactor structure which was fabricated using the AM technique. McDonough *et al.* (2019) studied the plug flow performance of coil-in-coil reactor using 3D-printing, see Figure 2.14. They designed and fabricated a complex geometry, which would be labour-intensive to produce similar dimensions using conventional method. These new designs allow achievement of plug flow behaviour at lower frequency ( $f = 0.25$  Hz) compared to a bigger dimension reactor.



*Figure 2.14. Various design of 3D-printed reactors (McDonough et al., 2019).*

In this work, a new orifice baffle design in mesoscale was designed and fabricated using 3D-printing technology for screening of continuous epoxidation of (R)-(+)-limonene and  $\alpha$ -pinene in the mesoOBR platform. The materials and dimension of the 3D-printed reactors are discussed in section 3.2.3 in Chapter 3.

## Chapter 3 Materials and Methods

This chapter describes the materials, experimental procedures, reactors, and analysis techniques used throughout this study.

### 3.1 Materials

The chemicals used in this study are shown in Table 3.1 below and were obtained from Sigma-Aldrich (Merck UK). Their physicochemical properties are shown in Table 3.2.

Chemicals	Molecular formula	% Assay	Description/purposes
(R)-(+)-limonene	C <sub>10</sub> H <sub>16</sub>	97 %	substrate
$\alpha$ -pinene	C <sub>10</sub> H <sub>16</sub>	98 %	substrate
hydrogen peroxide	H <sub>2</sub> O <sub>2</sub>	30 % wt. in H <sub>2</sub> O	oxidant preparation
sodium tungstate dihydrate	Na <sub>2</sub> WO <sub>4</sub> .2H <sub>2</sub> O	≥99 %	oxidant preparation
phosphoric acid (48.5 %)	H <sub>3</sub> PO <sub>4</sub>	85 wt. % in H <sub>2</sub> O	oxidant preparation
sulphuric acid (42.5 %)	H <sub>2</sub> SO <sub>4</sub>	≥95 %	increase acidity
potassium permanganate solution (0.02 M)	KMnO <sub>4</sub>	0.1 N	H <sub>2</sub> O <sub>2</sub> titration
sodium sulphate	Na <sub>2</sub> SO <sub>4</sub>	≥99 %	drying agent/salt
toluene	C <sub>7</sub> H <sub>8</sub>	99 %	solvent
1,2-dichloroethane	C <sub>2</sub> H <sub>4</sub> Cl <sub>2</sub>	99 %	solvent
<i>p</i> -cymene	C <sub>10</sub> H <sub>14</sub>	99 %	solvent

acetonitrile	$C_2H_3N$	99 %	solvent
methyltrialkyl (C <sub>8</sub> -C <sub>10</sub> ) ammonium chloride (Adogen 464™)	$C_{84}H_{180}Cl_3N_3$	NA	phase transfer catalyst
sodium chloride	NaCl	≥99 %	destabilise emulsion
naphthalene	$C_{10}H_8$	99 %	analysis/GC internal standard
chloroform	$CHCl_3$	99 %	analysis/GC sample dilution
limonene-1,2-epoxide	$C_{10}H_{16}O$	97 %	analysis/product identification
limonene-8,9-epoxide	$C_{10}H_{16}O$	97 %	analysis/product identification
bis-epoxide	$C_{10}H_{16}O_2$	≥98 %	analysis/product identification
limonene-1,2-diol	$C_{10}H_{18}O_2$	≥97 %	analysis/product identification
carveol	$C_{10}H_{16}O$	≥98 %	analysis/product identification
carvone	$C_{10}H_{14}O$	≥98.5 %	analysis/product identification
α-pinene oxide	$C_{10}H_{16}O$	97 %	analysis/product identification
sobrerol	$C_{10}H_{18}O_2$	99 %	analysis/product identification

campholenic aldehyde	C <sub>10</sub> H <sub>16</sub> O	≥96 %	analysis/product identification
pinanediol	C <sub>10</sub> H <sub>18</sub> O <sub>2</sub>	99 %	analysis/product identification
verbenone	C <sub>10</sub> H <sub>14</sub> O	≥99 %	analysis/product identification
verbenol	C <sub>10</sub> H <sub>16</sub> O	95 %	analysis/product identification

NA = Not available

*Table 3.1 List of chemicals used.*

<b>Chemicals</b>	<b>Molecular weight (g mol<sup>-1</sup>)</b>	<b>Boiling point (°C)<sup>a</sup></b>	<b>Density (kg m<sup>-3</sup>)<sup>b</sup></b>
(R)-(+)-limonene	136.24	176	841
α-pinene	136.24	155	858
hydrogen peroxide	34.01	150.2	1110
limonene-1,2-epoxide	152.24	197	929
α-pinene oxide	152.24	189	964
limonene bis-epoxide	168.24	242	1028 <sup>c</sup>
limonene-1,2-diol	170.25	241	925
carveol	152.24	226	952
carvone	150.22	231	959
campholenic aldehyde	152.24	201	926
sobrerol	170.25	270	1051
pinanediol	170.25	263	1091



verbenol	152.24	214	992
verbenone	150.22	227	975 <sup>c</sup>
toluene	92.14	110	867
1,2-dichloroethane	98.95	84	1253
<i>p</i> -cymene	134.21	177	857
acetonitrile	41.05	82	786

<sup>a</sup>Boiling point at 760 mmHg; <sup>b</sup>density at 25 °C; <sup>c</sup>density at 20 °C

*Table 3.2 Properties of the reactant, solvents, and products.*

## 3.2 Experimental set-up and equipment

### 3.2.1 Batch reactor

Batch epoxidation of (R)-(+)-limonene and  $\alpha$ -pinene was performed to identify the conditions with highest selectivity to epoxides and to benchmark the development of a continuous process. Batch epoxidation was performed in a 150 ml jacketed flask (Figure 3.1) fitted with a four-neck lid that allowed connection to a thermocouple, FTIR spectroscopy probe and two sampling ports (one sealed). The internal diameter of the flask was 8 cm with a height of 10 cm. A water bath provided heating via water circulation inside the jacket.

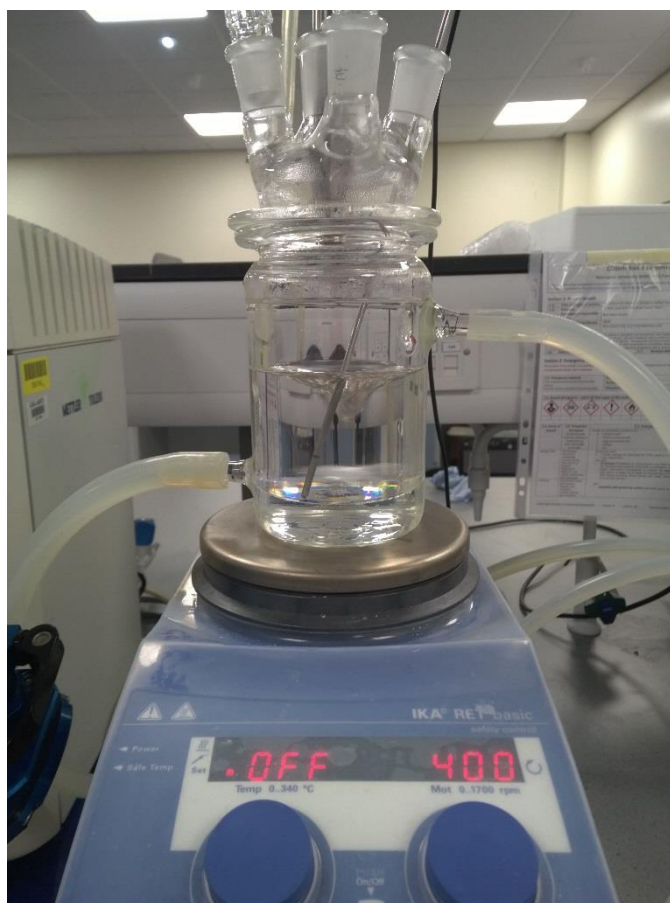


Figure 3.1. Jacketed four-neck batch reactor.

### 3.2.2 Helically and integrally baffled mesoOBR

Helical and integral baffle designs were used to perform the continuous epoxidation of (R)-(+)-limonene and  $\alpha$ -pinene with 30 wt.%  $\text{H}_2\text{O}_2$ . The performance of these reactors was compared to the orifice baffles. The mesoOBR consisted of two interconnected jacketed glass tubes with a total length of 1750 mm, 5 mm inner diameter and 8 mm outer diameter, with either helical baffles or an integral baffle design (Figure 3.2 (A) and (B)). The helical baffles used consisted of 1.2 mm thick stainless-steel coiled wire at 7.5 mm pitch and an inner diameter between the stainless-steel coiled wire of approximately 2.5 mm. The integral baffle design had smooth constrictions of 2.5 mm diameter, giving a 25 % open cross-sectional area and they were regularly spaced 7.5 mm apart (Eze *et al.*, 2017; Eze and Harvey, 2018). The total volumes for the integral and helical baffles designs were 28 mL and 30 mL, respectively. The helically and integrally baffled mesoOBR have been used previously in many mesoOBR studies (Phan and Harvey, 2010; Reis *et al.*, 2010; Phan and Harvey, 2011; Phan *et al.*, 2011b; Phan *et al.*, 2012; Harvey, 2013; Rasdi *et al.*, 2013; Eze *et al.*, 2017).

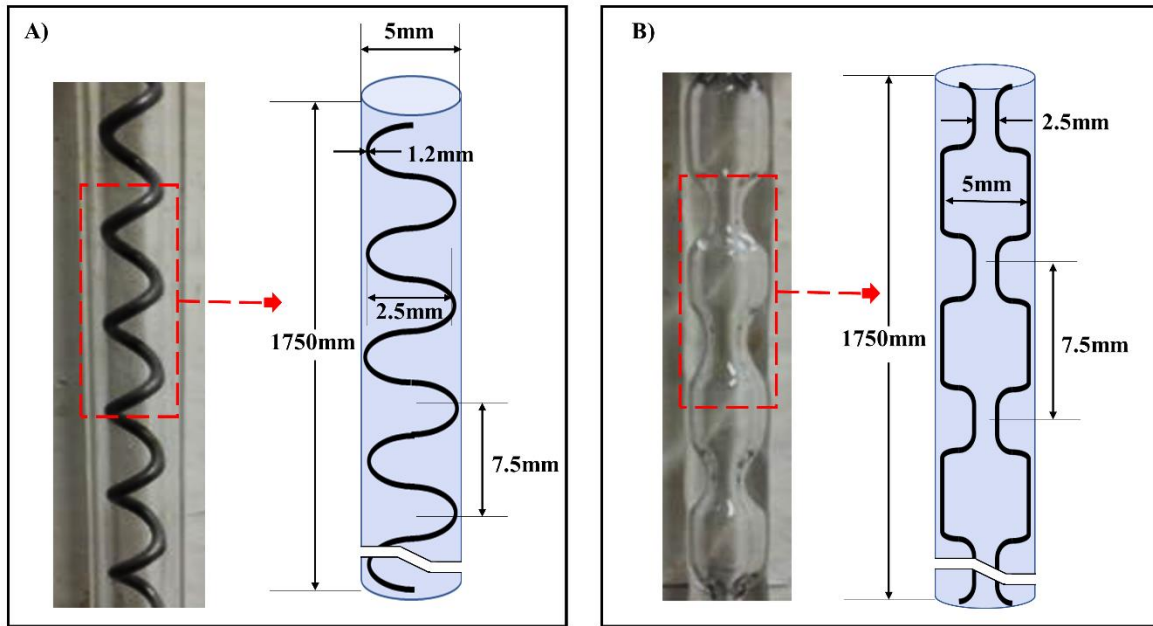
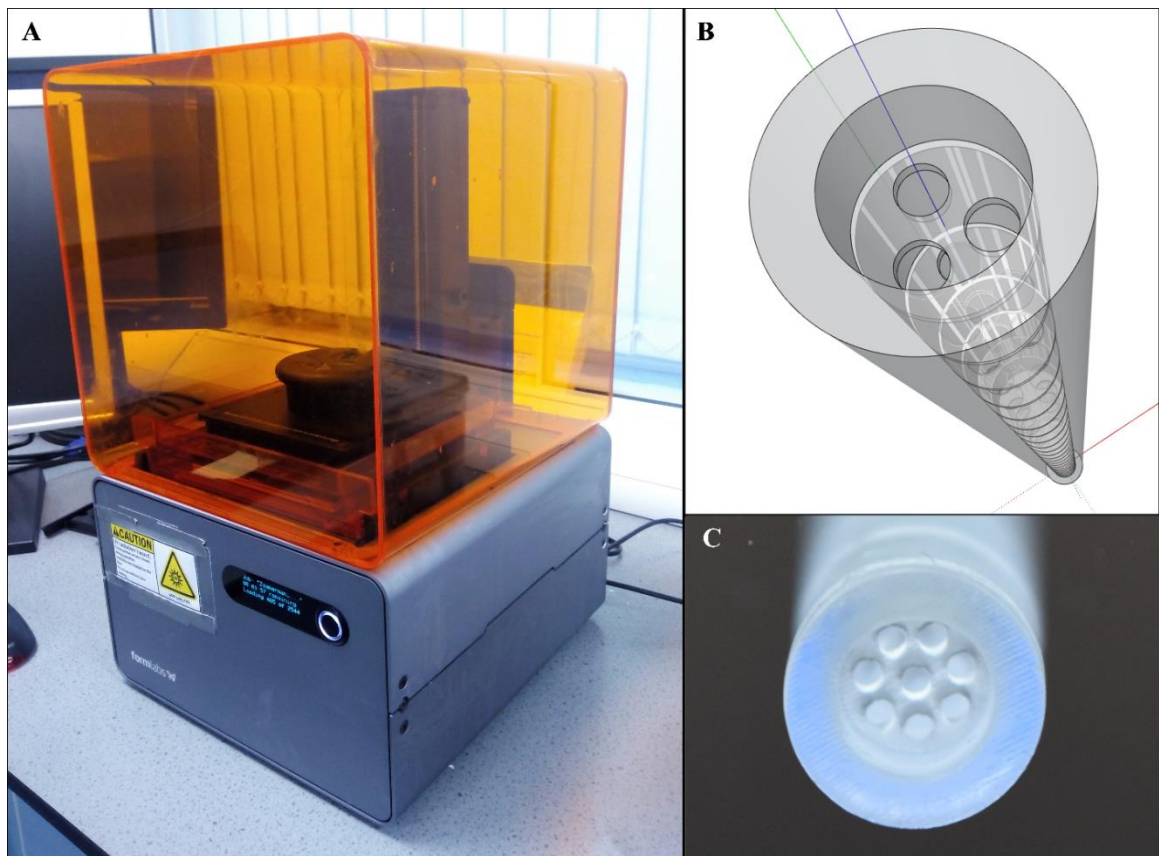


Figure 3.2. Configuration and schematics of the conventional mesoOBRs design: (A) helical baffles and (B) integral baffles.

### 3.2.3 Additive manufacturing for fabrication of orifice baffles using a 3D- printer

The AM technique was employed in the fabrication of orifice baffles at the mesoscale. This method allowed quick fabrication and printing of the desired reactor design using a high-resolution 3D-printer, the SLA-based Form2 3D-printer as shown in Figure 3.3 (A). The 3D-printed reactors were created using a single-point laser that tracked a bed of resin via photopolymerisation of resins consisting of methyl acrylate. Being translucent, this material has the advantage of identification of trapped bubbles, which can be purged. The printed reactor was built layer upon layer with an (x-y)-axis resolution of 140  $\mu\text{m}$  and z-axis resolution of 100  $\mu\text{m}$  (Figure 3.3 (C)), which ensured high rigidity after prior design work was conducted using SketchUp software as shown in Figure 3.3 (B).



*Figure 3.3. Application of the AM technique for the fabrication of orifice baffles at the millimetre scale: (A) Form2 SLA 3D-printer, (B) a SketchUp drawing model showing a tri-orifice baffle, and (C) a printed, cured and cleaned multi-orifice baffled mesoOBR reactor.*

The single orifice baffle was designed with an orifice diameter of 2.5 mm to fit in the existing 5 mm inner diameter glass tube (Figure 3.4 (A)). The tri-orifice and multi-orifice baffles were created as stand-alone reactors to ensure rigidity (Figure 3.4 (B) and (C)), with a diameter of 1.7 mm and 1 mm, respectively.

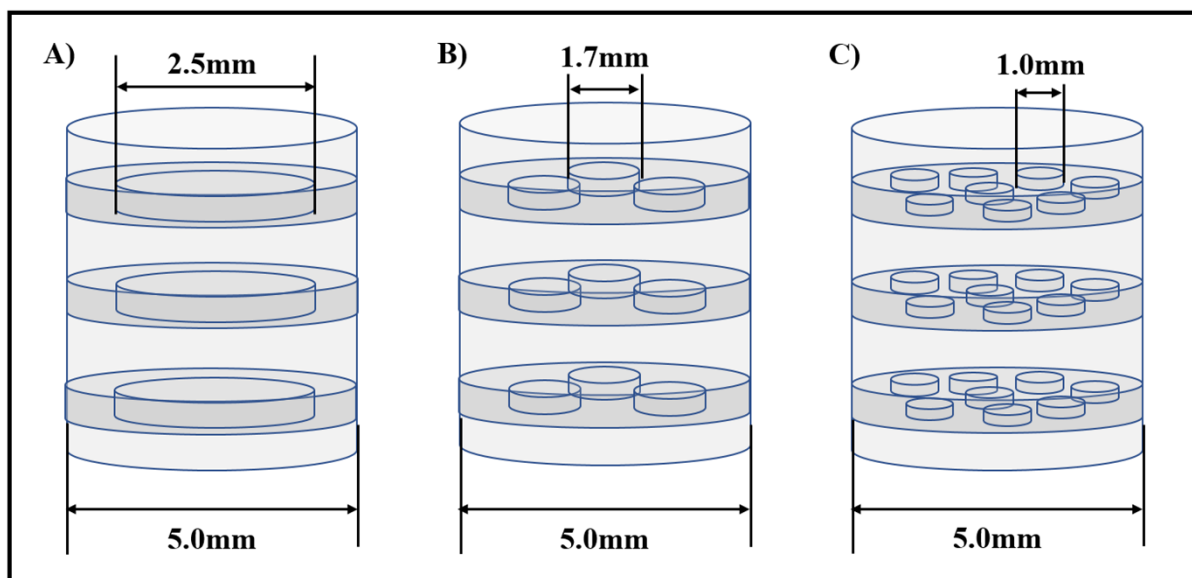
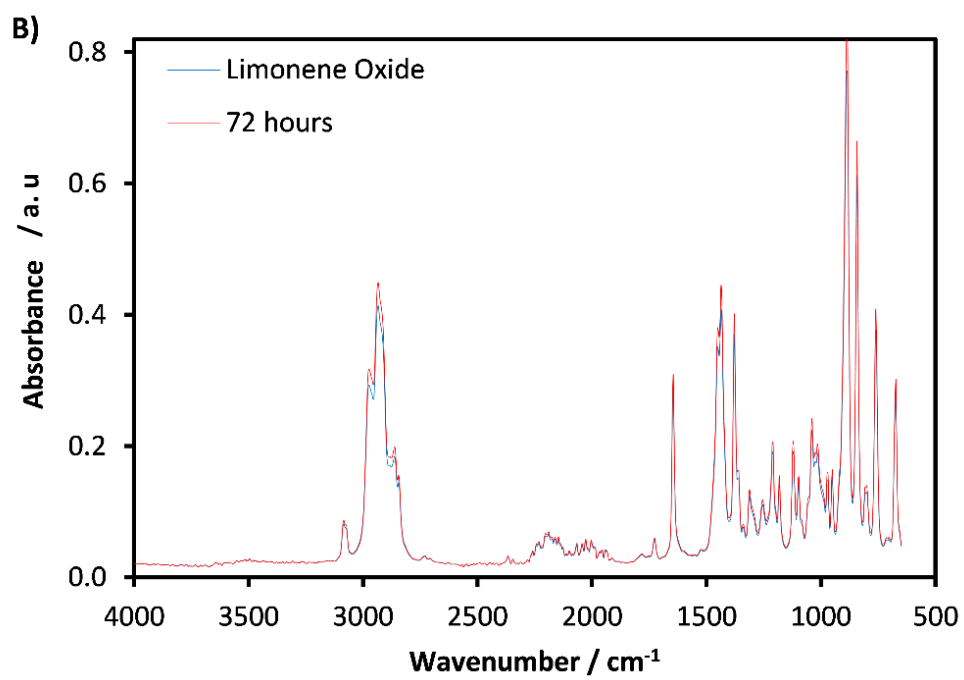
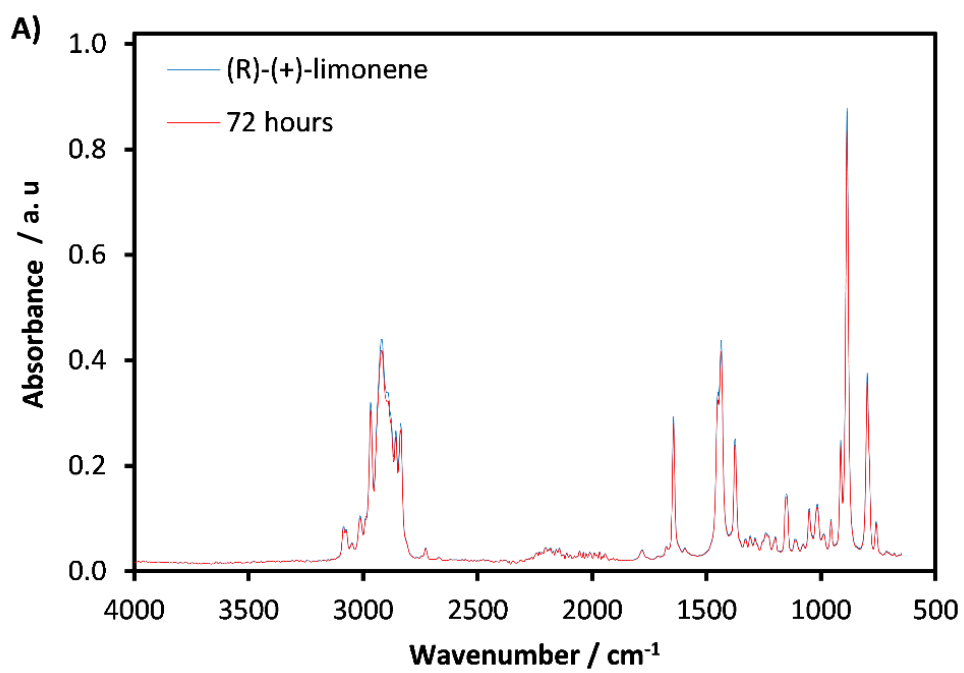


Figure 3.4. Configuration and schematics of the 3D-printed orifice mesoOBRs designs: (A) single orifice, (B) tri-orifice, and (C) multi-orifice.

Upon fabrication, the excess uncured resin was removed using isopropyl alcohol before being dried under sunlight at room temperature. Excess materials created as support during printing were removed. The total manufacturing time was typically up to 4 h. Compatibility of the 3D-printed material was tested with the chemicals used, by immersing in (R)-(+)-limonene,  $\alpha$ -pinene and limonene/ $\alpha$ -pinene oxides for 72 h. Analysis of the immersion liquids after 72 h using Fourier Transform Infra-red spectroscopy (FTIR) showed no degradation of the reactor material, which confirms their suitability for the epoxidation process, see Figure 3.5 (A – D).



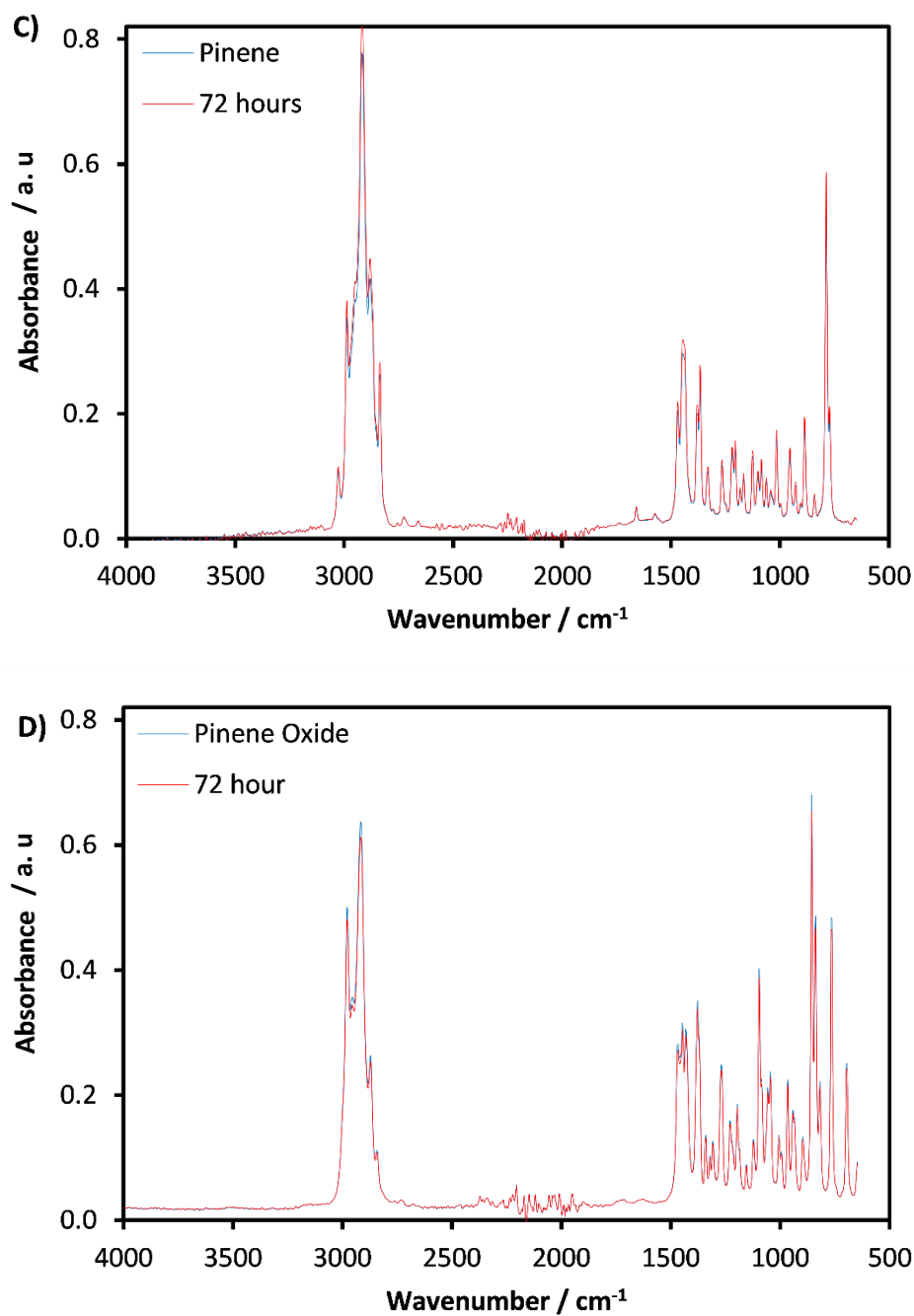


Figure 3.5. FTIR spectra of pure component and samples taken after submersion of 3D-printed materials for 72 hours; (A) (R)-(+)-limonene, (B) limonene-1,2-epoxide, (C)  $\alpha$ -pinene and (D)  $\alpha$ -pinene oxide.  $8\text{cm}^{-1}$  resolution, 40 averaged scans, 15 seconds per scan set.

The experimental set-up for the 3D-printed tri-orifice and multi-orifice baffles was similar to that of the mesoOBRs as described in section 3.4.4, except that the printed reactors had no heating jackets, so the temperature control was achieved by fully submerging the devices in a 28 L temperature-controlled water bath (LAUDA ECO Silver).

### 3.2.4 Laboratory equipment and accessories

The laboratory equipment, accessories and their errors are listed below:

- a) Water bath: temperature-controlled VWR MX7LR-20 provided heated water circulation for the jacketed mesoOBR ( $\pm 0.05$  °C), Grant (TX150) provided heated water circulation for the jacketed batch reactor ( $\pm 0.05$  °C) and LAUDA ECO Silver provided heating for tri-orifice and multi-orifice baffles in a 28 L tank ( $\pm 0.05$  °C).
- b) Hotplates and stirrer: IKA RCT Basic hotplates were used to provide heating and stirring for batch reactions, reagents for continuous reactions and catalyst preparation ( $\pm 0.05$  °C).
- c) Thermocouple: K-type Fuke thermocouple for temperature measurement ( $\pm 0.05$  °C).
- d) Rotary evaporator: BUCHI R-215 rotavapor for product purification.
- e) pH meter: Mettler Toledo (7excellence) pH meter to measure the pH of the aqueous phase ( $\pm 0.001$ ).
- f) Electronic weighing balance: Mettler Toledo (NewClassic MS,  $\pm 0.001$  g).
- g) Syringe pumps: Tri-Continent C3000 series syringe pumps were used to supply the reactant net flow rates and generate fluid oscillation.
- h) Sample storage: BioCold freezer operated at  $-20$  °C.

## 3.3 Experimental procedure

### 3.3.1 Preparation of the oxidant

The homogeneous polytungstophosphate catalyst ( $\{\text{PO}_4[\text{WO}(\text{O}_2)_2]_4\}^{3-}$ ) was prepared according to an existing procedure (Hachiya *et al.*, 2012). The tungsten source,  $\text{Na}_2\text{WO}_4 \cdot 2\text{H}_2\text{O}$  (0.4 g), was first added to a stirred  $\text{H}_2\text{O}_2$  (30 wt. % , 122 mmol) solution in a 25 mL beaker at the desired temperature, typically 50 °C. A hotplate (IKA RCT Basic) was used to heat and stir the solution at 750 rpm. Then, approximately 28  $\mu\text{L}$  of  $\text{H}_3\text{PO}_4$  (42.5 % , 0.06 mmol) was added to the well-mixed solution, and the pH of the solution was adjusted to  $< 1.0$  with 0.27 mL of  $\text{H}_2\text{SO}_4$  (48.5 % , 4 mmol) before the addition of the inorganic salt,  $\text{Na}_2\text{SO}_4$  (5.2 g), which was dissolved by continuous stirring until a clear and uniform solution was formed. The catalyst was characterised using NMR as shown in Figure 3.6 (A) and (B).



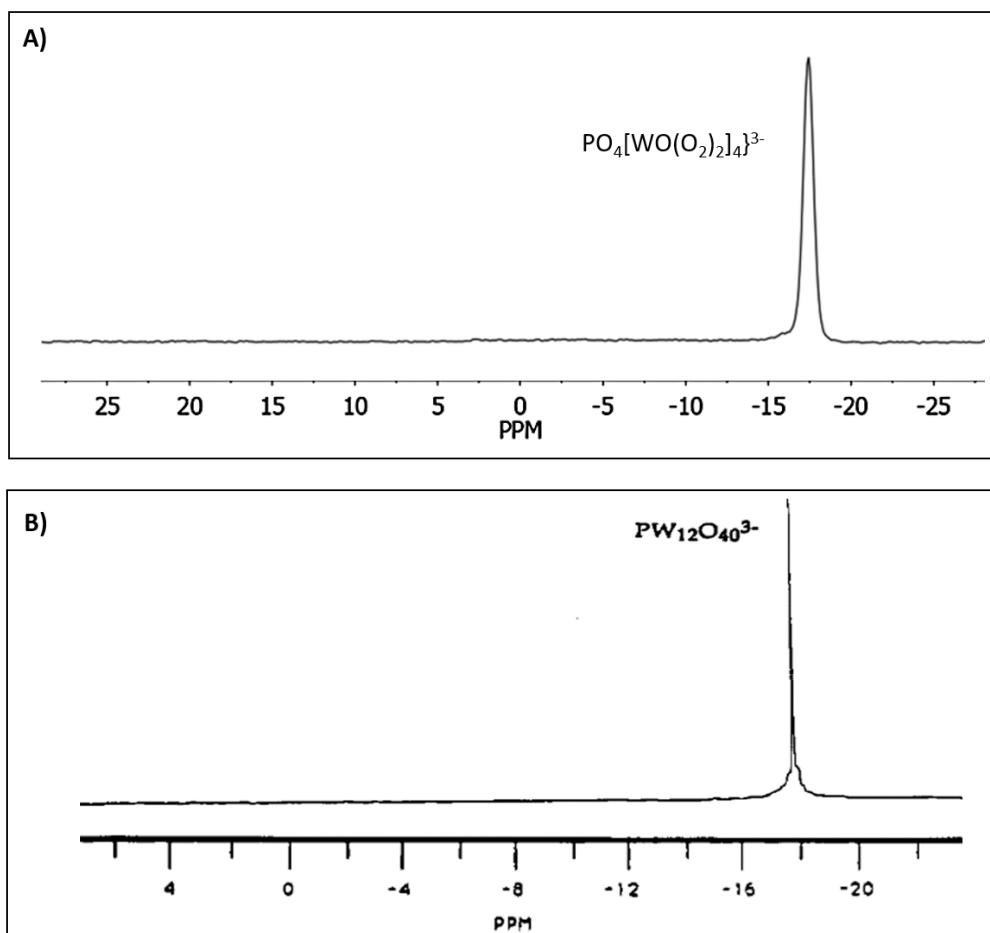


Figure 3.6. NMR spectra of (A) the prepared polytungstophosphate catalyst ( $\{PO_4[WO(O_2)_2]_4\}^{3-}$ ) and (B) polytungstophosphate characterized in (Duncan et al., 1995).

### 3.3.2 Batch epoxidation

The batch epoxidation experiments were conducted using a jacketed 150 mL flask reactor equipped with a thermocouple to provide temperature control, and heated via circulation of hot water from a temperature-controlled water bath (Grant TX 150). First, the reactor was charged with 16.62 g of (R)-(+)-limonene/ $\alpha$ -pinene (122 mmol) and 1 g of phase transfer catalyst, Adogen 464®, then the solvent (500 mol% relative to (R)-(+)-limonene or  $\alpha$ -pinene) was added to achieve isothermal conditions. The mixture was heated to the desired temperature (typically between 30 °C and 70 °C) and mixed vigorously using a magnetic stirrer at 1250 rpm (IKA RCT Basic). The mixing speed was chosen based on the mixing study performed on both (R)-(+)-limonene and  $\alpha$ -pinene (Chapter 4 and 5). The prepared oxidant (12.5 mL) was later added to the jacketed flask and allowed to react for up to 120 min. Samples (1 mL) were taken during the reaction at the selected time intervals of 5 min – 120 mins for quantification using gas chromatography (GC) analysis. The reaction was performed using an *in situ* FTIR for

qualification purpose. The FTIR probe was inserted in the reaction mixture to monitor the epoxides formation throughout the reaction time. Further discussion on the FTIR is in the analysis section (section 3.4.2). Figure 3.7 shows a typical experimental set-up for the batch (R)-(+)-limonene/ $\alpha$ -pinene epoxidation using *in situ* FTIR spectroscopy.

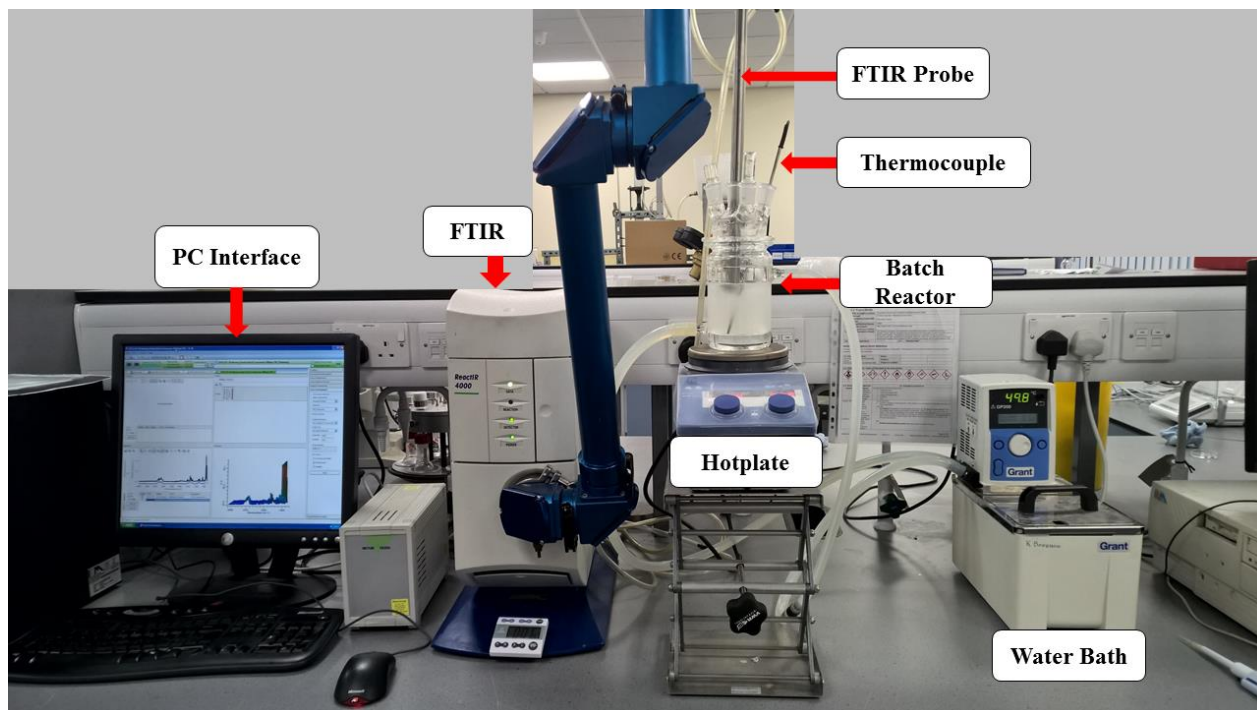


Figure 3.7. Experimental set-up for batch epoxidation using *in situ* FTIR spectroscopy.

### 3.3.3 Screening of process parameters

Seven process parameters were screened in batch mode to identify the process optima. The effect of mixing, amount of phase transfer catalyst, temperature, oxidant amount,  $\text{Na}_2\text{SO}_4$  amount, acid concentration and solvent type was screened for the epoxidation of (R)-(+)-limonene. Except for the amount of phase transfer catalyst and  $\text{Na}_2\text{SO}_4$ , all mentioned reaction parameters were screened for the epoxidation of  $\alpha$ -pinene, with the amount of catalyst precursor,  $\text{Na}_2\text{WO}_4 \cdot 2\text{H}_2\text{O}$  and  $\text{H}_3\text{PO}_4$  required for the epoxidation of  $\alpha$ -pinene being double that of (R)-(+)-limonene due to the lower overall reactivity of  $\alpha$ -pinene epoxidation. The range of operating parameters selected for the screening was guided by prior experiments, literature, and safety concern of using  $\text{H}_2\text{O}_2$ . The typical experimental conditions for the epoxidation of (R)-(+)-limonene and  $\alpha$ -pinene are shown in Table 3.3.

	(R)-(+)-limonene	$\alpha$ -pinene
mixing speed (rpm)	1250	1250
PTC (g)	1	1
temperature ( $^{\circ}$ C)	50	50
(R)-(+)-limonene or $\alpha$ -pinene (g)	16.62	16.62
H <sub>2</sub> O <sub>2</sub> (g)	13.83	13.83
Na <sub>2</sub> WO <sub>4</sub> .2H <sub>2</sub> O (g)	0.2	0.4
42.5 % wt. H <sub>3</sub> PO <sub>4</sub> (g)	0.038	0.076
Na <sub>2</sub> SO <sub>4</sub> (g)	5.7	5.7
48.5 % wt. H <sub>2</sub> SO <sub>4</sub> (g)	1.15	1.15
solvent (mol%)	toluene (500 mol%)	toluene (500 mol%)

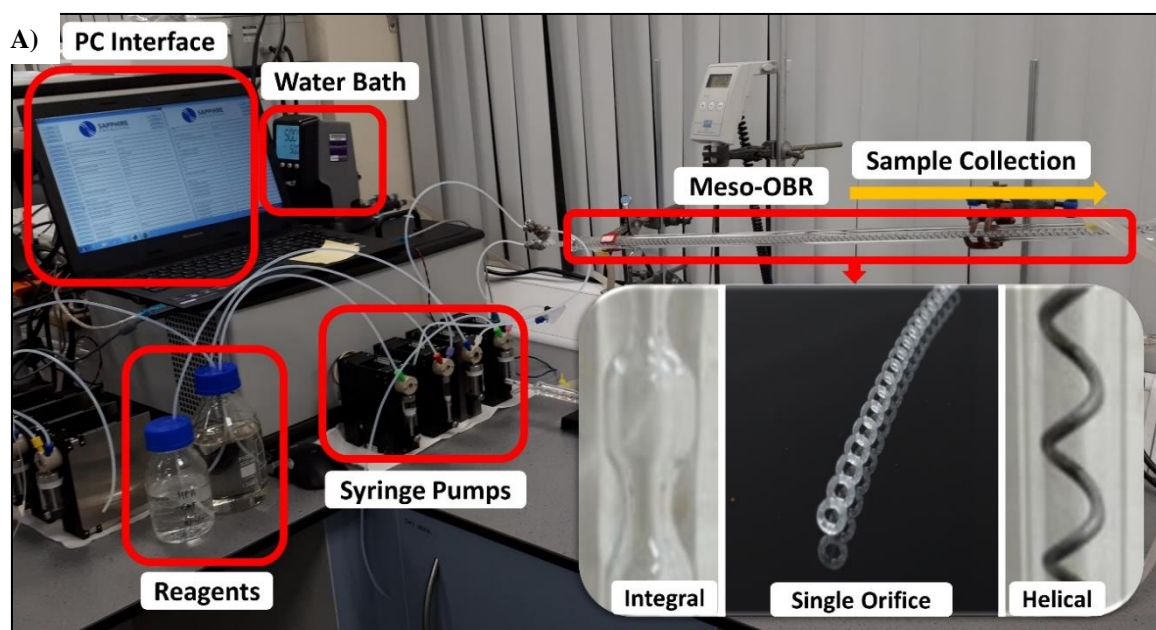
Table 3.3. Experimental conditions for the epoxidation of terpenes.

The effect of mixing was investigated by varying the stirring speed from 250 to 1500 rpm, while the other parameters in Table 3.3 were kept constant. The effect of PTC on the epoxidation was determined by varying the amount of PTC from 0 to 2.0 g using (R)-(+)-limonene as a representative terpene due to similarities of the catalytic system for (R)-(+)-limonene and  $\alpha$ -pinene. Reaction temperatures ranged from 30  $^{\circ}$ C to 60  $^{\circ}$ C for the (R)-(+)-limonene epoxidation and 30 $^{\circ}$ C to 70  $^{\circ}$ C for  $\alpha$ -pinene epoxidation to investigate the effects of reaction temperature. The effect of the amount of oxidant (H<sub>2</sub>O<sub>2</sub>) on the epoxidation of (R)-(+)-limonene and  $\alpha$ -pinene was studied by varying the amounts of H<sub>2</sub>O<sub>2</sub> from 13.83 g (100 mol%, 122 mmol) to 27.66 g (200 mol%, 244 mmol). The effect of the quantity of Na<sub>2</sub>SO<sub>4</sub> on the epoxidation of (R)-(+)-limonene was performed by varying the amount of Na<sub>2</sub>SO<sub>4</sub> from 2.5 g to 7.5 g. The amount used for screening (5.2 g and 5.7 g) was calculated from the saturation of Na<sub>2</sub>SO<sub>4</sub> in H<sub>2</sub>O at 30  $^{\circ}$ C and 50  $^{\circ}$ C, respectively. The calculation for the amount of Na<sub>2</sub>SO<sub>4</sub> is shown in Appendix A. A control experiment was also performed in the absence of Na<sub>2</sub>SO<sub>4</sub>. The effect of Na<sub>2</sub>SO<sub>4</sub>

was not studied on  $\alpha$ -pinene due to similarities of the system. The effect of acid concentration ( $\text{H}_2\text{SO}_4$ ) on the epoxidation of (R)-(+)-limonene and  $\alpha$ -pinene was performed by varying the amount of  $\text{H}_2\text{SO}_4$  from 0.38 g (0.02 M) to 1.15 g (0.06 M). The effect of solvent was determined by replacing toluene with either 1,2-dichloroethane, p-cymene or acetonitrile. The amount of solvent used was fixed at 500 mol% based on the amount of terpenes. Solvent-free conditions were set-up using terpenes in excess, between 16.62 g (100 mol%, 122 mmol) and 83.10 g (500 mol%, 610 mmol), while the other parameters were fixed.

### 3.3.4 Continuous epoxidation

Figure 3.8 (A) and (B) shows the typical experimental set-up for the continuous terpene epoxidation in the mesoOBRs, which were connected through Swagelok fittings to four C3000 series syringe pumps (TriContinent Ltd) via PTFE tubing of 1.5 mm inner diameter and 3.2 mm outer diameter.



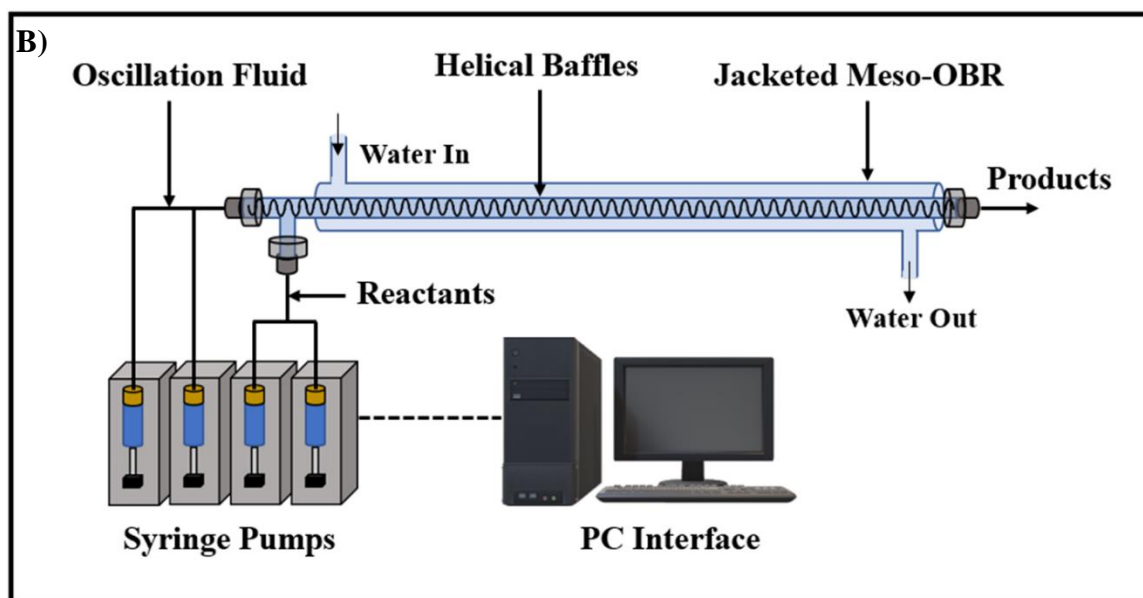


Figure 3.8. (A) Experimental set-up and (B) schematics for the continuous epoxidation of terpenes with  $H_2O_2$  using helically baffled mesoOBR.

Two of the syringe pumps were connected to the base of the mesoOBR and each fitted with 12.5 mL syringes to provide oscillations to the reactor through the bottom inlet. The oscillation fluid used was the organic phase ((R)-(+)-limonene or  $\alpha$ -pinene, phase transfer catalyst). The double oscillators provided vigorous multiphase mixing throughout the length of the mesoOBR in the range of frequencies of 1 Hz to 7.5 Hz and a centre-to-peak amplitude of 1 mm to 9 mm. The other two syringe pumps were fitted with a 5 mL syringe to provide net flow of both the organic phase and the prepared oxidant solution (aqueous phase). All pumps were connected to a PC interface which controlled the operation of the pumps and the desired flow rate. The oscillation frequency was regulated by the speed of syringe movement, while the oscillation amplitude was gained by the volume of liquid dispensed. A list of commands for the PC interface is shown in Appendix B. A temperature-controlled water bath (VWR MX7LR-20) was used to circulate water at a temperature between 30 °C to 60 °C through the outer jackets of the mesoOBRs to maintain the reaction temperature. The continuous epoxidation of (R)-(+)-limonene and  $\alpha$ -pinene was studied at 1:1 molar ratio to  $H_2O_2$  in an organic solvent-free condition. To prepare the organic phase, 16.62 g terpenes ((R)-(+)-limonene or  $\alpha$ -pinene) was weighed for every 1 g of phase transfer catalyst and placed in a 250 mL reagent bottle. The organic mixture was continuously stirred using a magnetic stirrer at 750 rpm and heated to the reaction temperature (50 °C) using a hotplate (IKA RCT Basic). To prepare the aqueous phase, 13.83 g of  $H_2O_2$  (30 wt. % in  $H_2O$ , 122 mmol), 0.4 g of  $Na_2WO_4 \cdot 2H_2O$ , 28  $\mu$ L of  $H_3PO_4$  (42.5 %, 0.06 mmol), 0.27 mL of  $H_2SO_4$  (48.5 %, 4 mmol) and 5.7 g of  $Na_2SO_4$  were placed in a 250 mL

reagent bottle. The mixture was continuously stirred using a magnetic stirrer at 750 rpm to ensure a uniform mixture and was heated to the reaction temperature (50 °C) using a hotplate (IKA RCT Basic). Prior to continuous reaction, the organic phase was initially pumped to fill the reactor, the organic phase was later pumped at specified flow rates depending on the residence times tested. The reaction began when the aqueous phase was pumped into the reactor at specified flow rates. The flow rates of both the aqueous and organic phases corresponded to an equimolar ratio of terpenes and H<sub>2</sub>O<sub>2</sub> and were calculated based on residence time between 5 min (6 mL min<sup>-1</sup>, Re<sub>n</sub> = 5.7) to 30 min (1 mL min<sup>-1</sup>, Re<sub>n</sub> = 1). A mixing study for various baffle types was performed at residence time between 5 min to 30 min and the mixing conditions used are shown in Appendix C. Various flow rates corresponding to different residence times are shown in Table 3.4.

<b>Flow rate (mL min<sup>-1</sup>)</b>	<b>Net flow Reynolds number (Re<sub>n</sub>)</b>	<b>Residence time (τ, min)</b>
6.0	5.7	5
3.0	2.9	10
2.0	1.9	15
1.5	1.4	20
1.2	1.1	25
1.0	1.0	30

*Table 3.4 Flow rate at each residence time for the continuous epoxidation in mesoOBR.*

To study the induction period, the performance of each baffle design (helical, integral, multi-orifice, tri-orifice and single orifice baffles) on the attainment of steady states for the continuous epoxidation was evaluated at a fixed residence time (τ) of 15 min (Re<sub>n</sub> = 2.0) with Re<sub>o</sub> ~ 1300. The mixing condition was chosen to provide enough mixing to overcome mass transfer limitation as discussed in section 6.3 of Chapter 6. The reactor was operated for 70 min for each baffle design tested, and samples were collected at 5 min intervals after 1 τ until 3 τ. The

reaction was performed continuously at 1:1 molar ratio of (R)-(+)-limonene to H<sub>2</sub>O<sub>2</sub> and 50 °C in an organic solvent-free environment.

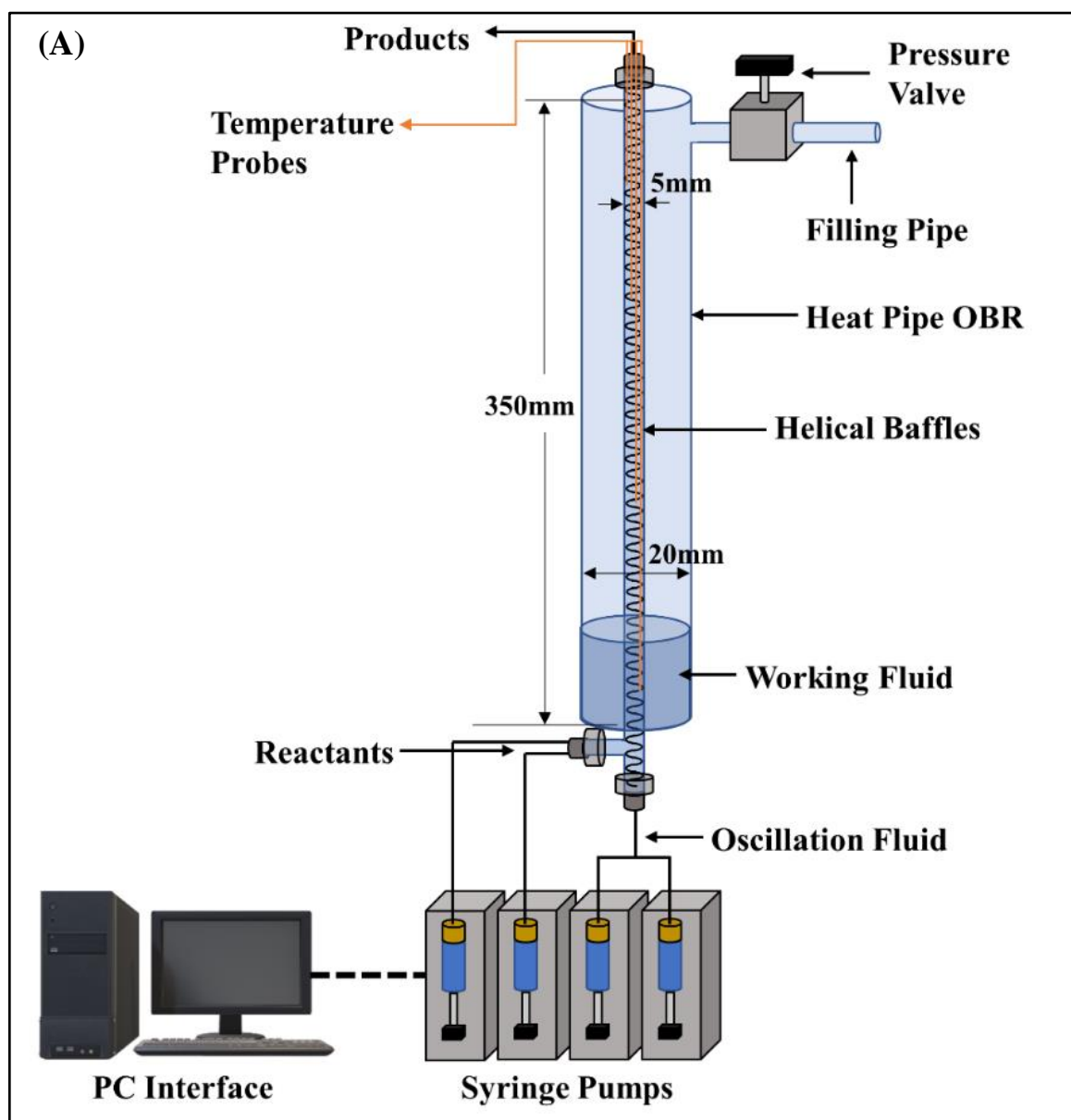
Steady state performances of the helically baffled and multi-orifice baffled mesoOBRs were evaluated through multi-steady state screening using ramped residence times, 1:1 molar ratio of terpenes to H<sub>2</sub>O<sub>2</sub> and 50 °C in an organic solvent-free environment. The mixing condition used was Re<sub>o</sub> of 1300 corresponding to a frequency of 5 Hz and an amplitude of 9 mm. The residence time was linearly ramped from  $\tau = 5$  min up to 25 min at an interval of 5 min.

### ***3.3.5 Heat pipe mesoOBR and temperature monitoring***

The heat pipe consisted of a helically baffled mesoOBR inner tube with a diameter of 5 mm within an annular outer tube of 20 mm with a total length of 350 mm (Figure 3.9 (A) and (B)). The heat pipe was constructed using stainless steel 316. The outer tube was welded and sealed to avoid leakage of the working fluid. A side inlet used for filling and draining was attached to the top part of the outer tube and was fitted with a pressure valve to maintain vacuum pressure. The inner tube mesoOBR was helically baffled to allow thermocouple placement. Four type-K thermocouples were fitted inside the inner tube and positioned at 23 mm (inlet), 123 mm, 230 mm, and 330 mm (outlet) from the bottom, respectively. The heat pipe mesoOBR had a volume of 6.5 mL, while the outer tube had a volume of 104 mL. The working fluid selected was methanol, because it has a boiling point of 65 °C, close to the reaction temperature for the epoxidation. The outer tube was filled with 25 mL of methanol before the vacuum was applied (10 mbar). It was envisaged that during operation, the exothermicity of the reaction near the inlet would be absorbed by the working fluid, causing the fluid to boil and evaporate. The evaporated fluid would then condense at the top part of the reactor, effectively distributing the exotherm at the inlet evenly throughout the reactor length, allowing an isothermal operation. The temperature measured by the thermocouples was channelled to a PC interface (PicoLog) through a data logger (TC-08). Average temperature values were recorded once the system reached a steady state. The temperature profile for the jacketed helically baffled mesoOBR was also investigated using type-K temperature probes placed inside the reactor at the designated points from the inlet, 23 mm, 123 mm, 230 mm and 330 mm, to match the similar point in the heat pipe mesoOBR. The temperature monitored by the probe at one point was allowed to reach steady state before the probe was moved to the next point.

The temperature profile for both heat pipe OBR and helically baffled mesoOBR was studied at a molar ratio of 1:1 of (R)-(+)-limonene to H<sub>2</sub>O<sub>2</sub> at an initial temperature of 50 °C in an organic

solvent-free environment. The initial temperature of the heat pipe was attained by preheating the reactants using hotplates prior to pumping into the reactor. The mixing condition used was  $Re_o$  of 1300 corresponding to a frequency of 5 Hz and an amplitude of 9 mm, and the reaction residence times were between 2.5 min and 20 min.





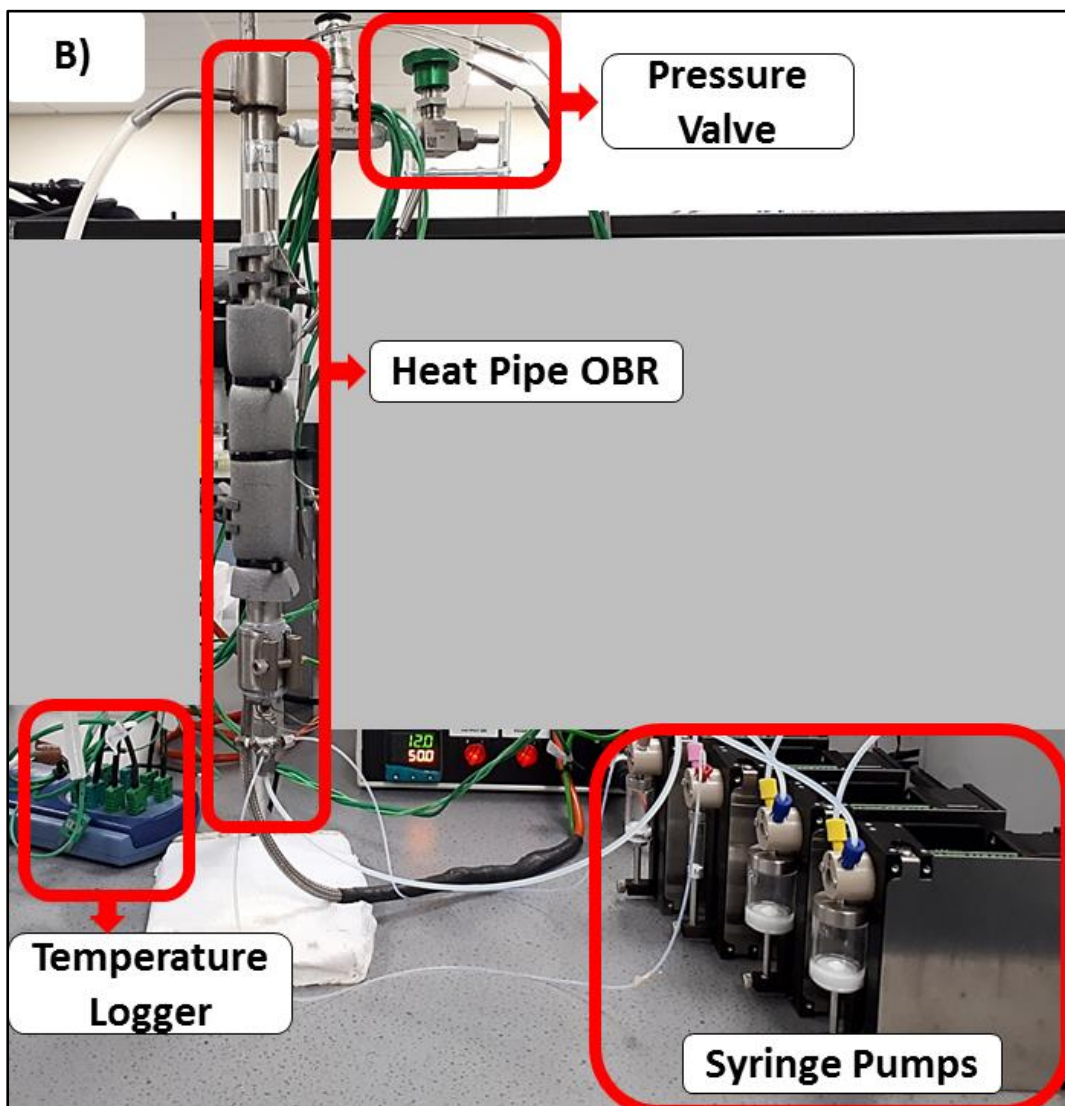


Figure 3.9. (A) Schematic diagram and (B) photograph of the heat pipe oscillatory baffled reactor (HPOBR) for continuous solvent-free epoxidation of terpenes with  $H_2O_2$ .

### ***3.3.6 Sampling and product purification***

Samples from both batch and continuous epoxidation were collected in 5 mL glass vials and immediately quenched using anhydrous Na<sub>2</sub>SO<sub>4</sub>. The addition of Na<sub>2</sub>SO<sub>4</sub> to the sample caused the polyoxometalates catalyst to be inactive due to the pH changes towards neutral. Moreover, Na<sub>2</sub>SO<sub>4</sub> facilitates in the drying of the organic phase. The top organic layer was collected and stored in a freezer at -20 °C for further analysis. For purification, following the batch reaction, the bulk biphasic mixture was placed in a separating funnel, and the phase transfer catalyst was destabilised by the addition of 5 mL of NaCl (0.1 M) with mixing before the phases were separated. The organic layer was dried with anhydrous Na<sub>2</sub>SO<sub>4</sub>. Unreacted (R)-(+)-limonene or  $\alpha$ -pinene was separated from the corresponding epoxides using a rotary evaporator coupled with a silicone oil bath at 150 °C and a reduced pressure of 50 mbar. The purity of the products obtained was  $\geq 98$  % as confirmed by analysis using a 5890 Hewlett Packard Series II gas chromatograph.

## **3.4 Product analysis techniques**

### ***3.4.1 H<sub>2</sub>O<sub>2</sub> titration method***

Titration was performed to determine the amount (wt. %) of H<sub>2</sub>O<sub>2</sub> in aqueous solution. First, 5 g of aliquot taken from the aqueous phase was weighed and placed into a 500 mL Erlenmeyer flask, before dilution with 200 mL of distilled water and addition of 20 mL of diluted sulphuric acid (diluted 1:4 in H<sub>2</sub>O). The titrant, 0.02 M potassium permanganate solution, was filled into a 50 mL burette and used to titrate the sample solution until a faint pink colour persisted for 30 seconds. The procedure was performed in triplicate to obtain an average value and the amount of H<sub>2</sub>O<sub>2</sub> was calculated using the following expression:

$$\%H_2O_2(\text{wt. \%}) = \frac{V_t N d (1.701)}{W} \quad (3.1)$$

Where: V<sub>t</sub> is the volume of KMnO<sub>4</sub> used in the titration (mL), N is the normality KMnO<sub>4</sub> of solution, d is the dilution factor, and W is the weight of the sample (g).

### 3.4.2 *In situ* Fourier transform infrared (FTIR) spectroscopy analysis

*In situ* FTIR spectroscopy monitoring was performed using the React IR-4000 FTIR spectrometer from Mettler Toledo (USA), fitted with a mercury cadmium telluride (MCT) band detector. The detector was cooled using liquid nitrogen filled in a specialised Dewar flask in the instrument. The FTIR was equipped with a K6 conduit with 6.35 mm DiComp (diamond) probe measuring from 4000 to 650  $\text{cm}^{-1}$ .

The instrument was connected to a PC interface on which spectra and data were recorded using iC-iR software (ver. 4.2.26). Initially, a signal to noise ratio (SNR) was determined to ensure IR spectra accuracy and consistency by minimising the variation between scans. The instrument was further calibrated by acquiring an air background spectrum and a water vapour spectrum to eliminate the response of the instrument to those factors. Spectra was collected with a spectral resolution of 8  $\text{cm}^{-1}$  with 40 co-added and averaged scans at 15 seconds per scan set in the absorbance mode. The area under the peak was measured using a two-point baseline that negates any variations due to changes in the baseline during a scan. Figure 3.10 (A) and (B) shows the FTIR spectra for pure (R)-(+)-limonene,  $\alpha$ -pinene, limonene-1,2-epoxide and  $\alpha$ -pinene oxide. Peaks of (R)-(+)-limonene and  $\alpha$ -pinene and their epoxides were found to be overlapping, except in the region from 1200  $\text{cm}^{-1}$  to 650  $\text{cm}^{-1}$ , where individual and isolated peaks can be monitored. The peaks for  $\alpha$ -pinene and  $\alpha$ -pinene oxide were monitored at wavenumber of 787  $\text{cm}^{-1}$  and 857  $\text{cm}^{-1}$ , respectively (Figure 3.10 (A)) (Stekrova *et al.*, 2014). Peaks for (R)-(+)-limonene and limonene-1,2-epoxide were monitored at the wavenumber of 1150  $\text{cm}^{-1}$  and 841  $\text{cm}^{-1}$ , respectively (Figure 3.10 (B)) (Caovilla *et al.*, 2008; Zapata *et al.*, 2009b). Peaks chosen for monitoring were isolated, sharp, and clear. The full spectra (4000  $\text{cm}^{-1}$  to 650  $\text{cm}^{-1}$ ) for both terpenes and their epoxides are shown in Appendix D.

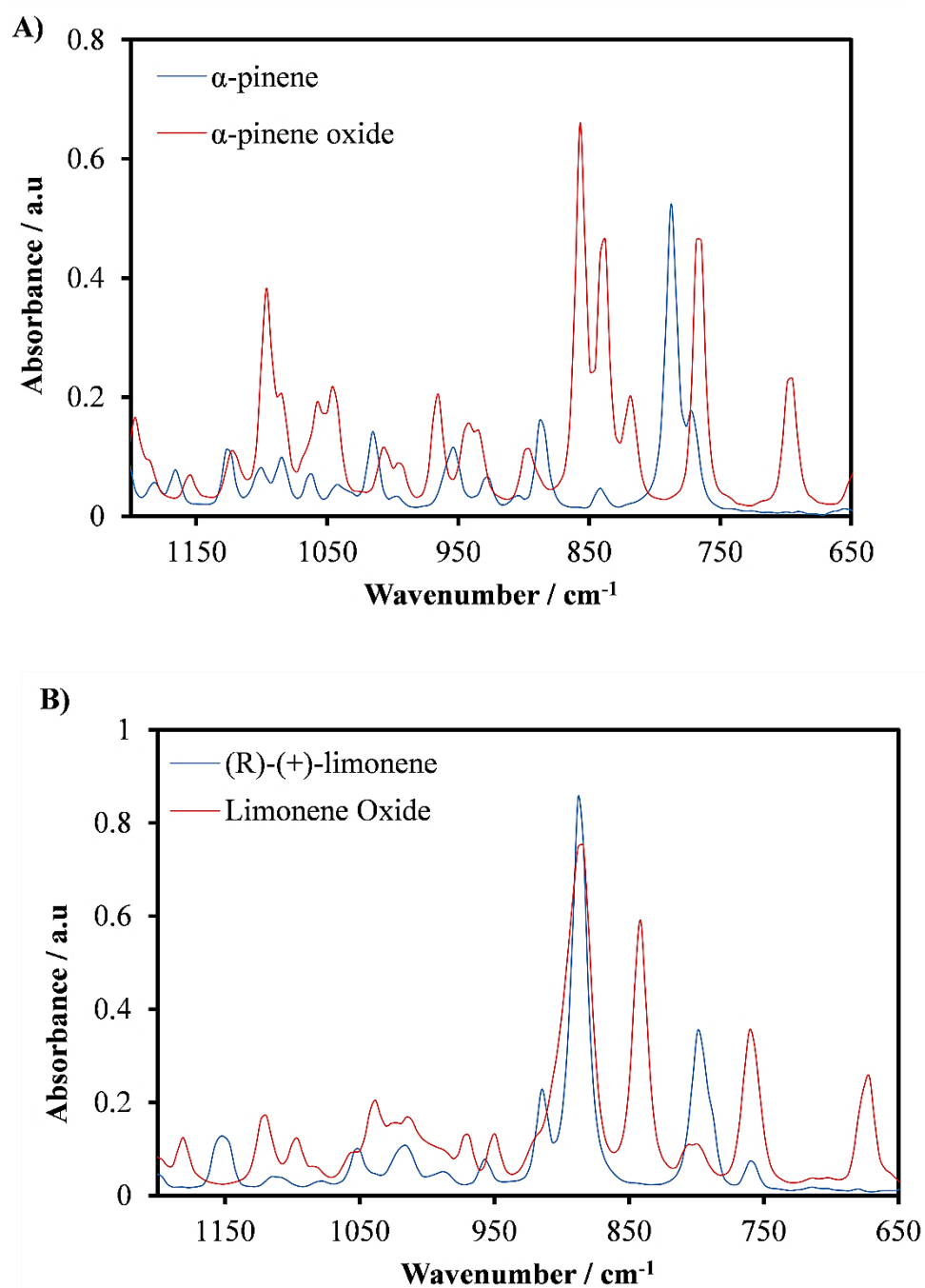


Figure 3.10. FTIR spectra of pure; (A)  $\alpha$ -pinene and  $\alpha$ -pinene oxide and (B) (R)-(+)-limonene and limonene-1,2-epoxide; collected between  $1200 \text{ cm}^{-1}$  and  $650 \text{ cm}^{-1}$  at  $8 \text{ cm}^{-1}$  resolution, 40 co-added and averaged scans and 15 seconds per scan set.

### 3.4.3 FTIR spectroscopy Calibration

Four sets of calibration curves were made to analyse the samples from the epoxidation of (R)-(+)-limonene and  $\alpha$ -pinene, respectively. Various concentrations of (R)-(+)-limonene, limonene-1,2-epoxide,  $\alpha$ -pinene and  $\alpha$ -pinene oxide were prepared in toluene as shown in Table 3.5. The concentration range selected for calibrations covered the concentration range of the experiments.

Compound	Concentrations (g L <sup>-1</sup> )									
	Run 1	Run 2	Run 3	Run 4	Run 5	Run 6	Run 7	Run 8	Run 9	Run 10
$\alpha$ -pinene	85.8	171.6	257.4	343.2	429.0	514.8	600.6	686.4	772.2	858.0
$\alpha$ -pinene-oxide	96.4	192.8	289.2	385.6	482	578.4	674.8	771.2	867.6	964.0
(R)-(+)-limonene	84.1	168.2	252.3	336.4	420.5	504.6	588.7	672.8	756.9	841.0
limonene-1,2-epoxide	92.9	185.8	278.7	371.6	464.5	557.4	650.3	743.2	836.1	929.0

Table 3.5. Various concentrations of  $\alpha$ -pinene,  $\alpha$ -pinene oxide, (R)-(+)-limonene and limonene-1,2-epoxide pure samples for FTIR spectroscopy calibration.

The spectrum for each calibration sample prepared was collected between 4000 cm<sup>-1</sup> and 650 cm<sup>-1</sup> at 8 cm<sup>-1</sup> resolution with 40 co-added and averaged scans and 15 seconds per scan set. The average peak area for all calibration samples was plotted against the sample concentration as shown in Figure 3.11 (A) and (B). The gradient of each plot represents the calibration value for the relationships between peak area and the concentration. The concentration of side-products from the epoxidation of (R)-(+)-limonene and  $\alpha$ -pinene with H<sub>2</sub>O<sub>2</sub> could not be analysed using the FTIR spectroscopy due to the absence of isolated peaks. The concentration of all side-products was determined using gas chromatography.

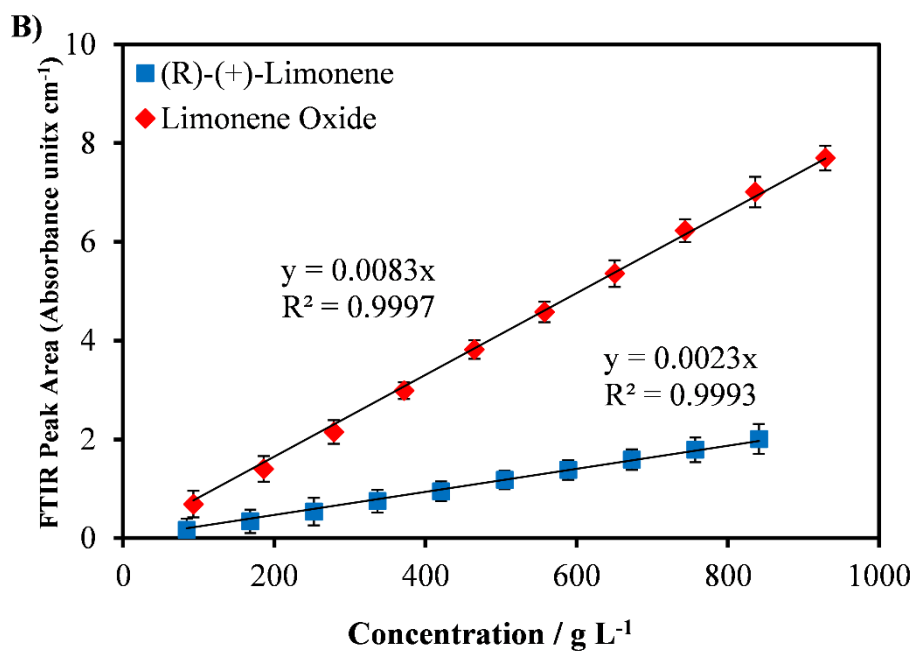
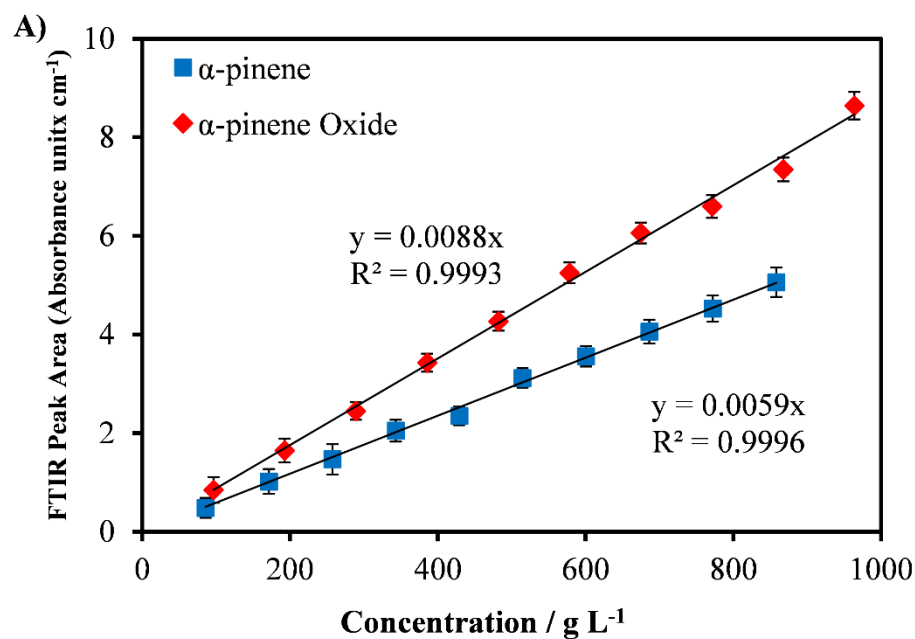


Figure 3.11. FTIR spectroscopy calibration curves showing the relationship between FTIR spectra peak area and pure component concentrations for (A)  $\alpha$ -pinene and  $\alpha$ -pinene oxide and (B) (R)-(+)-limonene and limonene-1,2-epoxide.

### 3.4.4 Gas chromatography

Samples were analysed by gas chromatography using a 5890 Hewlett Packard Series II instrument.

### 3.4.5 GC quantification via a calibration curve

Quantification of (R)-(+)-limonene,  $\alpha$ -pinene and their oxidative products using GC was performed using a prepared calibration curve. The mixture was prepared using various concentrations of (R)-(+)-limonene, limonene-1,2-epoxide, limonene bis-epoxide, limonene-1,2-diol, carveol, carvone,  $\alpha$ -pinene,  $\alpha$ -pinene oxide, sobrerol, campholenic aldehyde, pinanediol, verbenone and verbenol to determine the instrument response factors. Various volumes of these compounds were measured into 5 mL glass vials and naphthalene was used as an internal standard for all GC analysis as it has a different boiling point to other compounds in the sample mixture, allowing an isolated peak but within the residence time of all compounds in the GC column. Naphthalene (10 mg) was placed in each glass vial, followed by the addition of 1.96 mL chloroform to dilute the samples to be within the flame ionisation detector (FID) detection limit. Each prepared mixture was transferred into 2 mL GC autosampler vials, before 0.5  $\mu$ L was injected into the GC column by an autosampler using a 5- $\mu$ L GC syringe (SGE). The GC oven temperature was programmed as follows: a starting temperature of 80 °C was held for 4 min, then ramped up at a rate of 15 °C min<sup>-1</sup> to 260 °C, which was held for 10 min. The total run time was approximately 26 min per sample. Duplicated runs were performed to ensure minimal error. The GC column type used was a Varian CP Wax Capillary (BPX70). The GC injector and detector temperature were set at 260 °C, while helium was used as carrier gas at 7 psi (0.48 bar) input pressure.

The data obtained from the GC analysis of the calibration samples were correlated with the concentration of the mixture to calculate the response factors ( $R_f$ ) for each analyte. The response factors were calculated using the concentrations and peak areas ratios of each analyte to the naphthalene internal standard. Sample concentration of (R)-(+)-limonene, limonene-1,2-epoxide,  $\alpha$ -pinene and  $\alpha$ -pinene oxide for calibration were prepared as shown in Table 3.6. The calibration curve for these compounds and their responses factors (curve gradient) are shown in Figure 3.12 (A – D). The calibration curve for all side-products and their corresponding response factor are shown in Appendix E. The following expression (Equation 3.2) was used to calculate the response factor:

$$\left(\frac{C_s}{C_i}\right) = R_f \cdot \left(\frac{A_s}{A_i}\right) \quad (3.2)$$

Where,  $R_f$  is the response factor,  $C_s$  is the concentration of the analyte in the mixture ( $\text{mg L}^{-1}$ ),  $C_i$  is the concentration of the internal standard ( $\text{mg L}^{-1}$ ),  $A_s$  is the peak area of the analyte in the mixture (mVs), and  $A_i$  is the peak area of the internal standard (mVs).

Compounds	Concentration ( $\text{mg L}^{-1}$ )			
	Run 1	Run 2	Run 3	Run 4
(R)-(+)-limonene	1161.2	2322.5	3483.7	4645.0
limonene-1,2-epoxide	1401.6	2803.3	4205.0	5606.6
$\alpha$ -pinene	1337.0	2674.0	4011.0	5348.0
$\alpha$ -pinene oxide	1096.9	2193.9	3290.9	4387.8

*Table 3.6. Various concentrations of  $\alpha$ -pinene,  $\alpha$ -pinene oxide, (R)-(+)-limonene and limonene-1,2-epoxide pure samples for GC calibration.*



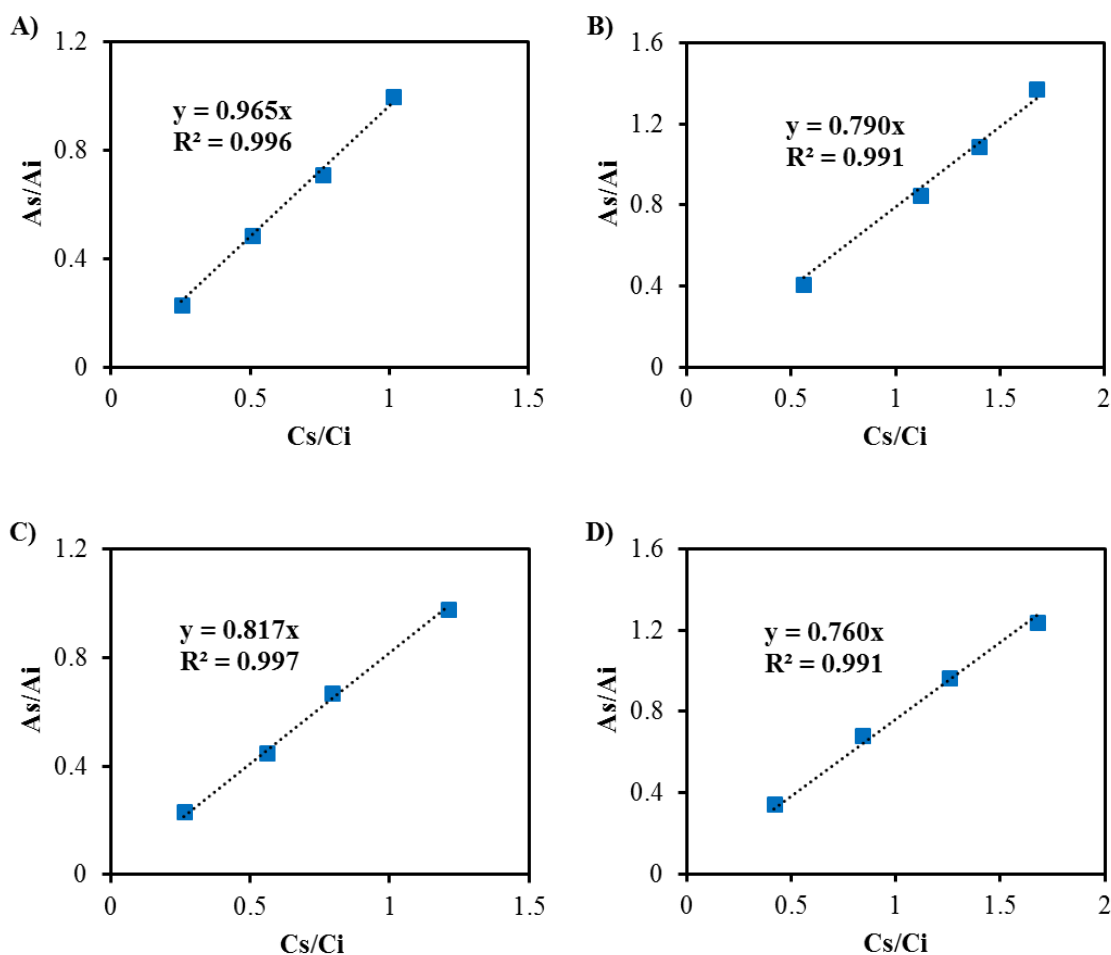


Figure 3.12. GC calibration curve for (A) (R)-(+)-limonene, (B) limonene-1,2-epoxide, (C)  $\alpha$ -pinene, and (D)  $\alpha$ -pinene oxide. The value of y-axis represents the ratio between the peak area of the analyte ( $A_s$ ) and the peak area of the internal standard ( $A_i$ ). The value of x-axis represents the ratio between the concentration of the analyte ( $C_s$ ) and the concentration of the internal standard ( $C_i$ ). The gradient of the curve represents the response factor ( $R_f$ ). The trendlines in Figure 3.12 each pass-through origin.

### 3.4.6 GC sample analysis and quantification

Approximately 40 mg of each sample was measured into 2 mL GC vials and diluted with 1.96 mL of chloroform ( $\text{CHCl}_3$ ), followed by the addition of naphthalene (10 mg) as an internal standard. Then, 0.5  $\mu\text{L}$  of the prepared sample was injected into the GC by an autosampler equipped with a 5- $\mu\text{L}$  GC syringe (SGE) and 0.5  $\mu\text{L}$  of the sample mixture was injected into the column manually using a 5- $\mu\text{L}$  GC syringe (SGE). The GC oven temperature was programmed as follows: a starting temperature of 80  $^\circ\text{C}$  was held for 4 min, then ramped up at a rate of 15  $^\circ\text{C min}^{-1}$  to 260  $^\circ\text{C}$ , which was held for 10 min. The total run time was approximately 26 min per sample. The instrument response factor obtained from the calibration curve was used to quantify each compound. Each peak area of the compound and the internal standard

were measured from the GC chromatogram. Prior to analysis of reaction samples, aliquots taken from pure standards of (R)-(+)-limonene, limonene-1,2-epoxide, limonene bis-epoxide, limonene-1,2-diol,  $\alpha$ -pinene,  $\alpha$ -pinene oxide, campholenic aldehyde, verbenol, verbenone, pinanediol and sobrerol were individually analysed using GC to facilitate the identification of peaks in reaction samples. Figure 3.13 (A) and (B) shows the GC chromatograms obtained from the analysis of samples from the epoxidation of (R)-(+)-limonene and  $\alpha$ -pinene, respectively.

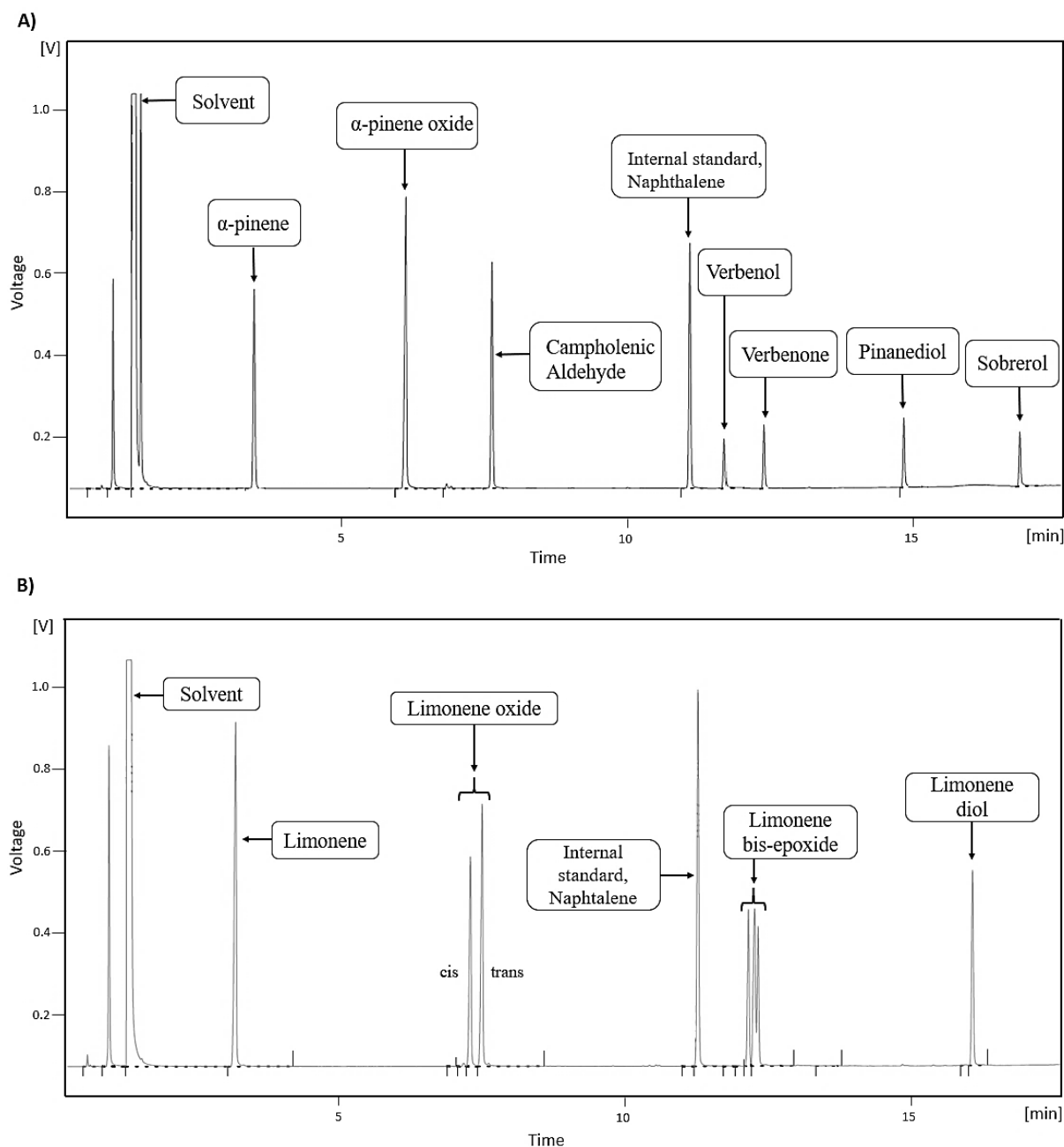


Figure 3.13. GC chromatogram of (A)  $\alpha$ -pinene, its oxidative products and the internal standard and (B) (R)-(+)-limonene, its oxidative products, and the internal standard.

As shown in Figure 3.13 (A), the first peak in the chromatogram represents the solvent, chloroform (CHCl<sub>3</sub>), which was used for sample dilution, followed by (R)-(+)-limonene, cis-limonene-1,2-epoxide, trans-limonene-1,2-epoxide, limonene bis-epoxide, the internal standard (naphthalene) and finally, limonene-1,2-diol. The peak of limonene bis-epoxide represents a collective of four isomers which overlapped in the chromatogram. The total area was taken to calculate the concentration of the mixture of bis-epoxides. In Figure 3.13 (B), the peaks are in the following order: solvent (CHCl<sub>3</sub>),  $\alpha$ -pinene,  $\alpha$ -pinene oxide, campholenic aldehyde, naphthalene, verbenol, verbenone, pinanediol and sobrerol. The concentration of each analyte was calculated as follows:

$$\text{Concentration (mg)} = R_f \cdot \left(\frac{A_s}{A_i}\right) \cdot (C_i) \times 100 \quad (3.3)$$

Reaction conversion and yields were calculated from the GC analysis based on the internal standard response factor. Analysis from batch parallel experiments showed less than ~2 % error for the mean value. The following expression determined the conversion:

$$\text{Conversion (\%)} = \frac{C_0 - C_i}{C_0} \times 100\% \quad (3.4)$$

Where, C<sub>0</sub> is the initial concentration of (R)-(+)-limonene and C<sub>i</sub> is the concentration of (R)-(+)-limonene in the sample as determined by the GC. When H<sub>2</sub>O<sub>2</sub> is the limiting reactant, the concentration of H<sub>2</sub>O<sub>2</sub> and its conversion were determined by the titration method. The yield of products was calculated using Equation 3.5, where X<sub>i</sub> is the concentration of products in the sample.

$$\text{Yield (\%)} = \frac{X_i}{C_0} \times 100\% \quad (3.5)$$

### 3.4.7 Nuclear magnetic resonance spectroscopy (NMR)

Purified product samples were identified by NMR spectroscopy performed externally by the School of Natural and Environmental Sciences, Newcastle University. A Bruker Advance III 700 MHz spectrometer was used to perform proton NMR spectroscopy (H-NMR). The spectrometer was equipped with a 24 position autosample changer and a triple-resonance nitrogen cooled cryoprobe. The probe was optimised for the observation of <sup>1</sup>H/<sup>19</sup>F and had a temperature range of 0 °C to 80 °C. Prior to the analysis, the organic samples were dried using anhydrous Na<sub>2</sub>SO<sub>4</sub> to remove any moisture and purified via rotary evaporation to remove any solvent. Each sample was dissolved in 0.6 mL of deuterated chloroform (CDCl<sub>3</sub>) before being analysis. The NMR spectra for (R)-(+)-limonene and  $\alpha$ -pinene are shown in Appendix F. The polytungstophosphate catalyst were sent to external facility for confirmation. A Varian Infinity

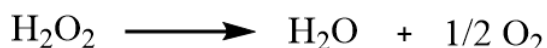
Plus 400 NMR spectrometer was used to perform NMR spectroscopy (P MAS NMR). The spectrometer was equipped with a 4 mm double resonance probe at frequency of 160 MHz measuring samples at room temperature using H<sub>3</sub>PO<sub>4</sub> as reference.

### 3.5 Kinetic modelling of the epoxidation of (R)-(+)-limonene and $\alpha$ -pinene with H<sub>2</sub>O<sub>2</sub>

#### 3.5.1 Kinetic study and models

In this study, the kinetic parameters and reaction order for the epoxidation of (R)-(+)-limonene and  $\alpha$ -pinene were determined experimentally by applying an initial-rate method based on pseudo-first order conditions. The rate laws used to develop models for the epoxidation of (R)-(+)-limonene and  $\alpha$ -pinene with H<sub>2</sub>O<sub>2</sub> using a polytungstophosphate catalyst was based on the description in section 2.5.3 of Chapter 2. The mathematical models developed in this work facilitate the understanding of the main products as well as the conditions that are prone to the formation of side-products. The model can be used to validate the kinetic parameters obtained from the experimental data.

The rate laws for all the reactions considered for the epoxidation of (R)-(+)-limonene are shown in Equation 3.6 – 3.11, where  $r_{decomp}$  is the rate of reaction for the H<sub>2</sub>O<sub>2</sub> decomposition,  $r_{oxidative}$  is the rate of formation of oxidative species,  $r_{lim}$  is the rate of (R)-(+)-limonene epoxidation,  $r_{bis}$  is the rate of formation of bis-epoxide,  $r_{diol}$  is the rate of formation of limonene-1,2-diol, and  $r_{bisdiol}$  is the rate of formation of bis-diol, while,  $k_{decomp}$ ,  $k_{oxidative}$ ,  $k_{lim}$ ,  $k_{bis}$ ,  $k_{diol}$  and  $k_{bisdiol}$  are the rate constants for each rate law. Scheme 3.1 shows the decomposition of H<sub>2</sub>O<sub>2</sub> to H<sub>2</sub>O and O<sub>2</sub>.



*Scheme 3.1. Decomposition of H<sub>2</sub>O<sub>2</sub> to H<sub>2</sub>O and O<sub>2</sub>.*

The reaction order with respect to the catalyst was studied using Na<sub>2</sub>WO<sub>4</sub>.2H<sub>2</sub>O concentrations in the range of 0.004 M to 0.008 M, and fixed initial concentrations of (R)-(+)-limonene (1.25 M), H<sub>2</sub>O<sub>2</sub> (1.25 M) and 500 mol% solvent (toluene). The reaction order with respect to (R)-(+)-limonene was determined by varying the initial concentration of (R)-(+)-limonene from 0.25 M to 1.25 M, while keeping the concentrations of H<sub>2</sub>O<sub>2</sub> (1.25 M) and Na<sub>2</sub>WO<sub>4</sub>.2H<sub>2</sub>O (0.006 M) constant and in excess. Similarly, the reaction order with respect to H<sub>2</sub>O<sub>2</sub> was determined by

varying the initial concentration of H<sub>2</sub>O<sub>2</sub> from 0.25 M to 1.25 M, with the initial concentration of (R)-(+)-limonene (1.25 M) and Na<sub>2</sub>WO<sub>4</sub>·2H<sub>2</sub>O (0.006 M) being kept constant and in excess.

$$r_{decomp} = k_{decomp} [\text{H}_2\text{O}_2] \quad (3.6)$$

$$r_{oxidative} = k_{oxidative} [\text{H}^+] ([8\text{H}_2\text{O}_2] [4\text{WO}_4^{2-}] [\text{PO}_4^{-3}] [3\text{Q}] - K_{eq}^{-1}[\text{Q}_3\text{POM}] [7\text{H}_2\text{O}]) \quad (3.7)$$

$$r_{lim} = k_{lim} [(R)\text{-}(+)\text{-limonene}] [\text{Q}_3\text{POM}] \quad (3.8)$$

$$r_{bis} = k_{bis} [\text{limonene-1,2-epoxide}] [\text{Q}_3\text{POM}] \quad (3.9)$$

$$r_{diol} = k_{diol} [\text{limonene-1,2-epoxide}] [\text{H}_2\text{O}] [\text{H}^+] \quad (3.10)$$

$$r_{bisdiol} = k_{bisdiol} [\text{bis-epoxide}] [\text{H}_2\text{O}] [\text{H}^+] \quad (3.11)$$

The rate laws for all the reactions considered for the epoxidation of  $\alpha$ -pinene are shown in Equation 3.12 – 3.14,  $r_{decomp}$ ,  $r_{oxidative}$  and  $r_{pinene}$  are the rates of reaction for the H<sub>2</sub>O<sub>2</sub> decomposition, the formation of oxidative species and  $\alpha$ -pinene epoxidation, respectively, while,  $k_{decomp}$ ,  $k_{oxidative}$  and  $k_{pinene}$  are the rate constants for each rate law. The reaction order with respect to the catalyst was studied using Na<sub>2</sub>WO<sub>4</sub>·2H<sub>2</sub>O concentrations in the range of 0.008 M to 0.016 M, and fixed initial concentrations of  $\alpha$ -pinene (1.25 M), H<sub>2</sub>O<sub>2</sub> (1.25 M) and 500 mol% solvent (toluene). The study was performed using a lower concentration of catalyst ( $\leq 0.016$  M) since higher metal loading is known to cause H<sub>2</sub>O<sub>2</sub> decomposition (Cánepa *et al.*, 2011). The reaction order with respect to  $\alpha$ -pinene was determined by varying the initial concentration of  $\alpha$ -pinene from 0.25 M to 1.25 M, while keeping the concentrations of H<sub>2</sub>O<sub>2</sub> (1.25 M) and Na<sub>2</sub>WO<sub>4</sub> (0.012 M) constant and in excess. Similarly, the reaction order with respect to H<sub>2</sub>O<sub>2</sub> was determined by varying the initial concentration of H<sub>2</sub>O<sub>2</sub> from 0.25 M to 1.25 M, with the initial concentration of  $\alpha$ -pinene (1.25 M) and Na<sub>2</sub>WO<sub>4</sub> (0.012 M) being kept constant and in excess.

$$r_{decomp} = k_{decomp} [\text{H}_2\text{O}_2] \quad (3.12)$$

$$r_{oxidative} = k_{oxidative} [\text{H}^+] ([8\text{H}_2\text{O}_2] [4\text{WO}_4^{2-}] [\text{PO}_4^{-3}] [3\text{Q}] - K_{eq}^{-1}[\text{Q}_3\text{POM}] [7\text{H}_2\text{O}]) \quad (3.13)$$

$$r_{pinene} = k_{pinene} [\alpha\text{-pinene}] [\text{Q}_3\text{POM}] \quad (3.14)$$

The model for the epoxidation of (R)-(+)-limonene does not consider the allylic oxidation of (R)-(+)-limonene to carveol and subsequent oxidative dehydrogenation to carvone. Likewise, the model for the epoxidation of  $\alpha$ -pinene does not consider the allylic oxidation of  $\alpha$ -pinene to

verbenol and subsequent dehydrogenation to verbenone. Furthermore,  $\alpha$ -pinene oxide rearrangement to campholenic aldehyde and the hydrolysis to sobrerol and pinanediol were not considered in the model. The main reason is the rate of conversion to these side-products is negligible under equimolar conditions and low acid concentration as investigated in Chapter 4 and 5. The inclusion of these side reactions in the models necessitates further isolated kinetic studies for each reaction to better understand the rate and the reaction order, which is beyond the scope of this study.

### 3.5.2 Modelling procedure

MATLAB version 2014b software was used to develop the model for the epoxidation of (R)-(+)-limonene and  $\alpha$ -pinene. The reactions represented by Equation 3.6 to 3.14 were expressed as ordinary differential equations (ODE) in the model. The ODE shows a derivative function of the changes in rate with respect to each concentration of the reactants and the rate constants. The initial concentration of the reactants involved, and an estimated value of the rate constant served as the initial boundary value to solve the ODE function. The ODE was solved numerically using the ODE15s function, a standard MATLAB function to solve stiff ODE equations. The function solver requires the initial condition ( $x = x_0$  at time  $t_0$ ) as shown in Equation 3.15. The function solves the equations by adjusting the kinetic parameters until it fits the experimental data within the error limits. The error between the experimental data and the model was quantified using the sum squares of errors (SSE) with tolerance fixed at  $\leq 1.0\%$  (Equation 3.16). A MATLAB code is presented in Appendix G showing the underlying code used by the solver for the epoxidation of (R)-(+)-limonene at 1:1 molar ratio with  $H_2O_2$  at  $50\text{ }^\circ\text{C}$  in the presence of toluene (500 mol%).

$$\frac{dx}{dt} = f(t, x), \quad x(t_0) = x_0 \quad (3.15)$$

$$SSE = \sum (C_{i_e} - C_{i_m})^2 x \quad 100 \quad (3.16)$$

Where,  $C_{i_e}$  is the concentration of reactants obtained from experimental data and  $C_{i_m}$  the concentration of reactants calculated by the model at time  $t$ .

## Chapter 4 Epoxidation of (R)-(+)-limonene

### 4.1 Introduction

This chapter presents the results and discussion from the screening of several parameters, including a kinetic study for the batch epoxidation of (R)-(+)-limonene. The batch screening was performed using four-necked jacketed flask. Results obtained from earlier works using tungstic-acid ( $\text{H}_2\text{WO}_4$ ) catalyst was also presented and compared to the polytungstophosphate catalyst.

### 4.2 Epoxidation of (R)-(+)-limonene with tungstic acid

Initially, the epoxidation of (R)-(+)-limonene was studied using tungstic acid ( $\text{H}_2\text{WO}_4$ ) catalyst before it was replaced by the polytungstophosphate catalyst. A series of experiments were performed to synthesise limonene-1,2-epoxide from (R)-(+)-limonene using tungstic acid as catalyst. The concentration of the tungstic acid was varied between 0.005 M and 0.01 M. The molar ratio of (R)-(+)-limonene to  $\text{H}_2\text{O}_2$  was fixed at 1:1.6 and the experiment was performed at 50 °C without using organic solvent. The study was performed using 1 g of phase transfer catalyst (methyltrialkyl-(C<sub>8</sub>-C<sub>10</sub>)-ammonium chloride, commercially: Adogen 464®). The reaction was performed using *in situ* FTIR to monitor the formation of epoxides. The spectra were collected between 1500  $\text{cm}^{-1}$  and 650  $\text{cm}^{-1}$  to increase the visibility of peaks during real-time monitoring of the reaction. The FTIR spectra of the reaction sample were compared to the FTIR spectra of pure (R)-(+)-limonene and limonene-1,2-epoxide, as shown in Figure 4.1.

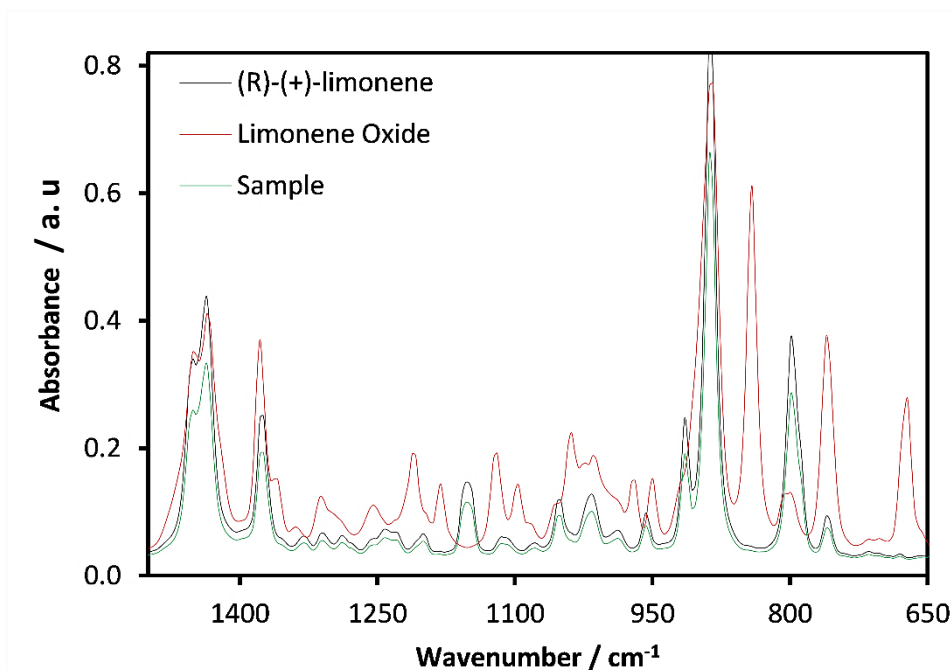


Figure 4.1. FTIR spectra of reaction sample from the batch epoxidation of (R)-(+)-limonene using tungstic acid catalyst at reaction condition of (R)-(+)-limonene (1.0 M),  $H_2O_2$  (1.6 M),  $H_2WO_4$  (0.009 M), phase transfer catalyst (PTC) amount 1 g, mixing speed of 1250 rpm, reaction time 2 hour, and temperature 50 °C. FTIR spectra collected between 1500  $cm^{-1}$  and 650  $cm^{-1}$  at 8  $cm^{-1}$  resolution, 40 averaged scans and 15 seconds per scan set.

As depicted in Figure 4.1, there was no formation of limonene-1,2-epoxide detected when using 0.009 M of  $H_2WO_4$ . The spectra of the reaction sample almost overlap the spectra of pure (R)-(+)-limonene. Furthermore, FTIR spectra of other samples collected from experiments using different tungstic acid concentration within the tested range shows a similar result. These results suggest that the tungstic acid catalyst was not active for the epoxidation of (R)-(+)-limonene at the reaction condition used. The selection of tungstic acid as a catalyst for the epoxidation reaction without co-catalyst to form a complex with  $H_2O_2$  can be the reason for such inactivity.

It is presumed that due to the absence of a suitable counter anion such as polyoxometalates (POM) for the phase transfer catalysed system caused the catalyst inactivity. It is reported that the commonly used central atom for the POM structure is phosphorus (P) and silica (Si) (Mizuno *et al.*, 2005). Mahha *et al.* (2007) found that the addition of a phosphate source in a POM structure significantly improve the conversion of alkenes in a phase transfer catalysed epoxidation reaction. They showed that a phosphate-free catalytic system exhibits poor conversion (< 5 %) of the alkene. In a similar study on phase transfer catalysed epoxidation, a combination of phosphate and tungstate for the formation of POM shows better catalytic activity compared to other POM structure (Chen *et al.*, 2004). Clearly, a phosphate source is



crucial for the formation of the polyoxometalates for the epoxidation. Therefore, a polytungstophosphate catalyst ( $\{PO_4[WO(O_2)_2]_4\}^{3-}$ ) was later employed for the epoxidation of (R)-(+)-limonene and  $\alpha$ -pinene. The polytungstophosphate catalyst was prepared using sodium tungstate dihydrate ( $Na_2WO_4 \cdot 2H_2O$ ) as the tungstate source and phosphoric acid ( $H_3PO_4$ ) as the phosphate source. The suitability of the catalyst was tested in a similarly conditioned reaction as the experiment with tungstic acid. Figure 4.2 shows the FTIR spectra of the reaction sample compared to the spectra of pure (R)-(+)-limonene and limonene-1,2-epoxide.

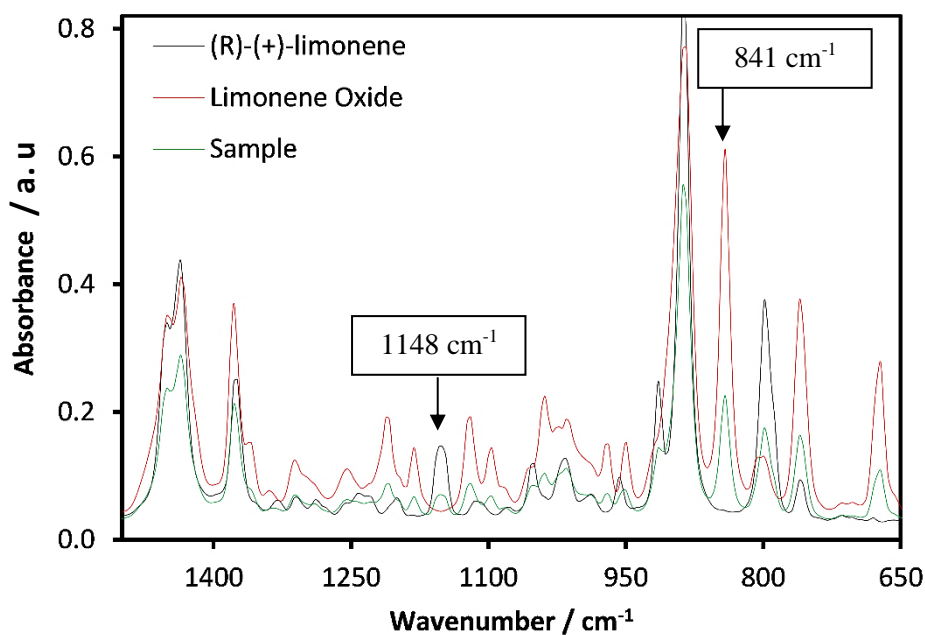


Figure 4.2. FTIR spectra of reaction sample from the batch epoxidation of (R)-(+)-limonene using polytungstophosphate catalyst at reaction condition of (R)-(+)-limonene (1.0 M),  $H_2O_2$  (1.6 M),  $Na_2WO_4 \cdot 2H_2O$  (0.009 M), phase transfer catalyst (PTC) amount 1 g, mixing speed of 1250 rpm, reaction time 2 hour, and temperature 50 °C. FTIR spectra collected between 1500  $cm^{-1}$  and 650  $cm^{-1}$  at 8  $cm^{-1}$  resolution, 40 averaged scans and 15 seconds per scan set.

As can be seen from Figure 4.2, the FTIR spectra of the sample shows the presence of a peak at 841  $cm^{-1}$ , which resembles the peak of limonene-1,2-epoxide. Furthermore, the peak at 1148  $cm^{-1}$  that marks the presence of (R)-(+)-limonene was found to be decreased. It can be deduced that the polytungstophosphate employed shows good activity toward the formation of limonene-1,2-epoxide. Further studies on the epoxidation of (R)-(+)-limonene and  $\alpha$ -pinene were performed using this catalyst.

### 4.3 Effects of mixing on (R)-(+)-limonene epoxidation

A series of experiments were performed to determine the mixing-independent region. This is the region where an increase in mixing speed no longer increases the reaction rates (< 15 minutes). The effects of stirrer speed on the epoxidation of (R)-(+)-limonene were investigated. The stirrer speed was varied between 250 rpm and 1500 rpm. The study was performed using 1 g of PTC (Adogen 464®). Figures 4.3 (A) and (B) present the results:

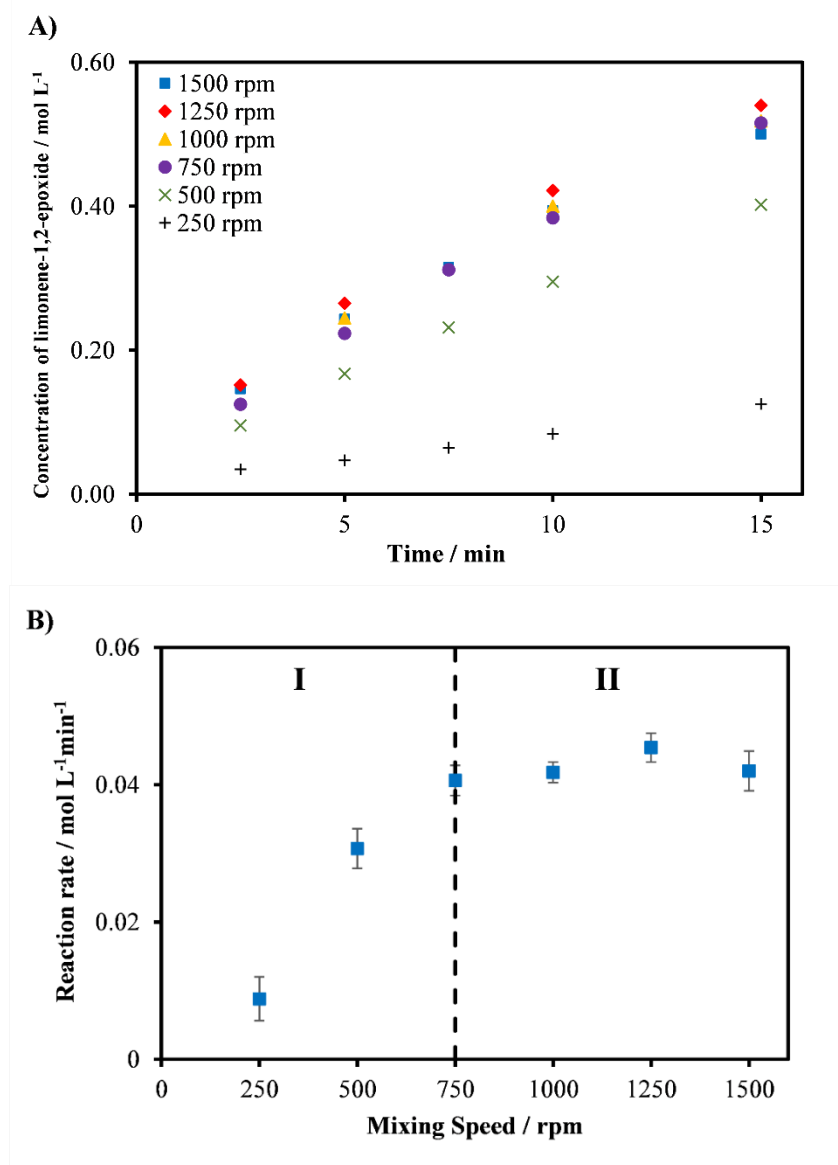


Figure 4.3. Batch epoxidation of (R)-(+)-limonene at reaction conditions of (R)-(+)-limonene (1.25 M), H<sub>2</sub>O<sub>2</sub> (1.25 M), Na<sub>2</sub>WO<sub>4</sub>·2H<sub>2</sub>O (0.006 M), Na<sub>2</sub>SO<sub>4</sub> (5.7 g), H<sub>2</sub>SO<sub>4</sub> (0.04 M), 1.0 g PTC, temperature (50 °C), toluene (500 mol%) and mixing speeds of 250 – 1500 rpm, (A) The concentration of limonene-1,2-epoxide versus time at various mixing speed. (B) The relationship between the initial reaction rate and the mixing speed.

As can be seen in Figure 4.3 (A), the reaction rate increased with increasing stirrer speed. The initial rates are obtained from the gradient of Figure 4.3 (A) measuring the increased in limonene-1,2-epoxide concentration over 15 minutes reaction time. The values of the initial rates are shown in Appendix H. The initial rates values are plotted against the stirrer mixing speed, as shown in Figure 4.3 (B). From this figure, it is clear that the initial reaction rate increases when the mixing speed is increased from 250 rpm to 750 rpm (region I). This region represents a mixing-dependent area where the reaction is mass transfer limited.

Further increases in the mixing speed from 750 rpm to 1500 rpm do not result in any increase in the initial reaction rate (region II). This is indicative of a mixing-independent area, where the reaction is not mass transfer limited. Operating within this mixing region allows a meaningful interpretation of reaction kinetic data, as well as results obtained from parametric studies. As such, all subsequent experiments for the batch epoxidation of (R)-(+)-limonene were performed at a stirrer speed of 1250 rpm.

#### **4.4 Effect of addition of a phase transfer catalyst on (R)-(+)-limonene epoxidation**

Figures 4.4 (A) and (B) show the effects of the concentration of the phase transfer catalyst (PTC) on the epoxidation process. In the biphasic epoxidation system, the polytungstophosphate catalyst ( $\{PO_4[WO(O_2)_2]_4\}^{3-}$ ) “shuttles” to and from the organic phase via a PTC. It is expected that the concentration of the PTC could affect the mass transfer rate of the peroxy species between the aqueous phase and the organic phase. Therefore, the effect of the PTC in the epoxidation system was investigated by varying the amount between 0.25 g and 2.0 g. A control experiment was also performed in the absence of the PTC.

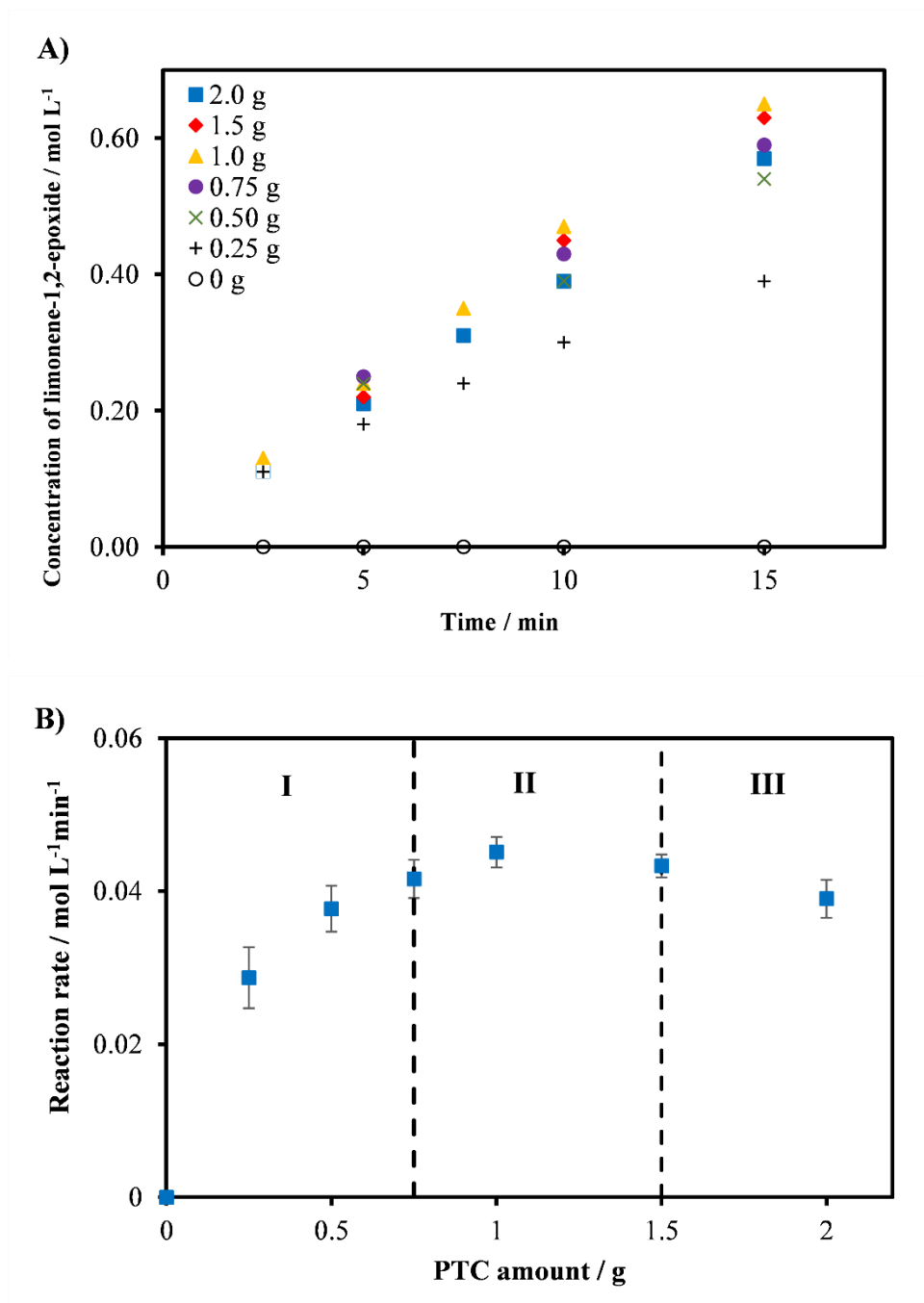


Figure 4.4. Batch epoxidation of (R)-(+)-limonene at reaction conditions of (R)-(+)-limonene (1.25 M), H<sub>2</sub>O<sub>2</sub> (1.25 M), Na<sub>2</sub>WO<sub>4</sub>·2H<sub>2</sub>O (0.006 M), Na<sub>2</sub>SO<sub>4</sub> (5.7 g), H<sub>2</sub>SO<sub>4</sub> (0.04 M), PTC ( 0 – 2.0 g), temperature (50 °C), toluene (500 mol%) and mixing speed of 1250 rpm, (A) The concentration of limonene-1,2-epoxide versus time at various amount of PTC. (B) The relationship between the initial reaction rate and the amount of PTC.

As depicted in Figure 4.4 (A), the reaction rate increases with increasing PTC. In the absence of a PTC, no conversion of (R)-(+)-limonene to any product was detected, as without the PTC, the mass transfer of the hydrophilic peroxy species between the phases would be negligible, so

the epoxidation would not occur due to the lack of active oxygen in the organic phase. The initial rates (15 minutes) values are obtained from the gradient of Figure 4.4 (A) and are tabulated in Appendix H. The initial rates values are plotted against the amount of PTC in Figure 4.4 (B). From this figure, three distinct regions can be observed. In region I, the initial reaction rate increases when the amount of PTC is increased from 0 g to 0.75 g. This clearly represents a mixing-dependent area where the reaction is mass transfer limited. In region II, the increase in the amount of PTC between 0.75 g and 1.5 g do not result in the increase of the initial reaction rate. It is presumed that this region presents the mixing-independent area where the rate of the epoxidation reaction is not limited by the mass transfer of the peroxy species.

Interestingly, further increase of the amount of PTC above 1.5 g, results in decreasing reaction rate (region III). This might be due to the increase in the viscosity of the reaction mixture. The PTC employed in this study is highly viscous and it is presumed that an excess of this compound significantly increases the viscosity of the reaction mixture, which in turn decreases the reaction rate. Similar observations were made by Shrikhande *et al.* (2010) for an aldol condensation reaction where an increase in phase transfer catalyst concentrations has a detrimental effect on the rates of reaction. Further experiments for the batch epoxidation of (R)-(+)-limonene were performed by fixing the amount of PTC at 1.0 g. This amount provides sufficient mass transfer between the phases while minimising the changes in the viscosity.

#### **4.5 Effects of metal catalyst and temperatures on decomposition of H<sub>2</sub>O<sub>2</sub>**

In this work, a tungsten-based polyoxometalates catalyst was employed for the epoxidation with H<sub>2</sub>O<sub>2</sub>. In the presence of a metal catalyst, H<sub>2</sub>O<sub>2</sub> decomposes to form oxygen (O<sub>2</sub>) and water (H<sub>2</sub>O) (Weiss, 1935). Elevated temperatures can promote the decomposition of the H<sub>2</sub>O<sub>2</sub> (Yazici and Deveci, 2010). Therefore, the effects of catalyst concentration and temperature on the decomposition of H<sub>2</sub>O<sub>2</sub> in the aqueous phase were investigated. In order to study the effect of catalyst concentration on the decomposition of H<sub>2</sub>O<sub>2</sub>, the concentration of catalyst precursor, Na<sub>2</sub>WO<sub>4</sub>·2H<sub>2</sub>O varied between 0.002 M and 0.02 M at a temperature of 70 °C. The effect of temperature on the decomposition of H<sub>2</sub>O<sub>2</sub> was studied within the temperature range 30 to 80 °C at a Na<sub>2</sub>WO<sub>4</sub>·2H<sub>2</sub>O concentration of 0.02 M. Both studies were performed for approximately 60 min. The initial concentration of H<sub>2</sub>O<sub>2</sub> (30 wt. % in H<sub>2</sub>O) stock solution as measured by titration with 0.02 M potassium permanganate solution was ~9.8 M. The results of these studies are shown in Figures 4.5 (A) and (B).

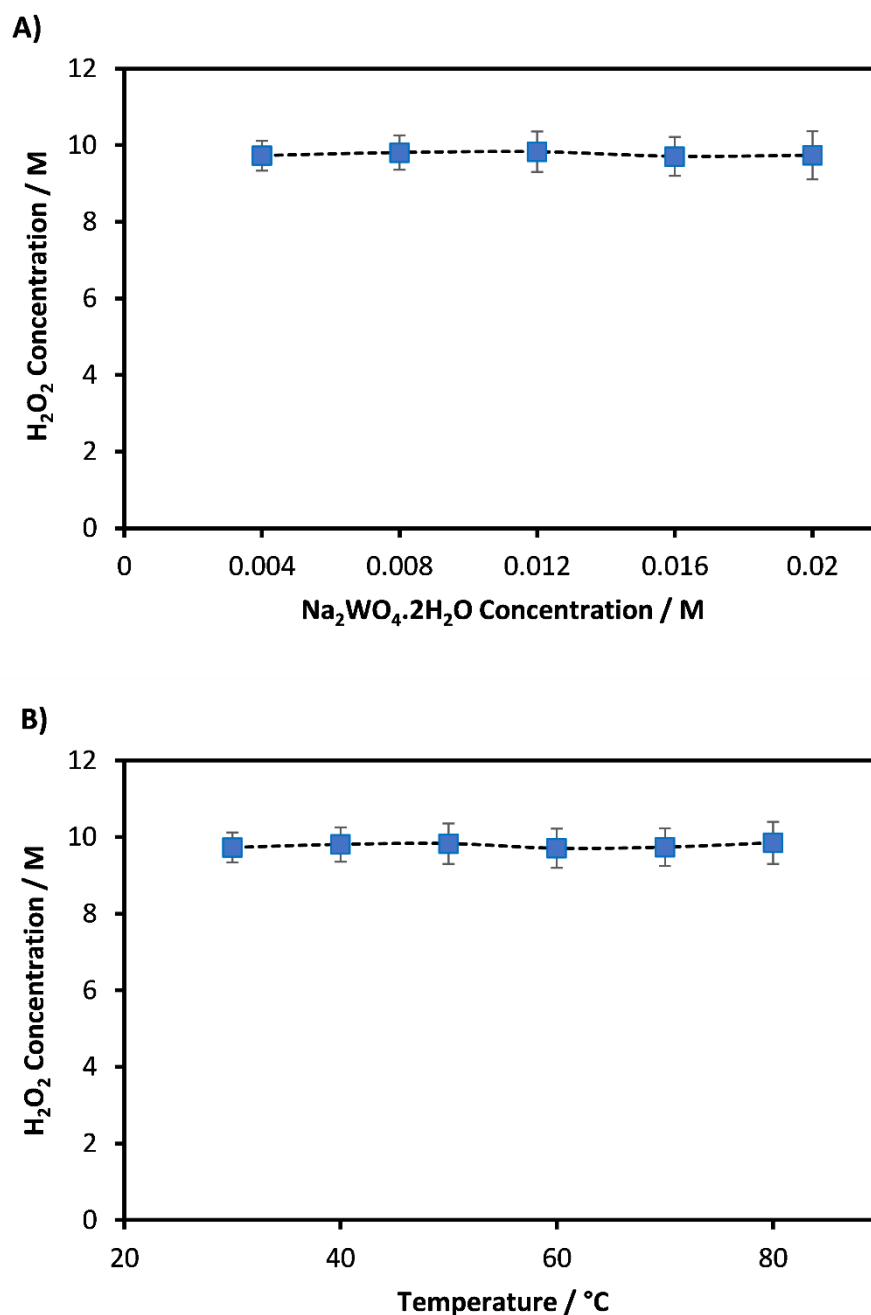


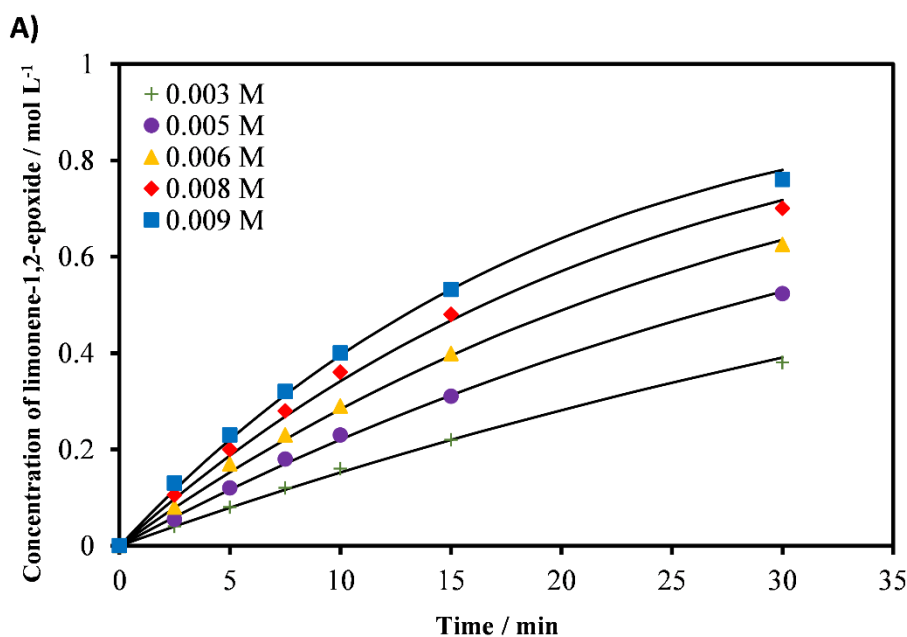
Figure 4.5. Effects of catalyst concentration and temperature on the decomposition of  $H_2O_2$ , (A) concentration of  $H_2O_2$  with increasing  $Na_2WO_4 \cdot 2H_2O$  catalyst concentration from 0.002 - 0.02 M at 70  $^{\circ}C$  temperature and 60 min, (B) concentration of  $H_2O_2$  with increasing temperature from 30 – 80  $^{\circ}C$ , 0.02 M  $Na_2WO_4 \cdot 2H_2O$  catalyst and 60 min.

As presented in Figure 4.5 (A), the concentration of  $H_2O_2$  in the aqueous phase remains constant with increasing  $Na_2WO_4 \cdot 2H_2O$  concentration from 0.002 M to 0.02 M. The concentration of  $H_2O_2$  for all experiments remained close to the stock concentration, ~9.8 M. Similarly, Figure 4.5 (B) shows that increasing the temperature up to 80  $^{\circ}C$ , had a negligible effect on the decomposition of  $H_2O_2$ . The concentration of  $H_2O_2$  in the aqueous phase remained constant

with increasing temperature. The results indicate that the decomposition of  $\text{H}_2\text{O}_2$  is negligible in the range of the catalyst concentrations and temperatures tested. These results are in accord with the literature, which states that a tungsten-based polyoxometalate catalyst has the least impact on  $\text{H}_2\text{O}_2$  decomposition compared to other metal catalyst (Sato *et al.*, 1996; Kon *et al.*, 2011; Takumi *et al.*, 2014). Further experiments in this study were carried out within these ranges of catalyst concentration and temperatures.

#### 4.6 Study of kinetics of (R)-(+)-limonene epoxidation

Figures 4.6 (A) and (B) shows the results for the kinetic study of (R)-(+)-limonene epoxidation using a polytungstophosphate catalyst. The initial rate method based on pseudo first-order conditions was applied to determine the kinetic parameters and the reaction orders. To determine the reaction order with respect to the catalyst, the concentrations of the catalyst precursor,  $\text{Na}_2\text{WO}_4 \cdot 2\text{H}_2\text{O}$  were varied between 0.003 M and 0.009 M, with the initial concentrations of (R)-(+)-limonene,  $\text{H}_2\text{O}_2$  and solvent kept constant (1.25 M each).



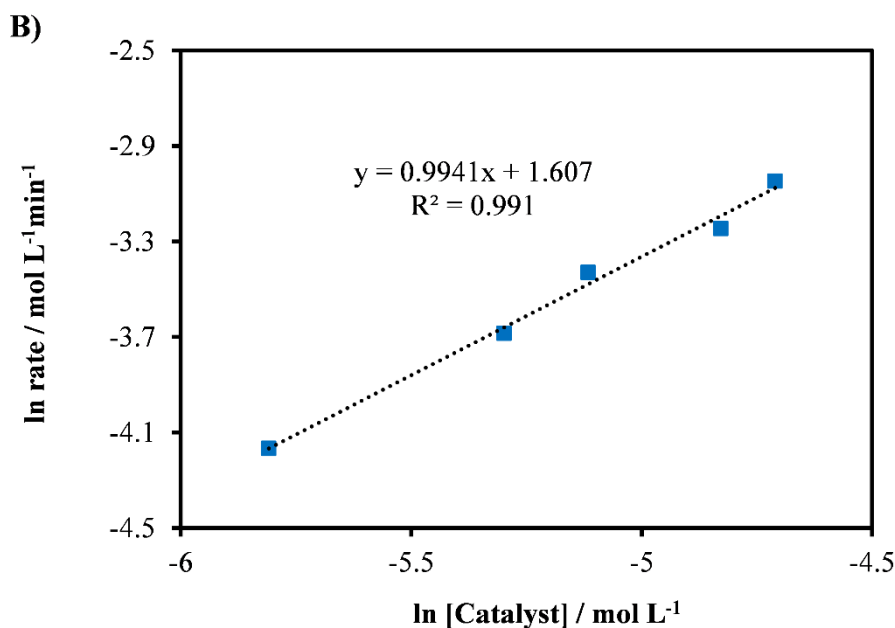


Figure 4.6. Batch epoxidation at reaction conditions of (R)-(+)-limonene (1.25 M),  $H_2O_2$  (1.25 M),  $Na_2WO_4 \cdot 2H_2O$  (0.003 M – 0.009 M),  $Na_2SO_4$  (5.7 g),  $H_2SO_4$  (0.04 M), 1.0 g PTC, temperature (50 °C), toluene (500 mol%), and 1250 rpm mixing speed, (A) The concentration of limonene-1,2-epoxide versus time at various concentration of  $Na_2WO_4 \cdot 2H_2O$ , (B) The plot of the natural log of the initial reaction rates and  $Na_2WO_4 \cdot 2H_2O$  concentrations. The lines in (A) are fitted to the kinetic model by using Equations (3.6) – (3.11) and the rate constant in Table 4.1.

As shown in Figure 4.6 (A), the reaction rate increases with increasing  $Na_2WO_4 \cdot 2H_2O$  concentration, as expected. The initial rates (15 minutes) values are obtained from the gradient of Figure 4.6 (A) and are tabulated in Appendix H. When  $Na_2WO_4 \cdot 2H_2O$  concentration is doubled from 0.003 M to 0.006 M, the initial rates increase from  $0.0155 \text{ mol L}^{-1} \text{ min}^{-1}$  to  $0.0324 \text{ mol L}^{-1} \text{ min}^{-1}$ , increasing by a factor of  $\sim 2$ . The plot of the natural log between the initial rates and  $Na_2WO_4 \cdot 2H_2O$  concentration is shown in Figure 4.6 (B). The plot produces a straight line with a gradient of  $\sim 1$  implying that this is a first-order reaction. In Figure 4.6 (A), the kinetic model (presented by the smooth lines) can predict the formation of limonene-1,2-epoxide at various catalyst concentration tested, and these were validated by the experimental data.

Figures 4.7 (A) and (B) presents the results for the determinations of the reaction order with respect to (R)-(+)-limonene by varying the initial concentration of (R)-(+)-limonene, from 0.25 M to 1.25 M. The concentrations of  $H_2O_2$  were kept constant (1.25 M). The solvent amount was varied accordingly to maintain a constant volume. Care was taken to ensure that the volume ratio between the organic and the aqueous phases was maintained constant.



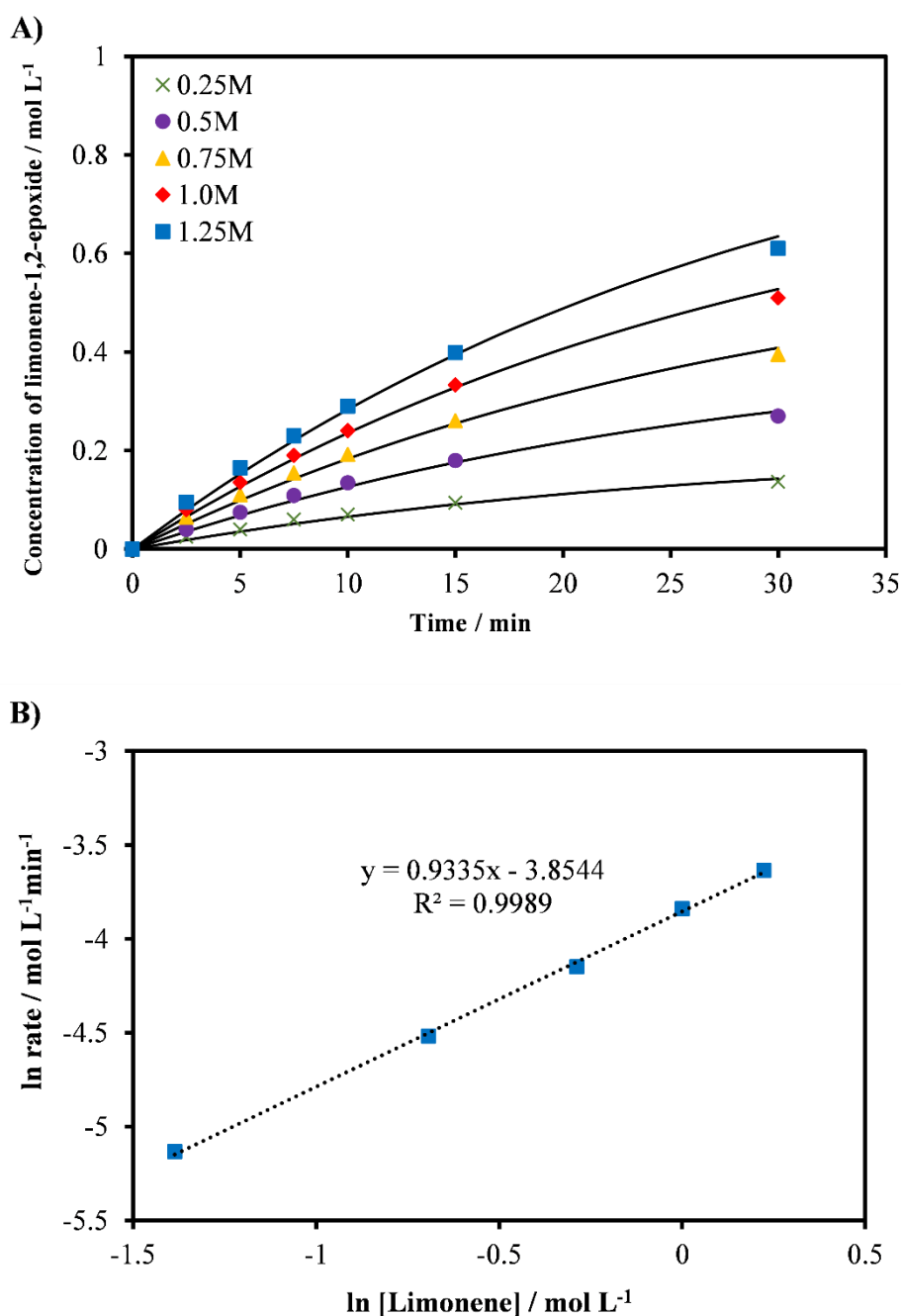
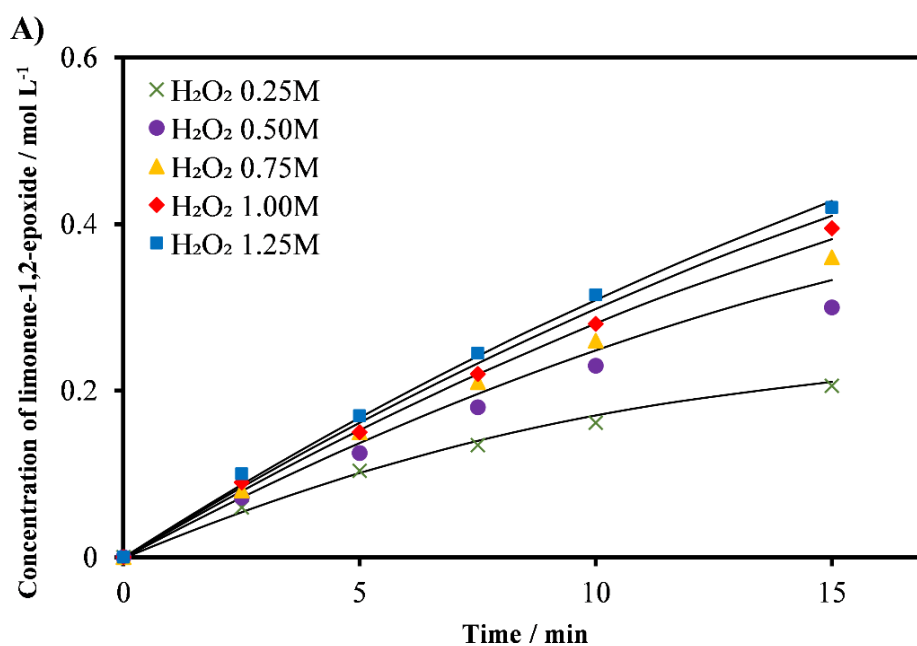


Figure 4.7. Batch epoxidation at reaction conditions of (R)-(+)-limonene (0.25 M - 1.25 M),  $H_2O_2$  (1.25 M),  $Na_2WO_4 \cdot 2H_2O$  (0.006 M),  $Na_2SO_4$  (5.7 g),  $H_2SO_4$  (0.04 M), 1.0 g PTC, temperature (50 °C), toluene (500 mol%), and 1250 rpm mixing speed, (A) The concentration of limonene-1,2-epoxide versus time at various initial (R)-(+)-limonene concentrations, (B) The plot of the natural log of the initial reaction rates and initial (R)-(+)-limonene concentrations. The lines in (A) are fitted to the kinetic model by using Equations (3.6) – (3.11) and the rate constant in Table 4.1.

As illustrated in Figure 4.7 (A), the reaction rates increase with increasing initial (R)-(+)-limonene concentration. The initial rates (15 minutes) values are obtained from the gradient of Figure 4.7 (A) and are tabulated in Appendix H. When the initial (R)-(+)-limonene concentration is doubled from 0.50 M to 1.00 M, the initial rates increase from  $0.013 \text{ mol L}^{-1} \text{ min}^{-1}$  to  $0.0252 \text{ mol L}^{-1} \text{ min}^{-1}$ , increasing by a factor of  $\sim 2$ . The gradient obtained from Figure 4.7 (B), approximately  $\sim 1$ , indicating that the reaction is first-order in terms of the concentration of (R)-(+)-limonene. As shown in Figure 4.7 (A), the kinetic model fits the experimental data with a slight deviation at the reaction time of 30 minutes for all concentrations of (R)-(+)-limonene tested.

The reaction order with respect to  $\text{H}_2\text{O}_2$  was determined by varying the initial concentration of  $\text{H}_2\text{O}_2$ , from 0.25 M to 1.25 M. In this case, the initial concentration of (R)-(+)-limonene was kept constant (1.25 M). The amounts of solvent were varied accordingly to maintain a constant volume. Figures 4.8 (A) and (B) presents the results.



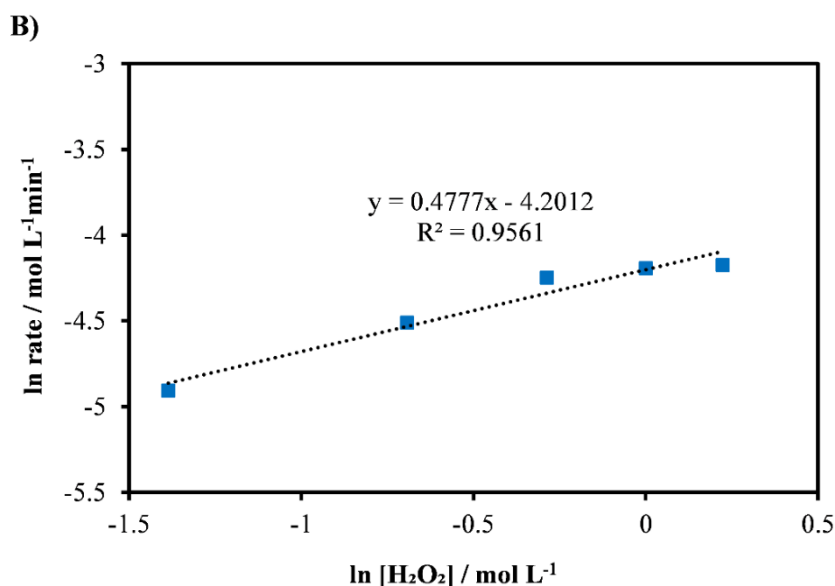


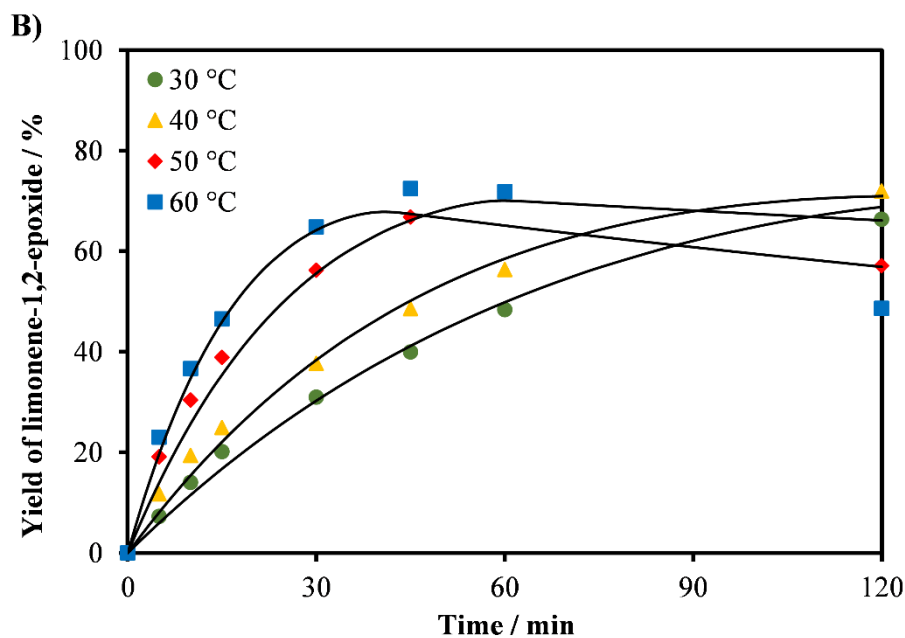
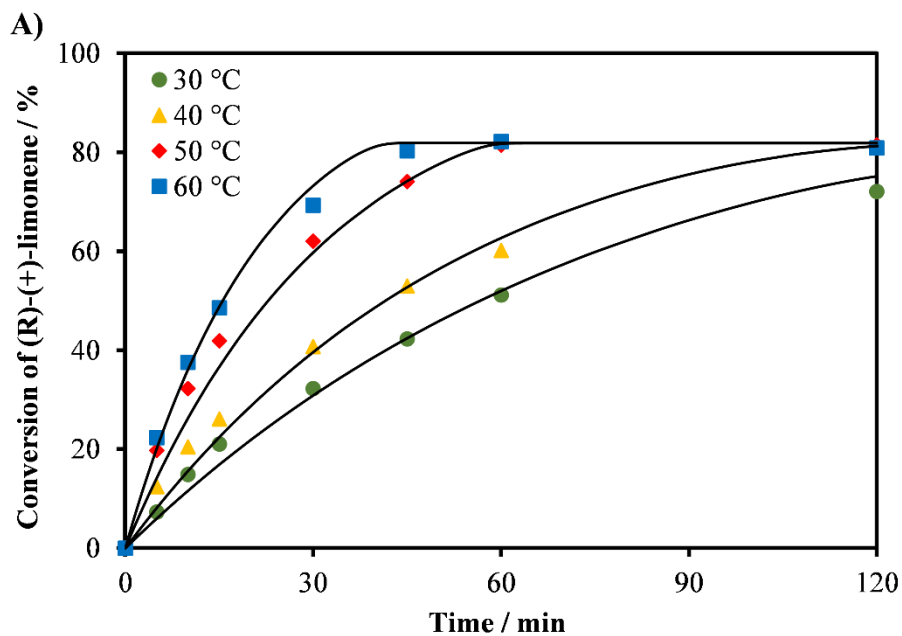
Figure 4.8. Batch epoxidation at reaction conditions of (R)-(+)-limonene (1.25 M), H<sub>2</sub>O<sub>2</sub> (0.25 M - 1.25 M), Na<sub>2</sub>WO<sub>4</sub>·2H<sub>2</sub>O (0.006 M), Na<sub>2</sub>SO<sub>4</sub> (5.7 g), H<sub>2</sub>SO<sub>4</sub> (0.04 M), 1.0 g PTC, temperature (50 °C), toluene (500 mol%), and 1250 rpm mixing speed, (A) The concentration of limonene-1,2-epoxide versus time at various initial H<sub>2</sub>O<sub>2</sub> concentrations, (B) The plot of the natural log of the initial reaction rates and initial H<sub>2</sub>O<sub>2</sub> concentrations. The lines in (A) are fitted to the kinetic model by using Equations (3.6) – (3.11) and the rate constant in Table 4.1.

Figure 4.8 (A) illustrates that increasing the concentration of H<sub>2</sub>O<sub>2</sub> increases the reaction rate. The initial rates (15 minutes) values are obtained from the gradient of Figure 4.8 (A) and are tabulated in Appendix H. The gradient obtained from Figure 4.8 (B) shows a fractional reaction order of ~0.5, indicating a complex mechanism as illustrated in Figure 2.8 in Chapter 2.

According to Equation (3.7), increasing the concentration of H<sub>2</sub>O<sub>2</sub> increases the formation of the polytungstophosphate but is limited to the concentration of tungstate (WO<sub>4</sub><sup>2-</sup>) and phosphate (PO<sub>4</sub><sup>3-</sup>). This finding also implied that the epoxidation of (R)-(+)-limonene, as shown by Equation (3.8), would probably be the rate-determining step. Hence, increasing the H<sub>2</sub>O<sub>2</sub> concentration would only increase the rate of formation of the peroxy species. Yadav and Satoskar (1997) reported similar behaviour for the epoxidation of undecylenic acid, where the rate was independent of the H<sub>2</sub>O<sub>2</sub> concentration when the ratio of the [H<sub>2</sub>O<sub>2</sub>]/[catalyst] was high. Kamata *et al.* (2004) also found an apparent zero-order dependence on the H<sub>2</sub>O<sub>2</sub> concentration for the epoxidation of alkene. The kinetic model shows a minor deviation especially at H<sub>2</sub>O<sub>2</sub> concentration between 0.5 M and 1.0 M, where the model predicts a slightly higher concentration of limonene-1,2-epoxide produced at 30 minutes reaction time (see Figure 4.8 (A)).

#### 4.7 Effect of temperature on the (R)-(+)-limonene epoxidation

Figures 4.9 (A) – (D) present the results for the effects of temperature on the epoxidation of (R)-(+)-limonene investigated at the reaction temperature between 30 °C and 60 °C. Care was taken to ensure isothermal temperature conditions are maintained throughout the reaction time.



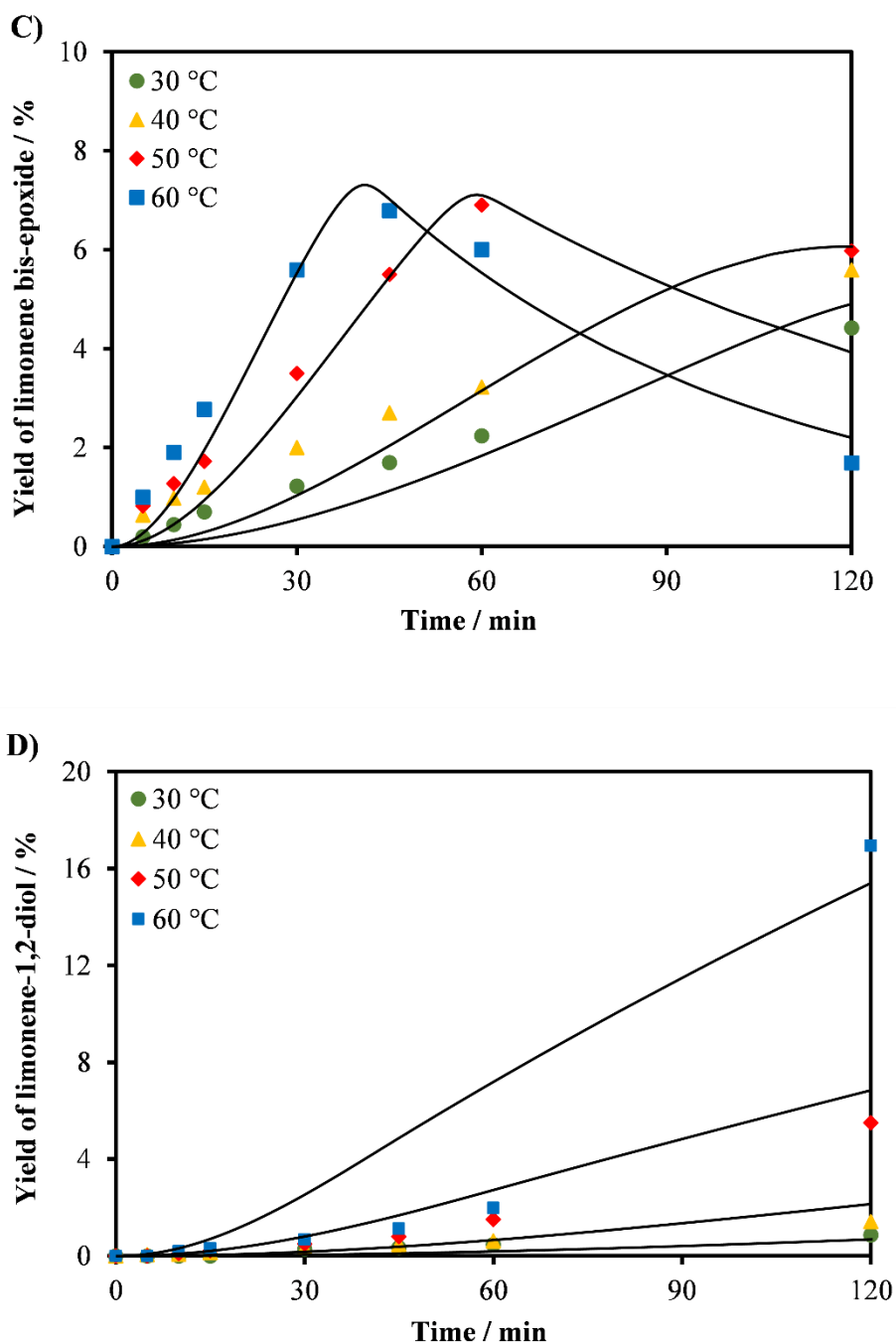
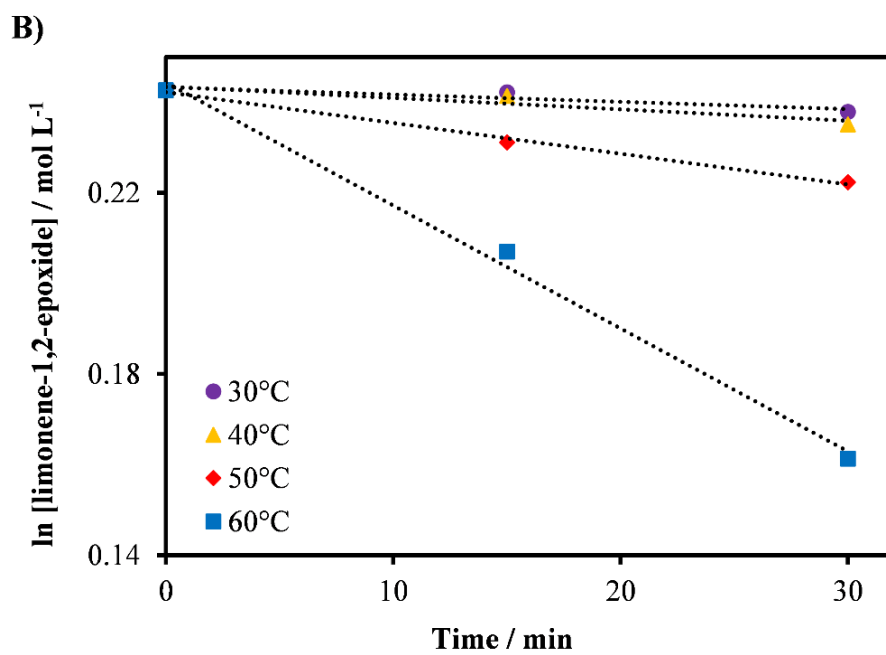
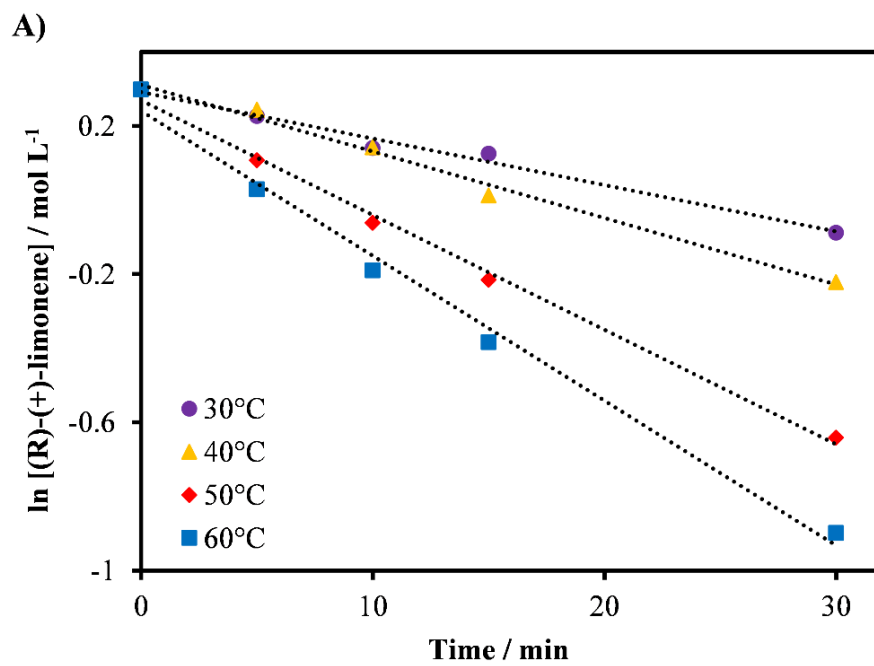


Figure 4.9. The effects of temperature on (R)-(+)-limonene epoxidation at reaction conditions of (R)-(+)-limonene (1.25 M),  $H_2O_2$  (1.25 M),  $Na_2WO_4 \cdot 2H_2O$  (0.006 M),  $Na_2SO_4$  (5.7 g),  $H_2SO_4$  (0.06M), 1.0 g PTC, temperature (30 – 60 °C), toluene (500 mol%) and 1250 rpm mixing. (A) conversion of (R)-(+)-limonene, (B) yield of limonene-1,2-epoxide, (C) yield of limonene bis-epoxide and (D) yield of limonene-1,2-diol. The lines are fitted to the kinetic model by using Equations (3.6) – (3.11) and the rate constant in Table 4.1.

As shown in Figure 4.9 (A), the rates of (R)-(+)-limonene conversions to various products increased monotonically with temperature, as expected. The conversion of (R)-(+)-limonene reaches equilibrium (80 %) at a reaction time of 120 min for all temperatures. However, as shown in Figure 4.9 (B), at a temperature higher than 50 °C, the yield of limonene-1,2-epoxide attains a maximum of 73 % before gradually decreasing. Figure 4.9 (C) shows that the yield of limonene bis-epoxide attains a maximum of 7 %. The decrease in both limonene-1,2-epoxide and limonene bis-epoxide yields over the reaction time can be explained by the rate of hydrolysis, which increases at a temperature above 50 °C (Hachiya *et al.*, 2012). Hydrolysis of limonene-1,2-epoxide and limonene bis-epoxide results in the formation of limonene-1,2-diol and limonene bis-diol, respectively (Grigoropoulou and Clark, 2006). Figure 4.9 (D) shows that the yield of limonene-1,2-diol at 60 °C is over 15 % at a reaction time of 120 min. This result is more than double the yield at 50 °C (7 %). Clearly, elevated temperatures are detrimental to the selectivity of limonene-1,2-epoxide.

As can be seen in Figure 4.9 (A) – (D), the kinetic model (presented by the smooth lines) is able to predict the formation of limonene bis-epoxide and limonene-1,2-diol at temperatures up to 60 °C and these were validated by experimental data. To ensure the highest selectivity towards the formation of limonene-1,2-epoxide, it is suggested that the epoxidation reaction be performed at a temperature below 50 °C.

The Arrhenius dependence for the formation of the desired product, limonene-1,2-epoxide, and a major by-product, limonene-1,2-diol, was determined by varying the reaction temperature between 30 °C and 60 °C. Figures 4.10 (A) – (B) presents the natural log of the concentrations of (R)-(+)-limonene (Figure 4.10 (A)) and limonene-1,2-epoxide (Figure 4.10 (B)) at various temperatures, and the temperature dependence of limonene-1,2-epoxide and limonene-1,2-diol formation as plots of  $\ln(k_{lim})$  and  $\ln(k_{diol})$  versus  $1/T$  (Figure 4.10 C).



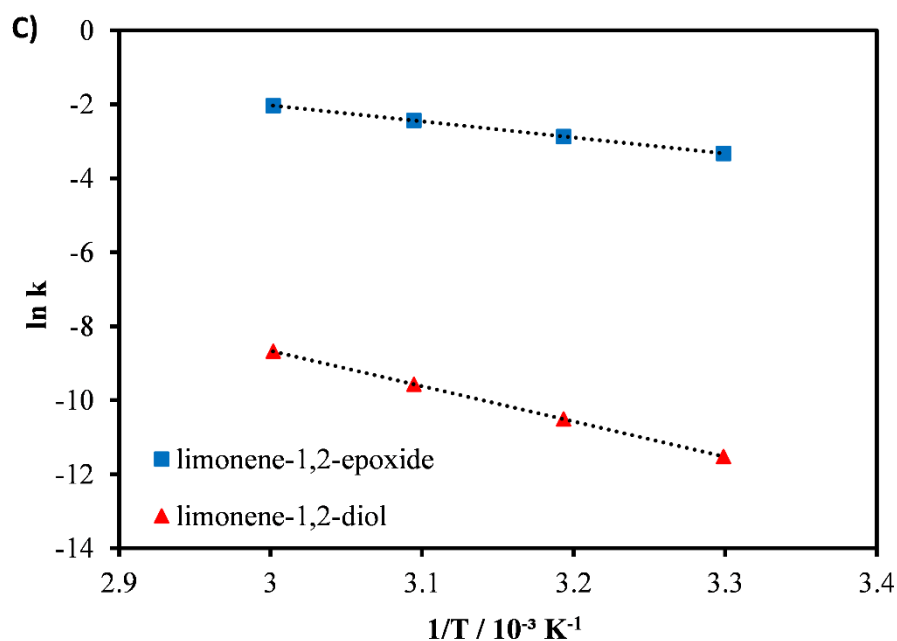


Figure 4.10. (A) The plot of the natural log of (R)-(+)-limonene concentration versus time at various temperatures for the formation of limonene-1,2-epoxide for batch epoxidation at reaction conditions of (R)-(+)-limonene (1.25 M),  $H_2O_2$  (1.25 M),  $Na_2WO_4 \cdot 2H_2O$  (0.006 M),  $H_2SO_4$  (0.04 M), 1.0 g PTC, toluene (500 mol%) and 1250 rpm mixing, and (B) limonene-1,2-diol formation for reactions at limonene-1,2-epoxide (1.27 M),  $H_2O_2$  (1.27 M),  $Na_2WO_4 \cdot 2H_2O$  (0.006 M),  $Na_2SO_4$  (5.7 g),  $H_2SO_4$  (0.04 M), 1.0 g PTC, toluene (500 mol%) and 1250 rpm mixing, (C) Arrhenius activation energies ( $E_a$ ) and temperature dependence of the rate constant for the formation of limonene-1,2-epoxide and limonene-1,2-diol.

The activation energy for the formation of limonene-1,2-epoxide obtained from the gradient of Figure 4.10 (C) was determined to be  $\sim 36 \text{ kJ mol}^{-1}$ . This figure is higher than the  $16 \text{ kJ mol}^{-1}$  reported by Cagnoli *et al.* (2005) for the epoxidation of (R)-(+)-limonene using a titanium-based catalyst. Villa *et al.* (2002) reported a much higher value ( $76 \text{ kJ mol}^{-1}$ ) for the epoxidation of (R)-(+)-limonene, but they had used a heterogeneous tungsten-based catalyst. On the other hand, the activation energy for the formation of limonene-1,2-diol was determined to be  $\sim 79 \text{ kJ mol}^{-1}$ . This result confirms that the formation of a side-product, limonene-1,2-diol proceeds more slowly at the lower temperatures in this range than with limonene-1,2-epoxide. However, at temperatures above  $50 \text{ }^\circ\text{C}$ , the reaction rate becomes more significant, resulting in a higher yield of limonene-1,2-diol, see Figure 4.10 (A) and (B). Table 4.1 lists the kinetic parameters obtained from the study.

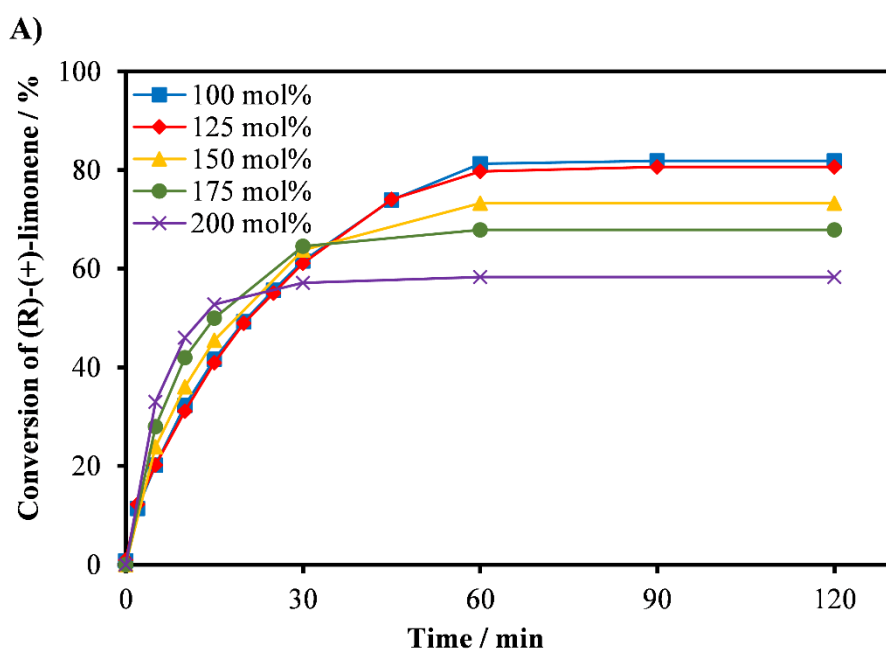


	Pre-exponential factor ( $A / s^{-1}$ )	Activation energy ( $E_a / kJ mol^{-1}$ )	
		This work	References
Formation of limonene-1,2-epoxide	$5.9 \times 10^4$	36	16 (Cagnoli <i>et al.</i> , 2005) 76 (Villa <i>et al.</i> , 2002)
Formation of limonene bis-epoxide	$8.6 \times 10^4$	43	-
Formation of limonene-1,2-diol	$4.9 \times 10^8$	79	-

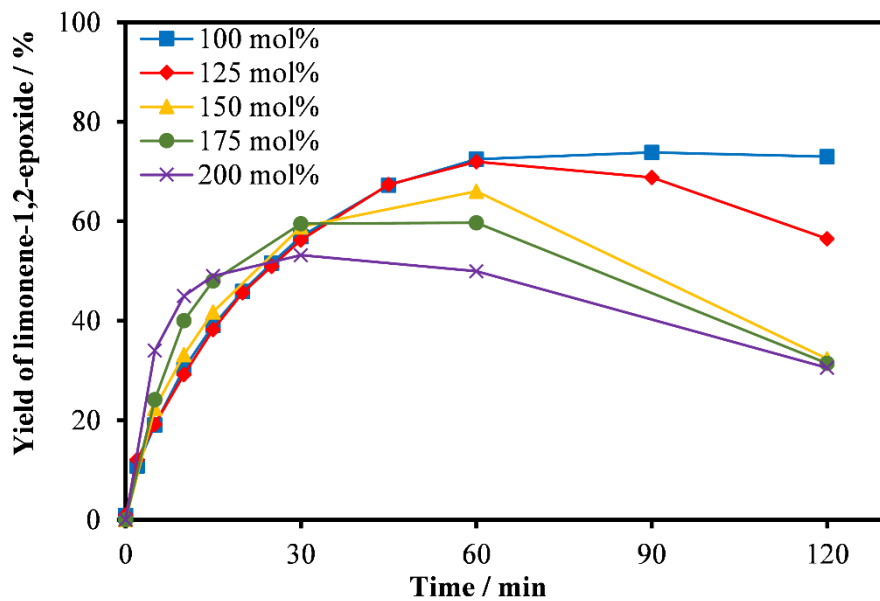
Table 4.1 The pre-exponential factor and the activation energy for the formation of limonene-1,2-epoxide, limonene bis-epoxide and limonene-1,2-diol.

#### 4.8 Effect of H<sub>2</sub>O<sub>2</sub> oxidant amount on (R)-(+)-limonene epoxidation

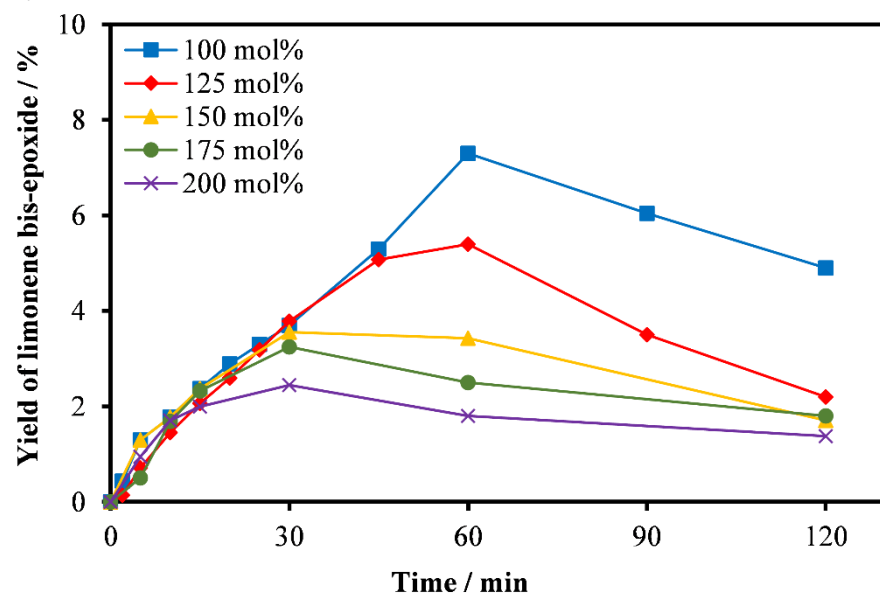
The results of the investigations of the effect of the H<sub>2</sub>O<sub>2</sub> amount by varying the initial amount of H<sub>2</sub>O<sub>2</sub> from 100 mol% to 200 mol% are shown in Figures 4.11 (A) – (D).



B)



C)



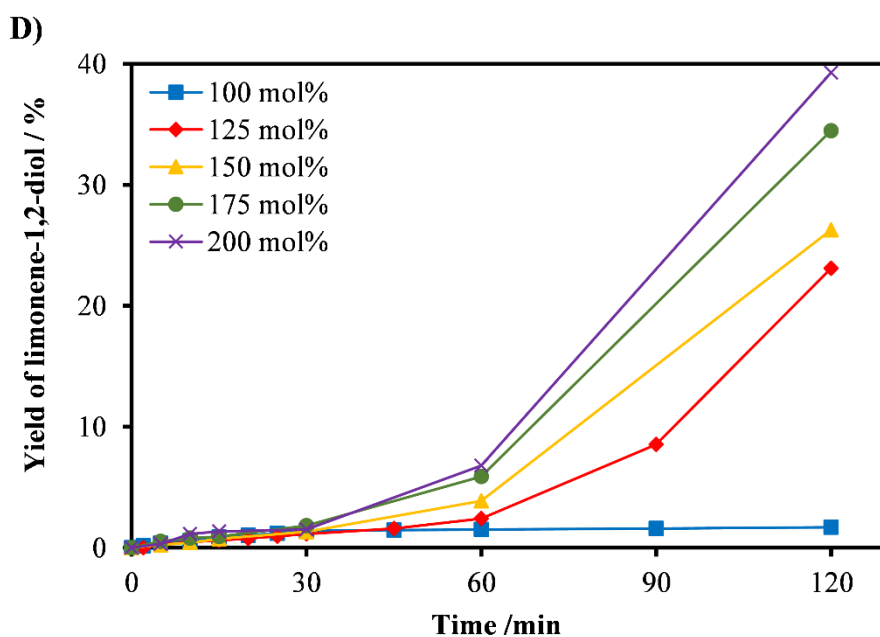


Figure 4.11. The effect of the  $H_2O_2$  amount on (R)-(+)-limonene epoxidation for reactions at (R)-(+)-limonene (1.25 M),  $H_2O_2$  (1.25 M – 2.50 M),  $Na_2WO_4 \cdot 2H_2O$  (0.006 M),  $H_2SO_4$  (0.06 M),  $Na_2SO_4$  (5.7 g), 1.0 g PTC, temperature (50 °C), toluene (500 mol%) and 1250 rpm mixing, (A) conversion of (R)-(+)-limonene, (B) yield of limonene-1,2-epoxide, (C) yield of limonene bis-epoxide, and (D) yield of limonene-1,2-diol.

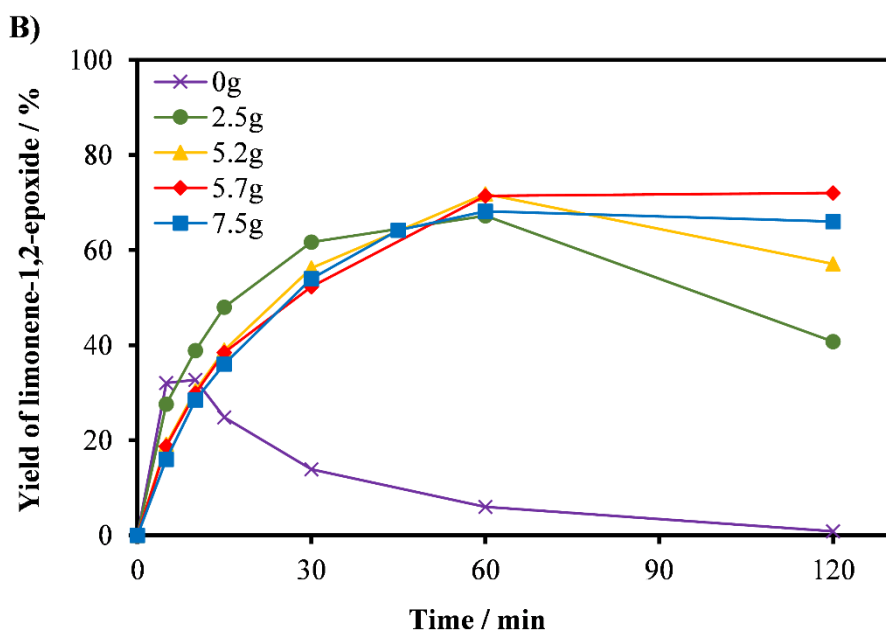
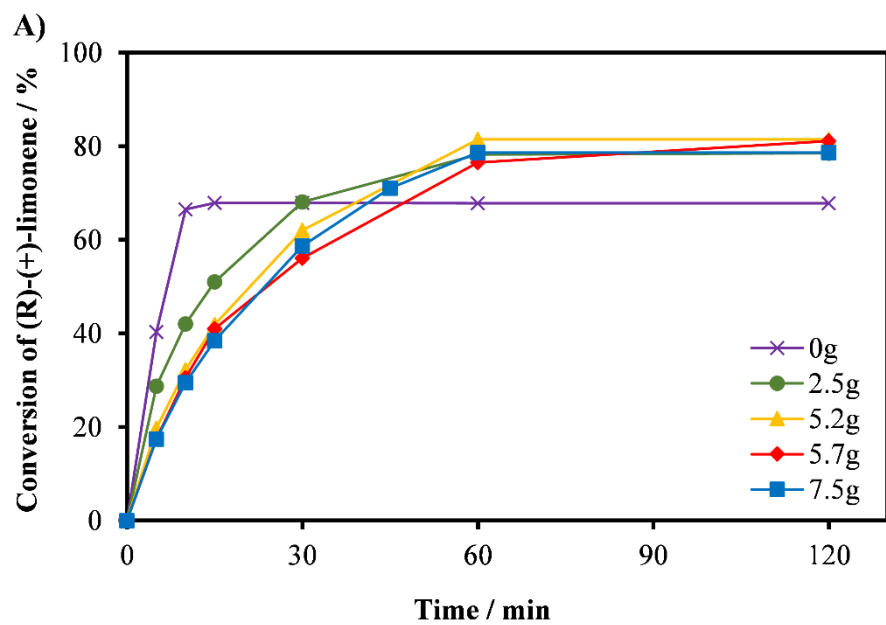
Figure 4.11 (A) shows that increasing the  $H_2O_2$  amount accelerates the initial reaction rates. However, the final conversions of (R)-(+)-limonene decrease with increasing  $H_2O_2$  amounts. The conversion of (R)-(+)-limonene decreases from 82 % to 58 % when the  $H_2O_2$  amount is increased from 100 mol% to 200 mol%. The decrease in conversion with the increasing amount of  $H_2O_2$  might be attributed to the dilution of the peroxy species in the aqueous phase since the amount of  $H_2O_2$  is in excess relative to a fixed amount of the peroxy species. The dilution results in a few oxidative species transferred to the organic phase to oxidise the double bond. This finding is similar to the observation of Wang and Huang, who reported a decrease in conversion for 1,7-octadiene with an increasing amount of oxidant ( $H_2O_2$ ) (Wang and Huang, 2004). As illustrated in Figure 4.11 (B), the yield of limonene-1,2-epoxide also decreased with an increasing  $H_2O_2$  amount. The yields are 74 % and 30 % for  $H_2O_2$  amounts of 100 mol% and 200 mol%, respectively. Above 125 mol%, the yield of limonene-1,2-epoxide attained a maximum before decreasing with time, becoming more pronounced as the  $H_2O_2$  amount increases. Increase in the  $H_2O_2$  amount from 100 mol% to 200 mol% also led to a decrease in the yield of limonene bis-epoxide (see Figure 4.11 C), which was not expected. The yield of limonene bis-epoxide is highest when the oxidant amount used is 100 mol%, achieving a

maximum of 8 % yield before gradually decreasing. This finding is in contrast with the observation of Takumi *et al.* (2014) who reported an increase of up to 40 % yield of limonene bis-epoxide with an increasing oxidant amount, which might be attributed to the lower acid concentration used in their study. Furthermore, they performed the reaction at a much lower temperature, decreasing the overall reaction rates, which in turn allowed the steady formation of limonene bis-epoxide. In this study, the decrease in the yields of both limonene-1,2-epoxide and limonene bis-epoxide when increasing the H<sub>2</sub>O<sub>2</sub> amount was due to the increased rate of diol formation.

The yield of limonene-1,2-diol increased dramatically with increasing H<sub>2</sub>O<sub>2</sub> amount, as shown in Figure 4.11 (D). The yield at a reaction time of 120 min rises from 8 % to about 40 % with increasing H<sub>2</sub>O<sub>2</sub>, due to the influence of H<sup>+</sup> and H<sub>2</sub>O on the formation of diol (Gunam Resul *et al.*, 2018). The increased H<sub>2</sub>O concentration is in proportion to the increase in the H<sub>2</sub>O<sub>2</sub> amount since 30 wt.% H<sub>2</sub>O<sub>2</sub> in H<sub>2</sub>O solution was used. The deleterious effect of H<sub>2</sub>O on the epoxidation of (R)-(+)-limonene can be inferred from this study. The increased H<sub>2</sub>O concentration leads to significantly higher hydrolysis of the epoxide ring. To maintain the high selectivity towards limonene-1,2-epoxide and to minimise the formation of limonene-1,2-diol, using an equivalent amount (100 mol%) of H<sub>2</sub>O<sub>2</sub> to (R)-(+)-limonene is therefore suggested.

#### **4.9 Effect of Na<sub>2</sub>SO<sub>4</sub> on the yield of limonene-1,2-epoxide**

The presence of H<sub>2</sub>O in an H<sub>2</sub>O<sub>2</sub> solution was found to adversely affect the selectivity of limonene-1,2-epoxide due to the hydrolysis of the epoxide ring. Many methods have been developed to suppress the hydrolysis process, including the addition of an inorganic salt, such as Na<sub>2</sub>SO<sub>4</sub>, which has been found to improve the selectivity to terpene oxides (Grigoropoulou and Clark, 2006; Hachiya *et al.*, 2012). Figure 4.12 (A) – (D) present the results for the investigations of the effect of Na<sub>2</sub>SO<sub>4</sub> on limonene-1,2-epoxide yields in (R)-(+)-limonene epoxidation using Na<sub>2</sub>SO<sub>4</sub> amounts from 2.5 g to 7.5 g. A control experiment was also performed in the absence of Na<sub>2</sub>SO<sub>4</sub>.



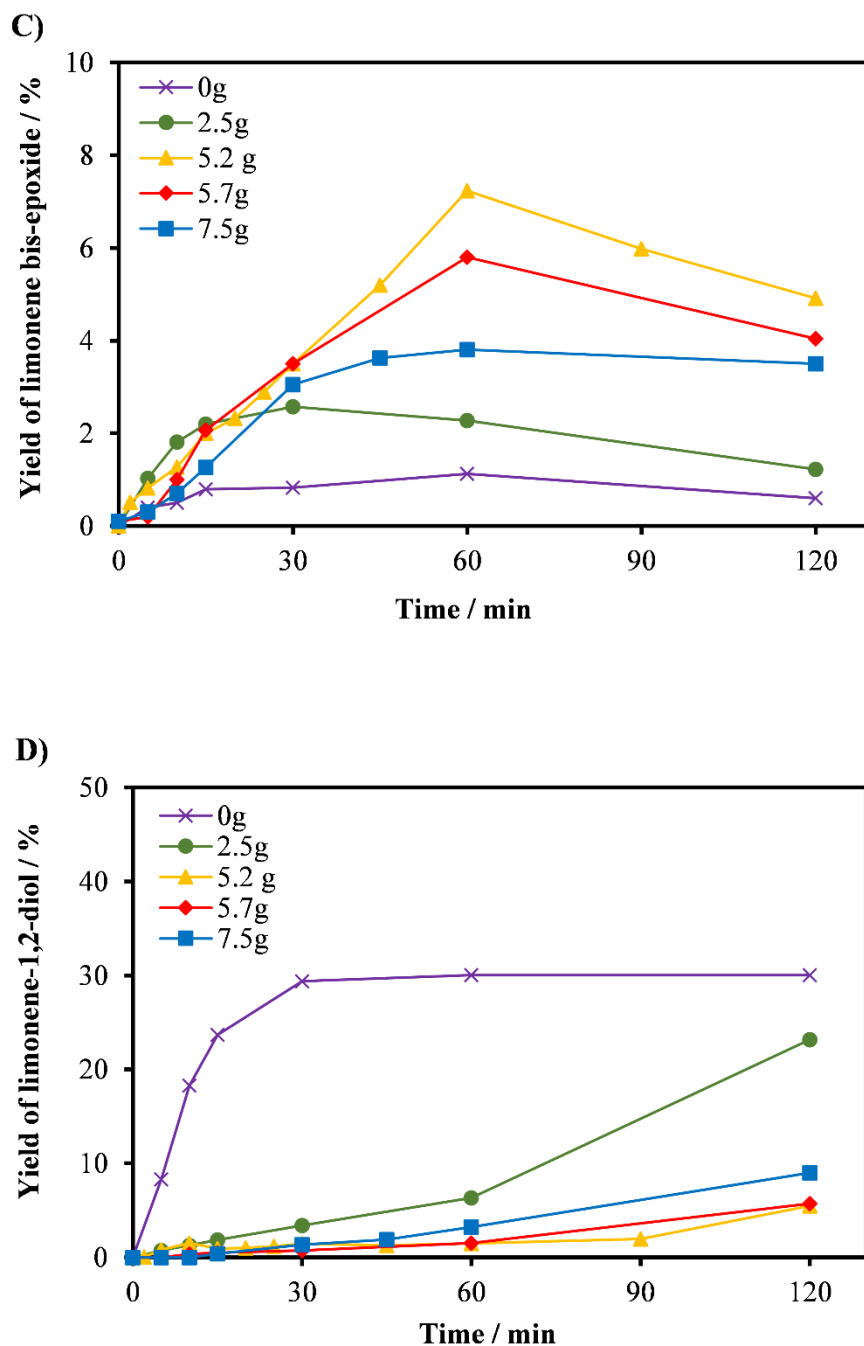


Figure 4.12. The effect of the  $\text{Na}_2\text{SO}_4$  amount on (R)-(+)-limonene epoxidation at reaction conditions of (R)-(+)-limonene (1.25 M),  $\text{H}_2\text{O}_2$  (1.25 M),  $\text{Na}_2\text{WO}_4 \cdot 2\text{H}_2\text{O}$  (0.006 M),  $\text{H}_2\text{SO}_4$  (0.06 M), 1.0 g PTC, temperature (50 °C), toluene (500 mol%) and 1250 rpm mixing, (A) conversion of (R)-(+)-limonene, (B) yield of limonene-1,2-epoxide, (C) yield of limonene bis-epoxide and (D) yield of limonene-1,2-diol.

As can be seen in Figure 4.12 (A), the conversion of (R)-(+)-limonene increased up to 80 % when the amount of  $\text{Na}_2\text{SO}_4$  was increased from 0 g to 7.5 g. Figure 4.12 (B) shows that the addition of  $\text{Na}_2\text{SO}_4$  increases the yield of limonene-1,2-epoxide. The yield at a reaction time of

120 min increases from less than 5 % to 75 % when the amount of  $\text{Na}_2\text{SO}_4$  is increased from 0 g to 5.7 g. There is no decrease in the yield of limonene-1,2-epoxide over time when more than 5.7 g of  $\text{Na}_2\text{SO}_4$  is used. Although the mechanism of the salt effect is difficult to determine, it has been postulated that the salt ionised into its respective ions, inducing a 'salting-out' process (Hyde *et al.*, 2017), as the ionic strength of the aqueous phase increases with the presence of  $\text{Na}_2\text{SO}_4$  (Grigoropoulou and Clark, 2006). The ions repulse nonelectrolyte compound such as limonene-1,2-epoxide in the aqueous phase, minimising the epoxide solubility at the interphase, which in turn suppresses the hydrolysis process.

As can be seen in Figure 4.12 (C), the yield of limonene bis-epoxide attains a maximum of 7 % at reaction time 60 min before gradually decreasing, when 5.7 g of  $\text{Na}_2\text{SO}_4$  was used. The yield of limonene bis-epoxide was much lower when other amount of  $\text{Na}_2\text{SO}_4$  was used. It is presumed that the decrease in the yield over the reaction time was due to hydrolysis of limonene bis-epoxide. Hydrolysis of limonene bis-epoxide might produce a combination of monoepoxide-diol and tetraol. However, these hydrolysis products were not detected in the GC analysis of the sample at reaction time 120 min, see Figure 4.13. This might be either due to the limitation of the GC method or the resulting diols dissolved in the aqueous phase. The latter might require a different analysis technique such as High-Performance Liquid Chromatography (HPLC).

Figure 4.12 (D) confirms the importance of  $\text{Na}_2\text{SO}_4$ , where the yield of limonene-1,2-diol decreases from 30 % to about 5 % with an increasing amount of  $\text{Na}_2\text{SO}_4$ . The utilisation of  $\text{Na}_2\text{SO}_4$  effectively reduces the hydrolysis of limonene-1,2-epoxide. The epoxidation of (R)-(+)-limonene using  $\text{H}_2\text{O}_2$  achieves the highest selectivity to limonene-1,2-epoxide when the aqueous phase is 100 % saturated with  $\text{Na}_2\text{SO}_4$  (5.7 g).

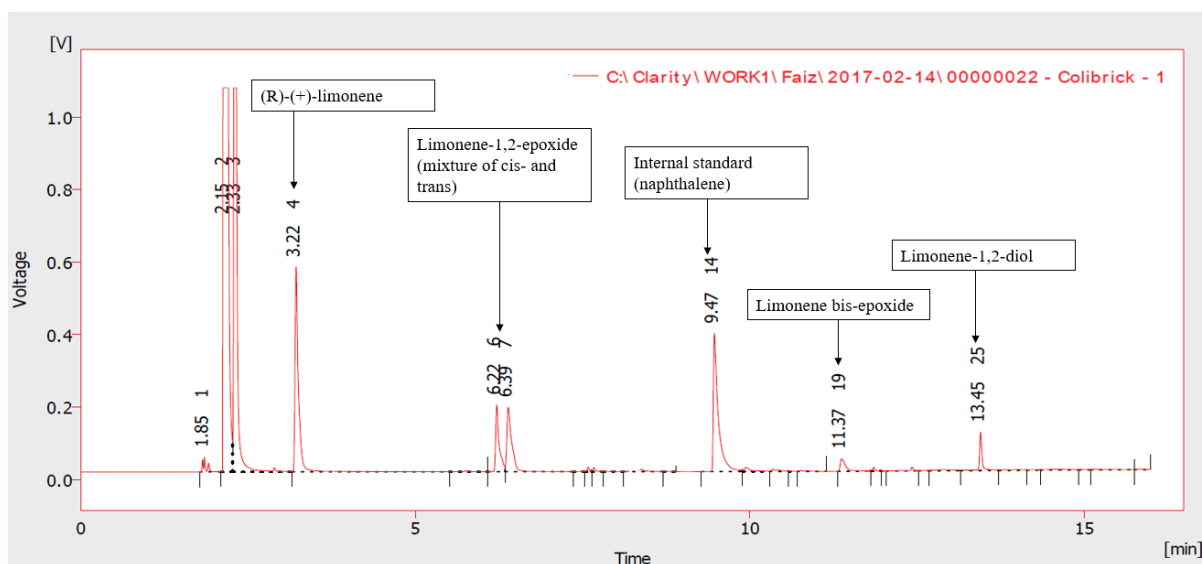
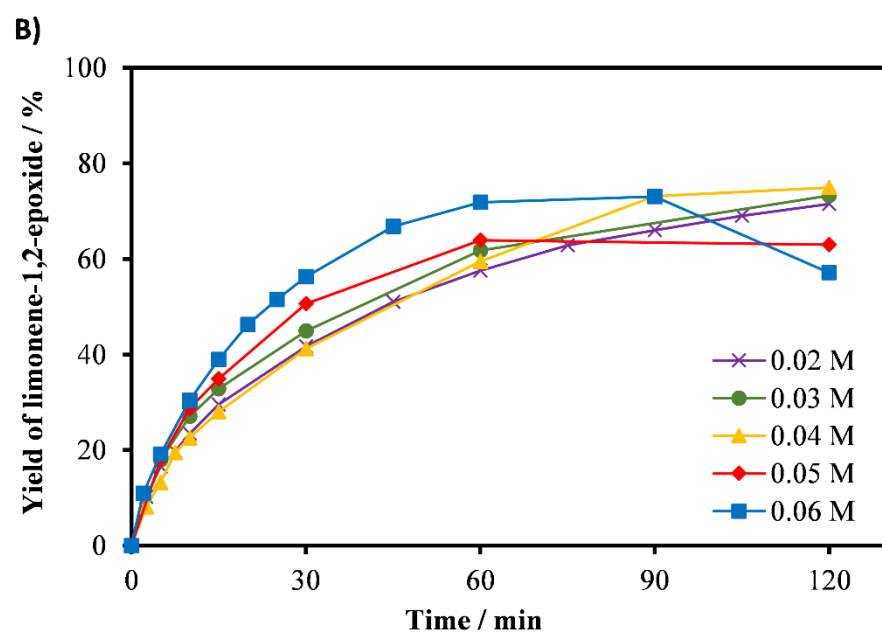
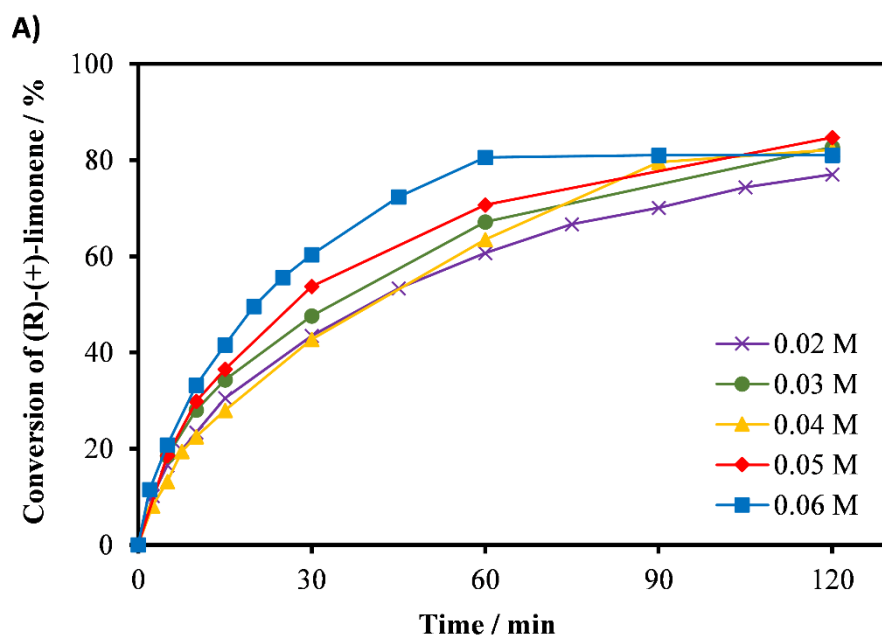


Figure 4.13. Gas chromatograph of samples at reaction time 120 min for the epoxidation of (R)-(+)-limonene using 5.7 g  $\text{Na}_2\text{SO}_4$ .

#### 4.10 Effect of acid concentration on (R)-(+)-limonene epoxidation

The concentration of acid ( $\text{H}_2\text{SO}_4$ ) in the reaction media affects the stability of the catalyst (Venturello *et al.*, 1983; Ishii *et al.*, 1988a; Venturello and D'Aloisio, 1988; Sato *et al.*, 1996; Grigoropoulou and Clark, 2006; Takumi *et al.*, 2014). Hence, the effect of acid on (R)-(+)-limonene epoxidation was studied by varying the initial concentration of  $\text{H}_2\text{SO}_4$  from 0.02 M to 0.06 M, and the results are shown in Figures 4.14 (A) – (D). The initial pH in all cases was lower than 1.





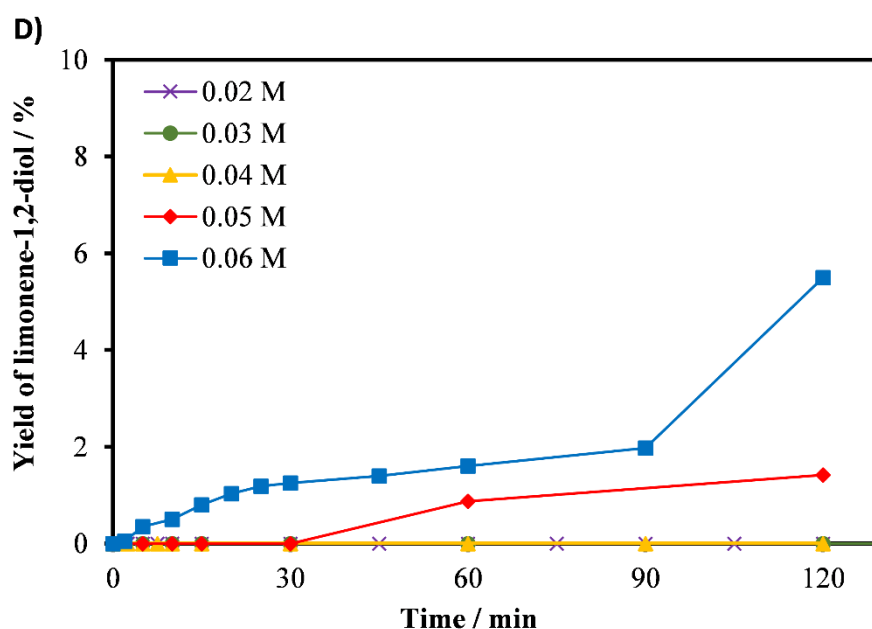
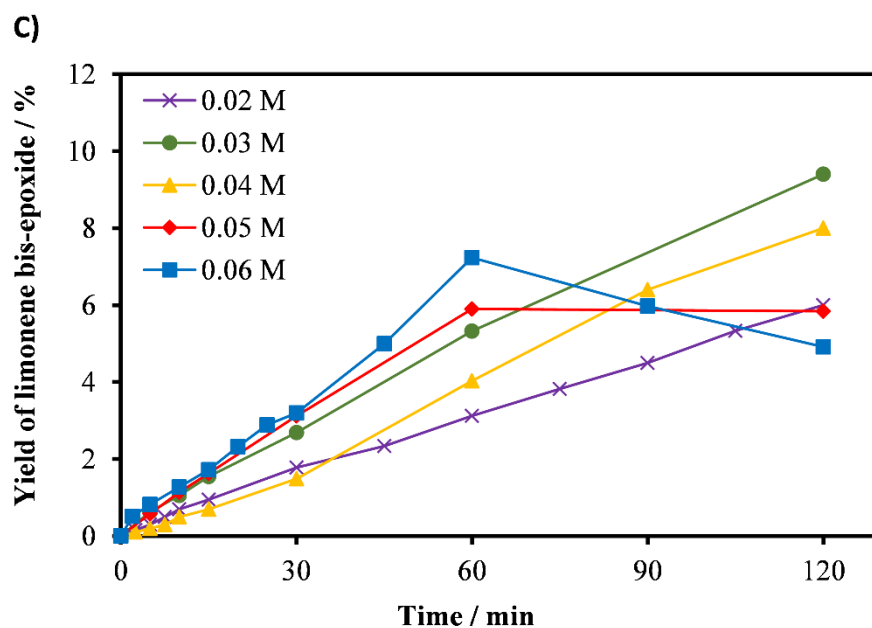


Figure 4.14. The effect of acid concentration on (R)-(+)-limonene epoxidation for reactions at (R)-(+)-limonene (1.25 M),  $H_2O_2$  (1.25 M),  $Na_2WO_4 \cdot 2H_2O$  (0.006 M),  $Na_2SO_4$  (5.7 g),  $H_2SO_4$  (0.02 M - 0.06 M), 1.0 g PTC, temperature (50 °C), toluene (500 mol%) and 1250 rpm mixing (A) conversion of (R)-(+)-limonene, (B) yield of limonene-1,2-epoxide, (C) yield of limonene bis-epoxide and (D) yield of limonene-1,2-diol.

As depicted in Figure 4.14 (A), the rates of (R)-(+)-limonene conversions increased with the acid concentrations. For instance, at a 30 min reaction time, the (R)-(+)-limonene conversion was more than 55 % for an acid concentration of 0.06 M, compared with 40 % for an acid concentration of 0.02 M. The conversion of (R)-(+)-limonene reached 80 % for all acid

concentrations at a reaction time of 120 min. Figure 4.14 (B) shows that at a reaction time of 120 min, the yield of limonene-1,2-epoxide increases with a decreasing acid concentration. The yield of limonene-1,2-epoxide rises from 57 % to 71 % when the acid concentration was decreased from 0.06 M to 0.02 M. Similarly, in Figure 4.14 (C), increasing the acid concentration decreased the yield of limonene bis-epoxide. For instance, the yield of limonene bis-epoxide at a reaction time of 120 min decreased from 10 % to 5 % when the acid concentration was increased from 0.03 M to 0.06 M. At an acid concentration of more than 0.05 M, the yield of limonene bis-epoxide attains a maximum before gradually decreasing. This suggests that the limonene bis-epoxide formed a diol (monoepoxide or tetraol) at higher acid concentration ( $> 0.05$  M). This was attributed to the effect of the acid on the hydrolysis of the epoxides of both limonene-1,2-epoxide and limonene bis-epoxide (Gunam Resul *et al.*, 2018). Therefore, a higher acid concentration ( $> 0.05$  M) is detrimental to the selectivity of the epoxides.

The yield of limonene-1,2-diol increased with an elevated acid concentration, as shown in Figure 4.14 (D). The yield of limonene-1,2-diol was only quantifiable when the acid concentration was more than 0.05 M. At acid concentrations below 0.04 M, no limonene-1,2-diol was detected in the reaction mixture. In all cases, the pH increases during the reaction. This might be due to the formation of  $H_2O$  as  $H_2O_2$  was progressively consumed. The final pH was above 2 when the acid concentration was less than 0.05 M, which shows the reduction in  $H^+$  concentration. The reduced acidity positively affects the selectivity of the epoxide as the acid-catalysed hydrolysis was suppressed. In this regard, a pH buffer might be detrimental to the epoxide selectivity since acid-catalysed hydrolysis could be enhanced throughout the reaction.

These results clearly demonstrated that acid concentration plays a vital role in the epoxidation of (R)-(+)-limonene with  $H_2O_2$  using polytungstophosphate catalyst. The highest selectivity towards limonene-1,2-epoxide with little to no diol formation can be achieved by optimising the acid concentration used in the reaction. The acid-catalysed regio-isomerisation of (R)-(+)-limonene to form products such as terpinolene and terpinene has been reported (Comelli *et al.*, 2005). However, the absence of such products in this work might be due to the lower acid concentration used and the different catalyst employed. It should be noted that prior control experiments were performed without the addition of  $H_2SO_4$ . Without the addition of acid, the initial pH of the aqueous phase is about 4.0. No conversion of (R)-(+)-limonene to any product was detected throughout the reaction time.

#### 4.11 Effects of various solvents on the epoxidation of (R)-(+)-limonene

Solvents can be used in epoxidation reactions to mitigate the exothermicity. The reactivity of (R)-(+)-limonene epoxidation is related to the nature and the polarity of solvents. Here, four different solvents, ranging from non-polar to polar, were used and compared for practical applications. A greener solvent, p-cymene was also evaluated. Additionally, an organic solvent-free system was studied by using (R)-(+)-limonene in a higher molar ratio (> 200 mol%). The results for the investigations of the effects of various solvents on (R)-(+)-limonene epoxidation is shown in Figure 4.15.

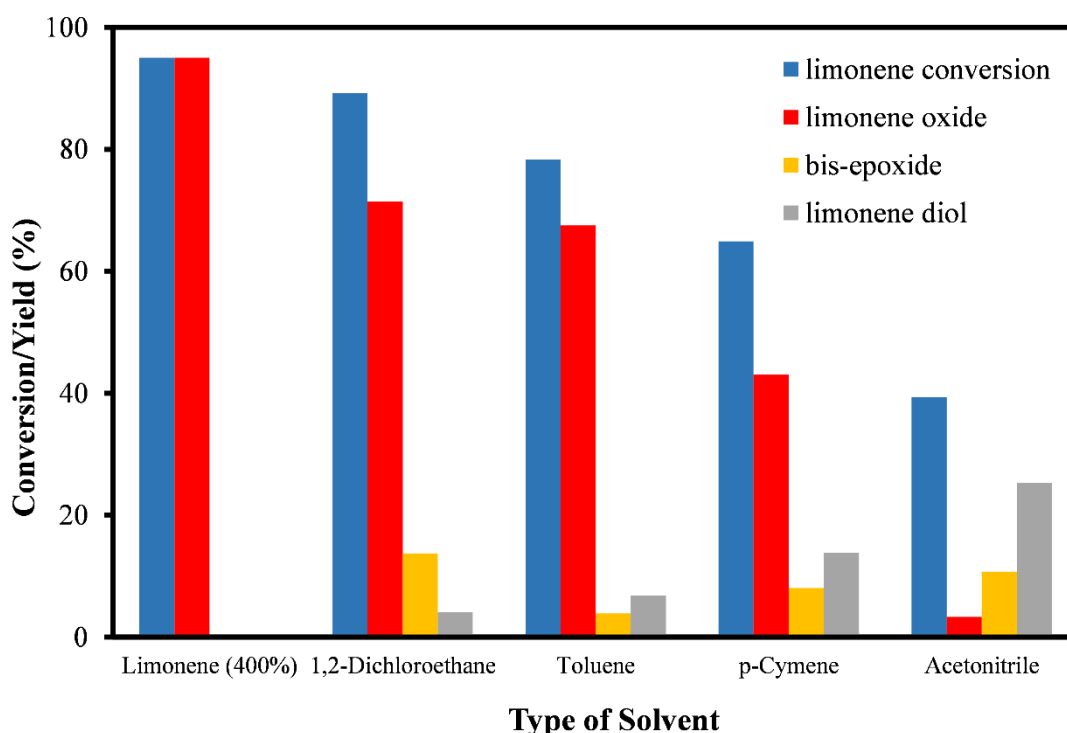


Figure 4.15. The effects of different solvents on (R)-(+)-limonene epoxidation for reactions at (R)-(+)-limonene (1.25 M),  $H_2O_2$  (1.25 M),  $Na_2WO_4 \cdot 2H_2O$  (0.006 M),  $Na_2SO_4$  (5.7 g),  $H_2SO_4$  (0.06 M), PTC, temperature (50 °C), reaction time (120 min) and solvent amount (500 mol%) for 1.0 g each solvent. (R)-(+)-limonene is represented by the calculated conversion on the y-axis, while limonene-1,2-epoxide, limonene bis-epoxide and limonene-1,2-diol are represented by the calculated yield.

As shown in Figure 4.15, the conversion of (R)-(+)-limonene increases in the following order: acetonitrile (39 %), < p-cymene (65 %), < toluene (78 %) and < 1,2-dichloroethane (89 %). The chlorinated solvent, 1,2-dichloroethane, significantly increases the conversion of (R)-(+)-limonene compared with the other tested solvents. However, the selectivity towards limonene-1,2-epoxide is reduced due to the formation of both limonene-1,2-diol and limonene bis-

epoxide. The yield of limonene-1,2-diol using this solvent is the lowest of all the solvents. Toluene has been used throughout this study, and it is found to have a lower activity than that of 1,2-dichloroethane. This work does not consider 1,2-dichloroethane as solvent for the screening of parameters in epoxidation reaction due its high toxicity and carcinogenic nature. The selectivity to limonene-1,2-epoxide in p-cymene was lower than in toluene and in 1,2-dichloroethane, where the yield of limonene-1,2-diol is slightly higher (14 %). The conversion of (R)-(+)-limonene was lowest when acetonitrile is used. The selectivity towards limonene-1,2-epoxide was also low, which in turn results in a much higher yield of limonene-1,2-diol (25 %). This might be due to the higher polarity of acetonitrile that enhances the hydrolysis of the epoxide. High selectivity to limonene-1,2-epoxide and high H<sub>2</sub>O<sub>2</sub> conversion are obtained when (R)-(+)-limonene is used in a higher molar ratio than H<sub>2</sub>O<sub>2</sub> without any other organic solvent. The conversion and yield were determined based on the concentration of H<sub>2</sub>O<sub>2</sub> as the limiting reactant.

Further studies were carried out on the effects of using excess (R)-(+)-limonene on the limonene-1,2-epoxide yields. Figure 4.16 shows that the yield of limonene-1,2-epoxide increased as the amount of (R)-(+)-limonene was increased up to 400 mol%. At the equimolar amount of (R)-(+)-limonene to H<sub>2</sub>O<sub>2</sub> (100 mol%), the maximum yield achieved was only 73 %. In this condition, the exothermic temperature (reaching ~105 °C) decomposes H<sub>2</sub>O<sub>2</sub>, resulting in lower conversion. The rate of hydrolysis also increases due to the temperature, which gradually consumes limonene-1,2-epoxide. However, the yield of limonene-1,2-epoxide was increased to 95 % at 100 % selectivity within 15 minutes reaction time by increasing the (R)-(+)-limonene amount up to 400 mol%. Furthermore, isothermal conditions were, achieved as the large amount of (R)-(+)-limonene helps mitigate the exotherm. Interestingly, there was no formation of limonene bis-epoxide, and no limonene-1,2-diol was detected when (R)-(+)-limonene was used in a higher ratio (> 200 mol%). This result was due to the rapid rate of formation of limonene-1,2-epoxide, which fully utilises the H<sub>2</sub>O<sub>2</sub> present in the system. This also prevents further epoxidation to limonene bis-epoxide. Due to the lower acid concentration used at 0.04 M, the epoxides remain stable throughout the reaction time, and no limonene-1,2-diol was detected by GC analysis.

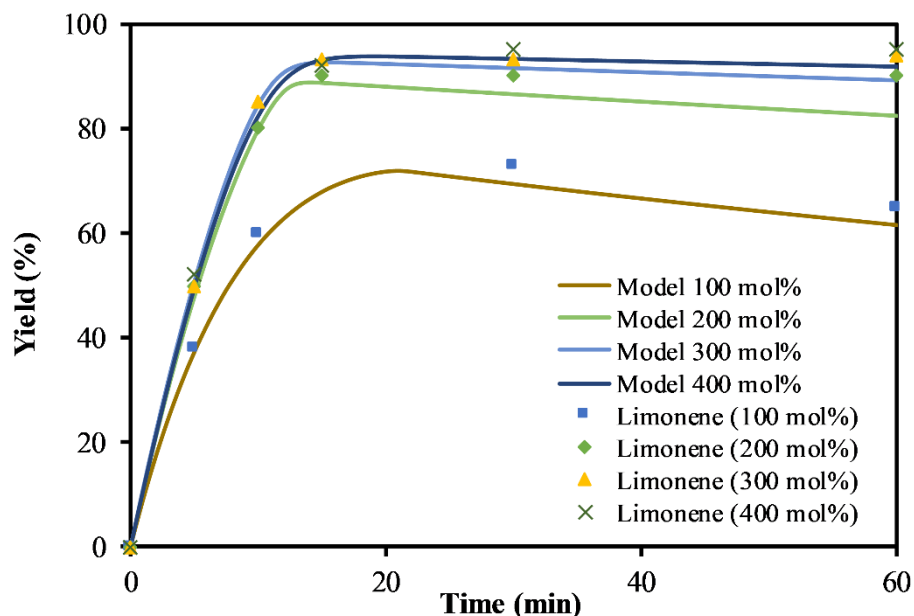


Figure 4.16. The yield of limonene-1,2-epoxide versus time as a function of the amount of (R)-(+)-limonene at reaction conditions of  $\text{H}_2\text{O}_2$  (1.25 M),  $\text{Na}_2\text{WO}_4 \cdot 2\text{H}_2\text{O}$  (0.006 M),  $\text{Na}_2\text{SO}_4$  (5.7 g), and  $\text{H}_2\text{SO}_4$  (0.04 M), 1.0 g PTC, temperature (50 °C) and 1250 rpm mixing. The lines are fitted to the kinetic model by using Equations (3.6) – (3.11) and the rate constant in Table 4.1.

The experimental data validates the kinetic model, especially at more than 300 mol% of (R)-(+)-limonene. The model predicted 93 % of the limonene-1,2-epoxide yield, which was remarkably close to the percentage in the experimental data (95 %). However, at a (R)-(+)-limonene amount of 200 mol%, the model predicts the formation of limonene bis-epoxide (5 %), which was not detected by GC analysis for the experimental data. Due to the absence of a solvent and the increased molar ratio of (R)-(+)-limonene to  $\text{H}_2\text{O}_2$ , the reaction temperature was slightly increased due to the exotherm at (R)-(+)-limonene amounts below 200 mol%. This situation causes the initial reaction rate to be slightly higher than predicted by the model, which uses a rate constant at 50 °C.

#### 4.12 Summary

Overall, it has been demonstrated that limonene-1,2-epoxide can be produced at 100% selectivity and 95 % conversion of  $\text{H}_2\text{O}_2$ . This requires the following conditions: temperature below 50 °C; an equimolar amount of  $\text{H}_2\text{O}_2$ ; saturated amount of  $\text{Na}_2\text{SO}_4$  (5.7g) and acid concentration below 0.04 M. The epoxidation of (R)-(+)-limonene could be performed organic solvent-free at a high yield and selectivity by using (R)-(+)-limonene in stoichiometric excess

(versus H<sub>2</sub>O<sub>2</sub>). This should be contrasted with a typical epoxidation reaction of (R)-(+)-limonene, which requires up to 500 mol% of solvent. In summary:

- i. Solvent-free epoxidation reaction to achieve 'greener' process.
- ii. The solvent-free process allows a shorter reaction time, 15 minutes instead of 60 minutes with solvent (toluene).
- iii. 100 % selectivity to limonene-1,2-epoxide at 95 % conversion of H<sub>2</sub>O<sub>2</sub>.
- iv. Up to 95 % yield of limonene-1,2-epoxide when using (R)-(+)-limonene in excess (400 mol%).
- v. Isothermal condition achieved by using (R)-(+)-limonene in excess.
- vi. Kinetic study reveals first-order reaction with respect to (R)-(+)-limonene and the catalyst.
- vii. Fractional order (~0.5) with respect to H<sub>2</sub>O<sub>2</sub>.
- viii. Predictive kinetic model has been developed, with a high level of agreement with the experimental data.
- ix. Reaction is not mass transfer limited when the stirrer speed is at 1250 rpm
- x. The employment of 1.0 g of the PTC is sufficient.
- xi. H<sub>2</sub>O<sub>2</sub> decomposition is negligible under the investigated operating conditions.

## Chapter 5 Epoxidation of $\alpha$ -pinene

### 5.1 Introduction

This chapter presents the results and discussion from the screening of a number of parameters, including a kinetic study, for the batch epoxidation of  $\alpha$ -pinene. The batch epoxidation was performed using a four-necked jacketed flask. The epoxidation of  $\alpha$ -pinene with  $\text{H}_2\text{O}_2$  using polytungstophosphate is similar in nature to that of (R)-(+)-limonene. The amount of phase-transfer catalyst (PTC) required would be similar to the (R)-(+)-limonene epoxidation. A similar approach was used to prepare the peroxy species in the aqueous phase using saturated amount of  $\text{Na}_2\text{SO}_4$ . Therefore, no further investigation on the effect of mixing, addition of PTC, effect of  $\text{Na}_2\text{SO}_4$ , and decomposition of  $\text{H}_2\text{O}_2$  is reported in this chapter.

### 5.2 Kinetics of $\alpha$ -pinene epoxidation

There have been a few kinetic studies on  $\alpha$ -pinene epoxidation with  $\text{H}_2\text{O}_2$  using various types of catalyst. Cánepa *et al.* (2011) studied the kinetics of the epoxidation of  $\alpha$ -pinene with  $\text{H}_2\text{O}_2$  using a titanium-based catalyst and reported an apparent first-order reaction with respect to the concentrations of the catalyst,  $\alpha$ -pinene and  $\text{H}_2\text{O}_2$ . As in the studies of (R)-(+)-limonene epoxidation, the kinetic parameters and reaction order for the epoxidation of  $\alpha$ -pinene were determined via an initial rate method based on pseudo first-order conditions.

Figures 5.1 (A) and (B) show the determination of the reaction order with respect to the catalyst, with the concentrations of the catalysts precursor ( $\text{Na}_2\text{WO}_4 \cdot 2\text{H}_2\text{O}$ ) varied between 0.008 M and 0.016 M, at constant initial concentrations of  $\alpha$ -pinene (1.25M),  $\text{H}_2\text{O}_2$  (1.25M) and the solvent (500 mol%).



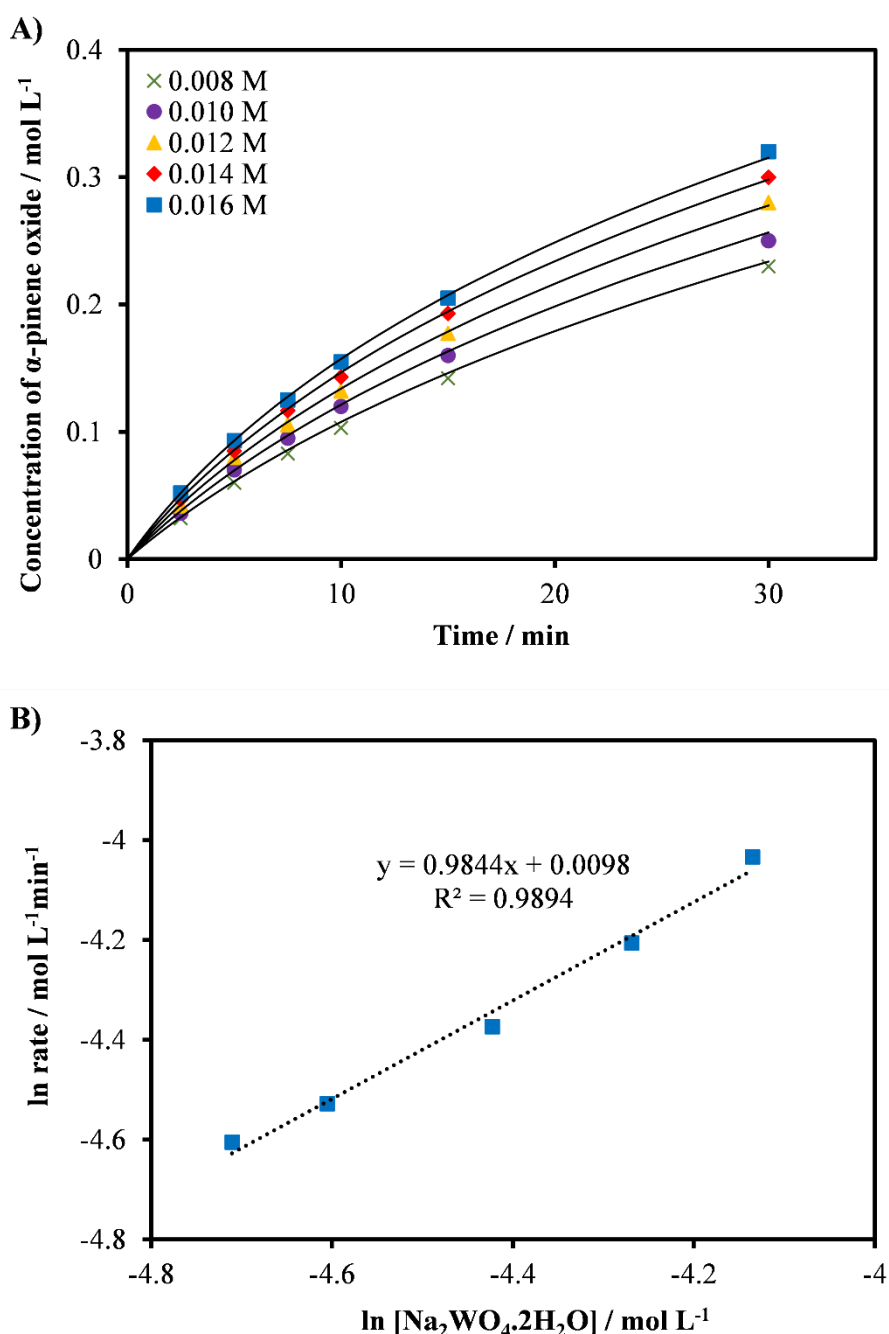
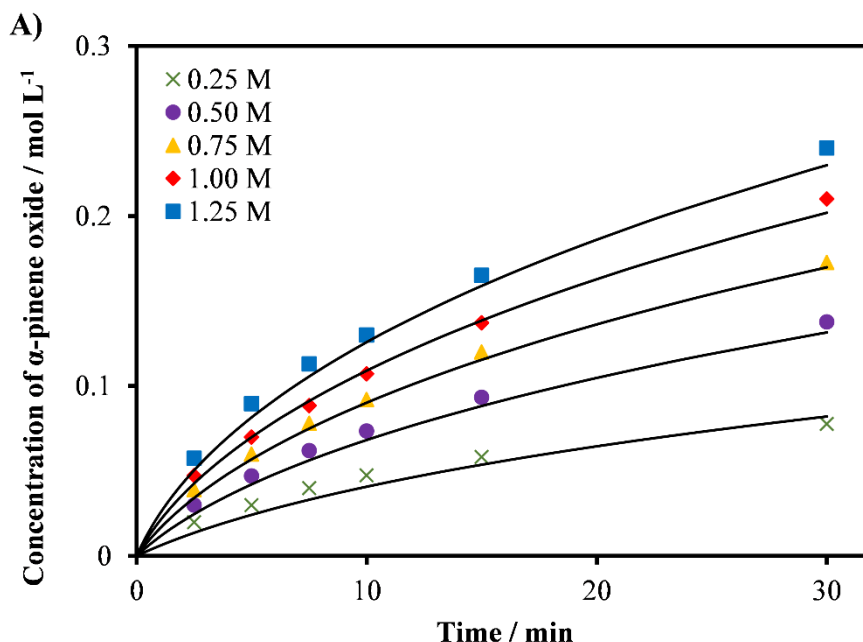


Figure 5.1. Batch epoxidation of  $\alpha$ -pinene at reaction conditions of  $\alpha$ -pinene (1.25 M), H<sub>2</sub>O<sub>2</sub> (1.25 M), Na<sub>2</sub>WO<sub>4</sub>·2H<sub>2</sub>O (0.008 M – 0.016 M), Na<sub>2</sub>SO<sub>4</sub> (5.7 g), H<sub>2</sub>SO<sub>4</sub> (0.05 M), 1.0 g PTC, temperature (50 °C), toluene (500 mol%) and 1250 rpm mixing, (A) The concentration of  $\alpha$ -pinene oxide versus time at various concentrations of Na<sub>2</sub>WO<sub>4</sub>·2H<sub>2</sub>O, (B) The plot of the natural log between the initial reaction rate and Na<sub>2</sub>WO<sub>4</sub>·2H<sub>2</sub>O concentration. The lines in (A) are fitted to the kinetic model using Equations (3.12) – (3.14) and the rate constant in Table 5.1.

As depicted in Figure 5.1 (A), the reaction rate increases with increasing Na<sub>2</sub>WO<sub>4</sub>·2H<sub>2</sub>O concentration, as expected. The initial rates (15 minutes) values are obtained from the gradient of Figure 5.1 (A) and are tabulated in Appendix I. When Na<sub>2</sub>WO<sub>4</sub>·2H<sub>2</sub>O concentration was

doubled from 0.008 M to 0.016 M, the initial rates increased from 0.0090 mol L<sup>-1</sup>min<sup>-1</sup> to 0.0177 mol L<sup>-1</sup>min<sup>-1</sup>, increasing by a factor of ~2. The plot of the natural log between the initial rates and Na<sub>2</sub>WO<sub>4</sub>·2H<sub>2</sub>O concentrations is shown in Figure 5.1 (B). The plot produces a straight line with a gradient of ~1, showing that the reaction is first-order in terms of catalyst concentration. In Figure 5.1 (A), the kinetic model (presented by the smooth lines) can predict the formation of  $\alpha$ -pinene oxide at various catalyst concentration tested, and these were validated by the experimental data. The study was performed using a higher concentration of Na<sub>2</sub>WO<sub>4</sub>·2H<sub>2</sub>O (up to 0.016 M) than the one used for (R)-(+)-limonene (up to 0.009 M) due to the lower reactivity of  $\alpha$ -pinene than (R)-(+)-limonene in epoxidation reaction (Caovilla *et al.*, 2008). Hence, Na<sub>2</sub>WO<sub>4</sub>·2H<sub>2</sub>O concentration was doubled. However, the Na<sub>2</sub>WO<sub>4</sub>·2H<sub>2</sub>O concentration was within the limit of this study (< 0.02 M).

The results used for determination of the reaction order with respect to  $\alpha$ -pinene are shown in Figures 5.2 (A) and (B). This was determined by varying the initial concentration of  $\alpha$ -pinene, from 0.25 M to 1.25 M while keeping the concentrations of H<sub>2</sub>O<sub>2</sub> constant (1.25 M). The solvent amount was varied accordingly to maintain a constant volume. Care was taken to ensure that the volume ratio between the organic and the aqueous phases was kept constant.



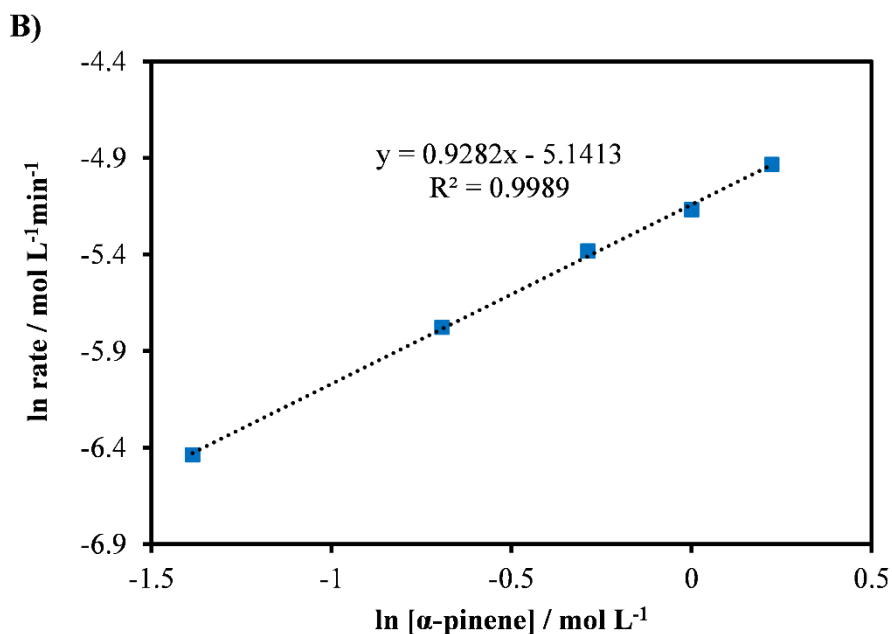


Figure 5.2. Batch epoxidations of  $\alpha$ -pinene at reaction conditions of  $\alpha$ -pinene (0.25 M - 1.25 M),  $\text{H}_2\text{O}_2$  (1.25 M),  $\text{Na}_2\text{WO}_4 \cdot 2\text{H}_2\text{O}$  (0.012 M),  $\text{Na}_2\text{SO}_4$  (5.7 g),  $\text{H}_2\text{SO}_4$  (0.05 M), 1.0 g PTC, temperature (50 °C), toluene (500 mol%) and 1250 rpm mixing, (A) The concentration of  $\alpha$ -pinene oxide versus time at various initial  $\alpha$ -pinene concentration, (B) The plot of the natural log between the initial reaction rate and initial  $\alpha$ -pinene concentration. The lines in (A) are fitted to the kinetic model using Equations (3.12) – (3.14) and the rate constant in Table 5.1.

As illustrated by Figure 5.2 (A), the reaction rates increase with an increasing initial  $\alpha$ -pinene concentration. The initial rates (15 minutes) values are obtained from the gradient of Figure 5.2 (A) and are tabulated in Appendix I. When the initial  $\alpha$ -pinene concentration is doubled from 0.50 M to 1.00 M, the initial rates increase from  $0.0031 \text{ mol L}^{-1}\text{min}^{-1}$  to  $0.0057 \text{ mol L}^{-1}\text{min}^{-1}$ , increasing by a factor of  $\sim 2$ . Figure 5.2 (B) shows the plot of the natural log between the initial rates and the initial  $\alpha$ -pinene concentration. The gradient obtained was approximately 1, confirming that this was a first-order reaction. As shown in Figure 5.2 (A), the kinetic model fits the experimental data with a slight deviation at the reaction time of 30 minutes for all concentrations of  $\alpha$ -pinene tested.

The reaction order with respect to  $\text{H}_2\text{O}_2$  was determined by varying the initial concentration of  $\text{H}_2\text{O}_2$ , from 0.25 M to 1.25 M, with the initial concentration of  $\alpha$ -pinene being kept constant. The amounts of solvent were varied accordingly to maintain a constant volume. Figures 5.3 (A) and (B) illustrates the results obtained.

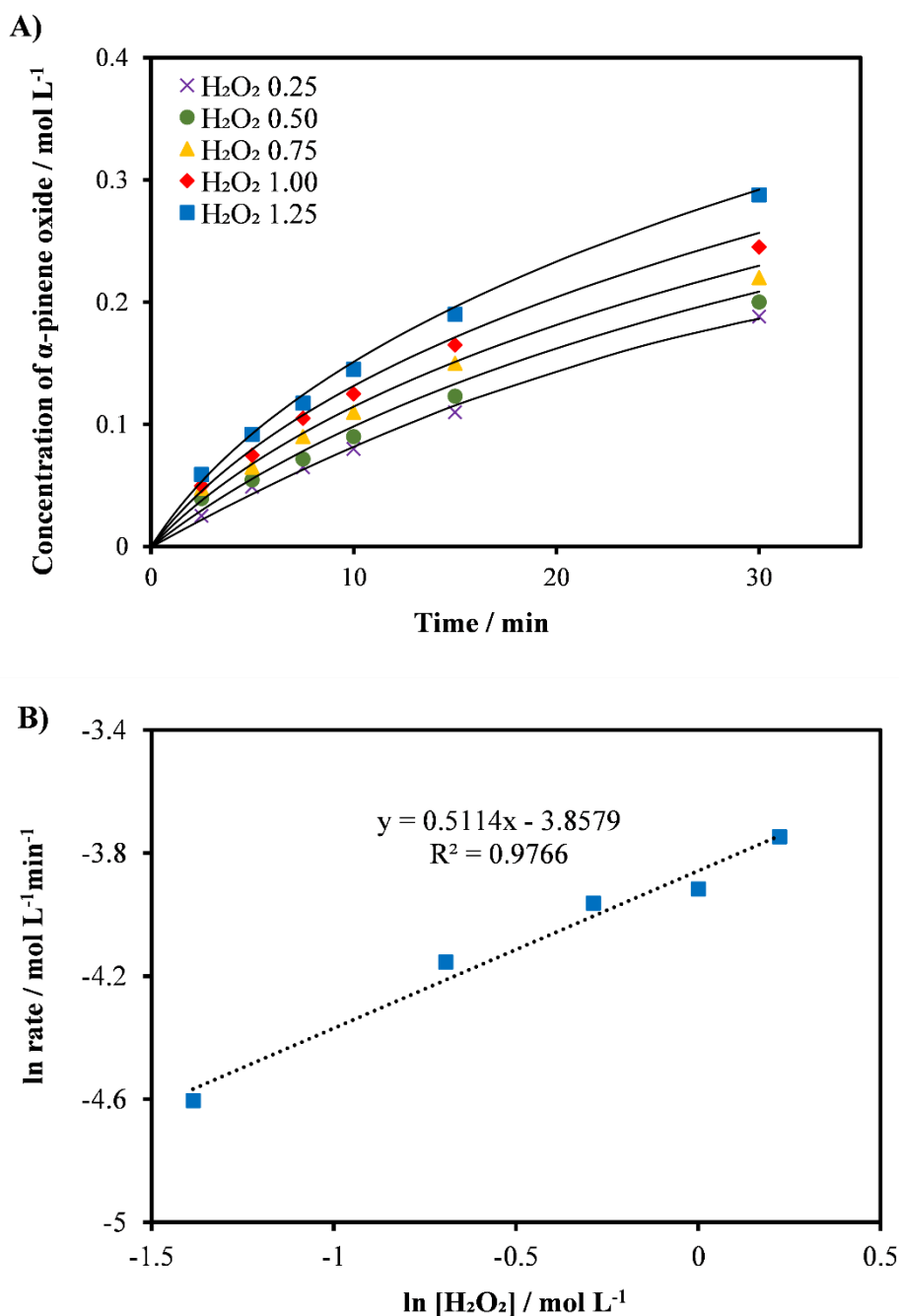


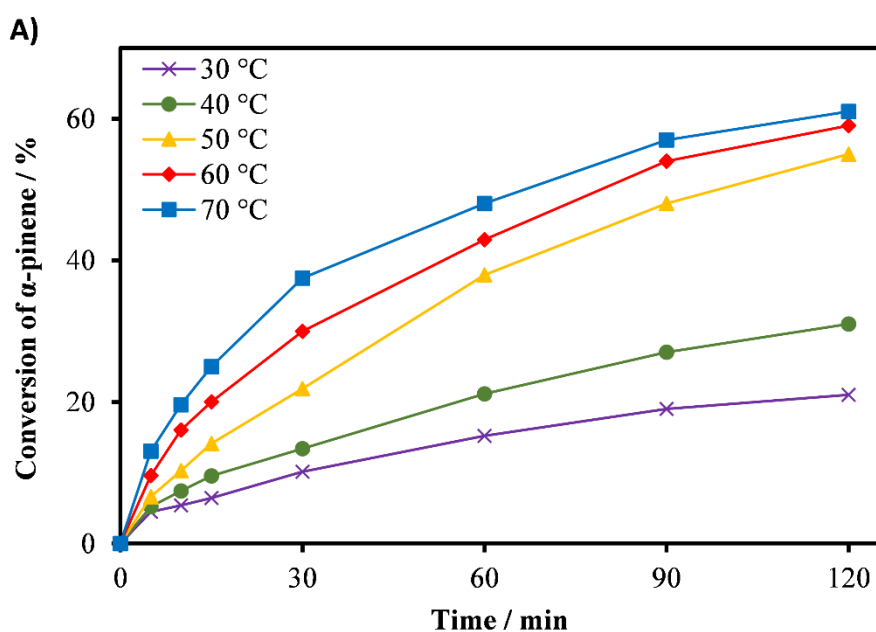
Figure 5.3. Batch epoxidations of  $\alpha$ -pinene at reaction conditions of  $\alpha$ -pinene (0.25 M),  $\text{H}_2\text{O}_2$  (0.25 M - 1.25 M),  $\text{Na}_2\text{WO}_4 \cdot 2\text{H}_2\text{O}$  (0.012 M),  $\text{Na}_2\text{SO}_4$  (5.7 g),  $\text{H}_2\text{SO}_4$  (0.05 M), 1.0 g PTC, temperature (50 °C), toluene (500 mol%) and 1250 rpm mixing, (A) The concentration of  $\alpha$ -pinene oxide versus time at various  $\text{H}_2\text{O}_2$  initial concentration. (B) The plot of the natural log between the initial reaction rate and initial  $\text{H}_2\text{O}_2$  concentration. The lines in (A) are fitted to the kinetic model using Equations (3.12)–(3.14) and the rate constant in Table 5.1.

Figure 5.3 (A) clearly shows that an increase in the initial concentration of  $\text{H}_2\text{O}_2$  increases the reaction rate. The initial rates (15 minutes) values are obtained from the gradient of Figure 5.3 (A) and are tabulated in Appendix I. The gradient of Figure 5.3 (B) shows a reaction order of

$\sim 0.5$ , which indicates a complex mechanism for the peroxide reaction. This result is similar to the findings for the epoxidation of (R)-(+)-limonene (section 4.6, Chapter 4). Increasing the concentration of  $\text{H}_2\text{O}_2$  increases the formation of the active peroxy species but this is limited by the concentration of tungstate ( $\text{WO}_4^{2-}$ ) and phosphate ( $\text{PO}_4^{3-}$ ). This finding also suggests that the epoxidation of  $\alpha$ -pinene, as shown by Equation (3.14), would most likely be the rate-limiting step. The model developed for the epoxidation of  $\alpha$ -pinene was able to predict the yield of  $\alpha$ -pinene oxide, as shown in Figure 5.3 (B). However, the model was limited to the conditions used in the kinetic studies, where a low acid concentration ( $0.05 \text{ M H}_2\text{SO}_4$ ) was used. Formation of other side-product was not included in the model, due to two factors; (i) lack of data on the rate constant of side reaction for the epoxidation of  $\alpha$ -pinene in the literature, (ii) the requirement of an individual kinetic study for each side reaction to obtain rate constants, which is outside the study scope. Therefore, the formation of these side-products could not be predicted by the model. The effect of acid concentration on the epoxidation of  $\alpha$ -pinene will be further discussed in the relevant section (section 5.5).

### 5.3 Effect of temperature on $\alpha$ -pinene epoxidation

The effects of reaction temperature on the epoxidation of  $\alpha$ -pinene were investigated. The temperature was varied between  $30 \text{ }^\circ\text{C}$  and  $70 \text{ }^\circ\text{C}$ . Care was taken to ensure isothermal temperature conditions are maintained throughout the reaction time. Figures 5.4 (A) and (B) illustrates the results.



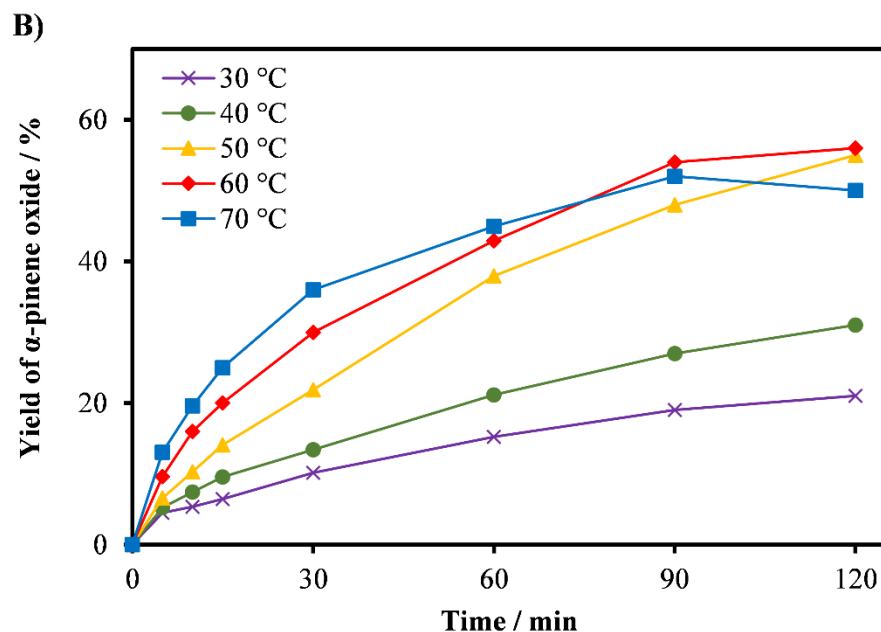


Figure 5.4. The effects of temperature on the epoxidation of  $\alpha$ -pinene at reaction conditions of  $\alpha$ -pinene (1.25 M),  $H_2O_2$  (1.25 M),  $Na_2WO_4 \cdot 2H_2O$  (0.012 M),  $Na_2SO_4$  (5.7 g),  $H_2SO_4$  (0.05 M), 1.0 g PTC, temperature (30 – 70 °C), toluene (500 mol%) and 1250 rpm mixing, (A) conversion of  $\alpha$ -pinene, (B) yield of  $\alpha$ -pinene oxide. The lines represent the trends between data points.

Figure 5.4 (A) shows the rates of conversions of  $\alpha$ -pinene clearly increased with temperatures from 30 °C to 70 °C. This trend was also followed by the  $\alpha$ -pinene oxide yields, except at 70 °C, where a decrease in the  $\alpha$ -pinene oxide yield was observed after 60 min reaction time (see Figure 5.4 B). The decrease in the  $\alpha$ -pinene oxide yield was due to the  $\alpha$ -pinene oxide undergoing both hydrolysis and rearrangement, resulting in the formation of side-products: mainly sobrerol (~3 %) and campholenic aldehyde (~1 %). Allylic oxidation becomes significant at temperatures higher than 60 °C, where the yield of verbenol is ~5 % (negligible verbenone). Similar observation was found by Stekrova *et al.* (2014), where allylic oxidation was prevalent at higher temperatures. While higher temperatures increase the rate of conversion of  $\alpha$ -pinene, they reduce selectivity to  $\alpha$ -pinene oxide. At temperatures below 50 °C, the process was highly selective to  $\alpha$ -pinene oxide, with little to no formation of any side-products. Hence this temperature was used in all subsequent experiments, as the highest temperature at which no side-products were detected.

The Arrhenius dependence of the formation of  $\alpha$ -pinene oxide was determined by varying the reaction temperature between 30 °C and 70 °C. Figure 5.5 (A) shows the natural log of the concentrations of  $\alpha$ -pinene at various temperatures, and Figure 5.5 (B) shows the temperature

dependence of  $\alpha$ -pinene oxide formation, as plots of  $\ln(k_{\text{pinene}})$  versus  $1/T$ , for determination of the Arrhenius activation energy.

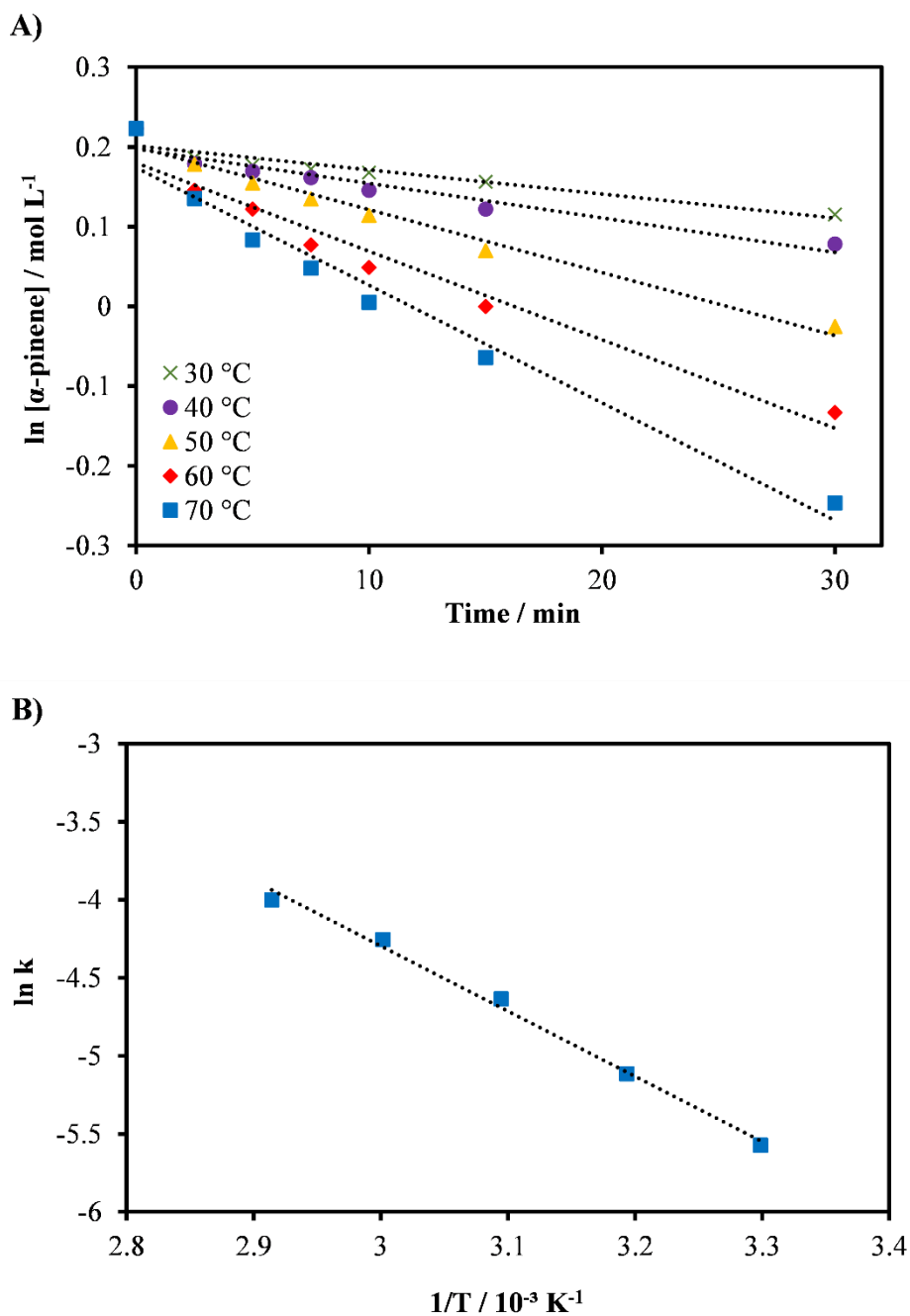


Figure 5.5. Arrhenius activation energy for the formation of  $\alpha$ -pinene oxide at reaction conditions of  $\alpha$ -pinene (1.25 M),  $\text{H}_2\text{O}_2$  (1.25 M),  $\text{Na}_2\text{WO}_4 \cdot 2\text{H}_2\text{O}$  (0.006 M),  $\text{Na}_2\text{SO}_4$  (5.7 g),  $\text{H}_2\text{SO}_4$  (0.04 M), 1.0 g PTC, temperature (30 – 70 °C), toluene (500 mol%) and 1250 rpm mixing, (A) The plot of the natural log of  $\alpha$ -pinene concentrations versus time at various temperatures for the epoxidation of  $\alpha$ -pinene. (B) Temperature dependence of the rate constant for the formation of  $\alpha$ -pinene oxide.

The Arrhenius activation energy for the formation of  $\alpha$ -pinene oxide in the epoxidation reaction was determined to be  $\sim 35 \text{ kJ mol}^{-1}$ , using the gradient of the plot of  $\ln(k_{\text{pinene}})$  versus  $1/T$  in the Figure 5.5 (B). This value is close to the  $\sim 40 \text{ kJ mol}^{-1}$  reported by Becerra *et al.* (2016) for the epoxidation of  $\alpha$ -pinene using an iron-based catalyst, and lower than  $68 \text{ kJ mol}^{-1}$  reported by Canepa *et al.* (2011) for the epoxidation of  $\alpha$ -pinene using heterogeneous titanium-based catalyst. A higher activation energy was obtained by Canepa *et al.* (2011) when a heterogeneous catalyst was used, indicating that the reaction rate obtained from this study should be lower, as would be expected for a homogeneous catalysis. Table 5.1 lists the kinetic parameters obtained from the study.

	Pre-exponential factor ( $\text{A / s}^{-1}$ )	Activation energy ( $\text{kJ mol}^{-1}$ )	
		This work	References
<b>Formation of <math>\alpha</math>-pinene oxide</b>	$3.7 \times 10^4$	35	40 (Becerra <i>et al.</i> , 2016) 68 (Canepa <i>et al.</i> , 2011)

Table 5.1. The pre-exponential factor and the activation energy for the formation of  $\alpha$ -pinene-oxide.

#### 5.4 Effect of $\text{H}_2\text{O}_2$ oxidant amount on the $\alpha$ -pinene epoxidation

The effect of the  $\text{H}_2\text{O}_2$  amount on the epoxidation of  $\alpha$ -pinene was studied by varying the quantity of  $\text{H}_2\text{O}_2$  from 100 mol% to 200 mol%. Figure 5.6 presents the results.



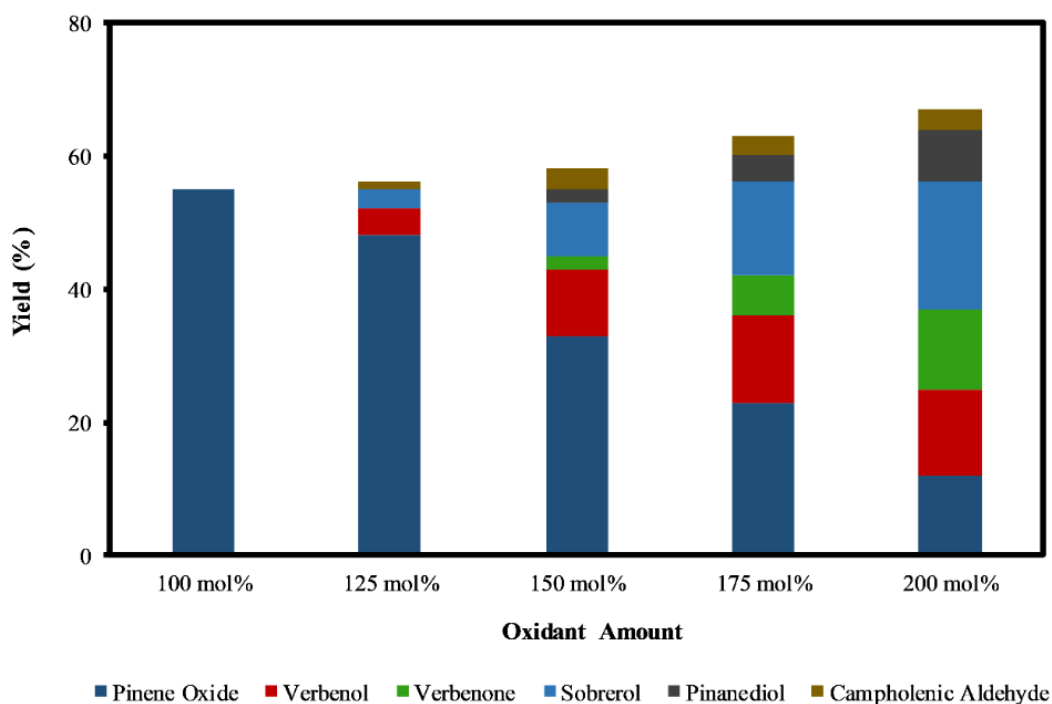


Figure 5.6. The effect of the oxidant amount on the epoxidation of  $\alpha$ -pinene and distribution of the products at reaction conditions of  $\alpha$ -pinene (1.25 M),  $H_2O_2$  (0.25 M - 1.25 M),  $Na_2WO_4 \cdot 2H_2O$  (0.012 M),  $Na_2SO_4$  (5.7 g),  $H_2SO_4$  (0.05 M), 1.0 g PTC, temperature (50 °C), reaction time (120 min), toluene (500 mol%) and 1250 rpm mixing.

Clearly, the selectivity to  $\alpha$ -pinene oxide, when above 1:1 (substrate:oxidant), decreases with increasing oxidant amount. The yields of  $\alpha$ -pinene oxide were 55 % and 12 % for oxidant amounts of 100 mol% and 200 mol%, respectively. At an excess amount of oxidant, epoxidation and allylic oxidation occur simultaneously (Cánepa *et al.*, 2015). The yield of verbenol increases from 4 % to 13 % when the oxidant amount is increased from 125 mol% to 200 mol%. These results are in accord with the literature, which states that an increase in  $H_2O_2$  concentration generates more radicals and favours the allylic oxidation route (which verbenol to verbenone) (Negoi *et al.*, 2018).

As shown in Figure 5.6, increasing the amount of oxidant also reduces the yield of  $\alpha$ -pinene oxide, as the rate of hydrolysis increases resulting in the formation of sobrerol and pinanediol. The increased rate of hydrolysis is mainly influenced by the increasing concentration of  $H_2O$ , which is in proportion to the oxidant amount as the  $H_2O_2$  is supplied in an aqueous solution. The yield of sobrerol rose from 3 % to 19 % as the oxidant amount was increased from 125 mol% to 200 mol%. Pinanediol was observed between 150 mol% and 200 mol%, with its yield increasing from 2 % to 8 %. A small amount of campholenic aldehyde (~3 %) is always present

in the reaction mixture at higher oxidant amounts but does not increase markedly with increasing amount of oxidant. As reported in the literature, the formation of campholenic aldehyde was due to the rearrangement of  $\alpha$ -pinene oxide, which requires higher acidity to occur (Sundravel *et al.*, 2016). Overall, there is a clear recommendation for this reaction: to maintain the highest selectivity towards  $\alpha$ -pinene oxide, an equimolar amount of oxidant and  $\alpha$ -pinene should be used.

### 5.5 Effect of acid concentrations on the $\alpha$ -pinene epoxidation

The concentration of acid ( $H_2SO_4$ ) in the reaction media affects the epoxidation reaction. The polytungstophosphate were reported to be stable in an acidic environment, but an acid-labile epoxide, such as  $\alpha$ -pinene oxide, could convert to many compounds in such an environment (Ishii *et al.*, 1988; Venturello and D'Aloisio, 1988; Grigoropoulou and Clark, 2006; Kon *et al.*, 2011; Hachiya *et al.*, 2012). The effect of sulphuric acid concentration on the epoxidation of  $\alpha$ -pinene are shown in Figure 5.7. In all cases, the initial pH was lower than  $\sim 1$ .

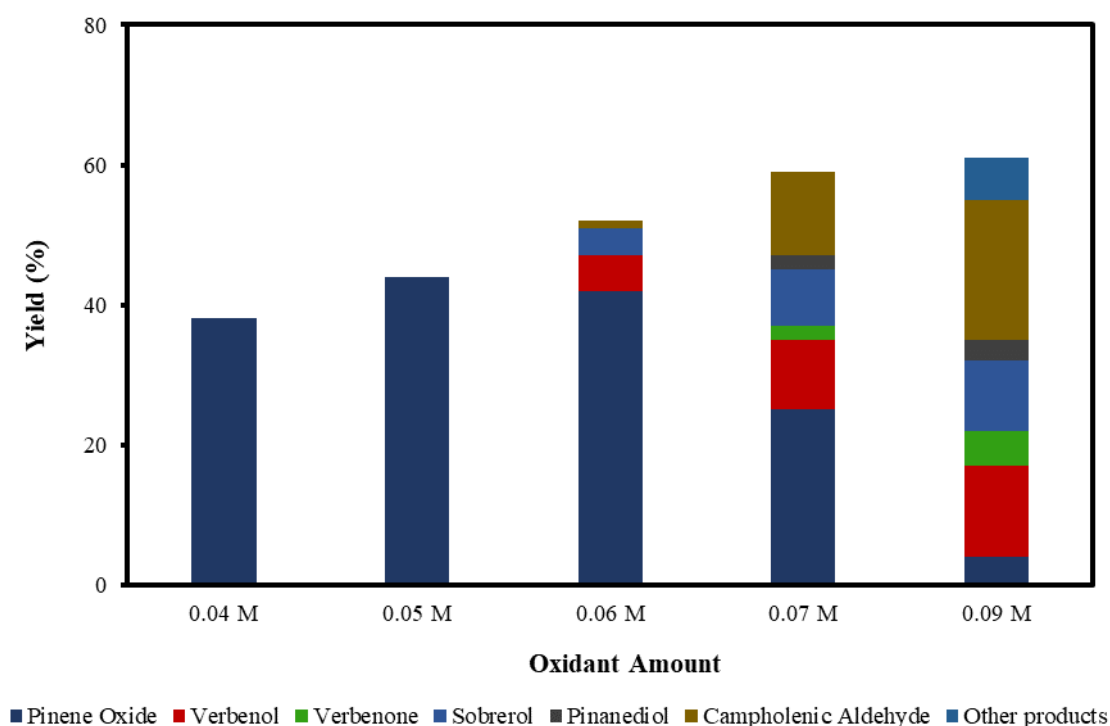


Figure 5.7. The effect of acid concentration on the epoxidation of  $\alpha$ -pinene and distribution of the products at reaction conditions of  $\alpha$ -pinene (1.25 M),  $H_2O_2$  (1.25 M),  $Na_2WO_4 \cdot 2H_2O$  (0.012 M),  $Na_2SO_4$  (5.7 g),  $H_2SO_4$  (0.04 M – 0.09 M), 1.0 g PTC, temperature (50 °C), reaction time (120 min), toluene (500 mol%) and 1250 rpm mixing.

As shown in Figure 5.7, the total yield of the product increases when the acid concentration increases from 0.04 M to 0.09 M. However, the selectivity to  $\alpha$ -pinene oxide decreases dramatically with increasing acid concentration, for example, the yields were 38 % at 0.04 M and 4 % at 0.09 M acid concentrations. At acid concentrations of 0.06 M and higher, the decrease in the final yield of  $\alpha$ -pinene oxide is primarily due to the significant increase in  $\alpha$ -pinene oxide rearrangement;  $\alpha$ -pinene oxide was progressively consumed to almost complete conversion, mainly forming campholenic aldehyde. The yield of campholenic aldehyde rises from ~1 % to ~20 % with increasing acid concentrations. Furthermore, at an acid concentration of 0.09 M, other products, mainly aldehydes and alcohols were detected using gas chromatography (GC), with a total calculated yield of 6 %. This is largely due to the increase in  $H^+$  concentration, which acts as a Lewis acid. The  $H^+$  reacts with the oxygen atoms in  $\alpha$ -pinene oxide, causing the C-C bonds to split and form aldehyde and alcohol (Stekrova *et al.*, 2014; Cánepa *et al.*, 2015).

The decrease in  $\alpha$ -pinene oxide yield is also due to increasing hydrolysis of the epoxide. The yield of sobrerol increases from 4 % to about 10 % with increasing acid concentration. On the other hand, the yield of pinanediol was only 2 % and 3 % at acid concentrations of 0.07 M and 0.09 M, respectively. The hydrolysis of  $\alpha$ -pinene oxide becomes less prevalent with increasing acid concentrations than with increases in the oxidant amount, as discussed in section 5.4. This confirms the need for high  $H_2O$  concentrations to degrade  $\alpha$ -pinene oxide through hydrolysis, while increasing acid ( $H^+$ ) concentrations favour the rearrangement process.

The competing allylic oxidation is apparent when the acid concentration is higher than 0.06 M, with the yield of verbenol increasing from 5 % to about 13 %. Verbenone was only observed at acid concentrations of 0.07 M and 0.09 M, with yields of ~2 % and 5 %, respectively. From these results, it can be deduced that the epoxidation route is more kinetically favoured than allylic oxidation, even when the acid concentration is increased, as confirmed by the increasing total yield of  $\alpha$ -pinene oxide rearrangement and hydrolysis products compared to allylic oxidation products.

The epoxidation of  $\alpha$ -pinene is only 100 % selective to  $\alpha$ -pinene oxide when the acid concentration is less than 0.05 M. The pH of the aqueous phase changes throughout the reaction time mainly caused by the formation of  $H_2O$  as  $H_2O_2$  was consumed. At acid concentrations of 0.06 M and higher, the final pH was less than 2, while acid concentrations lower than 0.05 M resulted in a final pH of about ~2.5. It is presumed that higher acid concentrations not only destabilise the peroxo species but also reduce  $H^+$  concentration, which could affect the

selectivity to  $\alpha$ -pinene oxide. In this regard, the use of a pH buffer might favour the acid-catalysed formation of side-products.

The reaction with an acid concentration of 0.05 M at 70 °C (section 5.3) did not yield as many side-products as the reaction using an acid concentration of 0.09 M at 50 °C. This clearly highlights the importance of acid concentration to this type of epoxidation, which holds the key to developing a highly selective epoxidation of  $\alpha$ -pinene. It should be noted that a control experiment was performed without the addition of acid. This raised the pH of the aqueous peroxide solution above 4, which presumably retarded the formation of the active peroxy species. No conversion of  $\alpha$ -pinene to any product was observed.

### **5.6 Effects of solvents on $\alpha$ -pinene epoxidation**

The exothermic nature of the  $\alpha$ -pinene epoxidation reaction with H<sub>2</sub>O<sub>2</sub> is typically mitigated by the drop-wise addition of H<sub>2</sub>O<sub>2</sub> or using a solvent. The choice of solvent can affect the conversion and selectivity of  $\alpha$ -pinene epoxidation. Four different solvents were studied and compared for the epoxidation of  $\alpha$ -pinene. Additionally, an organic solvent-free system was investigated by using  $\alpha$ -pinene in a higher molar ratio (> 200 mol%). The results for the investigations of the effects various solvents on  $\alpha$ -pinene epoxidation are shown in Figure 5.8.

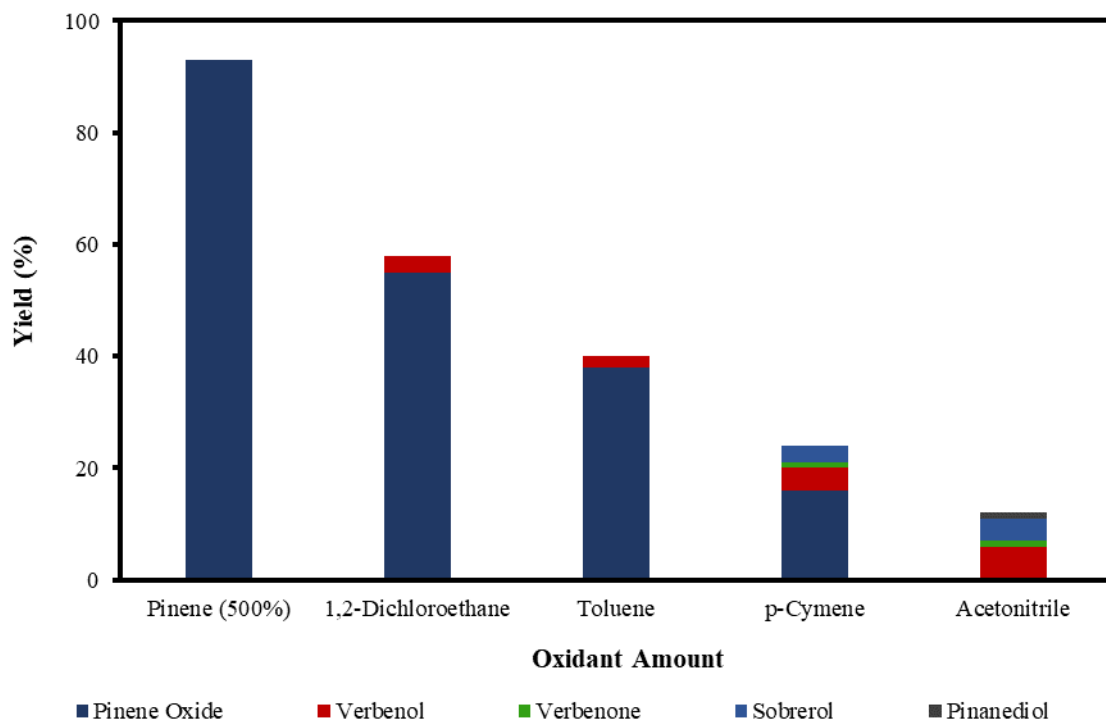


Figure 5.8. The effects of solvents on  $\alpha$ -pinene epoxidation at reaction conditions of  $\alpha$ -pinene (1.25 M),  $H_2O_2$  (1.25 M),  $Na_2WO_4 \cdot 2H_2O$  (0.012 M),  $Na_2SO_4$  (5.7 g),  $H_2SO_4$  (0.05 M), 1.0 g PTC, temperature (50 °C), reaction time (120 min), solvent amount (500 mol%) for each solvent and 1250 rpm mixing.

As depicted in Figure 5.8, the conversion of  $\alpha$ -pinene decreased when the solvents are used in the following order: 1,2-dichloroethane (58 %), > toluene (40 %), *p*-cymene (24 %), > acetonitrile (12 %). Of all the solvents, 1,2-dichloroethane improved the conversion of  $\alpha$ -pinene epoxidation most. Under these conditions, the yield of  $\alpha$ -pinene oxide was 55 %, with only verbenol (3 %) being observed as a side-product. Toluene afforded yields of  $\alpha$ -pinene oxide and verbenol of about 38 % and 2 %, respectively. The conversion of  $\alpha$ -pinene in *p*-cymene as a solvent after a reaction time of 120 min was about 24 %. *p*-Cymene was less selective to  $\alpha$ -pinene oxide than toluene and 1,2-dichloroethane. The conversion of  $\alpha$ -pinene is the lowest when acetonitrile is used, with no  $\alpha$ -pinene oxide being detected within a reaction time of 120 min. This is due to the complete conversion of  $\alpha$ -pinene oxide to its hydrolysis products, sobrerol (4 %) and pinanediol (~1 %). Allylic oxidation is more prevalent in acetonitrile, in which the yields of verbenol and verbenone are 6 % and ~1 %, respectively. This is in accordance with the literature showing that allylic oxidation is favoured when high polarity solvent such as acetonitrile is used (Shylesh and Singh, 2004). There was no formation of campholenic aldehyde with any of the solvents used. This might be due to the lower acid

concentration (0.05 M) used in this set of experiments, which hampered the rearrangement of  $\alpha$ -pinene oxide as explained in section 5.5.

The true reason for the different performances of the solvents might be complex and difficult to determine. Many researchers have ascribed the differing effects to the interactions between the solvent, catalyst and the active oxidant (Clerici and Ingallina, 1993; Corma *et al.*, 1996; Cánepa *et al.*, 2015). The highest yield and selectivity to  $\alpha$ -pinene oxide was obtained when  $\alpha$ -pinene was used in a higher molar ratio than  $\text{H}_2\text{O}_2$  without any additional solvent. Note that the calculated conversion and yield were based on the concentration of  $\text{H}_2\text{O}_2$  as the limiting reactant. The results are shown in Figure 5.9.

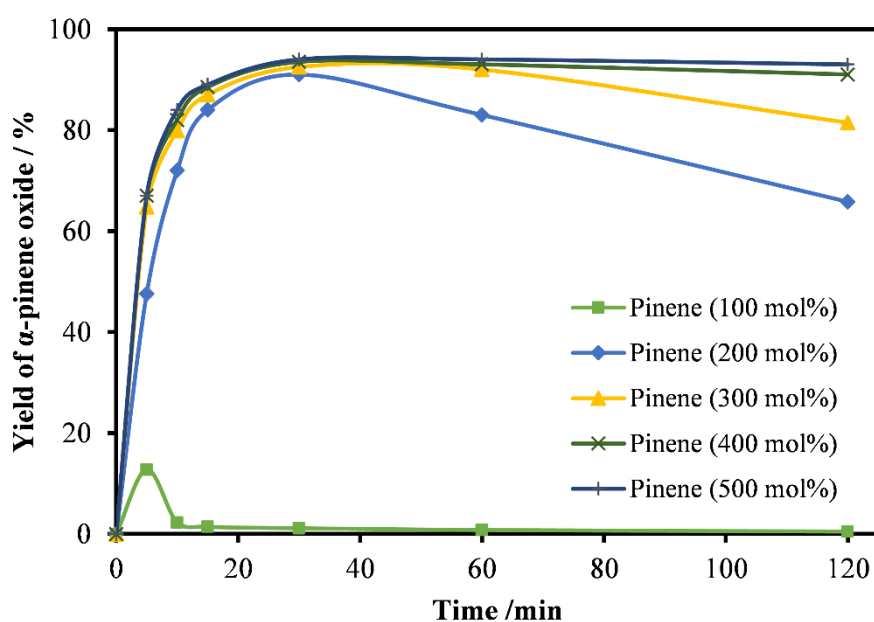


Figure 5.9. The yield of  $\alpha$ -pinene oxide versus time as a function of the amount of  $\alpha$ -pinene at reaction conditions of  $\text{H}_2\text{O}_2$  (1.25 M),  $\text{Na}_2\text{WO}_4 \cdot 2\text{H}_2\text{O}$  (0.012 M),  $\text{Na}_2\text{SO}_4$  (5.7 g),  $\text{H}_2\text{SO}_4$  (0.05 M), 1.0 g PTC, temperature (50 °C), reaction time (120 min), and 1250 rpm mixing. The lines represent the trends between data points.

As shown in Figure 5.9, there was an increase in the yield of  $\alpha$ -pinene oxide when the amount of  $\alpha$ -pinene was increased to 500 mol%. In the absence of a solvent and with an amount of  $\alpha$ -pinene equimolar to  $\text{H}_2\text{O}_2$  (100 mol%), the yield of  $\alpha$ -pinene oxide reached its maximum (12 %) before completely converting to various side-products. Interestingly, the mass balance shows that the conversion of  $\text{H}_2\text{O}_2$  does not account for all the products detected by GC. It is presumed that an oligomeric and polymeric compound was formed throughout the reaction time, assisted

by the exothermicity. This became evident when a viscous layer of liquid was observed in the organic phase, justifying the need for a solvent in such processes.

The yield of  $\alpha$ -pinene oxide improved significantly within 20 minutes when  $\alpha$ -pinene was used in a higher molar ratio ( $> 200$  mol%), due to a high reaction rate. The yields of  $\alpha$ -pinene oxide at 200 mol% and 300 mol% reached a maximum of 91 % and 93 %, respectively. However, the selectivity to  $\alpha$ -pinene oxide decreased gradually over time due to the combination of the hydrolysis and rearrangement processes. Further increasing the amount of  $\alpha$ -pinene up to 500 mol% improves the selectivity of  $\alpha$ -pinene oxide and results in isothermal conditions. At 500 mol% of  $\alpha$ -pinene, the yield of  $\alpha$ -pinene oxide reaches 93 %, with 100 % selectivity to  $\alpha$ -pinene oxide throughout the reaction time. This result can be explained by the rapid formation of  $\alpha$ -pinene oxide, which fully utilised the oxidant in the reaction. This is confirmed by the titration of  $\text{H}_2\text{O}_2$ . The rapid consumption of active oxygen, coupled with the lower acid concentration, significantly reduces the propagation of radicals. This, in turn, suppresses the allylic oxidation and favours epoxidation as the dominant route; at  $\alpha$ -pinene amounts of 200 mol% and higher, little to no formation of allylic products was observed. The large reservoir of  $\alpha$ -pinene not only helps to mitigate the exotherm, but also to isolate  $\alpha$ -pinene oxide in the organic phase, minimising its contact with  $\text{H}^+$  and  $\text{H}_2\text{O}$  in this biphasic reaction. The developed model was not able to predict the yield of  $\alpha$ -pinene oxide when  $\alpha$ -pinene was in excess under solvent-free conditions. This is due to the formation of various side-products, which was not incorporated into the model.

## 5.7 Summary

Screening of process parameters revealed that a 100 % selective reaction to  $\alpha$ -pinene oxide could be obtained at temperature under 50 °C, equimolar amount of  $\text{H}_2\text{O}_2$  and acid concentration of lower than 0.05 M. The findings showed that a highly selective process could be achieved, with 93 % conversion of the  $\text{H}_2\text{O}_2$  at 100 % selectivity to  $\alpha$ -pinene oxide within 20 minutes in an organic solvent-free environment. It shows that. In summary:

- i. High selectivity ( $\sim 100$  %) to  $\alpha$ -pinene oxide is possible with substantially suppressed allylic oxidation, rearrangement, and hydrolysis processes.
- ii. Greener process by using organic solvent-free conditions.
- iii. The organic solvent-free process allows a shorter reaction time, 20 minutes instead of 60 minutes with solvent (toluene).
- iv. 100 % selectivity to  $\alpha$ -pinene oxide at 93 % conversion of  $\text{H}_2\text{O}_2$ .
- v. Up to 93 % yield of  $\alpha$ -pinene oxide when using  $\alpha$ -pinene in excess.

- vi. Isothermal condition achieved by using  $\alpha$ -pinene in excess.
- vii. Kinetic study reveals first-order reaction with respect to  $\alpha$ -pinene and catalyst
- viii. Fractional order ( $\sim 0.5$ ) with respect to  $\text{H}_2\text{O}_2$ .
- ix. The activation energy was determined to be  $35 \text{ kJ mol}^{-1}$ .
- x. Predictive kinetic model has been developed, with a high level of agreement with the experimental data.

Among the objective of this work is to understand the nature of the epoxidation reaction of (R)-(+)-limonene and  $\alpha$ -pinene. Results from Chapter 4 and Chapter 5 shows the reactions could be optimised with 100 % selectivity towards the desired products (epoxides). The data gathered from these two chapters serves as a basis for the development of a continuous process, the aim for the next chapter (Chapter 6).



## Chapter 6 Continuous Epoxidation of (R)-(+)-limonene and $\alpha$ -pinene

### 6.1 Introduction

This chapter presents the results from continuous epoxidation of (R)-(+)-limonene and  $\alpha$ -pinene in mesoOBR. The reaction conditions used for the continuous epoxidation are based on the findings in Chapter 4 and 5.

The focus of this chapter is to develop a continuous process for the epoxidation of (R)-(+)-limonene and  $\alpha$ -pinene with  $H_2O_2$  in mesoOBR. A new design of orifices baffle at this scale (~5 mm) was fabricated through 3D-printing. The performance of the 3D-printed baffles was evaluated and compared with commonly used baffles (helical and integral). The reactor performances were evaluated in terms of achieving minimum induction period and quality steady states. Temperature control performance of the mesoOBR was evaluated and compared to a batch reactor. The possibility of using mesoOBR in a heat pipe assembly to achieve passive isothermalisation was also investigated.

### 6.2 Process limitation of an organic solvent-free epoxidation at equimolar conditions

The objective of this study is to develop an organic solvent-free process for the continuous epoxidation of (R)-(+)-limonene and  $\alpha$ -pinene. However, the epoxidation reaction is exothermic, and an organic solvent such as toluene was typically used to mitigate the exotherm. In an organic solvent-free batch reaction, with a single-step addition of the oxidant under equimolar ratio to the (R)-(+)-limonene, the reaction temperature rose to about 105 °C. This situation caused multiple adverse effects, including the decomposition of  $H_2O_2$ , the formation of many side-products such as diols and polymerisation of (R)-(+)-limonene and its oxidative products. Therefore, in such batch processes, the addition of either solvent or excess substrate were used to keep the temperature down. Since an isothermal condition could not be established for an equimolar, organic solvent-free condition experimentally, the initial rate for the epoxidation of (R)-(+)-limonene or  $\alpha$ -pinene in such conditions could not be determined directly.

The initial rate data is crucial to evaluate the performance of a continuous process in comparison to the performance of a batch process. In order to overcome this obstacle, data from the model developed for the epoxidation of (R)-(+)-limonene was used instead. The model, which was developed using Equations 3.6 to 3.11 was simulated under equimolar condition (1.25 M (R)-

(+)-limonene and 1.25 M H<sub>2</sub>O<sub>2</sub>) using 0.006 M Na<sub>2</sub>WO<sub>4</sub>·2H<sub>2</sub>O at a temperature of 50 °C. The simulated data are plotted as the yield of limonene-1,2-epoxide over 30 minutes reaction time as shown in Figure 6.1.

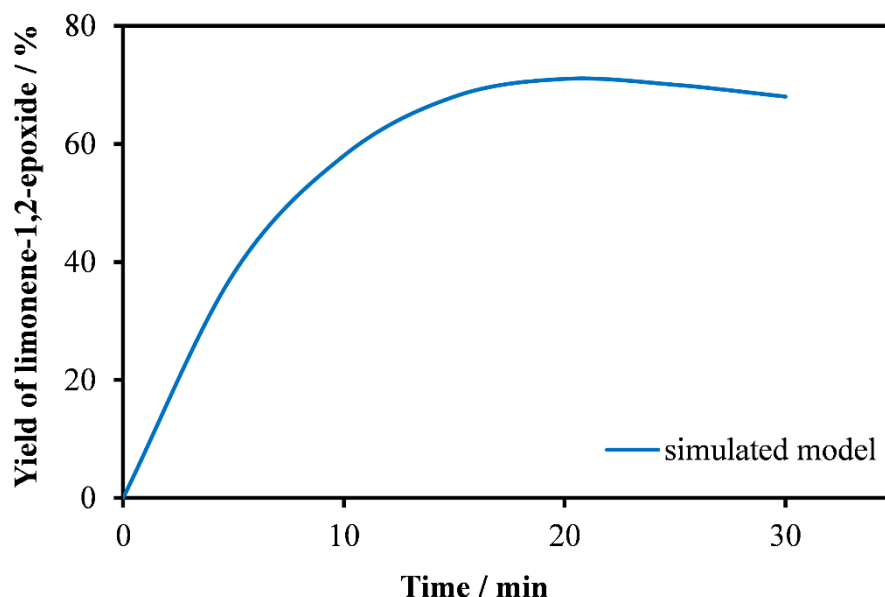


Figure 6.1. Simulated yield of limonene-1,2-epoxide. Reaction conditions: (R)-(+)-limonene (1.25 M), H<sub>2</sub>O<sub>2</sub> (1.25 M), Na<sub>2</sub>WO<sub>4</sub>·2H<sub>2</sub>O (0.006 M), H<sub>2</sub>SO<sub>4</sub> (0.04 M) and temperature (50 °C). The model is fitted using Equation (3.6) – (3.11) and the rate constant in Table 4.1.

As can be seen in Figure 6.1, the simulated model shows that the yield of limonene-1,2-epoxide reached a maximum of 71 % at a reaction time of 20 minutes. The amount of limonene-1,2-epoxide was predicted to be gradually decreasing over time due to the formation of diol, which was included in the model. The initial rate (5 minutes) for the epoxidation of (R)-(+)-limonene (model) was calculated to be 0.078 mol L<sup>-1</sup>min<sup>-1</sup>. This initial rate value was used to benchmark the continuous epoxidation process in an organic solvent-free and under equimolar conditions.

### 6.3 Mixing study for epoxidation of (R)-(+)-limonene in the continuous mesoOBR reactor

A series of experiments were performed to study the mixing performance of mesoOBR for the epoxidation of (R)-(+)-limonene in an organic solvent-free and under equimolar condition at temperature of 50 °C. The continuous epoxidation reaction performed under such condition shows little exothermicity in jacketed mesoOBR. This allows further studies on the isothermal epoxidation of (R)-(+)-limonene or  $\alpha$ -pinene in an organic solvent-free and equimolar

conditions, which were not possible using jacketed flask (batch reaction). This superior temperature control exhibited by the mesoOBR was discussed in the relevant section (section 6.8). Figure 6.2 show the initial rates achieved using five different baffle designs (integral baffle, helical, single orifice, tri-orifice, and multi-orifice) evaluated in this study.

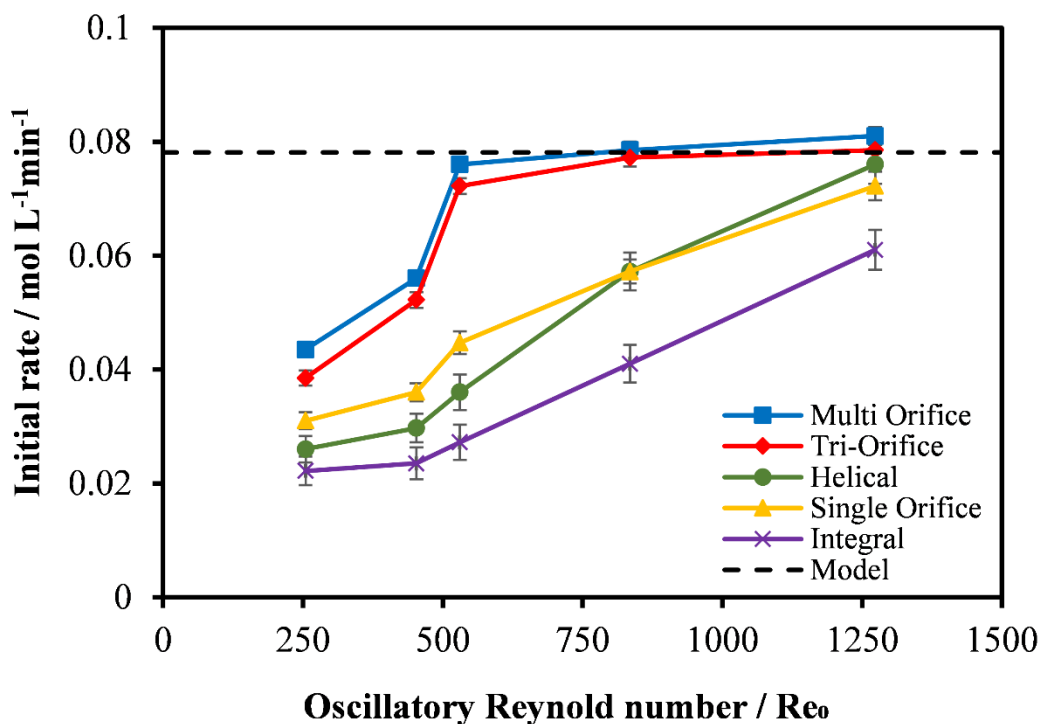


Figure 6.2. Effect of mixing on the initial rate of reaction for the epoxidation of (R)-(+)-limonene using various type of baffles. Reaction condition: (R)-(+)-limonene (1.25 M),  $\text{H}_2\text{O}_2$  (1.25 M),  $\text{Na}_2\text{WO}_4 \cdot 2\text{H}_2\text{O}$  (0.006 M),  $\text{H}_2\text{SO}_4$  (0.04 M), temperature (50 °C),  $Re_o \sim 1300$ , residence times ( $\tau$ ) 5 min to 15 min ( $Re_n$  2.0 – 5.7). Dashed line represents data from simulated model.

The baffles were tested on a range of mixing condition ( $Re_o$ ) ranging from less intense ( $Re_o \sim 250$ ) to very intense ( $Re_o \sim 1300$ ). This  $Re_o$  corresponds to frequency ranges from 3 Hz to 7.5 Hz, and the centre to peak amplitude ranges from 2.5 mm to 9 mm. The initial rate of reaction,  $0.078 \text{ mol L}^{-1}\text{min}^{-1}$  obtained from the simulated model of (R)-(+)-limonene epoxidation was used as a benchmark (dashed line in Figure 6.2). Clearly, in the mesoOBR, both a sufficient  $Re_o$  and a suitable baffle design were required.

As can be seen in Figure 6.2, using the integral baffle, even at highest  $Re_o$ , the observed reaction rates ( $0.061 \text{ mol L}^{-1}\text{min}^{-1}$ ) was much lower than the benchmark, indicating mass transfer limitations. The poor mixing performance is due to the absence of sharp edges, which allows

coalescence of smaller droplets generated during vortex formations (Phan *et al.*, 2011b). The helically baffled design exhibited poor mixing and low rate of reaction at  $Re_o < 850$ , but higher rates at the highest  $Re_o$  (1300), approaching the benchmark's performance. This design does not have sharp edges, but the improved mixing and enhanced reaction rates at  $Re_o \sim 1300$  can be explained by the formation of swirling flow in the helically baffled reactor (Ahmed *et al.*, 2017; McDonough *et al.*, 2017). The single orifice baffle design enhanced the two-phase mixing. At  $Re_o$  850 - 1300, its behaviour was similar to the helical baffle. The integral and single orifice baffles were not able to overcome mass transfer limitation, even at higher  $Re_o$ .

The tri-orifice and multi-orifice baffles designs achieved comparable reaction rates to the model at  $Re_o > 500$ , respectively. Figure 6.2 shows that the mixing performances of the tri-orifice baffles were remarkably similar to the multi-orifice at all  $Re_o$ . The performances of the tri-orifice and multi-orifice baffles were clearly better than the single orifice. This is probably due to a greater length of edge for flow separation, creating more vortices, thereby enhancing droplet break-up, which in turn increases the reaction rate. This allows both baffle designs to be operated without mass transfer limitation at  $Re_o > 500$ . It was also observed that at a lower  $Re_o (< 450)$ , effective mixing for all baffle designs could not be sustained which leads to phases segregation. The yield of limonene-1,2-epoxide obtained from the study at highest mixing intensity,  $Re_o \sim 1300$  for all the baffle designs were compared to the simulated model as shown in Figure 6.3.

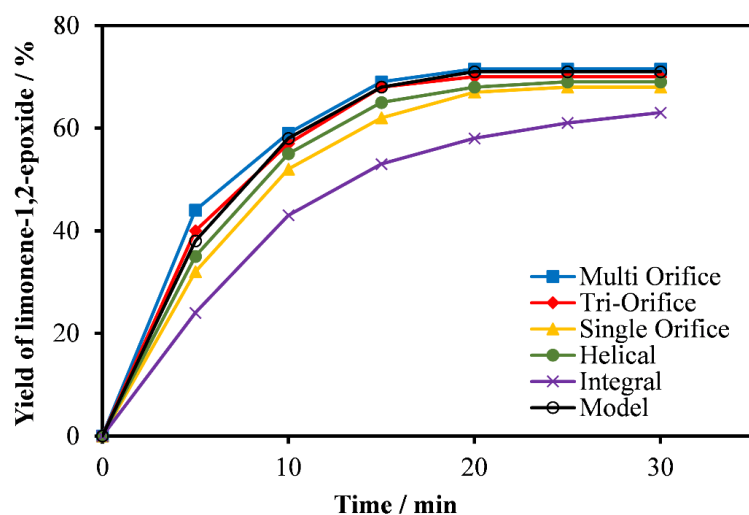


Figure 6.3. Comparison of the yield of limonene-1,2-epoxide of the simulated model and continuous mesoOBR using various baffles. Reaction condition: (R)-(+)-limonene (1.25 M),  $H_2O_2$  (1.25 M),  $Na_2WO_4 \cdot 2H_2O$  (0.006 M),  $H_2SO_4$  (0.04 M), temperature (50 °C),  $Re_o \sim 1300$ , residence times ( $\tau$ ) 30 min ( $Re_n$  2.0 – 5.7).

From Figure 6.3, the experimental yield of limonene-1,2-epoxide using tri-orifice and multi-orifice baffles was similar to the yield simulated by the model. This finding confirms that mass transfer was overcome using both tri-orifice and multi-orifice baffles and validates the models previously developed. The yield of limonene-1,2-epoxide for the helical baffle was slightly higher compared to the single orifice design. This is due to the better performance of the helical baffle at the mixing intensity of  $Re_o \sim 1300$ . The integral baffle suffered poor yield of limonene-1,2-epoxide compared to other baffle design, which clearly shows the importance of sharp-edges baffle design to break up droplets in a biphasic reaction.

#### 6.4 Steady states performance of the mesoOBRs

The performances of the mesoOBRs for the epoxidation reaction were evaluated based on criteria such as the attainment of steady states (induction period) and the consistency of the product. For a continuous reactor, the induction period refers to the period required to establish a steady state. The induction period should be minimised to reduced waste generated due to variations in product output (Phan *et al.*, 2012). The time to attainment of steady states for the continuous epoxidation of (R)-(+)-limonene with  $H_2O_2$  at 15 min residence time ( $\tau$ ) ( $Re_n \sim 2.0$ ) with  $Re_o \sim 1300$ , evaluated over 70 minutes in real time. The results are shown in Figure 6.4.

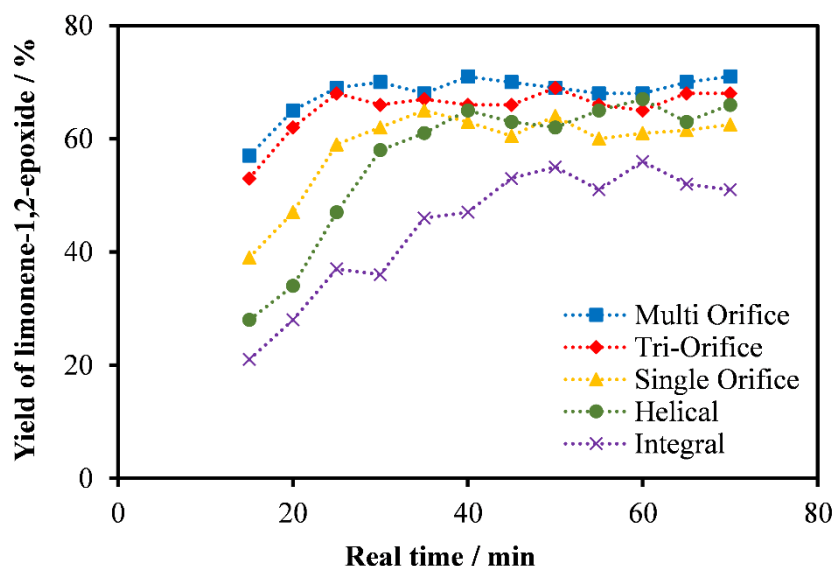


Figure 6.4. The effect of various baffle types on the achievement of steady states for the continuous epoxidation of (R)-(+)-limonene. Reaction condition: (R)-(+)-limonene (1.25 M),  $H_2O_2$  (1.25 M),  $Na_2WO_4 \cdot 2H_2O$  (0.006 M),  $H_2SO_4$  (0.04 M), temperature 50 °C, residence time ( $\tau$ ) 15 min ( $Re_n \sim 2.0$ ),  $Re_o \sim 1300$ .

Figure 6.4 shows that the baffle design strongly influenced the induction time. At  $1 \tau$  (15 min), the yield of limonene-1,2-epoxide for the integral baffles was very low (about 21 %), and steady states were not achieved in this reactor below 45 min, as the yield fluctuated in the range of 21 % -53 %. At 45 min ( $t = 3 \tau$ ) and longer, minimum variation was observed with steady state epoxide yield of  $53 \pm 2.1$  %. The large variances in the yield are due to mass transfer limitations inside the reactor, where the immiscible reactants visibly separated into two phases.

For helical baffles, the yield was low at 15 min ( $t = \tau$ ), but steady states could be achieved by 37 min ( $t = 2.5 \tau$ ), with the steady state epoxide yield reaching  $65 \pm 1.8$  %. The single orifice baffle achieves steady states slightly quicker than the helical, at time 30 min ( $t = 2 \tau$ ), however, the steady state yield was still low at  $62 \pm 1.6$  %. This result is consistent with the finding in section 3.2, where at  $Re_o \sim 1300$ , the helical baffle achieved higher initial reaction rates than the single orifice.

The tri-orifice and the multi-orifice baffles designs exhibited better performances than the other mesoOBR designs, achieving steady states by 22 min ( $t = 1.5 \tau$ ). The steady state epoxide yields were  $68 \pm 1.3$  % and  $69 \pm 1.2$  % for the tri-orifice and the multi-orifice baffles, respectively. The variances in epoxide yield for both multi-orifice and the tri-orifice baffles design were the lowest for the mesoOBR used, indicating uniform mixing throughout these reactors. This was attributed to the presence of sharp edges in these orifice baffles, which enhances and maintains droplets break-up. The tri-orifice and multi-orifice baffles showed better control of product quality and reproducibility, and these two qualities are typically associated with operating at a plug flow regime. A plug flow mixing exhibits excellent radial mixing with minimal axial dispersion, thus reducing product variations.

The mesoOBR has been demonstrated to perform rapid screening of process parameters, which allows the reduction in process development time and the amount of reagent used compared to a batch process (Rasdi *et al.*, 2013). In this work, the multi steady states performance of the mesoOBRs in (R)-(+)-limonene epoxidation was evaluated using ramped residence times from 5 min up to 25 min in a continuous mode, by imposing several consecutive residence times on the reaction in a single experiment (see Figure 6.5). The multi-orifice baffle design was used and compared to the helical baffles designs at  $Re_o \sim 1300$ .

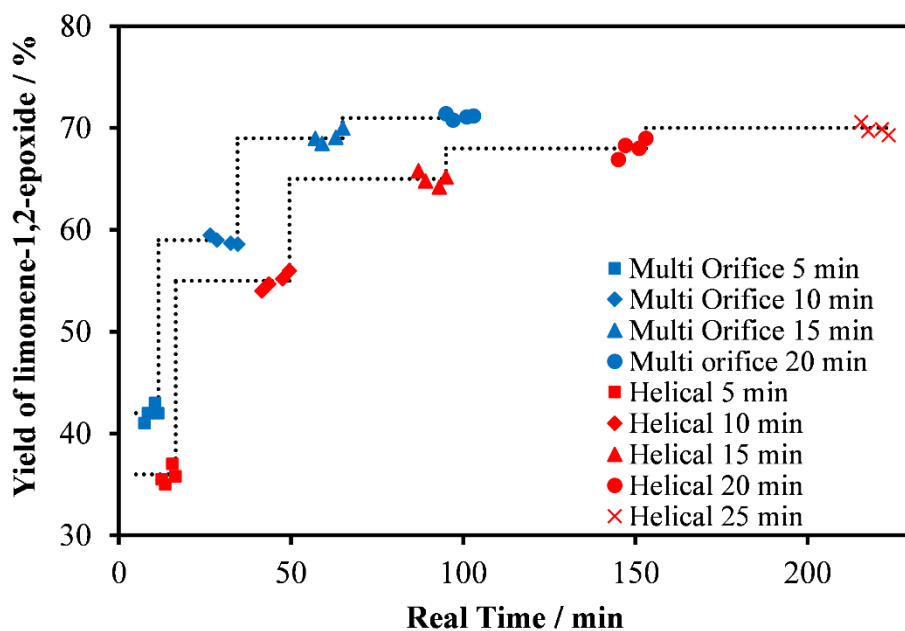


Figure 6.5. Comparison between the multi-orifice baffle and helically baffled mesoOBR for the screening of residence time for the continuous epoxidation of (R)-(+)-limonene in multi steady state mode. The dashed line represents ramped residence times. Reaction condition: (R)-(+)-limonene (1.25 M),  $H_2O_2$  (1.25 M),  $Na_2WO_4 \cdot 2H_2O$  (0.006 M),  $H_2SO_4$  (0.04 M) temperature 50 °C,  $Re_n$  1.0 – 5.7,  $Re_o \sim 1300$ .

As illustrated in Figure 6.5, steady states were achieved for both baffles designs at all residence times, and inductions periods of  $1.5 \tau$  for the multi-orifice and  $2.5 \tau$  for the helical baffles. Both baffles showed clear step changes, indicative of high levels of plug flow. The multi-orifice baffles had a shorter induction period due to the superior mixing in the reactor, as previously noted. The higher epoxide yields, and lower variances exhibited by the multi-orifice baffles design at all residence times compared to the helical baffle also indicates a higher degree of plug flow in the multi-orifice baffles. The total screening time for the multi-orifice baffle was about 100 minutes, while the helical baffle design required twice as long (200 min).

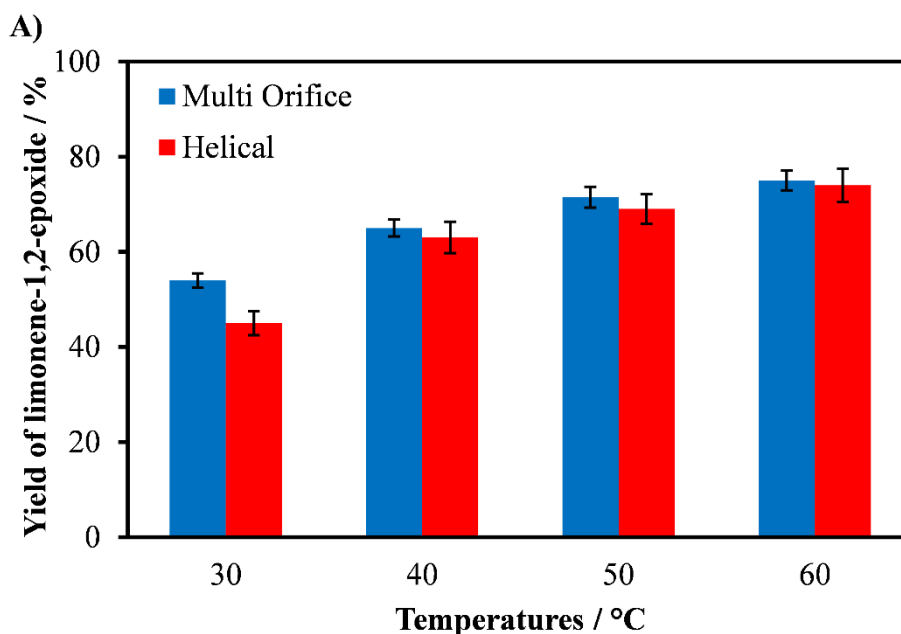
All of the data points shown in the Figure 6.5 is equivalent to one sample collected from a batch reaction, therefore, to obtain a similar number of data point as the mesoOBR, several independent experiments would need to be performed in batch, which would take several hours to complete. Here, especially with the multi-orifice baffle design, the variation was much lower than in batch and with other types of baffle. This clearly demonstrate the advantage of the mesoOBR as a rapid screening reactor, with consistent, reproducible data. Another advantage is that the multi-orifice baffle could probably be predictably scaled up. A recent scale-up study

on the helically baffled OBR between diameter 10 mm to 50 mm shows similar mixing pattern allowing reaction conditions to be extrapolated between these scales (Ahmed *et al.*, 2017). This scalability characteristic of the OBR would allow higher throughput of the continuous epoxidation reaction compared to a conventional fed-batch reactor.

The developed process condition using multi-orifice baffles for the epoxidation of (R)-(+)-limonene could be further extended to the epoxidation of  $\alpha$ -pinene. Further studies are performed to screen the reaction parameters such as residence time, temperature, and excess molar ratio.

### 6.5 Effect of temperature on the continuous epoxidation in mesoOBR

A series of experiments were performed using helical and multi-orifice baffled mesoOBR to evaluate the continuous epoxidation of (R)-(+)-limonene and  $\alpha$ -pinene at temperatures between 30 to 60 °C. The reaction was performed in an organic solvent-free under equimolar conditions. Figures 6.6 (A) and (B) present the results.





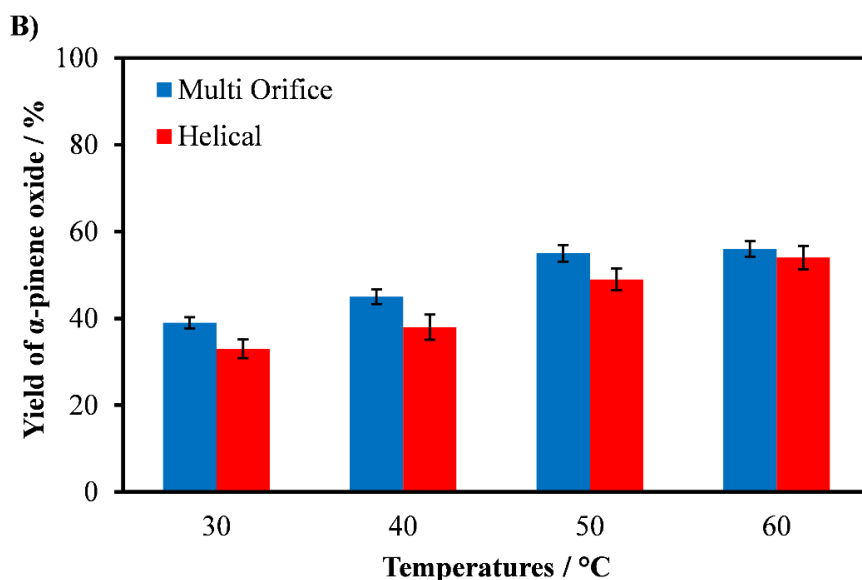


Figure 6.6. Comparison of yield for the continuous epoxidation using helical and multi-orifice mesoOBR at various temperature. (A) yield of limonene-1,2-epoxide (B) yield of  $\alpha$ -pinene oxide. Reaction conditions: (R)-(+)-limonene (1.25 M),  $H_2O_2$  (1.25 M),  $Na_2WO_4 \cdot 2H_2O$  (0.006 M),  $H_2SO_4$  (0.04 M), residence time ( $\tau$ ) 30 minutes ( $Re_n$  1.0), multi-orifice  $Re_o \sim 500$ , helical  $Re_o \sim 1300$ .

As can be seen in Figure 6.6 (A), the yield of limonene-1,2-epoxide for both types of baffle, increased with increasing temperature. The yield increased from 54 % to 75 % when the temperature is increased from 30 to 60 °C when using multi-orifice baffled mesoOBR. The helically baffled mesoOBR attained a lower yield than multi-orifice where the yield increased from 45 % to 74 % when the temperature is increased from 30 to 60 °C. Although the difference of yield of limonene-1,2-epoxide between both baffles were apparent at 30 °C, the yield was almost similar at 60 °C.

Figure 6.6 (B) depict the yield of  $\alpha$ -pinene oxide increased with increasing temperature for both baffles tested. The yield increased from 39 % to 56 % when the temperature is increased from 30 to 60 °C when using multi-orifice baffled mesoOBR. Similar to the study with (R)-(+)-limonene, the helical baffle exhibit lower yield than multi-orifice baffle at all temperature studied. The yield increased from 33 % to 54 % when the temperature is increased from 30 to 60 °C. The multi-orifice mesoOBR demonstrated better yield than helical baffle at all temperature tested for both substrates, (R)-(+)-limonene and  $\alpha$ -pinene. This confirms the superior feature of the multi-orifice baffle where the sharp edge design facilitates better mixing between the biphasic mixture. Furthermore, the multi-orifice baffles exhibit lower product variation (deduced from error bars) as compared to the helical mesoOBR.

## 6.6 Effect of residence time on the continuous epoxidation in mesoOBR

Figures 6.7 (A) and (B) present the results of the continuous epoxidation of (R)-(+)-limonene and  $\alpha$ -pinene was studied at residence time between 5 min to 30 minutes. The study was performed using both helical and multi-orifice baffled mesoOBR. The reaction was performed in an organic solvent-free under equimolar conditions.

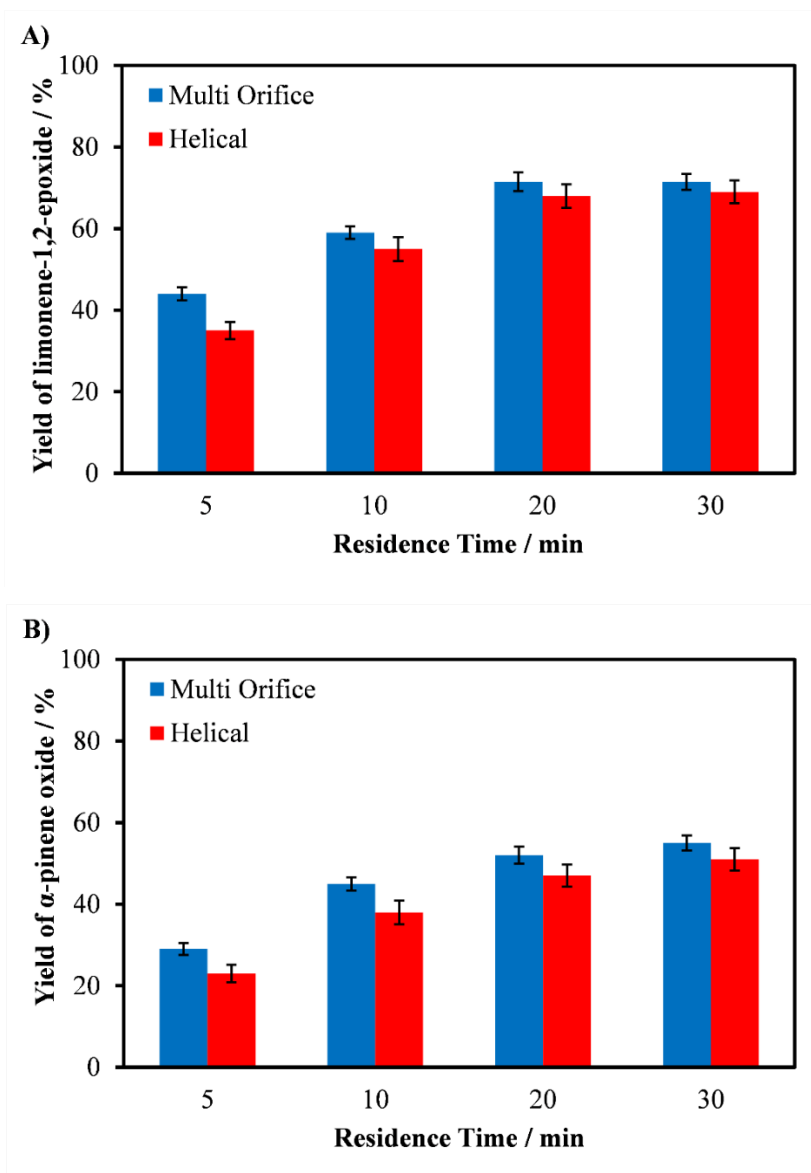


Figure 6.7. Comparison of yield for the continuous epoxidation using helical and multi-orifice mesoOBR at various residence time. (A) yield of limonene-1,2-epoxide (B) yield of  $\alpha$ -pinene oxide. Reaction conditions: (R)-(+)-limonene (1.25 M),  $H_2O_2$  (1.25 M),  $Na_2WO_4 \cdot 2H_2O$  (0.006 M),  $H_2SO_4$  (0.04 M), temperature 50 °C, (Ren 1.0 – 5.7), multi-orifice  $Re_o \sim 500$ , helical  $Re_o \sim 1300$ .

Figure 6.7 (A) shows the yield of limonene-1,2-epoxide for both baffle design, increased with increasing residence time, as expected. The multi-orifice and helical mesoOBR attains a maximum yield at 20 minutes residence time. In the epoxidation with multi-orifice mesoOBR, the yield increased from 44 % to 72 % when the residence time is increased from 5 min to 30 min. The helical mesoOBR shows a lower yield than multi-orifice mesoOBR where the yield increased from 35 % to 69 % when the residence time is increased from 5 min to 30 min. The difference between the yield of both type of mesoOBR is less apparent at higher residence time, 30 minutes.

As can be seen in Figure 6.7 (B), the yield of  $\alpha$ -pinene oxide increased when the residence time is increased up to 30 min. In multi-orifice mesoOBR, the yield was 29 % and 55 %, for the residence time of 5 min to 30 min, respectively. In helical mesoOBR, the yield increased from 23 % to 51 % when the residence time is increased from 5 min to 30 min. The study on the residence time for the epoxidation of (R)-(+)-limonene and  $\alpha$ -pinene showed similar behaviour to a typical batch epoxidation reaction the substrate, where the yield increases over time before attains a maximum. However, for a continuous process, apart from achieving similar performance (in terms of conversion or yield) to a batch reactor, it is important to be able to do so with minimum product variations. Here, the multi-orifice mesoOBR shown higher yield of both limonene-1,2-epoxide and  $\alpha$ -pinene oxide at each residence time tested with noticeably less variation than the helical mesoOBR.

### **6.7 Effect of molar ratio of (R)-(+)-limonene and $\alpha$ -pinene to $H_2O_2$ on the continuous epoxidation in mesoOBR**

A series of experiments were performed using helical and multi-orifice baffled mesoOBR to evaluate the effect of molar ratio of (R)-(+)-limonene and  $\alpha$ -pinene on the continuous epoxidation using a multi-orifice and a helical baffle mesoOBR. The reaction was performed in an organic solvent-free under equimolar conditions. The results are shown in Figure 6.8 (A) and (B).

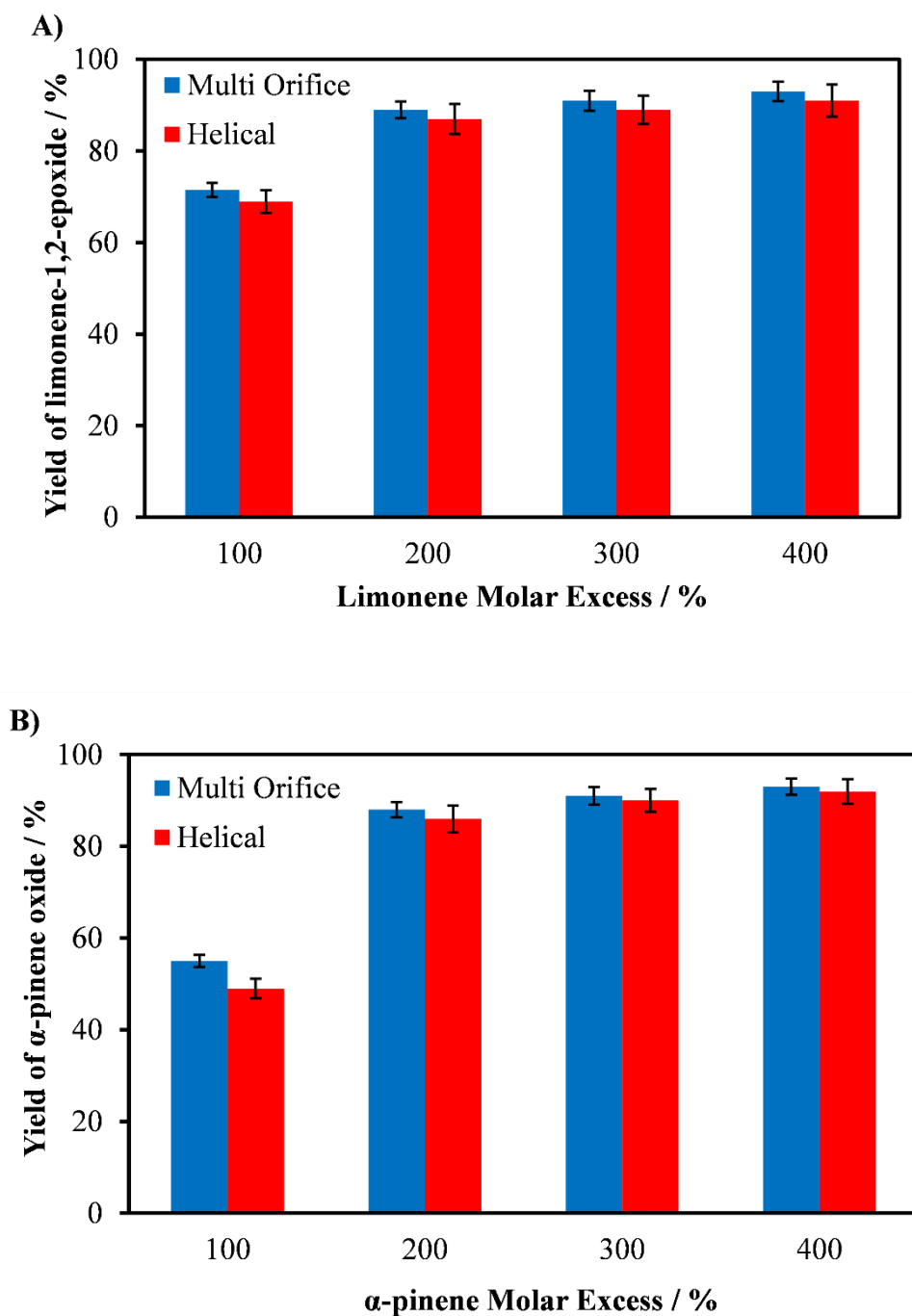


Figure 6.8. Comparison of yield for the continuous epoxidation using helical and multi-orifice mesoOBR at various molar ratio. (A) yield of limonene-1,2-epoxide (B) yield of  $\alpha$ -pinene oxide. Reaction conditions:  $\text{Na}_2\text{WO}_4 \cdot 2\text{H}_2\text{O}$  (0.006 M),  $\text{H}_2\text{SO}_4$  (0.04 M), residence time 30 minutes ( $Re_n$  1.0), multi-orifice  $Re_0 \sim 500$ , helical  $Re_o \sim 1300$ , 400 mol% = 4:1 substrate: $\text{H}_2\text{O}_2$ .

Figure 6.8 (A) shows the yield of limonene-1,2-epoxide for both baffle design increased with an increasing amount of (R)-(+)-limonene over  $\text{H}_2\text{O}_2$ . The yield of limonene-1,2-epoxide for multi-orifice and helical mesoOBR were 71.5 % and 69 % when 100 mol% of (R)-(+)-limonene

was used. When the amount of (R)-(+)-limonene was doubled (200 mol%), the yield increased dramatically. The yield of limonene-1,2-epoxide were 89 % and 87 % for multi-orifice and helical mesoOBR, respectively. Further increase in the amount of (R)-(+)-limonene of up to 400 mol%, afforded a merely 4 % increase in the yield of limonene-1,2-epoxide for each baffle design. Multi-orifice and helical mesoOBR attain a maximum of 93 % and 91 % yield of limonene-1,2-epoxide, respectively. This clearly shows that in meso OBR, especially when using the multi-orifice baffles, high yield of limonene-1,2-epoxide (~89 %) can be achieved while using less amount of excess limonene (~200 mol%) as compared to a batch epoxidation of (R)-(+)-limonene (~400 mol%) in a jacketed flask. This is due to the ability of the mesoOBR to operate isothermally despite using less solvents. In a batch epoxidation of (R)-(+)-limonene, a minimum of 400 mol% of (R)-(+)-limonene was required to maintain isothermal operation. This advantage of mesoOBR could save the number of reagents used and reduce wastage.

Similarly, in Figure 6.8 (B), the yield of  $\alpha$ -pinene oxide increased considerably, when the amount of  $\alpha$ -pinene was increased from 100 mol% to 200 mol% for both baffle design. The yield increase from 55 % to 88 %, and from 49 % to 86 %, for multi-orifice and helical mesoOBR, respectively. Further increase in the amount of  $\alpha$ -pinene of up to 400 mol% caused an increase of yield of  $\alpha$ -pinene oxide of up to 93 % and 92 % for both baffle design. Overall, the multi-orifice mesoOBR demonstrated higher yield of  $\alpha$ -pinene oxide than helical mesoOBR. However, the difference in yield of  $\alpha$ -pinene oxide is less pronounced at a higher amount of (R)-(+)-limonene and  $\alpha$ -pinene. It is noteworthy to mention that the multi-orifice achieved the maximum yield of limonene-1,2-epoxide and  $\alpha$ -pinene oxide at a lower mixing intensity ( $Re_0 \sim 500$ ), while the helical baffles requires more energy to obtain comparable yield ( $Re_0 \sim 1300$ ). The 3D-printed multi-orifice mesoOBR could achieved comparable performance to the batch using less energy than the commonly used baffle design such as the helical mesoOBR.

## **6.8 Passive isothermalisation of continuous epoxidation using heat-pipe OBR (HPOBR)**

The advantage of mesoOBR as seen in the previous section is the ability to achieve isothermal condition for the exothermic epoxidation reaction. This feature allows the mesoOBR to achieved high yield of limonene-1,2-epoxide in an organic solvent-free condition while using less amount of (R)-(+)-limonene. The mesoOBR used was jacketed in which a steady flow of water at specific temperature flows on the outer jacket. The flow rate of the water in the jacket was sufficient to removes the exothermic heat released by the reaction. Figure 6.9 shows the

temperature profile of jacketed mesoOBR compared to a jacketed four-necked flask, typically used for the batch epoxidation reaction. The batch reactor temperature profile includes solvent-free operation at an initial temperature of 50 °C in both non-jacketed and jacketed mode as well as with solvent in a jacketed mode. The mesoOBR temperature profile was measured at high flow rates (6 mL min<sup>-1</sup>,  $Re_n$  5.7) corresponding to 5 min residence time and low flow rates (1.0 mL min<sup>-1</sup>,  $Re_n$  1.0), corresponding to 30 min residence time. The epoxidation of (R)-(+)-limonene was used as a model reaction.

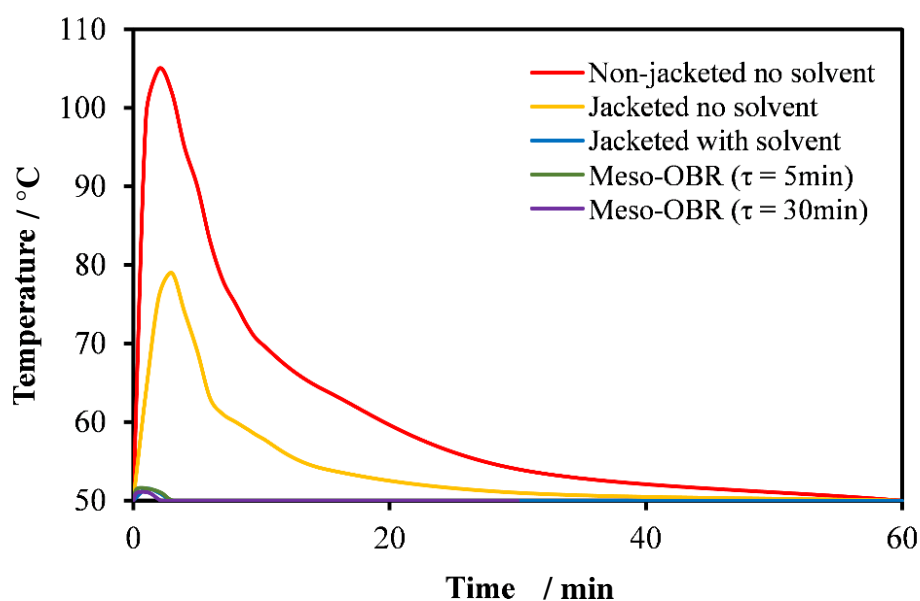


Figure 6.9. Temperature profile comparison between jacketed flask and mesoOBR. Condition for mesoOBR; 5 min residence time ( $Re_n = 5.7$ ) and 30 min residence time ( $Re_n = 1.0$ ).

As shown in Figure 6.9, regardless of the reactor type, the exothermicity of the epoxidation reaction was significant at the initial reaction time period (< 5 min). The temperature for the batch epoxidation using the flask in an organic solvent-free reaction in a non-jacketed mode (without water circulation) reached a maximum of 105 °C. At these temperatures, significant H<sub>2</sub>O<sub>2</sub> decomposition was observed, and multiple by-products, mainly diols, of up to 40 %, were obtained. When the flask was used in a jacketed mode (with water circulation) under the same reaction condition, the temperature rose to 80 °C, a reduction of about 25 °C. A near isothermal condition (to ±1 °C) can be achieved using the flask when a solvent amount equivalent to ~ 500 mol% was added.

In the jacketed mesoOBR, the temperature profile for both high ( $Re_n = 5.7$ , 5 min residence time) and slow flow rates ( $Re_n = 1.0$ , 30 min residence time) showed similar behaviour with only  $\pm 1$  °C variation in an organic solvent-free condition. Superior temperature control was evident in the jacketed mesoOBR regardless of the flow rate tested (up to  $6 \text{ mL min}^{-1}$ ,  $Re_n = 5.7$ ). This can be attributed to the high surface to volume ratio of the mesoOBR coupled with sufficient water circulation in the jacket. In a conventional process using a large batch reactor, the temperature variation would be significantly higher than in the lab scale reactor (flask) used here. Therefore, a drop-wise method of addition of the oxidant in a fed-batch reactor was typically required to maintain an isothermal process, which lengthens the reaction. Reaction times of up to 8 h are used in practice (Santacesaria *et al.*, 2011; Santacesaria *et al.*, 2012; Wu *et al.*, 2017). This obstacle could be overcome using the jacketed mesoOBR. A continuous isothermal reaction using the mesoOBR reactor would potentially increase the throughput of the process, reduce the processing time, and lead to safer epoxidation process.

Heat-pipe OBR (HPOBR) is typically a mesoOBR without the water jacket. Instead, the outer jacket was filled with a working fluid such as methanol, where the boiling and condensation of the working fluid allows the reactor to achieve isothermalisation passively (McDonough *et al.*, 2016). A series of experiments were performed to compare the performance of mesoOBR and the HPOBR on the epoxidation of (R)-(+)-limonene at residence time between 5 min to 30 min. Two type of baffle design were used for the mesoOBR, which the helical and multi-orifice baffle. The HPOBR used a helical baffle design to allow thermocouples to be fitted at specific length inside the inner tube (ID 5 mm). The reaction was performed in an organic solvent-free under equimolar conditions. The results are shown in Figure 6.10.

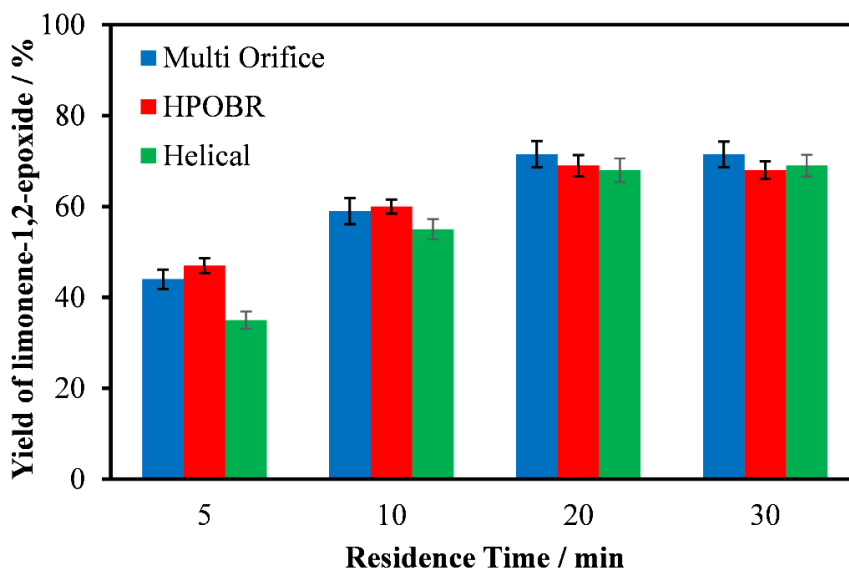


Figure 6.10. Comparison of yield of limonene-1,2-epoxide for the continuous epoxidation using helical mesoOBR, multi-orifice mesoOBR and helically baffled HPOBR at various residence time. Reaction conditions: (R)-(+)-limonene (1.25 M),  $H_2O_2$  (1.25 M),  $Na_2WO_4 \cdot 2H_2O$  (0.006 M),  $H_2SO_4$  (0.04 M),  $Re_n$  1.0 – 5.7, multi-orifice  $Re_o \sim 500$ , helical  $Re_o \sim 1300$ , HPOBR  $Re_o \sim 1300$ .

As can be seen in Figure 6.10, the yield of limonene-1,2-epoxide for both mesoOBR and HPOBR, increased with increasing residence time. The mesoOBRs and HPOBR attains a maximum yield at 20 minutes residence time. Interestingly the yield of limonene-1,2-epoxide at 5 min and 10 min residence time for the HPOBR was higher than both mesoOBRs. The yield for the HPOBR was 47 % and 60 % at 5 min and 10 min residence time, respectively, while the yield of multi-orifice mesoOBR was 44 % and 59 % at similar residence time. However, the multi-orifice mesoOBR achieved higher yield of limonene-1,2-epoxide than helical mesoOBR and HPOBR at 20 min and 30 min residence time.

At lower residence time (5 min and 10 min), the HPOBR achieved a slightly higher yield than the multi-orifice mesoOBR despite using a helical baffle. To better understand this result, more investigation was carried out using the HPOBR. Temperature profiles of the HPOBR were recorded at various reactor length (mm) for the epoxidation of (R)-(+)-limonene at residence time between 2.5 min and 20 min. The reaction was performed in an organic solvent-free under equimolar conditions. The reactants were preheated to 50 °C using a heating band. The temperature measured at each designated reactor length, for the experiments at residence time 2.5 min up to 20 min are shown in in Figure 6.11.



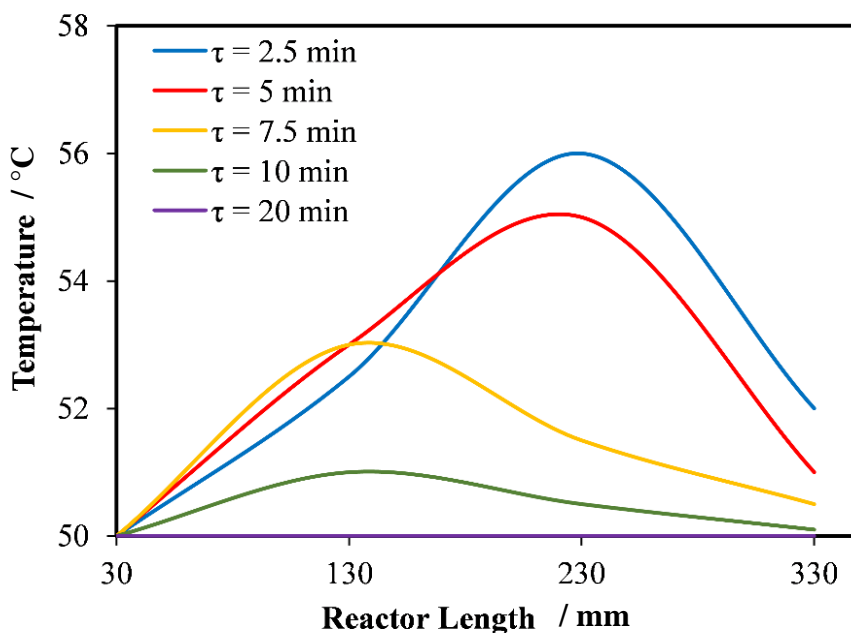


Figure 6.11. Temperature profile for HPOBR showing hot spot at certain reactor length. Reaction conditions: (R)-(+)-limonene (1.25 M),  $H_2O_2$  (1.25 M),  $Na_2WO_4 \cdot 2H_2O$  (0.006 M),  $H_2SO_4$  (0.04 M), initial temperature 50 °C, ( $Re_n$  1.0 – 11.2), HPOBR  $Re_o \sim 1300$ .

Figure 6.11 shows a maximum of ~6 °C difference between the inlet temperature and the temperature at 230 mm length of the reactor when operating at a residence time of < 7.5 min ( $Re_n > 4.5$ ). Higher  $Re_n$  (lower residence time) pushes the hot spot closer to the reactor outlet (at 330 mm). Decreasing the  $Re_n$  (residence time > 10 min) allows the reaction to be isothermalised. This results clearly shows that at lower residence time (< 10 min residence time), the HPOBR was up to 6 °C hotter than a mesoOBR operating at 50 °C. This explains the result in Figure 6.10, where the yield of limonene-1,2-epoxide was higher than the multi-orifice mesoOBR at residence time of less than 10 min. Nevertheless, the HPOBR could achieve passive isothermalisation at higher residence time (lower flow rates) which should allow isothermal epoxidation of (R)-(+)-limonene and  $\alpha$ -pinene using less energy.

In summary, the jacketed mesoOBR shows near isothermalisation with a temperature variation of  $\pm 1$  °C in an organic solvent-free condition, allowing the reaction time to be reduced from 8 hours (conventional reactor) to less than 30 minutes, a 16-fold reduction. The epoxidation reaction without solvent reduces the volume of the reactor required to 5-fold, resulting in an overall intensification factor of 80 for the continuous epoxidation process in mesoOBR.

## 6.9 Summary

New 3D-printed orifice baffle designs were developed and compared to existing integral and helical baffles in the mesoOBR for the biphasic and highly exothermic epoxidation of (R)-(+)-limonene and  $\alpha$ -pinene with  $\text{H}_2\text{O}_2$  in an organic solvent-free environment. The new baffles design performance was evaluated in terms of the mixing intensity, induction period, achievement of multiple steady states and heat removal capability. Passive isothermalisation was also investigated using a heat-pipe OBR. In summary:

- i) The tri-orifice and multi-orifice baffle designs exhibited removal of mixing limitations at  $\text{Re}_o > 500$ .
- ii) The tri-orifice and multi-orifice baffles exhibited shorter induction periods ( $\sim 1.5 \tau$ ) than single orifice baffle designs ( $\sim 2 \tau$ ), helical ( $\sim 2.5 \tau$ ) and the integral baffle designs ( $\sim 3 \tau$ ).
- iii) The shorter induction periods for the tri orifice and multi-orifice baffles reduce waste production in the start-up stage.
- iv) The multi-orifice baffles exhibited the lowest variances in limonene-1,2-epoxide yield among all the baffles designs investigated, indicating a high degree of plug flow.
- v) The multi-orifice mesoOBR was less energy intensive compared to the helical mesoOBR to achieve similar yield to the batch experiment.
- vi) The jacketed mesoOBR exhibited superior temperature control, with a  $\pm 1 \text{ }^\circ\text{C}$  variation in temperature.
- vii) Passive isothermalisation was possible when using HPOBR.

## Chapter 7 Conclusions and Future Work

### 7.1 Conclusions

A process was developed for the continuous epoxidation of (R)-(+)-limonene and  $\alpha$ -pinene using a mesoscale Oscillatory Baffled Reactor (mesoOBR). Waste biomass derived (R)-(+)-limonene and  $\alpha$ -pinene were used as sustainable alternatives to petrochemical sources for the synthesis of epoxides. The epoxidation reaction was performed using more “environmentally friendly” hydrogen peroxide ( $\text{H}_2\text{O}_2$ ) and a polytungstophosphate catalyst. The aim was to resolve the challenges associated with the epoxidation of (R)-(+)-limonene and  $\alpha$ -pinene with  $\text{H}_2\text{O}_2$ .

The three main processing challenges were: (i) selectivity to epoxides was often low (ii) mass transfer limitations occurred due to the immiscibility of the phases, reducing the reaction rate, and (iii) the reaction was exothermic, so the reaction was often operated in non-optimal conditions, where heat transfer was easier. The selectivity issues were addressed by optimising the reaction conditions through screening of various parameters including temperature, oxidant amount, sodium sulphate ( $\text{Na}_2\text{SO}_4$ ) amount, acid concentration ( $\text{H}_2\text{SO}_4$ ) and solvent type. Mass transfer limitation was observed in continuous epoxidation of (R)-(+)-limonene and  $\alpha$ -pinene with  $\text{H}_2\text{O}_2$  using commonly used helically and integrally baffled mesoOBR. The mass transfer issues were solved by developing new 3D-printed orifices baffles in mesoOBR. The mesoOBR platform allows isothermal conditions to be achieved in an organic solvent-free conditions. The performance of the mesoOBR was investigated via the mixing studies using various baffle designs, the attainment of the induction period, steady state performance and temperature profile. Passive isothermalisation can be achieved using HPOBR.

### 7.1.1 Batch (R)-(+)-limonene epoxidation

It has been demonstrated that the epoxidation of (R)-(+)-limonene can be performed solvent-free at a 95 % conversion of  $\text{H}_2\text{O}_2$  and 100 % selectivity to limonene-1,2-epoxide by using (R)-(+)-limonene in stoichiometric excess (versus  $\text{H}_2\text{O}_2$ ) with a single-step addition of the oxidant ( $\text{H}_2\text{O}_2$ ). The reaction was performed in a jacketed batch reactor with temperature control provided via a water bath. Process parameters were screened at temperature range from 30 °C to 60 °C,  $\text{H}_2\text{O}_2$  amount from 100 -200 mol%,  $\text{Na}_2\text{SO}_4$  amount from 0 – 7.5 g, and acid ( $\text{H}_2\text{SO}_4$ ) concentration of 0.02 – 0.06 M. The findings showed a process 100% selective to limonene-1,2-epoxide could be obtained at temperatures below 50 °C, equimolar amount of  $\text{H}_2\text{O}_2$  (100 mol%), saturated amount of  $\text{Na}_2\text{SO}_4$  (5.7g) and acid concentration of lower than 0.04 M. Above 50 °C, with  $\text{H}_2\text{O}_2$  above 100 mol%, no  $\text{Na}_2\text{SO}_4$  and acid concentration of above 0.04 M, caused significant hydrolysis of limonene-1,2-epoxide to limonene-1,2-diol.

The addition of  $\text{Na}_2\text{SO}_4$  has been shown to inhibit the hydrolysis of limonene-1,2-epoxide to limonene-1,2-diol through a ‘salting-out’ process. The selectivity towards limonene-1,2-epoxide is 100 % when enough  $\text{Na}_2\text{SO}_4$  (5.7 g) is used to saturate the aqueous phase. It was also found that the correct acid concentration (< 0.04 M) suppressed the formation of limonene-1,2-diol. Five solvents have also been compared, as follows: (R)-(+)-limonene itself (i.e., solvent-free operation), p-cymene, toluene, acetonitrile and 1,2-dichloroethane. Higher yield of limonene-1,2-epoxide was obtained when using (R)-(+)-limonene in excess. The developed process has a 95 % conversion of  $\text{H}_2\text{O}_2$  with 100 % selectivity towards limonene-1,2-epoxide and a significantly shorter reaction time (~15 minutes) than is conventionally used (8 h).

The (R)-(+)-limonene epoxidation was shown to be first-order with respect to (R)-(+)-limonene and the catalyst. A fractional order (~0.5) with respect to the  $\text{H}_2\text{O}_2$  concentration was obtained. The Arrhenius activation energies for the formation of limonene-1,2-epoxide and limonene-1,2-diol were determined to be 35 and 79  $\text{kJ mol}^{-1}$ , respectively. Based on these values, predictive kinetic model was developed. The model could predict the conversion of (R)-(+)-limonene and the yield of limonene-1,2-epoxide with a high level of agreement with the experimental data (~98 %). The formation of limonene bis-epoxides and the hydrolysis of epoxides was also incorporated into the model.

### **7.1.2 Batch $\alpha$ -pinene epoxidation**

The epoxidation of  $\alpha$ -pinene typically leads to a variety of side-products. It is usually performed in an excess of solvent or using drop-wise addition of the oxidant, as a mitigation due to the exotherm. This mode of operation reduces the reaction rate and lengthens the reaction time, while the use of solvent necessitates additional separation steps.

Here, it was shown that 93 % conversion of  $\text{H}_2\text{O}_2$  with 100 % selectivity to  $\alpha$ -pinene oxide within 20 minutes reaction time could be achieved using a single-step addition of the oxidant in the absence of a solvent. Screening of process parameters revealed a 100 % selective reaction to  $\alpha$ -pinene oxide could be obtained at a temperature under 50 °C, an equimolar amount of  $\text{H}_2\text{O}_2$  and acid concentration of lower than 0.05 M causing substantially suppressed allylic oxidation, rearrangement and hydrolysis processes. It was demonstrated that low concentration of acid ( $\leq 0.05$  M) should be used, as this prevented the formation of various side-products. It was found that by using  $\alpha$ -pinene in excess without any solvent, the reaction exhibited rapid and efficient consumption of oxidants, which coupled with the lower acid concentration allows a predominantly epoxidation reaction route. This study also found that increasing the amount of oxidant enhances the rate of undesired allylic oxidation.

Reaction kinetic studies revealed that the reaction is first order with respect to  $\alpha$ -pinene and the catalyst and has a reaction order of 0.5 with respect to the  $\text{H}_2\text{O}_2$ . The kinetic parameters (reaction orders) determined for the  $\alpha$ -pinene epoxidation were similar to the values obtained for (R)-(+)-limonene epoxidation. An Arrhenius activation energy for the  $\alpha$ -pinene epoxidation to an epoxide was determined to be 35 kJ mol<sup>-1</sup>. A MATLAB-based model was developed to predict the rates of the  $\alpha$ -pinene epoxidation numerically. The model was able to predict the yield of  $\alpha$ -pinene oxide using the optimised conditions.

### **7.1.3 Continuous (R)-(+)-limonene epoxidation using mesoOBR**

A continuous process was developed and implemented using novel designs of 3D-printed oscillatory baffled reactor. They were compared to conventional integral and helical baffles in mesoOBR for the biphasic and highly exothermic epoxidation reaction of (R)-(+)-limonene and  $\alpha$ -pinene with  $\text{H}_2\text{O}_2$  in an organic solvent-free environment. The new designs were able to overcome the mass and heat transfer challenges associated with the reaction.

The performance criteria investigated included mixing intensity, induction period, achievement of multiple steady states and the temperature profile of the mesoOBRs. The 3D-printed tri-

orifice and multi-orifice baffle mesoOBRs achieved comparable rate to the developed kinetic model ((R)-(+)-limonene) at  $Re_o > 850$  and  $Re_o > 500$ , respectively. The tri-orifice and multi-orifice baffles exhibited induction periods of  $1.5\tau$ , as compared to  $2.0\tau$  for single orifice baffles,  $2.5\tau$  for helical and  $3.0\tau$  for integral baffles designs. The shorter induction periods for the tri-orifice and multi-orifice baffles would reduce waste production in the start-up stage. The performance of the tri-orifice and multi-orifice baffles mesoOBRs was attributed to their smaller orifice diameters, which induces formations of smaller droplets sizes, increasing contact area that enhances the reaction rates.

The multi-orifice baffles exhibited the lowest variances ( $\pm 1.2\%$ ) in limonene epoxide yield among the baffle designs investigated, indicating a high degree of plug flow and high product reproducibility. In the screening of residence time in a multi steady state mode, the multi-orifice baffles were shown to be able to screen the parameter in half the time (100 min) required for the helical (200 min), and lesser time than in a batch reactor ( $> 4$  hours individual experiments). Clear, steady states were achieved at all residence times, an indication of tight control of process parameters and stable operations.

The jacketed mesoOBR showed superior temperature control to jacketed batch reactor, with a  $\pm 1$  °C variation in temperature at the inlet, which allows isothermal operation in an organic solvent-free condition for the highly exothermic epoxidation reaction. This reduces the reaction time from 8 hours to less than 30 minutes, a 16-fold reduction, which would mean a 16-fold reduction in reactor size. Low energy, passive isothermalisation was possible using the mesoOBR in a heat pipe assembly at a residence times of  $\tau > 10$  min. The epoxidation reaction in the jacketed mesoOBR could be operated without solvent, which would reduce the volume of the reactor required by a further factor of 5. Altogether, an intensification factor of 80 ( $5 \times 16$ ) could be achieved using the continuous epoxidation process in mesoOBR. The findings in this study could be applied in a larger process since the mesoOBR could be predictably scaled up.

## 7.2 Future Work

### 7.2.1 Heterogeneous catalyst

In this work, the catalyst used was a homogeneous polytungstophosphate. The homogeneous catalyst allowed the rapid development of a selective epoxidation reaction and ease of operation using mesoOBR platform. However, the catalyst was not recovered and recycled. Using a heterogeneous catalyst could solve this issue, leading to a greener epoxidation process. A heterogeneous tungsten-based polyoxometalates catalyst has been studied (Villa *et al.*, 2002) and shown to have comparable performance to a homogeneous catalyst in terms of selectivity to epoxides. The catalyst can be recovered and recycled for the epoxidation process. If used, it would be necessary to overcome the challenges of using heterogeneous catalyst in the mesoOBR. The geometry of the orifice's baffles could provide challenges on the packing of heterogeneous catalyst. However, the helically and integrally baffled mesoOBR have previously been proven to work well with heterogeneous catalysts (Eze *et al.*, 2013).

### 7.2.2 Residence Time Distributions (RTD)

In this study, new designs of orifice baffles were 3D-printed and used in a mesoOBR platform. The orifice baffle design was proven to enhance mass transfer between reactants in a biphasic reaction. However, this did not include the study of the residence time distribution (RTD) of these new baffles design. The RTD test is a tool in reactor engineering that allows the characterisation of flow patterns in a continuous reactor. The test represents the probability distribution function for the time fluid spends inside the reactor. This would allow quantification of the degree of plug flow in these reactor designs, as a function of operating conditions (net flow, frequency, and amplitude of oscillation).

### 7.2.3 Scalability of the mesoOBR

Scalability study of a helically baffled OBR from a diameter of 10 mm to 50 mm has been performed (Ahmed *et al.*, 2017). In the study, similar mixing behavior was observed regardless of the diameter. A scalability study of an orifice baffled OBR from a diameter of 24 mm to 150 mm has been conducted (Smith and Mackley, 2006). However, there is a lack of literature on the scalability study of an orifice baffle OBR at mesoscale (~5 mm), due to difficulties in manufacturing at such scale. In this work, orifice baffles were 3D-printed with a diameter of

5mm. Future works should be carried out to investigate the scalability of this orifice baffled mesoOBR. The result from the study should be able to confirm the scalability of mesoOBR.

#### ***7.2.4 Heat transfer study***

In this work, the heat removal capabilities of the mesoOBR was evaluated by the measurement of temperatures along the reactor. This temperature profile was compared to the temperature profile of the batch reactor. Future studies could be conducted to measure the temperature of the cooling water in the jacket and the enthalpy to fully understand the extent of heat transfer for this exothermic reaction.

#### ***7.2.5 Droplet diameter***

It is recommended to conduct future research on the droplet size in the biphasic epoxidation reaction between (R)-(+)-limonene and  $\alpha$ -pinene with  $H_2O_2$ , which might extend the explanations of the mass transfer between the immiscible reactants. It was observed in the mixing study of various baffles that the orifice diameter size plays a crucial role in enhancing the mass transfer between the reactants. It is postulated that the small diameter orifice caused smaller breakage of the droplets, thereby increases the contact area between the reactants. Future studies could explore this issue by measuring the droplet size and investigating the onset of which droplet size required to overcome mass transfer limitations.

#### ***7.2.6 Kinetic model***

The developed kinetic model for the epoxidation of (R)-(+)-limonene has incorporated the formation of limonene bis-epoxide and limonene-1,2-diol. The formation of these side-products was validated by experimental data. However, the kinetic model for the epoxidation of  $\alpha$ -pinene was not able to incorporate the formation of side-products. This is due to the challenging nature of  $\alpha$ -pinene epoxidation, where multiple reactions, including a possible polymerisation occur simultaneously. Future work should include developing a more robust model for the epoxidation of  $\alpha$ -pinene with  $H_2O_2$ . Investigations on the formation of side-products, especially of the allylic reaction, could provide better understanding of the conditions that formed each product, and how to maximise yield of desired  $\alpha$ -pinene derivatives.



## References

- Abbott, M.S.R., Valente Perez, G., Harvey, A.P. and Theodorou, M.K. (2014) 'Reduced power consumption compared to a traditional stirred tank reactor (STR) for enzymatic saccharification of alpha-cellulose using oscillatory baffled reactor (OBR) technology', *Chemical Engineering Research and Design*, 92(10), pp. 1969-1975.
- Ahmed, S.M.R., Phan, A.N. and Harvey, A.P. (2017) 'Scale-Up of Oscillatory Helical Baffled Reactors Based on Residence Time Distribution', *Chemical Engineering & Technology*, 40(5), pp. 907-914.
- Al-Abduly, A., Christensen, P., Harvey, A. and Zahng, K. (2014) 'Characterization and optimization of an oscillatory baffled reactor (OBR) for ozone-water mass transfer', *Chemical Engineering and Processing*, 84, pp. 82-89.
- Albanese, D.C.M., Foschi, F. and Penso, M. (2016) 'Sustainable Oxidations under Phase-Transfer Catalysis Conditions', *Organic Process Research & Development*, 20(2), pp. 129-139.
- Albert, R.M. and Webb, R.L. (1989) in *Fragrance and Flavor Chemicals*. New York: Pulp chemical Association.
- Amini, M., Haghdoost, M.M. and Bagherzadeh, M. (2014) 'Monomeric and dimeric oxido-peroxido tungsten (VI) complexes in catalytic and stoichiometric epoxidation', *Coordination Chemistry Reviews*, 268, pp. 83-100.
- Anastas, P.T. and Kirchhoff, M.M. (2002) 'Origins, Current Status, and Future Challenges of Green Chemistry', *Acc. Chem. Res.*, 35, pp. 686-694.
- Arends, I. and Sheldon, R. (2002) 'Recent developments in selective catalytic epoxidations with H<sub>2</sub>O<sub>2</sub>', *Topics in Catalysis*, 19(1), pp. 133-141.
- Attwood, D., Mallon, C. and Taylor, C. (1992) 'Phase studies on oil-in-water phospholipid microemulsions', *International journal of pharmaceuticals*, 84(2), pp. R5-R8.
- Bártolo, P.J. and Gibson, I. (2011) 'History of stereolithographic processes', in *Stereolithography*. Springer, pp. 37-56.
- Bauer, K., Garbe, D. and Surburg, H. (2008) *Common fragrance and flavor materials: preparation, properties and uses*. John Wiley & Sons.
- Becerra, J.-A., González, L.-M. and Villa, A.-L. (2016) 'Kinetic study of  $\alpha$ -pinene allylic oxidation over FePcCl<sub>16</sub>-NH<sub>2</sub>-SiO<sub>2</sub> catalyst', *Journal of Molecular Catalysis A: Chemical*, 423, pp. 12-21.
- Becerra, J.-A., González, L.-M. and Villa, A.-L. (2018) 'A bio-inspired heterogeneous catalyst for the transformation of limonene from orange peel waste biomass into value-added products', *Catalysis Today*, 302, pp. 250-260.
- Belgacem, M.N. and Gandini, A. (2008) *Monomers, Polymers and Composites from Renewable Resources*. The Boulevard, Langford Lane, Kidlington, Oxford OX5 1GB, UK: Elsevier.

- Bishopp, S.D., Scott, J.L. and Torrente-Murciano, L. (2014) 'Insights into biphasic oxidations with hydrogen peroxide; towards scaling up', *Green Chemistry*, 16(6), pp. 3281-3285.
- Bonon, A.J., Kozlov, Y.N., Bahú, J.O., Filho, R.M., Mandelli, D. and Shul'pin, G.B. (2014) 'Limonene epoxidation with H<sub>2</sub>O<sub>2</sub> promoted by Al<sub>2</sub>O<sub>3</sub>: Kinetic study, experimental design', *Journal of Catalysis*, 319, pp. 71-86.
- Breitmaier, E. (2006) *Terpenes: Flavors, Fragrance, Pharmaca, Pheromones*. Weinham: Wiley-VCH.
- Brunold, C.R., Hunns, J.C.B., Mackley, M.R. and Thompson, J.W. (1989) 'Experimental-Observations on Flow Patterns and Energy-Losses for Oscillatory Flow in Ducts Containing Sharp Edges', *Chemical Engineering Science*, 44(5), pp. 1227-1244.
- Cagnoli, M.V., Casuscelli, S.G., Alvarez, A.M., Bengoa, J.F., Gallegos, N.G., Samaniego, N.M., Crivello, M.E., Ghione, G.E., Pérez, C.F., Herrero, E.R. and Marchetti, S.G. (2005) "'Clean" limonene epoxidation using Ti-MCM-41 catalyst', *Applied Catalysis A: General*, 287(2), pp. 227-235.
- Calogirou, A., Larsen, B. and Kotzias, D. (1999) 'Gas-phase terpene oxidation products: a review', *Atmospheric Environment*, 33(9), pp. 1423-1439.
- Campanella, A. and Baltanás, M.A. (2006) 'Degradation of the oxirane ring of epoxidized vegetable oils in liquid-liquid heterogeneous reaction systems', *Chemical Engineering Journal*, 118(3), pp. 141-152.
- Cánepa, A.L., Chanquía, C.M., Vaschetti, V.M., Eimer, G.A. and Casuscelli, S.G. (2015) 'Biomass toward fine chemical products: Oxidation of  $\alpha$ -pinene over sieves nanostructured modified with vanadium', *Journal of Molecular Catalysis A: Chemical*, 404, pp. 65-73.
- Cánepa, A.L., Herrero, E.R., Crivello, M.E., Eimer, G.A. and Casuscelli, S.G. (2011) 'H<sub>2</sub>O<sub>2</sub> based  $\alpha$ -pinene oxidation over Ti-MCM-41. A kinetic study', *Journal of Molecular Catalysis A: Chemical*, 347(1-2), pp. 1-7.
- Caovilla, M., Caovilla, A., Pergher, S.B., Esmelindro, M.C., Fernandes, C., Dariva, C., Bernardo-Gusmão, K., Oestreicher, E. and Antunes, O. (2008) 'Catalytic oxidation of limonene,  $\alpha$ -pinene and  $\beta$ -pinene by the complex [FeIII (BPMP) Cl ( $\mu$ -O) FeIII Cl<sub>3</sub>] biomimetic to MMO enzyme', *Catalysis Today*, 133, pp. 695-698.
- Carr, G., Dosanjh, G., Millar, A.P. and Whittaker, D. (1994) 'Ring opening of  $\alpha$ -pinene epoxide', *Journal of the Chemical Society, Perkin Transactions 2*, (7), pp. 1419-1422.
- Casuscelli, S., Herrero, E., Crivello, M., Pérez, C., Egusquiza, M.G., Cabello, C.I. and Botto, I.L. (2005) 'Application of complex heteropolytungstates in limonene epoxidation by H<sub>2</sub>O<sub>2</sub> in biphasic medium', *Catalysis today*, 107, pp. 230-234.
- Casuscelli, S.G., Crivello, M.E., Perez, C.F., Ghione, G., Herrero, E.R., Pizzio, L.R., Vázquez, P.G., Cáceres, C.V. and Blanco, M.N. (2004) 'Effect of reaction conditions on limonene epoxidation with H<sub>2</sub>O<sub>2</sub> catalyzed by supported Keggin heteropolycompounds', *Applied Catalysis A: General*, 274(1-2), pp. 115-122.

Cavani, F. (1998) 'Heteropolycompound-based catalysts:: A blend of acid and oxidizing properties', *Catalysis Today*, 41(1-3), pp. 73-86.

Chapuis, C. and Jacoby, D. (2001) 'Catalysis in the preparation of fragrances and flavours', *Applied Catalysis A: General*, 221(1-2), pp. 93-117.

Charbonneau, L. and Kaliaguine, S. (2017) 'Epoxidation of limonene over low coordination Ti in Ti-SBA-16', *Applied Catalysis a-General*, 533, pp. 1-8.

Chen, Y.Y., Zhuang, J.Q., Liu, X.M., Gao, J.B., Han, X.W., Bao, X.H., Zhou, N., Gao, S. and Xi, Z.W. (2004) 'On the nature of reaction-controlled phase transfer catalysts for epoxidation of olefin: a P-31 NMR investigation', *Catalysis Letters*, 93(1-2), pp. 41-46.

Chiker, F., Launay, F., Nogier, J.P. and Bonardet, J.L. (2003) 'Green and selective epoxidation of alkenes catalysed by new TiO<sub>2</sub>-SiO<sub>2</sub>SBA mesoporous solids', *Green Chem.*, 5(3), pp. 318-322.

Clerici, M.G. and Ingallina, P. (1993) 'Epoxidation of lower olefins with hydrogen peroxide and titanium silicalite', *Journal of Catalysis*, 140(1), pp. 71-83.

Comelli, N.A., Ponzi, E.N. and Ponzi, M.I. (2005) 'Isomerization of  $\alpha$ -pinene, limonene,  $\alpha$ -terpinene, and terpinolene on sulfated zirconia', *Journal of the American Oil Chemists' Society*, 82(7), pp. 531-535.

Corma, A., Esteve, P. and Martínez, A. (1996) 'Solvent effects during the oxidation of olefins and alcohols with hydrogen peroxide on Ti-beta catalyst: the influence of the hydrophilicity-hydrophobicity of the zeolite', *Journal of Catalysis*, 161(1), pp. 11-19.

Corma, A., Iborra, S. and Velty, A. (2007) 'Chemical Routes for the Transformation of Biomass into Chemicals', *Chem.Rev.*, 107, p. 2411-2502.

da Rosa, R.G., de Campos, J.D.R. and Buffon, R. (2000) 'The effect of water on the rhodium-catalyzed carbonylation of isopropylallylamine', *Journal of Molecular Catalysis A: Chemical*, 153(1-2), pp. 19-24.

De Vos, D.E., Sels, B.F. and Jacobs, P.A. (2003) 'Practical heterogeneous catalysts for epoxide production', *Advanced synthesis & catalysis*, 345(4), pp. 457-473.

Derfer, J.M. and Traynor, S.G. (1989) *Chemistry of Turpentine*. New York: Pulp Chemical Association.

Desikan, S. and Doraiswamy, L. (2000) 'Enhanced activity of polymer-supported phase transfer catalysts', *Chemical engineering science*, 55(24), pp. 6119-6127.

Di Giuseppe, A., Crucianelli, M., Passacantando, M., Nisi, S. and Saladino, R. (2010) 'Chitin- and chitosan-anchored methyltrioxorhenium: An innovative approach for selective heterogeneous catalytic epoxidations of olefins', *Journal of Catalysis*, 276(2), pp. 412-422.

Doong, R.-a., Wu, Y.-W. and Lei, W.-g. (1998) 'Surfactant enhanced remediation of cadmium contaminated soils', *Water Science and Technology*, 37(8), pp. 65-71.

- Dragone, V., Sans, V., Rosnes, M.H., Kitson, P.J. and Cronin, L. (2013) '3D-printed devices for continuous-flow organic chemistry', *Beilstein journal of organic chemistry*, 9, p. 951.
- Duncan, D.C., Chambers, R.C., Hecht, E. and Hill, C.L. (1995) 'Mechanism and dynamics in the H<sub>3</sub> [PW<sub>12</sub>O<sub>40</sub>]-catalyzed selective epoxidation of terminal olefins by H<sub>2</sub>O<sub>2</sub>. Formation, reactivity, and stability of {PO<sub>4</sub> [WO (O<sub>2</sub>)<sub>2</sub>]<sub>4</sub>}<sup>3-</sup>', *Journal of the American Chemical Society*, 117(2), pp. 681-691.
- Dutta, B., Jana, S., Bhattacharjee, A., Gütllich, P., Iijima, S.-I. and Koner, S. (2010) 'γ-Fe<sub>2</sub>O<sub>3</sub> nanoparticle in NaY-zeolite matrix: Preparation, characterization, and heterogeneous catalytic epoxidation of olefins', *Inorganica Chimica Acta*, 363(4), pp. 696-704.
- Duynstee, E. and Grunwald, E. (1959) 'Organic Reactions Occurring in or on Micelles. I. Reaction Rate Studies of the Alkaline Fading of Triphenylmethane Dyes and Sulphonphthalein Indicators in the Presence of Detergent Salts<sup>1</sup>', *Journal of the American Chemical Society*, 81(17), pp. 4540-4542.
- Egusquiza, M.G., Cabello, C.I., Botto, I.L., Thomas, H.J., Casuscelli, S., Herrero, E. and Gazzoli, D. (2012) 'Advance in the study of limonene epoxidation with H<sub>2</sub>O<sub>2</sub> catalyzed by Cu(II) complex heteropolytungstates', *Catalysis Communications*, 26, pp. 117-121.
- Englard, S. and Seifter, S. (1990) '[22] Precipitation techniques', in *Methods in enzymology*. Elsevier, pp. 285-300.
- Erman, W.F. (1985) *Chemistry of Monoterpenes*. New York: Marcel Dekker.
- Eze, V.C., Fisher, J.C., Phan, A.N. and Harvey, A.P. (2017) 'Intensification of carboxylic acid esterification using a solid catalyst in a mesoscale oscillatory baffled reactor platform', *Chemical Engineering Journal*, 322, pp. 205-214.
- Eze, V.C. and Harvey, A.P. (2018) 'Continuous reactive coupling of glycerol and acetone – A strategy for triglyceride transesterification and in-situ valorisation of glycerol by-product', *Chemical Engineering Journal*, 347, pp. 41-51.
- Eze, V.C., Phan, A.N., Pirez, C., Harvey, A.P., Lee, A.F. and Wilson, K. (2013) 'Heterogeneous catalysis in an oscillatory baffled flow reactor', *Catalysis Science & Technology*, 3(9), pp. 2373-2379.
- Fabiyi, M.E. and Skelton, R.L. (1999) 'The application of oscillatory flow mixing to photocatalytic wet oxidation', *Journal of Photochemistry and Photobiology A: Chemistry*, 129(1-2), pp. 17-24.
- Fdil, N., Romane, A., Allaoud, S., Karim, A., Castanet, Y. and Mortreux, A. (1996) 'Terpenic olefin epoxidation using metals acetylacetonates as catalysts', *Journal of Molecular Catalysis A: Chemical*, 108(1), pp. 15-21.
- Fráter, G., Bajgrowicz, J.A. and Kraft, P. (1998) 'Fragrance chemistry', *Tetrahedron*, 54(27), pp. 7633-7703.
- Gallezot, P. (2007) 'Process options for converting renewable feedstocks to bioproducts', *Green Chemistry*, 9(4), pp. 295-302.

Gao, J.B., Chen, Y.Y., Han, B., Feng, Z.C., Li, C., Zhou, N., Gao, S.A. and Xi, Z.W. (2004) 'A spectroscopic study on the reaction-controlled phase transfer catalyst in the epoxidation of cyclohexene', *Journal of Molecular Catalysis a-Chemical*, 210(1-2), pp. 197-204.

Garcia-Castello, E.M., Mayor, L., Chorques, S., Argüelles, A., Vidal-Brotons, D. and Gras, M. (2011) 'Reverse osmosis concentration of press liquid from orange juice solid wastes: flux decline mechanisms', *Journal of food engineering*, 106(3), pp. 199-205.

Ghazi, A., Resul, M.G., Yunus, R. and Yaw, T.S. (2008) 'Preliminary design of oscillatory flow biodiesel reactor for continuous biodiesel production from jatropha triglycerides', *Journal of Engineering Science and Technology*, 3(2), pp. 138-145.

Goud, V.V., Patwardhan, A.V., Dinda, S. and Pradhan, N.C. (2007) 'Kinetics of epoxidation of jatropha oil with peroxyacetic and peroxyformic acid catalysed by acidic ion exchange resin', *Chemical Engineering Science*, 62(15), pp. 4065-4076.

Grigoropoulou, G. and Clark, J.H. (2006) 'A catalytic, environmentally benign method for the epoxidation of unsaturated terpenes with hydrogen peroxide', *Tetrahedron Letters*, 47(26), pp. 4461-4463.

Grigoropoulou, G., Clark, J.H. and Elings, J.A. (2003) 'Recent developments on the epoxidation of alkenes using hydrogen peroxide as an oxidant', *Green Chemistry*, 5(1), pp. 1-7.

Guidotti, M., Psaro, R., Batonneau-Gener, I. and Gavrilova, E. (2011) 'Heterogeneous Catalytic Epoxidation: High Limonene Oxide Yields by Surface Silylation of Ti-MCM-41', *Chemical Engineering & Technology*, 34(11), pp. 1924-1927.

Gunam Resul, M.F.M., López Fernández, A.M., Rehman, A. and Harvey, A.P. (2018) 'Development of a selective, solvent-free epoxidation of limonene using hydrogen peroxide and a tungsten-based catalyst', *Reaction Chemistry & Engineering*, (3), pp. 747-756.

Gupta, K., Sutar, A.K. and Lin, C.-C. (2009) 'Polymer-supported Schiff base complexes in oxidation reactions', *Coordination Chemistry Reviews*, 253(13-14), pp. 1926-1946.

Hachiya, H., Kon, Y., Ono, Y., Takumi, K., Sasagawa, N., Ezaki, Y. and Sato, K. (2012) 'Unique Salt Effect on Highly Selective Synthesis of Acid-Labile Terpene and Styrene Oxides with a Tungsten/H<sub>2</sub>O<sub>2</sub> Catalytic System under Acidic Aqueous Conditions', *Synthesis-Stuttgart*, 44(11), pp. 1672-1678.

Halpern, M. (2000) 'Phase-Transfer Catalysis', *Ullmann's Encyclopedia of Industrial Chemistry*.  
Harvey, A. (2013) 'An Overview of Research into Mesoscale Oscillatory Baffled Reactors at Newcastle' University, N.

Harvey, A., Mackley, M., Reis, N., Teixeira, J.A. and Vicente, A.A. (2003a) 'The fluid mechanics relating to a novel oscillatory flow micro reactor', *4th european Congress of Chemical Engineering*. Granada.

Harvey, A.P., Mackley, M.R. and Seliger, T. (2003b) 'Process intensification of biodiesel production using a continuous oscillatory flow reactor', *Journal of Chemical Technology & Biotechnology*, 78(2-3), pp. 338-341.

- Harvey, A.P., Mackley, M.R. and Stonestreet, P. (2001) 'Operation and Optimization of an Oscillatory Flow Continuous Reactor', *Ind. Eng. Chem. Res.*, 40, pp. 5371-5377.
- Hauenstein, O., Reiter, M., Agarwal, S., Rieger, B. and Greiner, A. (2016) 'Bio-based polycarbonate from limonene oxide and CO<sub>2</sub> with high molecular weight, excellent thermal resistance, hardness and transparency', *Green Chemistry*, 18(3), pp. 760-770.
- Herzberger, J., Niederer, K., Pohlit, H., Seiwert, J., Worm, M., Wurm, F.R. and Frey, H. (2015) 'Polymerization of ethylene oxide, propylene oxide, and other alkylene oxides: synthesis, novel polymer architectures, and bioconjugation', *Chemical reviews*, 116(4), pp. 2170-2243.
- Hill, C.L. (1998) 'Introduction: polyoxometalates multicomponent molecular vehicles to probe fundamental issues and practical problems'. ACS Publications.
- Hill, C.L. (2007) 'Progress and challenges in polyoxometalate-based catalysis and catalytic materials chemistry', *Journal of Molecular Catalysis A: Chemical*, 262(1-2), pp. 2-6.
- Holmberg, K. (2007) 'Organic reactions in microemulsions', *European journal of organic chemistry*, 2007(5), pp. 731-742.
- Hull, C.W. (1984) *Apparatus for production of three-dimensional objects by stereolithography*.
- Hunter, J.E. and Fowler Jr, J.F. (1998) 'Safety to human skin of cocamidopropyl betaine: A mild surfactant for personal-care products', *Journal of Surfactants and Detergents*, 1(2), pp. 235-239.
- Hyde, A.M., Zultanski, S.L., Waldman, J.H., Zhong, Y.-L., Shevlin, M. and Peng, F. (2017) 'General Principles and Strategies for Salting-Out Informed by the Hofmeister Series', *Organic Process Research & Development*, 21(9), pp. 1355-1370.
- Ishii, Y., Sakaguchi, S. and Iwahama, T. (2001) 'Innovation of hydrocarbon oxidation with molecular oxygen and related reactions', *Advanced Synthesis & Catalysis*, 343(5), pp. 393-427.
- Ishii, Y., Yamawaki, K., Ura, T., Yamada, H., Yoshida, T. and Ogawa, M. (1988) 'Hydrogen-Peroxide Oxidation Catalyzed by Heteropoly Acids Combined with Cetylpyridinium Chloride - Epoxidation of Olefins and Allylic Alcohols, Ketonization of Alcohols and Diols, and Oxidative Cleavage of 1,2-Diols and Olefins', *Journal of Organic Chemistry*, 53(15), pp. 3587-3593.
- Jones, C.W. (1999) *Applications of Hydrogen Peroxide and Derivatives*. Cambridge: Roy. Soc. Chem.
- Kamata, K., Yonehara, K., Sumida, Y., Yamaguchi, K., Hikichi, S. and Mizuno, N. (2003) 'Efficient epoxidation of olefins with  $\geq 99\%$  selectivity and use of hydrogen peroxide', *Science*, 300(5621), pp. 964-966.
- Katsoulis, D.E. (1998) 'A survey of applications of polyoxometalates', *Chemical Reviews*, 98(1), pp. 359-388.
- Keggin, J. (1934) 'The structure and formula of 12-phosphotungstic acid', *Proc. R. Soc. Lond. A*, 144(851), pp. 75-100.

- Kimura, Y., Kirszensztejn, P. and Regen, S.L. (1983) 'Poly (ethylene glycol)-graft copolymers as synthetic equivalents of benzyltriethylammonium chloride for triphase catalytic alkylation', *The Journal of Organic Chemistry*, 48(3), pp. 385-386.
- Kitson, P.J., Glatzel, S., Chen, W., Lin, C.-G., Song, Y.-F. and Cronin, L. (2016) '3D printing of versatile reactionware for chemical synthesis', *nature protocols*, 11(5), p. 920.
- Kitson, P.J., Rosnes, M.H., Sans, V., Dragone, V. and Cronin, L. (2012) 'Configurable 3D-Printed millifluidic and microfluidic 'lab on a chip' reactionware devices', *Lab on a Chip*, 12(18), pp. 3267-3271.
- Kobe, J., Evans, W., June, R. and Lemanski, M. (2002) 'Epoxidation—Industrial', *Encyclopedia of catalysis*.
- Kojima, I. and Davis, S. (1984) 'The effect of salt concentration on the distribution of phenol between aqueous sodium chloride and carbon tetrachloride', *International journal of pharmaceuticals*, 20(1-2), pp. 203-207.
- Kon, Y., Hachiya, H., Ono, Y., Matsumoto, T. and Sato, K. (2011) 'An Effective Synthesis of Acid-Sensitive Epoxides via Oxidation of Terpenes and Styrenes Using Hydrogen Peroxide under Organic Solvent-Free Conditions', *Synthesis-Stuttgart*, 7(7), pp. 1092-1098.
- Korenman, Y.I., Mokshina, N.Y. and Zykov, A. (2010) 'Distribution coefficients of vitamin B 2 in hydrophilic organic solvent-aqueous salt solution systems', *Russian Journal of Physical Chemistry A*, 84(3), pp. 415-418.
- Kosswig, K. (2000) 'Surfactants', *Ullmann's encyclopedia of industrial chemistry*.
- Kurti, L. and Czakó, B. (2005) *Strategic applications of named reactions in organic synthesis*. Elsevier.
- Lane, B.S. and Burgess, K. (2003) 'Metal-catalyzed epoxidations of alkenes with hydrogen peroxide', *Chem Rev*, 103(7), pp. 2457-73.
- Law, R., Ahmed, S.M., Tang, N., Phan, A.N. and Harvey, A.P. (2018) 'Development of a more robust correlation for predicting heat transfer performance in oscillatory baffled reactors', *Chemical Engineering and Processing-Process Intensification*, 125, pp. 133-138.
- Lawton, S., Steele, G., Shering, P., Zhao, L., Laird, I. and Ni, X.-W. (2009) 'Continuous crystallization of pharmaceuticals using a continuous oscillatory baffled crystallizer', *Organic Process Research & Development*, 13(6), pp. 1357-1363.
- Lee, D.G. and Chang, V.S. (1978) 'Oxidation of hydrocarbons. 8. Use of dimethyl polyethylene glycol as a phase transfer agent for the oxidation of alkenes by potassium permanganate', *The Journal of Organic Chemistry*, 43(8), pp. 1532-1536.
- Letts, K. and Mackay, R. (1975) 'Reactions in microemulsions. I. Metal ion incorporation by tetraphenylporphine', *Inorganic Chemistry*, 14(12), pp. 2990-2993.
- Loncaric, C., Manabe, K. and Kobayashi, S. (2003) 'AgOTf-Catalyzed Aza-Diels–Alder Reactions of Danishefsky's Diene with Imines in Water', *Advanced Synthesis & Catalysis*, 345(4), pp. 475-477.

- Löwe, H., Axinte, R., Breuch, D. and Hofmann, C. (2009) 'Heat pipe controlled syntheses of ionic liquids in microstructured reactors', *Chemical Engineering Journal*, 155(1-2), pp. 548-550.
- Mackley, M.R., Smith, K.B. and Wise, N.P. (1993) 'Mixing and separation of particle suspensions using oscillatory flow in baffled tubes', *Chemical Engineering Research and Design*, 71(A6), pp. 649-656.
- Maheswari, P.U., de Hoog, P., Hage, R., Gamez, P. and Reedijk, J. (2005) 'A Na<sub>2</sub>WO<sub>4</sub>/H<sub>2</sub>WO<sub>4</sub>-Based Highly Efficient Biphasic Catalyst towards Alkene Epoxidation, using Dihydrogen Peroxide as Oxidant', *Advanced Synthesis & Catalysis*, 347(14), pp. 1759-1764.
- Mahha, Y., Salles, L., Piquemal, J., Briot, E., Atlamsani, A. and Bregeault, J. (2007) 'Environmentally friendly epoxidation of olefins under phase-transfer catalysis conditions with hydrogen peroxide', *Journal of Catalysis*, 249(2), pp. 338-348.
- Makosza, M. (2000) 'Phase-transfer catalysis. A general green methodology in organic synthesis', *Pure and applied chemistry*, 72(7), pp. 1399-1403.
- Martín, C. and Kleij, A.W. (2016) 'Terpolymers derived from limonene oxide and carbon dioxide: access to cross-linked polycarbonates with improved thermal properties', *Macromolecules*, 49(17), pp. 6285-6295.
- Mathieson, J.S., Rosnes, M.H., Sans, V., Kitson, P.J. and Cronin, L. (2013) 'Continuous parallel ESI-MS analysis of reactions carried out in a bespoke 3D printed device', *Beilstein journal of nanotechnology*, 4, p. 285.
- Matoba, Y., Inoue, H., Akagi, J.-i., Okabayashi, T., Ishii, Y. and Ogawa, M. (1984) 'Epoxidation of Allylic Alcohols with Hydrogen Peroxide Catalyzed by [PMO<sub>12</sub>O<sub>40</sub>] 3-[C<sub>5</sub>H<sub>5</sub>N<sup>+</sup> (CH<sub>2</sub>)<sub>15</sub>CH<sub>3</sub>]<sup>3-</sup>', *Synthetic Communications*, 14(9), pp. 865-873.
- Mazzola, P.G., Lopes, A.M., Hasmann, F.A., Jozala, A.F., Penna, T.C., Magalhaes, P.O., Rangel-Yagui, C.O. and Pessoa Jr, A. (2008) 'Liquid-liquid extraction of biomolecules: an overview and update of the main techniques', *Journal of Chemical Technology & Biotechnology: International Research in Process, Environmental & Clean Technology*, 83(2), pp. 143-157.
- McDonough, J., Ahmed, S., Phan, A. and Harvey, A. (2017) 'A study of the flow structures generated by oscillating flows in a helical baffled tube', *Chemical Engineering Science*, 171, pp. 160-178.
- McDonough, J.R., Armett, J., Law, R. and Harvey, A.P. (2019) 'Coil-in-Coil Reactor: Augmenting Plug Flow Performance by Combining Different Geometric Features Using 3D Printing', *Industrial & Engineering Chemistry Research*, 58(47), pp. 21363-21371.
- McDonough, J.R., Phan, A.N. and Harvey, A.P. (2015) 'Rapid process development using oscillatory baffled mesoreactors - A state-of-the-art review', *Chemical Engineering Journal*, 265, pp. 110-121.
- McDonough, J.R., Phan, A.N., Reay, D.A. and Harvey, A.P. (2016) 'Passive isothermalisation of an exothermic reaction in flow using a novel "Heat Pipe Oscillatory Baffled Reactor (HPOBR)"', *Chemical Engineering and Processing: Process Intensification*, 110, pp. 201-213.



- Mcpherson, A. (2001) 'A comparison of salts for the crystallization of macromolecules', *Protein Science*, 10(2), pp. 418-422.
- Michel, T., Cokoja, M., Sieber, V. and Kuhn, F.E. (2012) 'Selective epoxidation of (+)-limonene employing methyltrioxorhenium as catalyst', *Journal of Molecular Catalysis a-Chemical*, 358, pp. 159-165.
- Mimoun, H. (1996) 'Catalytic opportunities in the flavor and fragrance industry', *CHIMIA International Journal for Chemistry*, 50(12), pp. 620-625.
- Mizuno, N. and Misono, M. (1998) 'Heterogeneous catalysis', *Chemical Reviews*, 98(1), pp. 199-218.
- Mizuno, N., Yamaguchi, K. and Kamata, K. (2005) 'Epoxidation of olefins with hydrogen peroxide catalyzed by polyoxometalates', *Coordination chemistry reviews*, 249(17-18), pp. 1944-1956.
- Mouret, A., Leclercq, L., Mühlbauer, A. and Nardello-Rataj, V. (2014) 'Eco-friendly solvents and amphiphilic catalytic polyoxometalate nanoparticles: a winning combination for olefin epoxidation', *Green Chem.*, 16(1), pp. 269-278.
- Negoi, A., Parvulescu, V.I. and Tudorache, M. (2018) 'Peroxidase-based biocatalysis in a two-phase system for allylic oxidation of  $\alpha$ -pinene', *Catalysis Today*, 306, pp. 199-206.
- Neuenschwander, U., Guignard, F. and Hermans, I. (2010) 'Mechanism of the Aerobic Oxidation of  $\alpha$ -Pinene', *ChemSusChem*, 3(1), pp. 75-84.
- Neuenschwander, U., Meier, E. and Hermans, I. (2011) 'Peculiarities of  $\beta$ -Pinene Autoxidation', *ChemSusChem*, 4(11), pp. 1613-1621.
- Neumann, R. and Gara, M. (1994) 'Highly active manganese-containing polyoxometalate as catalyst for epoxidation of alkenes with hydrogen peroxide', *Journal of the American Chemical Society*, 116(12), pp. 5509-5510.
- Ni, X. and Gough, P. (1997) 'On the discussion of the dimensionless groups governing oscillatory flow in a baffled tube', *Chemical Engineering Science*, 82(18), pp. 3209-3212.
- Ni, X., Jian, H. and Fitch, A. (2002) 'Computational fluid dynamic modelling of flow patterns in an oscillatory baffled column', *Chemical Engineering Science*, 57(14), pp. 2849-2862.
- Ni, X. and Pereira, N.E. (2000) 'Parameters affecting fluid dispersion in a continuous oscillatory baffled tube', *AIChE Journal*, 46(1), pp. 37-45.
- Ni, X. and Stevenson, C.C. (1999) 'On the effect of gap size between baffle outer diameter and tube inner diameter on the mixing characteristics in an oscillatory-baffled column', *J. Chem. Technol. Biotechnol.*, 74, pp. 587-593.
- Noyori, R., Aoki, M. and Sato, K. (2003) 'Green oxidation with aqueous hydrogen peroxide', *Chemical Communications*, (16), p. 1977.

- Okafor, O., Weilhard, A., Fernandes, J.A., Karjalainen, E., Goodridge, R. and Sans, V. (2017) 'Advanced reactor engineering with 3D printing for the continuous-flow synthesis of silver nanoparticles', *Reaction Chemistry & Engineering*, 2(2), pp. 129-136.
- Oyama, S.T. (2008) 'Rates, kinetics, and mechanisms of epoxidation: homogeneous, heterogeneous, and biological routes', in *Mechanisms in homogeneous and heterogeneous epoxidation catalysis*. Elsevier, pp. 3-99.
- Pagliaro, M., Fidalgo, A., Palmisano, L., Ilharco, L.M., Parrino, F. and Ciriminna, R. (2018) 'Polymers of Limonene Oxide and Carbon Dioxide: Polycarbonates of the Solar Economy'.
- Palumbo, C., Tiozzo, C., Ravasio, N., Psaro, R., Carniato, F., Bisio, C. and Guidotti, M. (2016) 'An efficient epoxidation of terminal aliphatic alkenes over heterogeneous catalysts: when solvent matters', *Catalysis Science & Technology*, 6(11), pp. 3832-3839.
- Paquette, L.A. (1999) *Handbook of Reagents for Organic Synthesis, Chiral Reagents for Asymmetric Synthesis*. John Wiley & Sons.
- Patil, M.V., Yadav, M.K. and Jasra, R.V. (2007) 'Catalytic epoxidation of  $\alpha$ -pinene with molecular oxygen using cobalt (II)-exchanged zeolite Y-based heterogeneous catalysts', *Journal of Molecular Catalysis A: Chemical*, 277(1-2), pp. 72-80.
- Pena, A., Veiga, S., Sapelli, M., Martínez, N., Márquez, V., Dellacassa, E. and Bussi, J. (2012) 'Limonene oxidation by molecular oxygen under solvent-free conditions: the influence of peroxides and catalysts on the reaction rate', *Reaction Kinetics, Mechanisms and Catalysis*, 107(2), pp. 263-275.
- Phan, A.N. and Harvey, A. (2010) 'Development and evaluation of novel designs of continuous mesoscale oscillatory baffled reactors', *Chemical Engineering Journal*, 159(1-3), pp. 212-219.
- Phan, A.N., Harvey, A. and Lavender, J. (2011a) 'Characterisation of fluid mixing in novel designs of mesoscale oscillatory baffled reactors operating at low flow rates (0.3-0.6 ml/min)', *Chemical Engineering and Processing*, 50(3), pp. 254-263.
- Phan, A.N. and Harvey, A.P. (2011b) 'Effect of geometrical parameters on fluid mixing in novel mesoscale oscillatory helical baffled designs', *Chemical Engineering Journal*, 169(1-3), pp. 339-347.
- Phan, A.N. and Harvey, A.P. (2012a) 'Characterisation of mesoscale oscillatory helical baffled reactor-Experimental approach', *Chemical Engineering Journal*, 180, pp. 229-236.
- Phan, A.N., Harvey, A.P. and Eze, V. (2012b) 'Rapid Production of Biodiesel in Mesoscale Oscillatory Baffled Reactors', *Chemical Engineering & Technology*, 35(7), pp. 1214-1220.
- Phan, A.N., Harvey, A.P. and Rawcliffe, M. (2011c) 'Continuous screening of base-catalysed biodiesel production using New designs of mesoscale oscillatory baffled reactors', *Fuel Processing Technology*, 92(8), pp. 1560-1567.
- Philp, J.C., Bartsev, A., Ritchie, R.J., Baucher, M.-A. and Guy, K. (2013) 'Bioplastics science from a policy vantage point', *New biotechnology*, 30(6), pp. 635-646.

Piquemal, J.Y., Bois, C. and Bregeault, J.M. (1997) 'Synthesis, reactivity, x-ray crystal and molecular structures of a novel dimeric tungsten(VI) polyoxoperoxo complex: [PPh(4)](2)[Ph(2)SiO(2){W2O2(mu-O-2)(2)(O-2)(2)}] and of a molybdenum(VI) analogue', *Chemical Communications*, (5), pp. 473-474.

Ramshaw, C. (1999) 'Process Intensification and Green Chemistry', *Green Chemistry*, 1(1), pp. G15-G17.

Randall, M. and Failey, C.F. (1927) 'The Activity Coefficient of Non-Electrolytes in Aqueous Salt Solutions from Solubility Measurements. The Salting-out Order of the Ions', *Chemical Reviews*, 4(3), pp. 285-290.

Rasdi, F.R.M., Phan, A.N. and Harvey, A.P. (2013) 'Rapid determination of reaction order and rate constants of an imine synthesis reaction using a mesoscale oscillatory baffled reactor', *Chemical Engineering Journal*, 222, pp. 282-291.

Rehman, A., Fernández, A.M.L., Resul, M.G. and Harvey, A. (2019) 'Highly selective, sustainable synthesis of limonene cyclic carbonate from bio-based limonene oxide and CO<sub>2</sub>: A kinetic study', *Journal of CO<sub>2</sub> Utilization*, 29, pp. 126-133.

Reis, N., Harvey, A.P., Mackley, M.R., Vicente, A.A. and Teixeira, J.A. (2005) 'Fluid mechanics and design aspects of a novel oscillatory flow screening mesoreactor', *Chemical Engineering Research and Design*, 83(4 A), pp. 357-371.

Reis, N., Vicente, A.A. and Teixeira, J.A. (2010) 'Liquid backmixing in oscillatory flow through a periodically constricted meso-tube', *Chemical Engineering and Processing: Process Intensification*, 49(7), pp. 793-803.

Reis, N., Vicente, A.A., Teixeira, J.A. and Mackley, M.R. (2004) 'Residence times and mixing of a novel continuous oscillatory flow screening reactor', *Chemical Engineering Science*, 59(22-23), pp. 4967-4974.

Reiter, M., Vagin, S., Kronast, A., Jandl, C. and Rieger, B. (2017) 'A Lewis acid  $\beta$ -diiminato-zinc-complex as all-rounder for co- and terpolymerisation of various epoxides with carbon dioxide', *Chemical science*, 8(3), pp. 1876-1882.

Ruckel, E.R. and Arlt, H.J. (1989) in *Polyterpenes Resins*. New York: Pulp Chemical Association.

Santacesaria, E., Renken, A., Russo, V., Turco, R., Tesser, R. and Di Serio, M. (2012) 'Biphasic Model Describing Soybean Oil Epoxidation with H<sub>2</sub>O<sub>2</sub> in Continuous Reactors', *Industrial & Engineering Chemistry Research*, 51(26), pp. 8760-8767.

Santacesaria, E., Tesser, R., Di Serio, M., Turco, R., Russo, V. and Verde, D. (2011) 'A biphasic model describing soybean oil epoxidation with H<sub>2</sub>O<sub>2</sub> in a fed-batch reactor', *Chemical Engineering Journal*, 173(1), pp. 198-209.

Sato, K., Aoki, M., Ogawa, M., Hashimoto, T. and Noyori, R. (1996) 'A practical method for epoxidation of terminal olefins with 30% hydrogen peroxide under halide-free conditions', *Journal of Organic Chemistry*, 61(23), pp. 8310-8311.

- Schirmann, J.P. and Delavarenne, S.Y. (1979) *Hydrogen Peroxide in Organic Chemistry*. Paris: EDI.
- Seki, T. and Baiker, A. (2009) 'Catalytic Oxidations in Dense Carbon Dioxide', *Chem. Rev.*, 109, pp. 2409–2454.
- Shen, L., Worrell, E. and Patel, M. (2010) 'Present and future development in plastics from biomass', *Biofuels, Bioproducts and Biorefining: Innovation for a sustainable economy*, 4(1), pp. 25-40.
- Shylesh, S. and Singh, A. (2004) 'Synthesis, characterization, and catalytic activity of vanadium-incorporated,-grafted, and-immobilized mesoporous MCM-41 in the oxidation of aromatics', *Journal of Catalysis*, 228(2), pp. 333-346.
- Sienel, G., Rieth, R. and Rowbottom, K.T. (2003) *Ullmann's Encyclopedia of Industrial Chemistry*. sixth edn. Weinheim: Verlag Chemie.
- Silva, J.M.d.S.e., Vinhado, F.a.S., Mandelli, D., Schuchardt, U. and Rinaldi, R. (2006) 'The chemical reactivity of some terpenes investigated by alumina catalyzed epoxidation with hydrogen peroxide and by DFT calculations', *Journal of Molecular Catalysis A: Chemical*, 252, pp. 186–193.
- Silvestre, A.J. and Gandini, A. (2008) 'Terpenes: major sources, properties and applications', in *Monomers, Polymers and Composites from Renewable Resources*. Elsevier, pp. 17-38.
- Sinou, D., Rabeyrin, C. and Nguéfacq, C. (2003) 'Catalytic asymmetric alkylation in water in the presence of surfactants', *Advanced Synthesis & Catalysis*, 345(3), pp. 357-363.
- Smith, K.B. and Mackley, M.R. (2006) 'An Experimental Investigation into the Scale-up of Oscillatory Flow Mixing in Baffled Tubes', *Chemical Engineering Research and Design*, 84(11), pp. 1001-1011.
- Starks, C.M. (1971) 'Phase-transfer catalysis. I. Heterogeneous reactions involving anion transfer by quaternary ammonium and phosphonium salts', *Journal of the American Chemical Society*, 93(1), pp. 195-199.
- Stekrova, M., Kumar, N., Aho, A., Sinev, I., Grünert, W., Dahl, J., Roine, J., Arzumanov, S.S., Mäki-Arvela, P. and Murzin, D.Y. (2014) 'Isomerization of  $\alpha$ -pinene oxide using Fe-supported catalysts: Selective synthesis of campholenic aldehyde', *Applied Catalysis A: General*, 470, pp. 162-176.
- Stonestreet, P. and Harvey, A.P. (2002a) 'A mixing-based design methodology for continuous oscillatory flow reactors', *Chemical Engineering Research & Design*, 80(A1), pp. 31-44.
- Stonestreet, P. and Harvey, A.P. (2002b) 'A mixing-based design methodology for continuous oscillatory flow reactors', *Chemical Engineering Research and Design*, 80(1), pp. 31-44.
- Stonestreet, P. and Van Der Veecken, P.M.J. (1999) 'The Effects of Oscillatory Flow and Bulk Flow Components on Residence Time Distribution in Baffled Tube Reactors', *Chemical Engineering Research and Design*, 77(8), pp. 671-684.
- Strukul, G. (1992) *Catalytic Oxidation with Hydrogen Peroxide as Oxidant*. Dordrecht: Kluwer.

- Swern, D. (1971) *Organic Peroxides*. New York: Wiley Interscience.
- Sundaravel, B., Babu, C.M., Vinodh, R., Cha, W.S. and Jang, H.-T. (2016) 'Synthesis of campholenic aldehyde from  $\alpha$ -pinene using bi-functional PrAlPO-5 molecular sieves', *Journal of the Taiwan Institute of Chemical Engineers*, 63, pp. 157-165.
- Swift, K.A.D. (2004) 'Catalytic transformations of the major terpene feedstocks', *Topics in Catalysis*, 27(1-4), pp. 143-155.
- Symes, M.D., Kitson, P.J., Yan, J., Richmond, C.J., Cooper, G.J., Bowman, R.W., Vilbrandt, T. and Cronin, L. (2012) 'Integrated 3D-printed reactionware for chemical synthesis and analysis', *Nature chemistry*, 4(5), p. 349.
- Takumi, K., Sasagawa, N., Ezaki, Y., Yoshihiro, K. O. N., Ono, Y., & Sato, K. (2014). U.S. Patent No. 8,742,145. Washington, DC: U.S. Patent and Trademark Office.
- Thompson, R.C., Swan, S.H., Moore, C.J. and vom Saal, F.S. (2009) 'Our plastic age', *Philos Trans R Soc Lond B Biol Sci*, 364(1526), pp. 1973-6.
- Uguina, M.A., Delgado, J.A., Rodríguez, A., Carretero, J. and Gómez-Díaz, D. (2006) 'Alumina as heterogeneous catalyst for the regioselective epoxidation of terpenic diolefins with hydrogen peroxide', *Journal of Molecular Catalysis A: Chemical*, 256(1-2), pp. 208-215.
- Vanoye, L., Wang, J., Pablos, M., de Bellefon, C. and Favre-Réguillon, A. (2016) 'Epoxidation using molecular oxygen in flow: facts and questions on the mechanism of the Mukaiyama epoxidation', *Catalysis Science & Technology*, 6(13), pp. 4724-4732.
- Vecitis, C.D., Park, H., Cheng, J., Mader, B.T. and Hoffmann, M.R. (2008) 'Kinetics and mechanism of the sonolytic conversion of the aqueous perfluorinated surfactants, perfluorooctanoate (PFOA), and perfluorooctane sulfonate (PFOS) into inorganic products', *The Journal of Physical Chemistry A*, 112(18), pp. 4261-4270.
- Venturello, C., Alneri, E. and Ricci, M. (1983) 'A New, Effective Catalytic-System for Epoxidation of Olefins by Hydrogen-Peroxide under Phase-Transfer Conditions', *Journal of Organic Chemistry*, 48(21), pp. 3831-3833.
- Venturello, C. and D'Aloisio, R. (1988) 'Quaternary Ammonium Tetrakis(diperoxotungsto)phosphates(3-) as a New Class of Catalysts for Efficient Alkene Epoxidation with Hydrogen Peroxide', *J. Org. Chem.*, 53, pp. 1553-1557.
- Villa, A.L., A., F.T. and de Correa, C.M. (2002) 'Kinetics of limonene epoxidation by hydrogen peroxide on PW-Amberlite', *Journal of Molecular Catalysis A: Chemical*, 185, pp. 269-277.
- Wang, L.-M., Jiao, N., Qiu, J., Yu, J.-J., Liu, J.-Q., Guo, F.-L. and Liu, Y. (2010) 'Sodium stearate-catalyzed multicomponent reactions for efficient synthesis of spirooxindoles in aqueous micellar media', *Tetrahedron*, 66(1), pp. 339-343.
- Wang, M.-L. and Huang, T.-H. (2004) 'Kinetic study of the epoxidation of 1, 7-octadiene under phase-transfer-catalysis conditions', *Industrial & engineering chemistry research*, 43(3), pp. 675-681.

- Wang, M.L. and Rajendran, V. (2007) 'Ultrasound assisted phase-transfer catalytic epoxidation of 1,7-octadiene - a kinetic study', *Ultrason Sonochem*, 14(1), pp. 46-54.
- Weber, W.P. and Gokel, G.W. (1977) *Phase transfer catalysis in organic synthesis, reactivity and structure*. Berlin: Springer.
- Weiss, J. (1935) 'The catalytic decomposition of hydrogen peroxide on different metals', *Transactions of the Faraday Society*, 31, pp. 1547-1557.
- Wender, P.A. and Mucciari, T.P. (1992) 'A new and practical approach to the synthesis of taxol and taxol analogs: the pinene path', *Journal of the American Chemical Society*, 114(14), pp. 5878-5879.
- Wiebus, E. and Cornils, B. (2006) 'Biphasic Systems: Water—Organic', in *Catalyst Separation, Recovery and Recycling*. Springer, pp. 105-143.
- Wikandari, R., Nguyen, H., Millati, R., Niklasson, C. and Taherzadeh, M.J. (2015) 'Improvement of biogas production from orange peel waste by leaching of limonene', *BioMed research international*, 2015.
- Wilkinson, S.G. (1975) *Int. Rev. Sci., Org. Chem.*, 2(2), pp. 111-129.
- Wong, S.-C., Hsiao, H.-C. and Lo, K.-F. (2014) 'Improving temperature uniformity and performance of CO preferential oxidation for hydrogen-rich reformat with a heat pipe', *International Journal of Hydrogen Energy*, 39(12), pp. 6492-6496.
- Wroblewska, A. (2014) 'The epoxidation of limonene over the TS-1 and Ti-SBA-15 catalysts', *Molecules*, 19(12), pp. 19907-22.
- Wu, Z., Zheng, T., Wu, L., Lou, H., Xie, Q., Lu, M., Zhang, L., Nie, Y. and Ji, J. (2017) 'Novel Reactor for Exothermic Heterogeneous Reaction Systems: Intensification of Mass and Heat Transfer and Application to Vegetable Oil Epoxidation', *Industrial & Engineering Chemistry Research*, 56(18), pp. 5231-5238.
- Xiong, Y., Zhao, Z., Zhu, L., Chen, Y., Ji, H. and Yang, D. (2013) 'Removal of three kinds of phthalates from sweet orange oil by molecular distillation', *LWT-Food Science and Technology*, 53(2), pp. 487-491.
- Yadav, G. and Pujari, A. (2000) 'Epoxidation of Styrene to Styrene Oxide: Synergism of Heteropoly Acid and Phase-Transfer Catalyst under Ishii–Venturello Mechanism', *Organic Process Research & Development*, 4(2), pp. 88-93.
- Yadav, G. and Satoskar, D. (1997) 'Kinetics of epoxidation of alkyl esters of undecylenic acid: comparison of traditional routes vs. Ishii-Venturello chemistry', *Journal of the American Oil Chemists' Society*, 74(4), pp. 397-407.
- Yang, X., Gao, S. and Xi, Z. (2005) 'Reaction-controlled phase transfer catalysis for styrene epoxidation to styrene oxide with aqueous hydrogen peroxide', *Organic process research & development*, 9(3), pp. 294-296.

- Yang, Z., Ebihara, M. and Kawamura, T. (2000) 'Homogeneous hydrogenation of olefins catalyzed by a novel tetrarhodium (II) complex as precursor in aqueous solution', *Journal of Molecular Catalysis A: Chemical*, 158(2), pp. 509-514.
- Yao, M.-Y., Huang, Y.-B., Niu, X. and Pan, H. (2016) 'Highly Efficient Silica-Supported Peroxycarboxylic Acid for the Epoxidation of Unsaturated Fatty Acid Methyl Esters and Vegetable Oils', *ACS Sustainable Chemistry & Engineering*, 4(7), pp. 3840-3849.
- Yazici, E.Y. and Deveci, H., (2010), October. Factors affecting decomposition of hydrogen peroxide. In Proceedings of the XIIth International Mineral Processing Symposium, Cappadocia, Turkey, pp. 6-10.
- Zapata, R.B., Villa, A.L. and de Correa, C.M. (2009a) 'Kinetic Modeling of Limonene Epoxidation over PW-Amberlite', *Industrial & Engineering Chemistry Research*, 48(2), pp. 647-653.
- Zapata, R.B., Villa, A.L., de Correa, C.M. and Williams, C.T. (2009b) 'In situ Fourier transform infrared spectroscopic studies of limonene epoxidation over PW-Amberlite', *Applied Catalysis A: General*, 365(1), pp. 42-47.
- Zheng, M., Skelton, R.L. and Mackley, M.R. (2007) 'Biodiesel Reaction Screening Using Oscillatory Flow Meso Reactors', *Process Safety and Environmental Protection*, 85(5), pp. 365-371.
- Zheng, M., Tang, J.S., Yin, D.L. and Xu, Q. (2012) 'Oxidation of  $\alpha$ -Pinene with Hydrogen Peroxide Catalyzed by VO(OAc)<sub>2</sub>', *Advanced Materials Research*, 550-553, pp. 179-182.
- Zhu, Y., Romain, C. and Williams, C.K. (2016) 'Sustainable polymers from renewable resources', *Nature*, 540(7633), p. 354.
- Zhu, Z., Tain, R. and Rhodes, C. (2003) 'A study of the decomposition behaviour of 12-tungstophosphate heteropolyacid in solution', *Canadian journal of chemistry*, 81(10), pp. 1044-1050.

## Appendices

### Appendix A. Calculation for Na<sub>2</sub>SO<sub>4</sub> solubility

Temperature (°C)	Solubility of 1 g Na <sub>2</sub> SO <sub>4</sub> in 100 mL of H <sub>2</sub> O
0	4.9
10	9.1
20	19.5
30	41.7
40	48.8
50	45.7
60	45.3
80	43.7
90	42.7
100	42.5

*Table A.1. Solubility of Na<sub>2</sub>SO<sub>4</sub> in H<sub>2</sub>O at various temperature.*

Example:

Solubility of Na<sub>2</sub>SO<sub>4</sub> in 100 mL H<sub>2</sub>O at 50 °C = 45.7 g

Solubility in 12.47 mL solution =  $45.7 / 100 \times 12.47 = \mathbf{5.7 \text{ g}}$

Solubility of Na<sub>2</sub>SO<sub>4</sub> in 100 mL H<sub>2</sub>O at 30 °C = 41.7 g

Solubility in 12.47 mL solution =  $41.7 / 100 \times 12.47 = \mathbf{5.2 \text{ g}}$



## Appendix B. Syringe pump commands

The pumps were operated through commands input in the Sapphire Commander software. Table B.1 shows some commonly used commands.

/nZR	Initialise pump no. <b>n</b>
/nT	Stop pump no. <b>n</b>
/_T	Stop all pumps
/nZA3000R	Move syringe <b>n</b> to bottom position (for cleaning)
/nIV5800A3000OA0GmR	Dispense fluid from pump <b>n</b> using full volume of syringe at maximum speed for <b>m</b> cycles (pump runs continually with $m = 0$ )
/nIV5800A3000OVXA0GmR	Dispense fluid from pump <b>n</b> using full volume of syringe at speed <b>X</b> for <b>m</b> cycles (pump runs continually with $m = 0$ ). <b>X</b> can be calculated using Equation B.1 below.
/nZS1LpOv1000Vqc2700gOArA0GmR	Fluid oscillation from pump <b>n</b> for <b>m</b> cycles (pump runs continually with $m = 0$ ). Commands <b>p/q</b> control the frequency and command <b>r</b> controls the amplitude. <b>p</b> is usually fixed at a maximum value of 20. <b>q/r</b> can be obtained from the table B-3 below.

Table B.1. Commonly used pump commands.

Z	Initialises the piston, turns the valve outlet to the right (to the dispense position)
R	Executes a command or command sequence
T	Termination
A	Absolute syringe position. A0 refers to the syringe at the outlet position while position A3000 refers to the syringe at the bottom.
I	Moves the valve to its inlet position (to fill the syringe)
V	Sets the maximum speed in Hz (5 = slowest, 5800 = fastest)
O	Move the valve to its output position (to dispense from the syringe)
G	Marks the start of a repeat sequence
S	Sets the maximum syringe speed (1 = fastest, 40 = slowest)
L	Sets the acceleration (1 = slowest, 20 = fastest)
v	Sets the initial speed in Hz
c	Sets the final speed in Hz
g	Marks the beginning of a loop

Table B.2. Description of abbreviations in Table B.1.

Input flow rates of the reactants are necessary in estimation of the  $X$  parameter for the pumps. This is a function of the volume of the pump syringe. For instance, when 1 mL (1000  $\mu\text{L}$ ) syringe is used to pump fluid at volumetric rate  $Q$  ( $\mu\text{L s}^{-1}$ ) into the reactor, the flow output parameter ( $X$ ) is calculated using the following expression:

$$X = \frac{(2)(3000)Q}{1000} = 6Q \quad (\text{B.1})$$

$q$	$r$	Corresponding frequency, $f$ (Hz)	Corresponding centre-to-peak amplitude (mm)
4500	60	5	9
4500	50	5.3	7.5
4500	40	5.9	5
4500	30	6.3	3.5
4500	20	7.5	2.5
4500	10	8.0	0.5
100	10	1	1
200	10	2	2
500	20	3	3
700	25	4	4
1500	30	5	5

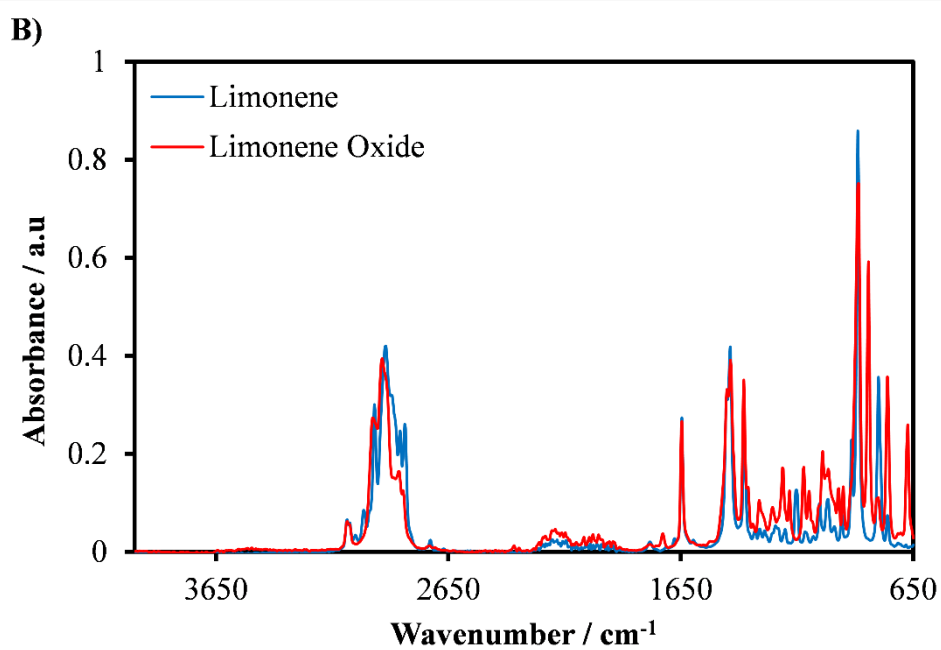
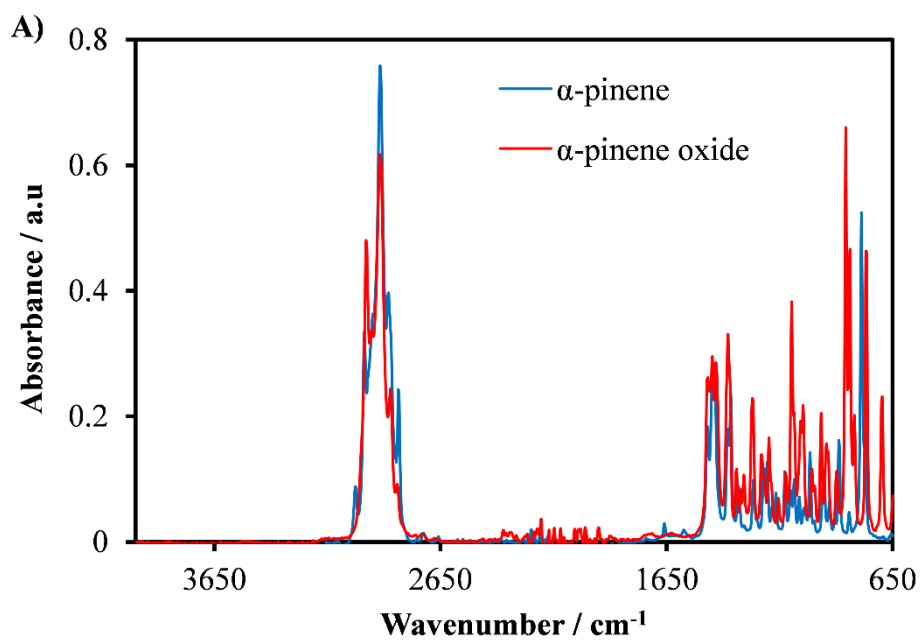
Table B.3.  $q$  and  $r$  parameters and its corresponding frequency and amplitude when using two 12.5 mL syringe for oscillation.

**Appendix C. Flow condition used in the continuous experiments using mesoOBR**

<b>Re<sub>0</sub></b>	<b>St</b>	<b>X<sub>0</sub> (mm)</b>	<b>f (Hz)</b>
254	0.13	3	3
452	0.10	4	4
530	0.16	2.5	7.5
834	0.08	5	5.9
1273	0.04	9	5

*Table C.1. Mixing condition (Re<sub>0</sub>), strouhal number (St) and its corresponding centre-to-peak amplitude (X<sub>0</sub>) and frequency (f).*

## Appendix D. Full FTIR spectra



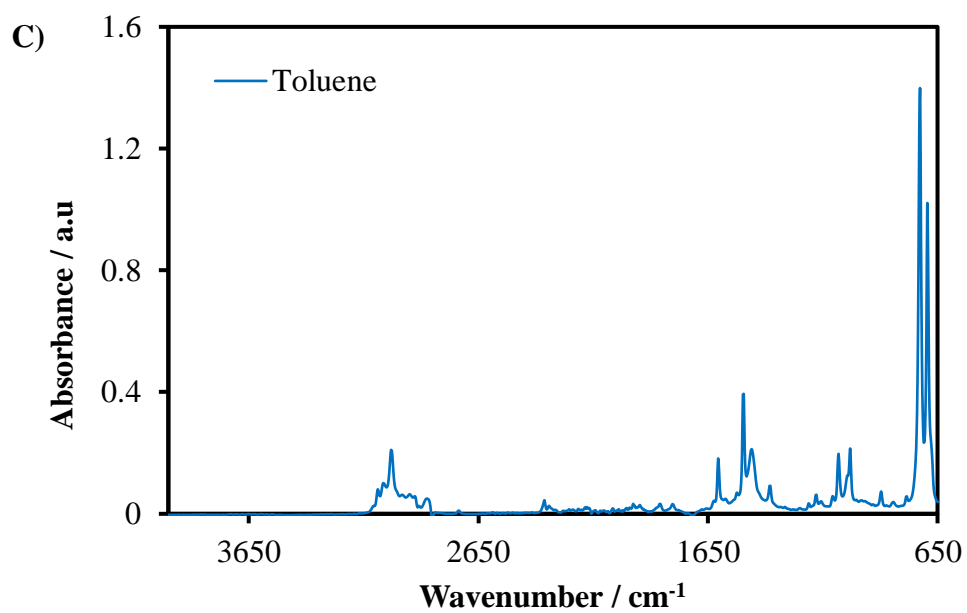


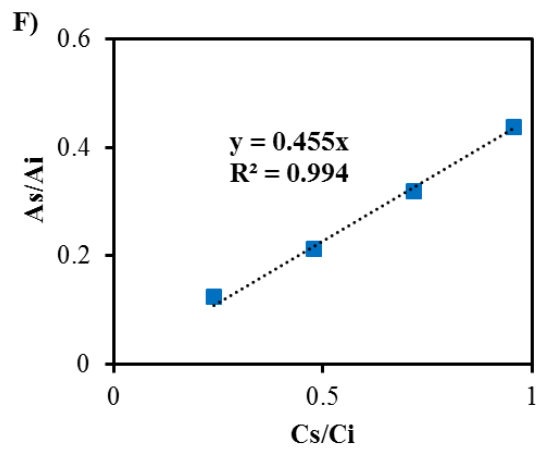
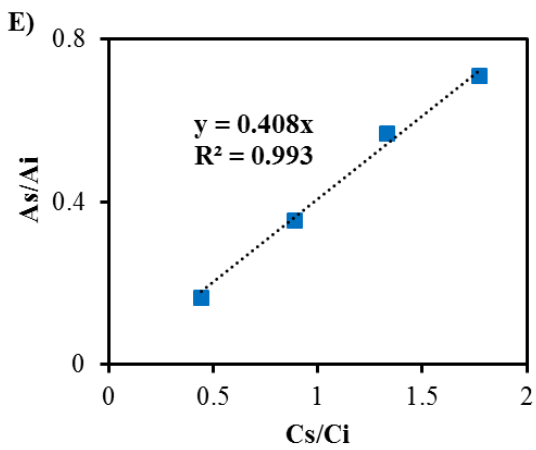
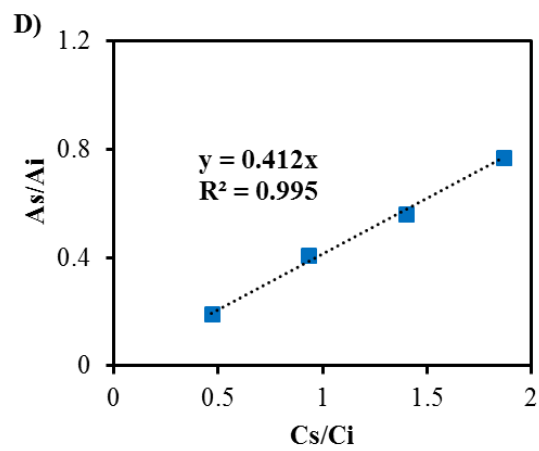
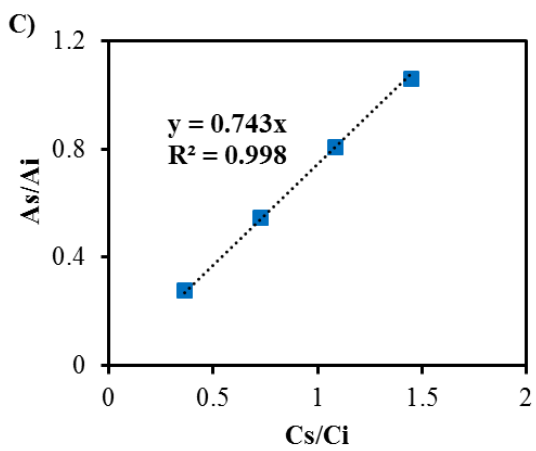
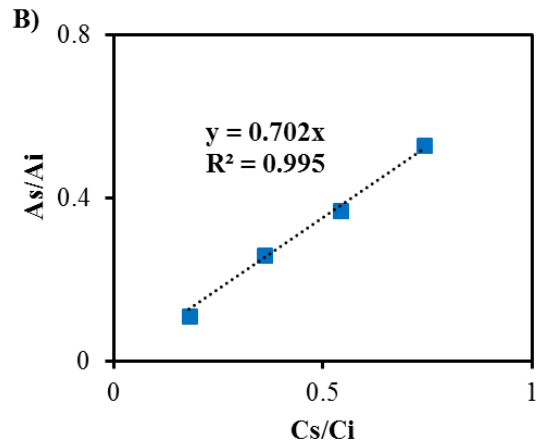
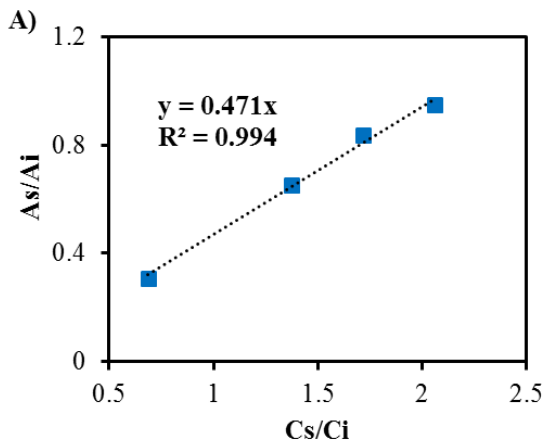
Figure D.1. Full (4000 – 650  $\text{cm}^{-1}$ ) FTIR spectra for A)  $\alpha$ -pinene and  $\alpha$ -pinene oxide B) limonene and limonene oxide C) toluene (solvent).

## Appendix E. GC response factor and calibration curves

<b>Compound</b>	<b>Response factor (f)</b>
limonene	0.965
limonene oxide	0.790
$\alpha$ -pinene	0.817
$\alpha$ -pinene oxide	0.760
limonene-bis-epoxide	0.471
limonene-1,2-diol	0.702
campholenic aldehyde	0.743
sobrerol	0.412
pinanediol	0.408
verbenol	0.455
verbenone	0.644

*Table E.1. GC response factor for limonene,  $\alpha$ -pinene and all oxidative products.*

Calibration curve:



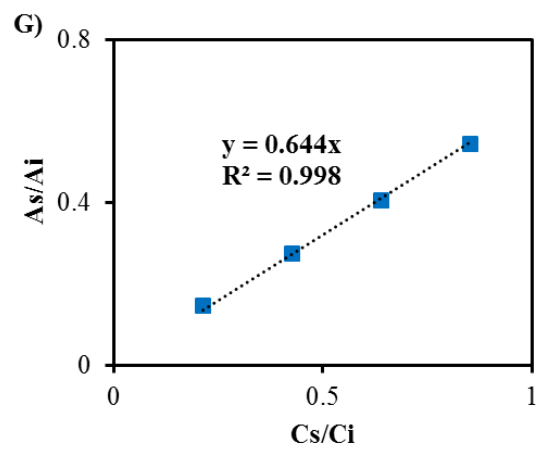
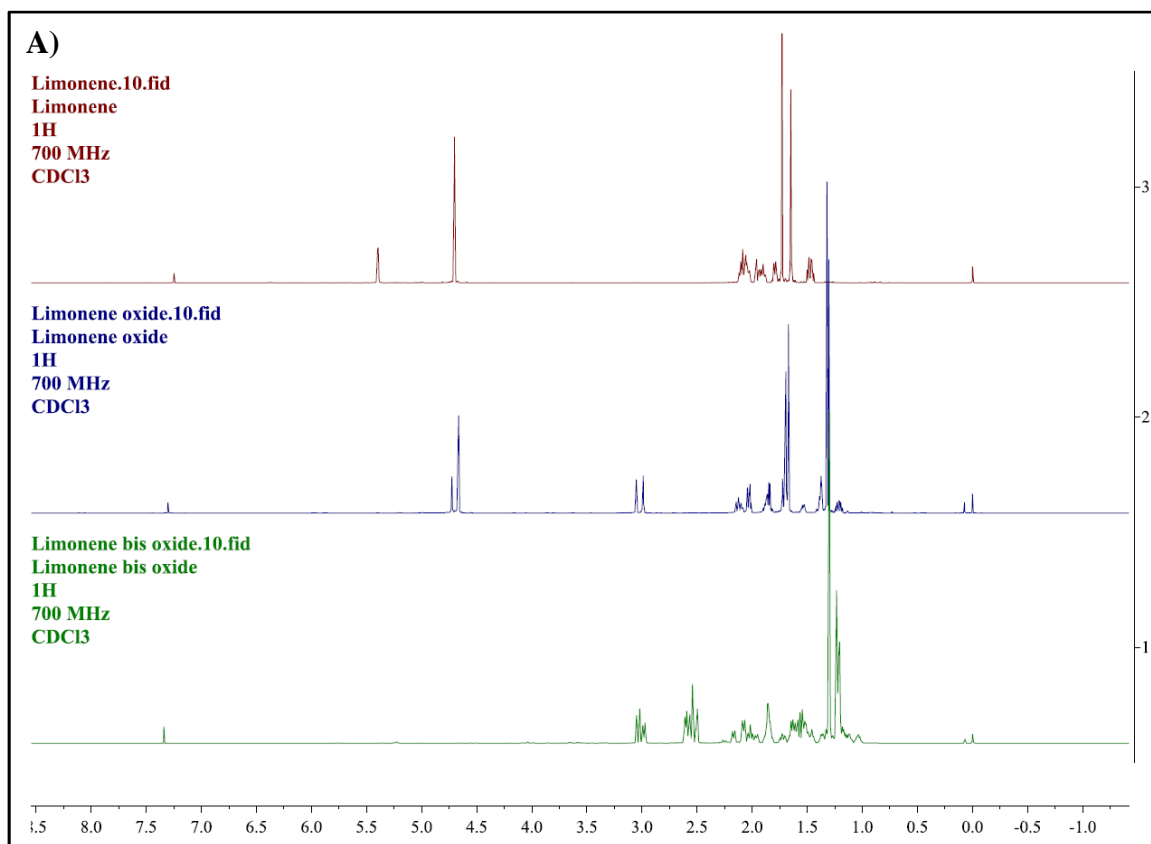


Figure E.1. GC Calibration curve for (A) Limonene bis-epoxide (B) Limonene-1,2-diol (C) Campholenic aldehyde (D) Sobrerol (E) Pinanediol (F) Verbenol (G) Verbenone.



## Appendix F. NMR Spectra



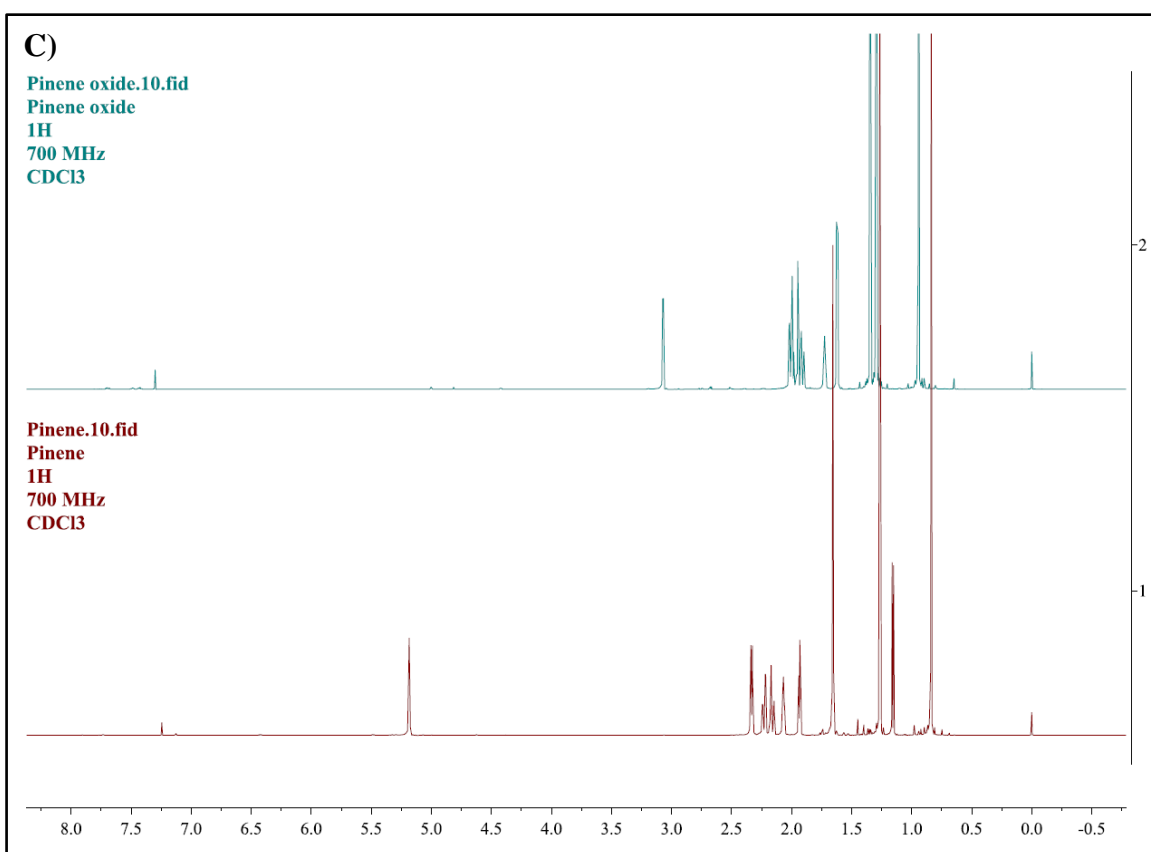
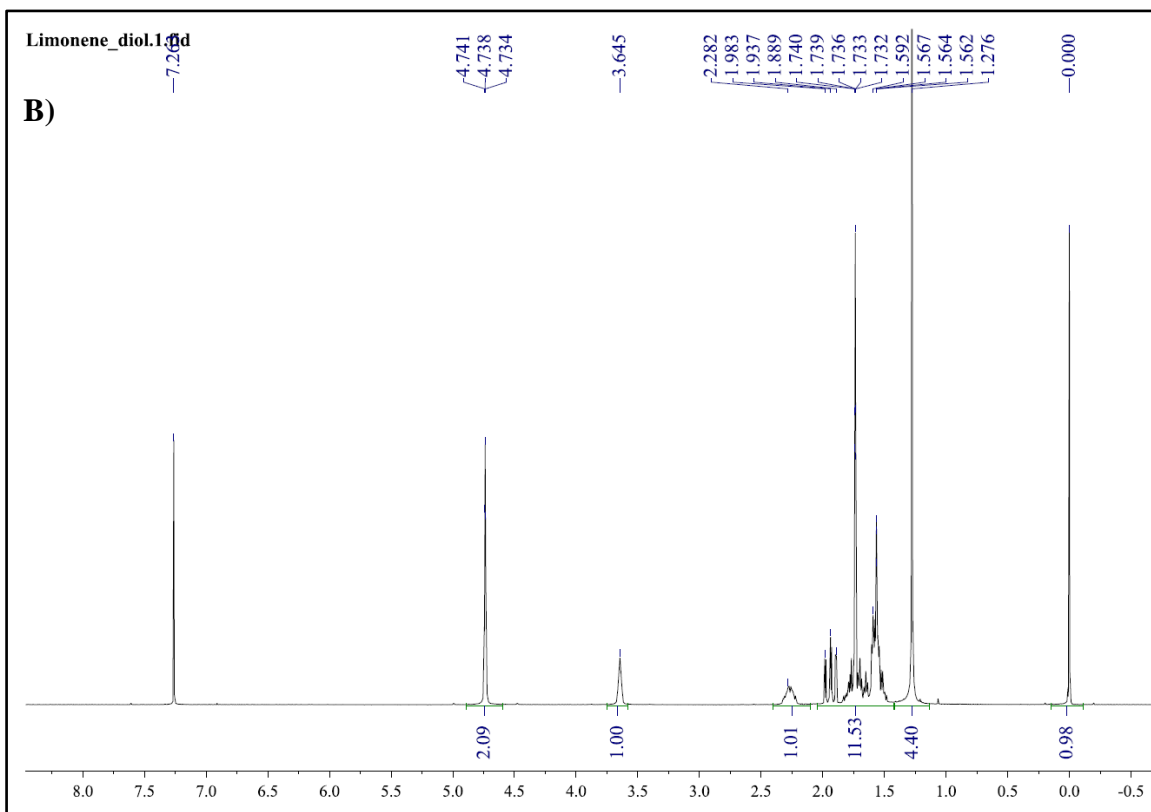


Figure F.1. NMR spectra for (A) limonene, limonene-1,2-epoxide, and limonene bis-epoxide (B) limonene-1,2-diol (C)  $\alpha$ -pinene and  $\alpha$ -pinene oxide.

## Appendix G. MATLAB code (epoxidation of limonene)

```
% Define initial concentrations
```

```
% [Lim, LO, LimDiol, Bis, BisDiol, H2O2, H2O, Cat,Pom, Na2SO4, Na2SO4H2O]
```

```
C0 = [1.25, 0, 0, 0, 0, 1.25, 5.52, 0.006, 0, 0.376, 0];
```

```
%Define time span
```

```
tspan = [0, 120];
```

```
%Run ODE Solver
```

```
[t, y] = ode15s(@Lim_Epox_MechanismV, tspan, C0);
```

```
plot(t,y)
```

```
legend('Lim','LO','LimDiol','Bis','BisDiol','H2O2','H2O','Cat','Pom','Na2SO4','Na2SO4H2O');
```

```
t1=[];
```

```
function dC = Lim_Epox_MechanismV(t, C)
```

```
% Variable names
```

```
CLim = C(1); CLO = C(2);
```

```
CLimDiol = C(3); CBis = C(4);
```

```
CBisDiol = C(5); CH2O2 = C(6);
```

```
CH2O = C(7); CCat = C(8);
```

```
CPom = C(9); CNa2SO4 = C(10);
```

```
CNa2SO4H2O = C(11);
```

```
CH = 0.038;
```

$$k1 = 0.00000001;$$

$$k2 = 1;$$

$$k3 = 0.03119;$$

$$k4 = 0.001;$$

$$k5 = 0.0008979;$$

$$k6 = 0.0009;$$

$$k7 = 10;$$

### %Rate laws

$$r1 = k1*CH2O2;$$

$$r2 = k2*CH2O2*CCat*CH;$$

$$r3 = k3*CLim*CPom;$$

$$r4 = k4*CLO*CPom;$$

$$r5 = k5*CLO*CH2O*CH;$$

$$r6 = k6*CBis*CH2O*CH;$$

$$r7 = k7*CNa2SO4*CH2O;$$

### %Mass balance

$$dCLim = -r3;$$

$$dCLO = r3 - r4 - r5;$$

$$dCLimDiol = r5;$$

$$dCBis = r4 - r6;$$

$$dCBisDiol = r6;$$

$$dCH2O2 = -r1 - r2;$$

$$dCH_2O = r_1 + r_2 - r_5 - r_6 - (10 * r_7);$$

$$dCCat = -r_2 + r_3 + r_4;$$

$$dCPom = r_2 - r_3 - r_4;$$

$$dCNa_2SO_4 = -r_7;$$

$$dCNa_2SO_4H_2O = r_7;$$

**%Assign output variables**

$$dC(1,:) = dCLim;$$

$$dC(2,:) = dCLO;$$

$$dC(3,:) = dCLimDiol;$$

$$dC(4,:) = dCBis;$$

$$dC(5,:) = dCBisDiol;$$

$$dC(6,:) = dCH_2O_2;$$

$$dC(7,:) = dCH_2O;$$

$$dC(8,:) = dCCat;$$

$$dC(9,:) = dCPom;$$

$$dC(10,:) = dCNa_2SO_4;$$

$$dC(11,:) = dCNa_2SO_4H_2O;$$

## Appendix H. Initial rates values (limonene epoxidation)

Appendix H presented the values of initial rates obtained from the mixing and kinetic study of limonene epoxidation. The initial rates values were obtained from the gradient of slope of plot of limonene-1,2-epoxide concentration vs time (15 minutes).

Mixing speed / rpm	Rate / mol L <sup>-1</sup> min <sup>-1</sup>
250	0.0088
500	0.0307
750	0.0406
1000	0.0418
1250	0.0454
1500	0.042

Table H.1. Initial rates obtained from the mixing study of limonene epoxidation.

PTC Amount / g	Rate / mol L <sup>-1</sup> min <sup>-1</sup>
0	0
0.25	0.0287
0.5	0.0377
0.75	0.0416
1	0.0451
1.5	0.0433
2	0.039

Table H.2. Initial rates obtained from the PTC amount study for limonene epoxidation.

Catalyst Concentration / mol L <sup>-1</sup>	Rate / mol L <sup>-1</sup> min <sup>-1</sup>
0.003	0.0155
0.005	0.0251
0.006	0.0324
0.008	0.0389
0.009	0.0475

Table H.3. Initial rates obtained from the kinetic study of limonene epoxidation (catalyst concentration).

Limonene Concentration / mol L <sup>-1</sup>	Rate / mol L <sup>-1</sup> min <sup>-1</sup>
0.25	0.0082
0.5	0.013
0.75	0.0184
1	0.0252
1.25	0.0308

*Table H.4. Initial rates obtained from the kinetic study of limonene epoxidation (limonene concentration).*

H <sub>2</sub> O <sub>2</sub> Concentration / mol L <sup>-1</sup>	Rate / mol L <sup>-1</sup> min <sup>-1</sup>
0.25	0.0133
0.5	0.0141
0.75	0.0179
1	0.0196
1.25	0.0267

*Table H.5. Initial rates obtained from the kinetic study of limonene epoxidation (H<sub>2</sub>O<sub>2</sub> concentration).*

## Appendix I. Initial rates values ( $\alpha$ -pinene epoxidation)

Appendix I presented the values of initial rates obtained from the mixing and kinetic study of  $\alpha$ -pinene epoxidation. The initial rates values were obtained from the gradient of slope of plot of  $\alpha$ -pinene oxide concentration vs time (15 minutes).

Catalyst Concentration / mol L <sup>-1</sup>	Rate / mol L <sup>-1</sup> min <sup>-1</sup>
0.008	0.009
0.010	0.0108
0.012	0.0126
0.014	0.0139
0.016	0.0177

Table I.1. Initial rates obtained from the kinetic study of  $\alpha$ -pinene epoxidation (catalyst concentration).

$\alpha$ -pinene Concentration / mol L <sup>-1</sup>	Rate / mol L <sup>-1</sup> min <sup>-1</sup>
0.25	0.0016
0.5	0.0031
0.75	0.0046
1	0.0057
1.25	0.0072

Table I.2. Initial rates obtained from the kinetic study of  $\alpha$ -pinene epoxidation ( $\alpha$ -pinene concentration).

H <sub>2</sub> O <sub>2</sub> Concentration / mol L <sup>-1</sup>	Rate / mol L <sup>-1</sup> min <sup>-1</sup>
0.25	0.0098
0.5	0.0109
0.75	0.0130
1	0.0149
1.25	0.0184

Table I.3. Initial rates obtained from the kinetic study of  $\alpha$ -pinene epoxidation (H<sub>2</sub>O<sub>2</sub> concentration).